

# **Synthesis, characterisation, and application of conjugated polyene modified TiO<sub>2</sub> photocatalysts for the treatment of selected pharmaceuticals in water**

A dissertation submitted in fulfilment of the requirements for the degree

of

Philosophiae Doctor (PhD): Chemistry

in the

Faculty of Applied and Computer Sciences

Department of Chemistry

at the

Vaal University of Technology

2020



*Your world to a better future*

Candidate name: Olayinka Oladimeji Samuel **Awofiranye**

Student No.: 217044050

**Promoter: Prof. SJ Modise**

**Co-Promoter: Prof. EB Naidoo**

## Declaration

I, Olayinka Oladimeji Samuel **Awofiranye**, hereby declare that this work is my own work and that all sources of materials used were duly acknowledged. This work has been submitted in partial fulfilment of the requirements of PhD degree at the Vaal University of Technology.

I solemnly declare that this project has not been submitted to any other institution anywhere for any other academic degree.

.....

Signature

.....

Date

## Acknowledgments

First and foremost, I want to offer this effort to God Almighty. To Him be all the glory and honour for the wisdom, strength, good health and the spirit of perseverance He bestowed upon me to finish this research.

This research work and the thesis became a reality with the kind support and useful assistance of many individuals. I would like to sincerely thank all of them.

Foremost, I offer my sincere gratitude to my principal supervisor, Professor SJ Modise; thank you for being a good and supportive supervisor. Thank you for the continual guidance and for allowing me to work in my own way.

I also owe my deep gratitude to my co-supervisor, Professor EB Naidoo, former HOD chemistry, for his endless patience and willingness to help whenever I needed his advice and support. I also appreciate Professor M. Moloto, the current HOD chemistry for caring for students.

I would like to express my gratitude to the Research Directorate at the Vaal University of Technology, South Africa, for the funding.

My sincere thanks also go to Mr Mike Ngoyi, the analytical laboratory technician, Chemistry Department, who willingly helped during the initial HPLC trauma and several other times his assistance was needed in the lab.

I would like to express my deepest appreciation towards my family for the encouragement, which helped me in the completion of this study. My beloved and highly supportive wife, Omolara, I say thank you for your endurance and taking over virtually all the responsibilities at home while I was not available. I appreciate my lovable and understanding children Esther, Joshua and Daniel who serve as sources of my inspiration to pursue this endeavour. Uncle Yemi, my brother-in-law, thank you for caring for these children while I was away for research.

My thanks and appreciations also go to my colleagues and people who have willingly helped me out with their abilities– Mr Ola Saka, Mr Attah-Daniel, Mr Benton, Dr. Sam

in biotechnology laboratory, Dr W. Omwoyo, Dr. Seth and Linda Apolo and Mr. Oluwayimika Oluokun. The useful advice from Dr. Ekemena Oseghe is highly appreciated.

My immeasurable appreciation and deepest gratitude go to Dr and Dr (Mrs) OS Adeyinka. Thank you for allowing yourself to be used by God to support me at a time when stopping was an option.

## Abstract

This research has investigated the effects of conjugation on the visible light absorption capacity of polyene modified  $\text{TiO}_2$  nanoparticles as well as the efficiency of these nanoparticles for the mineralisation of acetaminophen (APAP), a non-antibiotic and chloramphenicol (CAP), an antibiotic pharmaceutical compound (PC) which are commonly used worldwide. The efficiency of polyene modified  $\text{TiO}_2$  (CPE- $\text{TiO}_2$ ) compared with bare  $\text{TiO}_2$  was further assessed for the mineralisation of the selected PCs under visible light.

To achieve this aim, the synthesised nanoparticles were appropriately characterised and tested for the photocatalytic degradation of acetaminophen (APAP) and chloramphenicol (CAP), under visible light. Furthermore, the mechanism and the kinetics of photocatalytic degradation of the PCs were investigated by using high-performance liquid chromatography (HPLC) to monitor the photodegradation intermediates, e.g. Hydroquinone, p-nitrophenol and oxamic acid.

The DRS UV-vis spectra result of the CPE- $\text{TiO}_2$  indicated that it has a lower band-gap than bare  $\text{TiO}_2$  nanoparticles and demonstrated a better absorption ability in the wavelength range of 400-800 nm. This result was further confirmed by other optical analyses, such as electrochemical impedance spectrometry (EIS) and photoluminescence (PL). The analysis indicated a less recombination rate of electron/hole pairs in CPE- $\text{TiO}_2$  compared to  $\text{TiO}_2$ . Notably, CPE- $\text{TiO}_2$  nanocomposite exhibited higher photocatalytic properties for both pollutants, compared to bare  $\text{TiO}_2$  under visible light.

Importantly, photocatalytic degradation experiments demonstrated that the CPE modified nanoparticles were significantly more efficient for PCs degradation (94.21 % for APAP and 80.47% for CAP) compared to bare  $\text{TiO}_2$  (27.12% for APAP and 36.12% for CAP). The role of CPE- $\text{TiO}_2$  photocatalysis in degrading APAP and CAP was examined by varying experimental parameters such as PC concentrations, catalyst loading and solution pH. All the parameters were observed to influence the degradation of the PCs to some extent, albeit, at optimum conditions, most of these PCs were degraded within 210 minutes of visible light irradiation.

A significant relationship between the ionic state (+ve or -ve based on the pH) of the solution and CPE-TiO<sub>2</sub> photocatalytic process was observed. For the mineralisation, CPE-TiO<sub>2</sub> photocatalysis led to higher oxidation rates compared to direct photolysis and bare TiO<sub>2</sub> photocatalysis. The results confirm that the co-existence of multiple bonds in poly-conjugated carbon chains with a reduced band-gap in CPE-TiO<sub>2</sub> composite were able to enhance charge separation and migration as well as improve the photocatalytic efficiency.

This study has clearly demonstrated that polyene modified TiO<sub>2</sub> nanoparticles can be applied to degrade PCs in aqueous solution and offers an attractive option for small-scale pharmaceutical wastewater treatment. However, the complex nature of real effluents with co-existing pollutants and higher levels of organic and inorganic matter may call for possible coupling of a biological process as pre- or post-treatment to improve their biodegradability.

# TABLE OF CONTENTS

DECLARATION .....	II
ACKNOWLEDGMENTS.....	III
ABSTRACT.....	V
TABLE OF CONTENTS.....	VII
LIST OF FIGURES .....	X
LIST OF TABLES.....	XIV
LIST OF EQUATIONS .....	XV
NOMENCLATURE.....	XVII
<b>CHAPTER 1: GENERAL INTRODUCTION AND RESEARCH OVERVIEW.....</b>	<b>1</b>
1.1 INTRODUCTION .....	3
1.2 PROBLEM STATEMENT AND JUSTIFICATION.....	8
1.3 AIM AND OBJECTIVES OF THE STUDY.....	9
1.4 PROJECT SCOPE AND DELINEATION OF THE ATUDY .....	10
REFERENCES .....	12
<b>CHAPTER 2: LITERATURE REVIEW .....</b>	<b>17</b>
2.1 INTRODUCTION .....	19
2.2 PHOTOCATALYSIS .....	26
2.3 LIMITATIONS OF TiO <sub>2</sub> PHOTOCATALYST AND IMPROVEMENT WITH POLYMER MODIFICATIONS.....	34
2.4 PHOTOCATALYTIC APPLICATIONS OF POLYMER-TiO <sub>2</sub> .....	36
2.5 PHOTOCATALYTIC INTERMEDIATES FOR SELECTED PHARMACEUTICALS USING TiO <sub>2</sub> .....	43
CONCLUSION.....	48
REFERENCES .....	49
<b>CHAPTER 3: MATERIALS AND METHODS.....</b>	<b>65</b>
3.1 PHOTOCATALYTIC MATERIALS AND MODEL PHARMACEUTICALS.....	69

3.2 MATERIALS AND METHODS FOR EXPERIMENTAL STUDIES.....	69
3.3 ANALYTICAL TECHNIQUES AND EQUIPMENT .....	72
3.4 PHOTOCATALYTIC DEGRADATION EXPERIMENTS.....	77
REFERENCES .....	83

## **CHAPTER 4: RESULT AND DISCUSSIONS .....84**

### **SECTION A: STRUCTURAL AND MORPHOLOGICAL CHARACTERISATION .....87**

INTRODUCTION .....	87
4.1 STRUCTURAL CHARACTERISATION.....	87
4.2 MORPHOLOGICAL AND COMPOSITIONAL CHARACTERISATION.....	94
CONCLUSION.....	101

### **SECTION B: OPTICAL AND ELECTROCHEMICAL CHARACTERISATION.....102**

INTRODUCTION .....	102
4.3 OPTICAL CHARACTERISATION.....	102
4.4 ELECTROCHEMICAL CHARACTERISATION.....	108
CONCLUSION.....	110

### **SECTION C: THE PHOTOCATALYTIC PARAMETERS INVESTIGATION FOR THE DEGRADATION OF APAP, CAP AND DURABILITY TEST OF THE CATALYST MATERIALS .....112**

INTRODUCTION .....	112
4.5 EFFECTS OF CATALYST DOSAGE.....	112
4.6 EFFECTS OF INITIAL CONCENTRATION.....	115
4.7 EFFECT OF THE SOLUTION PH.....	118
4.8 EFFECT OF IRRADIATION TIME .....	121
4.9 PHOTOCATALYTIC DEGRADATION AT OPTIMUM CONDITIONS .....	123
4.10 THE TOTAL ORGANIC CARBON (TOC) REMOVAL FOR THE PHARMACEUTICALS.....	127
4.11 THE DURABILITY AND REUSABILITY TEST FOR THE CATALYST .....	129
CONCLUSION.....	130

### **SECTION D: THE KINETICS AND MECHANISMS OF APAP AND CAP PHOTOCATALYTIC DEGRADATIONS .....131**



INTRODUCTION .....	131
4.12 KINETICS OF PHOTODEGRADATION .....	131
4.13 POSSIBLE PHOTODEGRADATION MECHANISM AND INTERMEDIATE IDENTIFICATIONS.....	143
REFERENCES .....	150
 <b>CHAPTER 5: GENERAL CONCLUSION AND RECOMMENDATIONS .....</b>	<b>158</b>
5.1 GENERAL CONCLUSION .....	160
5.2 RECOMMENDATIONS .....	162
APENDICES .....	<b>164</b>

## LIST OF FIGURES

Figure 1.1: The chemical structures of acetaminophen and chloramphenicol.....	4
Figure 2.1: The proposed classifications of advanced oxidation processes (AOP) based on reaction mechanisms .....	26
Figure 2.2: The scheme of redox process mechanism of semiconductor (SC) photocatalyst in the presence of light. ....	33
Figure 2.3: The flow chart of the mechanistic route for semiconductor (TiO <sub>2</sub> ) photocatalysis. ....	34
Figure 2.4: The scheme of chitosan-TiO <sub>2</sub> composite fibre treated with different metal salt solutions. Source: Ali <i>et al.</i> (2018) .....	38
Figure 2.5: The mechanism of CP modified TiO <sub>2</sub> photocatalyst under light irradiation. ....	42
Figure 2.6: The summary of intermediates and final degradation products of pharmaceuticals .....	44
Figure 3.1: Homogenised sol-gel synthesis set up; (A) Refluxing (B) Homogenising .....	70
Figure 3.2: The schematic diagram for HPLC analytical technique: Source; Cruzan, (2012) .....	77
Figure 4.1: The FTIR spectra of (A) conjugated polyene (CPE) and PVA and (B) CPE, TiO <sub>2</sub> and CPE-TiO <sub>2</sub> materials .....	88
Figure 4.2: Powder X-ray diffraction (PXRD) of (A) TiO <sub>2</sub> and CPE-TiO <sub>2</sub> at varying CPE modifications and (B) synthesised TiO <sub>2</sub> and 0.6% CPE-TiO <sub>2</sub> . ....	90
Figure 4.3: Optimisation of CPE modified TiO <sub>2</sub> for photodegradation of acetaminophen and chloramphenicol.....	92
Figure 4.4: (A) The thermal gravimetric analysis (TGA) (B) the derivative thermal analysis (DTA) of TiO <sub>2</sub> and CPE-TiO <sub>2</sub> . ....	93

Figure 4.5: Scanning electron microscopy (SEM) images of (A) $\text{TiO}_2$ (B) 0.2% CPE- $\text{TiO}_2$ (C) 0.4% CPE- $\text{TiO}_2$ (D) 0.6% CPE- $\text{TiO}_2$ (E) 0.8% CPE- $\text{TiO}_2$ .....	95
Figure 4.6: Transmission electron microscopy (TEM) analysis for (A) $\text{TiO}_2$ (B) 0.2% CPE- $\text{TiO}_2$ (C) 0.4% CPE- $\text{TiO}_2$ (D) 0.6% CPE- $\text{TiO}_2$ and (E) 0.8% CPE- $\text{TiO}_2$ .....	96
Figure 4.7: Energy dispersive X-ray spectroscopy (EDS) analysis of (A) $\text{TiO}_2$ (B) 0.2% CPE- $\text{TiO}_2$ (C) 0.4% CPE- $\text{TiO}_2$ (D) 0.6% CPE- $\text{TiO}_2$ .....	97
Figure 4.8: Gaussian fit particle size distribution plots from TEM micrograph for (A) $\text{TiO}_2$ , (B) 0.2% CPE- $\text{TiO}_2$ , (C) 0.4% CPE- $\text{TiO}_2$ , (D) 0.6% CPE- $\text{TiO}_2$ , (E) 0.8% CPE- $\text{TiO}_2$ .....	100
Figure 4.9: UV-Vis electronic absorption spectra of PVA and CPE .....	103
Figure 4.10: (A) Uv-vis DRS spectra of bare $\text{TiO}_2$ and 0.6% CPE- $\text{TiO}_2$ and (B) Tauc plot for bare $\text{TiO}_2$ and 0.6% CPE- $\text{TiO}_2$ .....	104
Figure 4.11: The photoluminescence (PL) spectra of (A) $\text{TiO}_2$ and CPE- $\text{TiO}_2$ at varying polyene percentage modification (B) $\text{TiO}_2$ and 0.6% CPE- $\text{TiO}_2$ .....	107
Figure 4.12: CV curve for (A) $\text{TiO}_2$ and CPE- $\text{TiO}_2$ at varying polyene percentage modification (B) bare-electrode, $\text{TiO}_2$ and 0.6% CPE- $\text{TiO}_2$ .....	109
Figure 4.13: The EIS Nyquist plots of (A) $\text{TiO}_2$ and CPE- $\text{TiO}_2$ at varying polyene percentage modification and (B) $\text{TiO}_2$ and 0.6% CPE- $\text{TiO}_2$ .....	110
Figure 4.14: Visible light degradation of APAP by (A) bare $\text{TiO}_2$ and CPE- $\text{TiO}_2$ at various catalysts dosages (pH 8) and (B) the corresponding degradation rate (using CPE- $\text{TiO}_2$ ) with respect to time .....	113
Figure 4.15: Visible light degradation of CAP by (A) pure $\text{TiO}_2$ and CPE- $\text{TiO}_2$ at various catalysts dosages (pH 8) and (B) the corresponding degradation rate (using CPE- $\text{TiO}_2$ ) with respect to time .....	114
Figure 4.16: Visible light degradation of APAP by (A) bare $\text{TiO}_2$ and CPE- $\text{TiO}_2$ at various initial concentrations and (B) the corresponding degradation rate (using CPE- $\text{TiO}_2$ ) with respect to time .....	116
Figure 4.17: Visible light degradation of CAP by (A) bare $\text{TiO}_2$ and CPE- $\text{TiO}_2$ at various initial concentrations and (B) the corresponding degradation rate (using CPE- $\text{TiO}_2$ ) with respect to time .....	117

Figure 4.18: Visible light degradation of APAP by (A) bare $\text{TiO}_2$ and CPE- $\text{TiO}_2$ at various pH and (B) the corresponding degradation rate (using CPE- $\text{TiO}_2$ ) with respect to time .....	119
Figure 4.19: Visible light degradation of CAP by (A) bare $\text{TiO}_2$ and CPE- $\text{TiO}_2$ at various pH and (B) the corresponding degradation rate (using CPE- $\text{TiO}_2$ ) with respect to time .....	120
Figure 4.20: Visible light degradation of paracetamol by (A) pure $\text{TiO}_2$ and CPE- $\text{TiO}_2$ at different irradiation time and (B) the corresponding degradation rate.....	122
Figure 4.21: Visible light degradation of chloramphenicol by (A) pure $\text{TiO}_2$ and CPE- $\text{TiO}_2$ at different irradiation time and (B) the corresponding degradation rate.....	123
Figure 4.22: UV-Vis absorption spectra during photocatalytic degradation monitoring of (A) APAP (B) CAP using CPE- $\text{TiO}_2$ as a catalyst .....	124
Figure 4.23: Visible light photodegradation of APAP; (A) degradation rate with respect to time and (B) Relative % degradations (with no catalyst, pure $\text{TiO}_2$ and CPE- $\text{TiO}_2$ ) at optimum conditions .....	125
Figure 4.24: Visible light photodegradation of CAP; (A) degradation rate with respect to time and (B) Relative % degradations (with no catalyst, bare $\text{TiO}_2$ and CPE- $\text{TiO}_2$ ) at optimum conditions .....	126
Figure 4.25: Total organic carbon (TOC) removal percentage for (A) CAP and (B) APAP photocatalytic degradation after 210 min of visible light irradiation .....	128
Figure 4.26: Recycled photocatalytic degradation of acetaminophen in aqueous solution using CPE- $\text{TiO}_2$ nanocomposite.....	130
Figure 4.27: The rate plot for photocatalytic degradation of APAP with respect to time at varying Initial concentrations .....	136
Figure 4.28: The rate plot for photocatalytic degradation of CAP with respect to time at varying initial concentrations.....	136
Figure 4.29: The rate plot for photocatalytic degradation of APAP with respect to time at varying catalyst dosages.....	138
Figure 4.30: The rate plot for photocatalytic degradation of CAP with respect to time at varying catalyst dosages.....	138

Figure 4.31: The rate plot for photocatalytic degradation of APAP with respect to time at varying pH. ....	140
Figure 4.32: The rate plot for photocatalytic degradation of CAP with respect to time at varying pH. ....	140
Figure 4.33: The rate plot for photocatalytic degradation of APAP with respect to time at optimum conditions (pH = 8, Initial conc. = 25 mgL <sup>-1</sup> , catalyst dosage = 15 mg 200mgL <sup>-1</sup> ). .....	142
Figure 4.34: The rate plot for photocatalytic degradation of CAP with respect to time at optimum conditions (pH = 8, Initial conc. = 25 mgL <sup>-1</sup> , catalyst dosage = 15 mg 200 mgL <sup>-1</sup> ) . .....	143
Figure 4.35: Effect of scavengers on the photocatalytic degradation of paracetamol and chloramphenicol using CPE-TiO <sub>2</sub> .....	145
Figure 4.36: HPLC of APAP solution during photocatalytic degradation of 25mgL <sup>-1</sup> initial concentration at different irradiation times (min): at (A) 0, (B) 100 and (C) 210 .....	147
Figure 4.37: HPLC of APAP solution during photocatalytic degradation of 25mgL <sup>-1</sup> initial concentration at different irradiation times (min): at (A) 0, (B) 120 and (C) 210 .....	149

## LIST OF TABLES

Table 2.1: Formation rate of OH• on some metal oxide photocatalysts and their OH•- index values.....	30
Table 2.2: Application of TiO <sub>2</sub> photocatalyst for pharmaceutical degradation in solution .....	40
Table 2.3: Photodegradation of pharmaceuticals and other pollutants using polymer-TiO <sub>2</sub> catalysts.....	40
Table 2.4: Paracetamol photodegradation intermediates and products .....	45
Table 2.5: Chloramphenicol photodegradation intermediates and products .....	47
Table 3.1: Physicochemical properties of chloramphenicol and acetaminophen .....	70
Table 3.2: Methods of separation by HPLC for the pollutants during photocatalytic process	76
Table 3.3: Experimental set-up and conditions for the photocatalytic process .....	78
Table 3.4: Variable experimental parameters .....	79
Table 3.5: Preliminary experimental design for condition optimisation .....	80
Table 4.1: The estimated crystallite sizes of the materials from PXRD plots.....	91
Table 4.2: The crystallite sizes and bandgaps for bare TiO <sub>2</sub> and CPE-TiO <sub>2</sub> .....	105
Table 4.3: Acetaminophen % removal, half-life, rate constants ( $k_{app}$ ) and $R^2$ values for pseudo first order (PFO) kinetic model in the photocatalytic experiments using CPE-TiO <sub>2</sub>	134
Table 4.4: Chloramphenicol % removal, rate constants ( $k_{app}$ ) and $R^2$ values for pseudo first order (PFO) kinetic model in the photocatalytic experiments using CPE-TiO <sub>2</sub> bear.....	135
Table 4.5: The photo-oxidation reactive species and the scavenging reagents .....	144

## LIST OF EQUATIONS

$\text{Rate} = \frac{d[C]}{dt} = K[C]^{n-1}$	Equation 2.1..... 30
$\text{Rate}(r) = \frac{d[C]}{dt} = \frac{kKC}{1+KC}$	Equation 2.2.....31
$\ln\left(\frac{C_0}{C}\right) = kK_t = k_{app}t$	Equation 2.3..... 31
$\ln\left(\frac{C_0}{C}\right) = k_{app}$	Equation 2.4.....32
$OH - index = \frac{r}{r_0} \times 100$	Equation 2.5.....42
$CP + h\nu \rightarrow CP^*$	Equation 2.6.....43
$CP^* + TiO_2 \rightarrow CP^{++} + TiO_2(e^-)$	Equation 2.7.....43
$TiO_2(e^-) + O_2 \rightarrow O_2^-$	Equation 2.8.....43
$O_2^- + H^+ \rightarrow HO_2^{\cdot}$	Equation 2.9.....43
$O_2^- + H_2O \rightarrow HO_2^{\cdot} + OH^{\cdot}$	Equation 2.10.....43
$O_2^- (or HO_2^{\cdot} or OH^{\cdot} + PP) \rightarrow Intermediates$	Equation 2.11.....43
$Intermediate + O_2^- (or HO_2^{\cdot} or OH^{\cdot}) \rightarrow CO_2 + H_2O$	Equation 2.12.....43
$A = \log\left(\frac{I_0}{I}\right) = ECL$	Equation 3.1.....77
$Degradation\ Efficiency\ (\%) = \frac{C_0 - C_t}{C_t} \times 100$	Equation 3.2.....80
$D = \frac{K\lambda}{\beta \cos\theta}$	Equation 4.1.....93

$$(\propto hv)^2 = A(hv - Ebg) \quad \text{Equation 4.2.....102}$$

$$r = -\frac{dc}{dt} = k(p)\theta \quad \text{Equation 4.3.....135}$$

$$\theta = \frac{K_L c}{1 - K_L c} \quad \text{Equation 4.4.....135}$$

$$r = K_p \frac{K_L c}{1 + K_L c} \quad \text{Equation 4.5.....135}$$

$$r = \frac{dc}{dt} = \frac{k_r K_{ads}}{1 - K_{ads} c} \quad \text{Equation 4.6.....136}$$

$$\frac{1}{K_{ads}} = \frac{1}{k_r c} + \frac{1}{k_r K_{ads}} \quad \text{Equation 4.7.....136}$$

$$\ln\left(\frac{c}{c_0}\right) = -k_r K_{ads} t \quad k_{app} t \quad \text{Equation 4.8.....138}$$

$$r_{app} = -k_{app} t \quad \text{Equation 4.9.....137}$$

$$t_{\frac{1}{2}} = \ln 2 \frac{\ln 2}{k_{app}} = \frac{0.69309}{k_{app}} \quad \text{Equation 4.10.....137}$$



## Nomenclature

APAP	: Acetaminophen (paracetamol)
AOP	: Advanced oxidation process
CAP	: Chloramphenicol
CB	: Conduction band
CP	: Conjugated polymer
CPE	: Conjugated polyene
EF	: Electro Fenton
EUWED	: European Union of Water Directive
GC	: Gas chromatography
GC-MS	: Gas chromatography mass-spectrometer
HPLC	: High performance liquid chromatography
HOMO	: Highest occupied molecular orbitals
HO·	: Hydroxyl radical
LUMO	: Lowest unoccupied molecular orbitals
NSAIDs	: Non-steroid anti-inflammatory drugs
PCs	: Pharmaceutical compounds
PF	: Photo Fenton
PP	: Pharmaceutical pollutants
PPM	: Part per million
TCs	: Therapeutic compounds
SC	: Semiconductor
TOCs	: Total organic carbons
UV	: Ultraviolet
USEPA	: United States Environmental Protection Agency
VB	: Valence band

## **Chapter 1: General Introduction and Research Overview**

This chapter presents an overview of the research study. It provided the facts on the prevalence of pharmaceutical compounds as water pollutants. The theoretical background of some of the treatment methods is given. A brief description of photocatalysis as a method of water treatment is explained. The rationale behind this study is clarified and the aims and objectives are stated. The scope of the study is also outlined.

## TABLE OF CONTENTS

<b>CHAPTER 1: GENERAL INTRODUCTION AND RESEARCH OVERVIEW.....</b>	<b>1</b>
1.1 INTRODUCTION .....	3
1.2 PROBLEM STATEMENT AND JUSTIFICATION.....	8
1.3 AIM AND OBJECTIVES OF THE STUDY.....	9
<i>1.3.1 Aim of the study.....</i>	<i>9</i>
<i>1.3.2 The objectives of the study .....</i>	<i>9</i>
1.4 PROJECT SCOPE .....	10
REFERENCES .....	12

## 1.1 Introduction

The world is faced with a number of environmental challenges such as contaminated air, soil and water, which are great health concerns. These problems are a result of advanced industrialisation and anthropogenic activities in different fields of human endeavor. They have led to drastic increases in the production of different types of waste (Mandloi, 2014). The insufficient waste management in many developing countries, the waste produced often being uncontrollably discharged into the environment, thus leading to serious impact on human health (Teh *et al.*, 2017). Organic waste originating from industrial, hospital and urban sewages contains many hazardous compounds, such as pharmaceuticals, herbicides, detergents, phenol and their derivatives, estrogens and contraceptives (Shahidi *et al.*, 2015).

Among many other organic contaminants, pharmaceutical compounds (PCs) are emerging as new unregulated pollutants that are an environmental source of concern. Interestingly, these newly emerging pharmaceutical pollutants mainly come from products used in large quantities worldwide and in everyday life (Liu *et al.*, 2015; Ashfaq *et al.*, 2017). The prevalence of PCs mainly in the aquatic environment, via waste water, has become a universal issue of growing environmental concern.

In the last few decades, PCs have been considered probable contaminants of negative health consequence in the aquatic systems throughout the world (Yang *et al.*, 2010; Kaur *et al.*, 2016). The occurrence of PCs in the environment is detrimental to aquatic and human life due to their adverse health impact, such as hormonal disruption (Zhang *et al.*, 2018; An *et al.*, 2010), particularly on an untargeted human. Other adverse health effects of PCs include their genotoxicity, ability to promote antibiotic resistance in both animal and man, toxicity in aquatic environments and hormonal disturbance (Yang *et al.*, 2009; An *et al.*, 2010).

Antibiotics and non-antibiotic PCs are used to treat diseases and to relieve pain in both humans and animals worldwide (Jin *et al.*, 2018; Nie *et al.*, 2014). As a prominent antibiotic, chloramphenicol (CAP) has been widely used to inhibit bacterial infections (Jin *et al.*, 2018), while acetaminophen (APAP) has been one of the most

popularly used pain relievers (Glavanović *et al.*, 2016). However, due to its chronic side effect of aplastic anaemia and bone marrow suppression, CAP has been banned in some developed countries such as the USA (Jin *et al.*, 2018). Although CAP is not banned in South Africa, but its usage is a point of concern. On the other hand, the toxic effects of APAP have been identified in some studies (López Zavala & Estrada, 2016; Ayanda *et al.*, 2017). Therefore, the existence of these PCs, even at a low concentration in the environment for a prolonged duration is undesirable and their removal is of utmost importance, particularly from aquatic systems (Chatzitakis *et al.*, 2008; Klavarioti *et al.*, 2009). **Figure 1.1** illustrates the chemical structures of APAP and CAP.

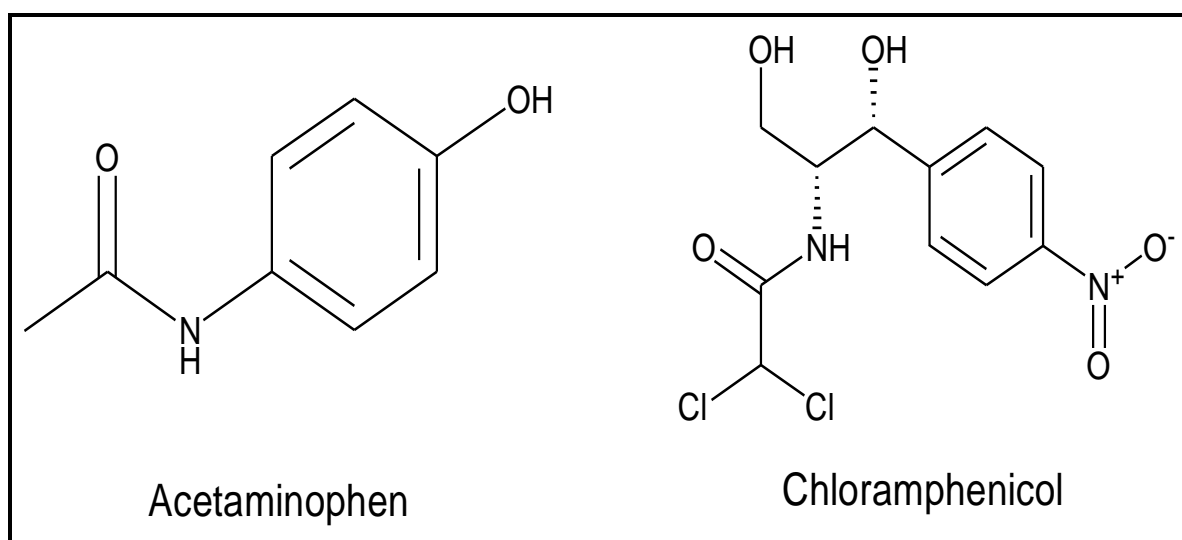


**Figure 1.1:** The chemical structures of acetaminophen and chloramphenicol

Most PCs co-exist in a mixture with several other contaminants in the environment, which makes their removal a bit challenging. Also, some of the active pharmaceutical ingredients (APIs), which are commonly used by pharmaceutical industries to produce desired drugs, are not only pharmacologically active, but they are also toxic (Chelliapan *et al.*, 2006). In addition, most of the APIs are unaffected by biodegradation, thereby are persistent in the environment (Kaur *et al.*, 2016). Besides, there are no legally permissible limits for these pharmaceuticals in wastewater, possibly because their exact impact of chronic exposure of PCs on the

aquatic environment remains unidentified (Rivera-Utrilla *et al.*, 2013). Therefore, an urgent need for their removal from the ecological system is necessary.

Treatment of pharmaceutical containing wastewater is essential to decontaminate the environment and protect living beings from several water-borne diseases (Kaur *et al.*, 2016). Various conventional treatment approaches such as coagulation, sedimentation, precipitations, filtrations as applied in municipal wastewater treatment plants (MWWTPs) and adsorption have their limitation in the removal of active PCs (Radjenovic *et al.*, 2007). The efficiency of natural (Biological) treatment procedures also are limited to effluents containing biodegradable compounds, which must not be harmful to the biological culture (Elmolla & Chaudhuri, 2010).

However, in a further quest for lasting solutions to this real threat to animal and human lives, many commendable efforts have again been directed towards the remediation of water sources contaminated with recalcitrant organic pollutants (Baccile & Babonneau, 2008; Mohan *et al.*, 2014). Several other methods have been applied for the treatment of water. These methods include adsorption, phytoremediation, chemical oxidation and biological treatment (Atul *et al.*, 2013). Although these methods have some useful applications, they have disadvantages such as slow operations and they do not remove many organic pollutants (Atul *et al.*, 2013), such as recalcitrant APIs. For instance, activated carbon adsorption only involves a transfer of pollutants onto the solid phase, without their destruction hence, the introduction of a new pollution challenges. Conventional chemical oxidation is also unable to mineralise all organic substances and is only economical if the pollutants are at high levels of concentration. In the case of biological treatment, the main disadvantages have been slow rates of reactions, and challenges associated with unsafe disposal of the sludge and the necessity for strict control of pH, temperature and some other environmental conditions.

Lately, it has been demonstrated that advanced oxidation processes (AOPs) shows outstanding features for superior, robust and multifunctional treatment processes that can enhance pollutant treatment efficiency (Chakma *et al.*, 2015). Past studies confirmed the effectiveness of AOPs, which are far more efficient in the removal of various API contaminants (He *et al.*, 2016; He *et al.*, 2018). However, all AOPs operate based on the same principle of generating highly reactive species such as

$O_2^{\bullet-}$ ,  $HO_2^{\bullet}$  and hydroxyl radicals ( $OH^{\bullet}$ ), which are non-selective and have the potential to oxidise many recalcitrant pollutants, in the process converting them to harmless end-products. Hydroxyl radicals are one of the most potent oxidants with an extraordinary ability to oxidise most organic contaminants with less or no discrimination. However, as a result of their high reactivity and very low selectivity,  $OH^{\bullet}$  are quickly used up therefore, they must be continuously generated simultaneously as the process proceeds.

Heterogeneous photocatalysis, a form of AOP technology has gained prominence in its applications as an improved environmentally remediation method. The mineralisation of hazardous and outlawed organic contaminants is being achieved by their conversion from toxic to non-toxic forms via this method (Ibrahim *et al.*, 2016). In heterogeneous photocatalysis, both the pollutant and the catalyst are usually not in the same phase. Typically, while the pollutants are in the aqueous phase, the applied catalyst is commonly in the form of a solid. The solid catalyst enhances the continuous generation of the rapidly used-up reactive radicals during heterogeneous process. This process can be achieved using metal oxide semiconductor (Liu *et al.*, 2015).

The application of metal oxide semiconductors as photocatalysts have gained much interest in heterogeneous photocatalytic processes, for continuous generation of the required reactive species. Various metal oxides have been used as photocatalysts for the degradation of many organic pollutants.

Ideally, an efficient photocatalyst should be stable, durable under constant irradiation and have good electron transfer with a long-distance transmission (Teh *et al.*, 2017;). Consequently, among other materials,  $TiO_2$  based photocatalysis has been commonly used. Its application in organic pollution control technology is based on its simple preparation method, good catalytic activities, stability and non-toxicity (Luo *et al.*, 2016; Wei *et al.*, 2017). Nevertheless, the photocatalytic activity of  $TiO_2$  under visible-light is meager, due to its poor visible-light absorption ability and relatively high recombination rate of the generated electron-hole pairs (Wang *et al.*, 2015; Vignesh *et al.*, 2014), Including poor recoverability after use. However, alternatives that have the advantages regarding versatility, economics, stability and abundance and non-toxicity possessed by  $TiO_2$  are rare (Wei *et al.*, 2017).

Therefore, the search for new and functional photocatalytic materials with activities exceeding titanium-based photocatalysts is critical for economical and effective environmental pollution control. Hence, the choice of improving TiO<sub>2</sub> using various approaches seems to be the most feasible and practical means to obtain a photocatalyst suitable for real-life applications even at a large scale (Teh *et al.*, 2017).

Several attempts have been made by researchers to modify photocatalysts for effective mineralisation of recalcitrant pollutants like some PCs. Some of such approaches include doping with metallic (Wang *et al.*, 2015) or non-metallic species (Warkhade *et al.*, 2017), combining with different metal oxides and the formation of mesoporous-base structures (Akhundi & Habibi-Yangjeh, 2017). All these methods are usually aimed at promoting the separation of photo-generated electrons and holes through interfacial charge transfer (ICT) (Zhang *et al.*, 2016). However, the photocatalytic activity and versatility of TiO<sub>2</sub> photocatalyst could be enhanced under visible light, if combined with band-gap narrowing poly-conjugated molecules (Xu *et al.*, 2017a).

Poly-conjugated molecules are a peculiar class of molecules or polymers that interact with light. They have band-gap energy in the range of 1 eV to 3 eV, that is, in the range of visible light. For example, metal porphyrin contains an aromatic conjugation system with central lone pairs of electrons capable of binding metal (Fe/Co) to improve the magnetic recoverability in the photocatalytic apparatus. Others include polyene, a linear poly-conjugated polymer (CP). Although CPs have proven to be good photo-sensitizers, they are underutilised for this purpose. Under irradiation, poly-conjugated polymers can produce electron-hole pairs that are delocalised (Hwang & Scholes, 2011), therefore, coupling TiO<sub>2</sub> photocatalysts with these photosensitive polymer molecules could be a better alternative and more efficient way to improve their photocatalytic performance (Xu *et al.*, 2017b).

Capping of TiO<sub>2</sub> with appropriate photo-sensitizers may allow for the extension of its absorption spectra into the visible region as well as enhance the production of reactive species. In this approach, a conjugated molecule can absorb visible light to produce a singlet or triplet state, which then releases an electron into the conduction band (energy level) of the semiconductor. The released electron can reduce surface



adsorbed oxygen molecule to produce more oxidising radicals such as  $\text{OH}^\bullet$ , which can oxidize any organic pollutant. Therefore, the fabricated photocatalysts should possess the following properties: High photocatalytic rate, low cost, high environmental stability and mechanical strength, which could improve the performance of the catalyst in the photodegradation process.

## 1.2 Problem statement and justification

Sustainable water supply is in increasing demand in today's world. Besides the enormous amount of water needed for agricultural purpose, the amount of quality water supply is inadequate for human sustenance. Among various challenges concerning water, the reduction of contaminants is a major issue. Therefore, the removal of environmentally-threatening chemicals, particularly PCs in water is a matter of concern that requires urgent attention. For example, methotrexate (MTX), an API classified as an antineoplastic drug is normally detected in wastewater, and been reported for its damaging effect on the human liver and kidney; it causes renal failure when tested on rats (Armagan *et al.*, 2015). Among other adverse effects of these APIs are hepatic and pulmonary toxicity while high dosage may result in renal failure (Kivity *et al.*, 2014). In an aquatic medium, Tribskom *et al.* (2004) demonstrated the toxic cytological effects of diclofenac in liver, kidney, gills and the intestine of rainbow trout, in their studies. Nevertheless, the environmental remediation of all these harmful pharmaceuticals can be a great challenge.

Considering the fact that these contaminants in the waste sources are usually resistant to natural removal and degradation, they tend to accumulate in the environment and eventually become a hazard to living organisms (Tremblay *et al.*, 2011). An appropriate technology suggested for their removal is photocatalysis using an appropriate semiconductor. Also, most available semiconductor photocatalysts have a relatively wide bandgap (e.g.  $\text{TiO}_2 = 3.2\text{eV}$  and  $\text{ZnO} = 3.2\text{eV}$ ) and cannot be optimally utilise in the visible light range, which is about 46% of the available solar energy, for the effective degradation of PCs. Besides, separation of used photocatalysts from the treated systems for reuse, is another major problem for photocatalytic processes using the common photocatalysts.

To mitigate these challenges posed by pollutants due to rapid industrialisation and urbanisation, there is a need to develop a robust and efficient technology (Islam *et al.*, 2012), for organic pollutant treatment. Furthermore, since water quality management is the key to a healthy human population and a vibrant economy, research focusing on developing alternatives for wastewater treatment is necessary. There has been some exploratory research in the area of doping and immobilisation of semiconductors to improve their photocatalytic performances. Nonetheless, to the best of our knowledge, hardly any studies have been reported on the modification of TiO<sub>2</sub> and other photocatalysts by coupling them with poly-conjugated molecules such as polyene, and their application in the removal of PC's and in particular APAP including CAP..

### **1.3 Aim and objectives of the study**

#### **1.3.1 Aim of the study**

The aim of this study was to synthesise and characterise a conjugated-polymer modified TiO<sub>2</sub> photocatalyst and investigate its photocatalytic activities in the photodegradation of selected pharmaceutical compounds in aqueous systems under visible light irradiation.

#### **1.3.2 The objectives of the study**

- ❖ To synthesise pure titania (TiO<sub>2</sub>) nanoparticles
- ❖ To prepare conjugated-polyene/titania (CPE-TiO<sub>2</sub>) nanocomposites using polyvinyl alcohol (PVA) as a precursor for polyene photosensitizer
- ❖ To characterise the synthesised photo-catalysts using SEM, TEM, XRD, EDS, FTIR, UV-Vis DRS, PL, CV, EIS and TGA
- ❖ To investigate the photocatalytic efficiency for the degradation of acetaminophen (a non-antibiotic) and chloramphenicol (an antibiotic), using the prepared photosensitizer modified catalysts as compared with unmodified TiO<sub>2</sub> under visible light irradiation

- ❖ To investigate the reusability of the synthesised nano-composites for pollutant degradation in a photocatalysis process
- ❖ To investigate the degradation kinetics of the organic contaminants (PCs) using Langmuir-Hinshelwood (L-H) kinetic models
- ❖ To investigate the mechanism and photodegradation by-products of acetaminophen and chloramphenicol.

#### **1.4 Project scope and delineation of the study**

This work covers the synthesis of pure  $\text{TiO}_2$  nanoparticles using a homogenised sol-gel method and from an isopropoxide organic precursor, preparation of conjugated-polyene/titanium oxide photocatalysts from dehydrated polyvinyl alcohol to obtain CPE- $\text{TiO}_2$  hybrid nanocomposites. It also covers both structural and optical characterisation, as well as photocatalytic degradation studies.

The dissertation consists of five chapters:

Chapter 1 gives the background and the introduction to the study. It highlights the problem statement, aim and the objective and the scope of the work.

Chapter 2 gives the details of the literature review on the area of the study. It identifies some of the studies that have been carried out in heterogeneous photocatalysis using  $\text{TiO}_2$  photocatalyst and the results obtained.

Chapter 3 gives the details of the research methodologies on material synthesis, characterisation and instrumental analysis for the data generated.

Chapter 4 presents the results obtained, the detailed discussion and the sub-conclusions. This chapter is divided into four sections: Section A gives the results and the discussion on structural and morphological characterisation. Section B presents the results and the discussion on electrochemical and optical characterisation. Section C presents the results obtained and the discussion on photocatalytic degradation and parameter investigations. While section D presents the results and the discussion on the kinetics, the mechanisms of the photocatalytic degradations, and the intermediate by product identification.

Chapter 5 gives a general conclusion and the recommendations for further studies. This chapter summarises all the findings and the challenges encountered during the project execution. It clearly and unambiguously highlights the contribution of the project to the body of knowledge in photocatalysis and wastewater treatment.

## References

- AKHUNDI, A. & HABIBI-YANGJEH, A. 2017. High performance magnetically recoverable g-C<sub>3</sub>N<sub>4</sub>/Fe<sub>3</sub>O<sub>4</sub>/Ag/Ag<sub>2</sub>SO<sub>3</sub> plasmonic photocatalyst for enhanced photocatalytic degradation of water pollutants. *Adv. Powd. Tech.*, 28(2):565–574.
- ARMAGAN, I., BAYRAM, D., CANDAN I.A., YIGIT, A., CELIK, E, ARMAGAN, H.H., & UĞUZ, A.C. 2015. Effects of pentoxifylline and alpha lipoic acid on methotrexate-induced damage in liver and kidney of rats. *Environ. Tox. Pharm.* 39:1122-1131.
- AN, T., YANG, H., SONG, W., LI, G., LUO, H., & COOPER, W.J. 2010. Mechanistic considerations for the advanced oxidation treatment of fluoroquinolone pharmaceutical compounds using TiO<sub>2</sub> heterogeneous catalysis. *J. Phy. Chem., A*:2569–2575.
- ASHFAQ, M., NAWAZ KHAN, K., SAIF UR REHMAN, M., MUSTAFA, G., FAIZAN NAZAR, M., SUN, Q., IQBAL, J., MULLA, S.I., & YU, C.P. 2017. Ecological risk assessment of pharmaceuticals in the receiving environment of pharmaceutical wastewater in Pakistan. *Ecotox. Environ. Safety*, 136 , 31–39.
- ATUL, W., GAIKWARD, G., DONDHE, M., & KHATY, N. 2013. Removal of organic pollutant from water by heterogeneous photocatalysis: a review. *Res. J. Chem. Environ.*, 17 (September), 84–94.
- AYANDA, O.S., NELANA, S.M., PETRIK, L.F. & NAIDOO, E.B., 2017. Nano-TiO<sub>2</sub>, ultrasound and sequential nano-TiO<sub>2</sub>/ultrasonic degradation of N-acetyl-para-aminophenol from aqueous solution. *J. Water Health*, 15 (6), 1015–1027.
- BACCILE, N. & BABONNEAU, F. 2008. Organo-modified mesoporous silicas for organic pollutant removal in water: Solid-state NMR study of the organic/silica interactions. *Microp. Mesop. Mat.*, 110 (2–3), 534–542.
- CHAKMA, S., DAS, L., & MOHOLKAR, V.S. 2015. Dye decolorization with hybrid advanced oxidation processes comprising sonolysis/Fenton-like/photo-ferrioxalate systems: A mechanistic investigation. *Sep. Pur. Tech.*, 156 (October),

596–607.

- CHATZITAKIS, A., BERBERIDOU, C., PASPALTSIS, I., KYRIAKOU, G., SKLAVIADIS, T., & POULIOS, I. 2008. Photocatalytic degradation and drug activity reduction of Chloramphenicol. *Water Res.*, 42 (1–2), 386–394.
- CHELLIAPAN, S., WILBY, T., & SALLIS, P.J. 2006. Performance of an up-flow anaerobic stage reactor (UASR) in the treatment of pharmaceutical wastewater containing macrolide antibiotics. *Water Res.*, 40 (3), 507–516.
- ELMOLLA, E.S. & CHAUDHURI, M. 2010. Comparison of different advanced oxidation processes for treatment of antibiotic aqueous solution. *Desalination*, 256 (1–3), 43–47.
- GLAVANOVIĆ, S., GLAVANOVIĆ, M., & TOMIŠIĆ, V. 2016. Simultaneous quantitative determination of paracetamol and tramadol in tablet formulation using UV spectrophotometry and chemometric methods. *Spectrochimica Acta - Part A: Mol. Biomol. Spec.*, 157, 258–264.
- HE, Y., SUTTON, N.B., RIJNAARTS, H.H.H., & LANGENHOFF, A.A.M. 2016. Degradation of pharmaceuticals in wastewater using immobilized TiO<sub>2</sub> photocatalysis under simulated solar irradiation. *Appl. Catal. B: Environ.*, 182, 132–141.
- HE, Y., WANG, X., HUANG, W., CHEN, R., ZHANG, W., LI, H., & LIN, H. 2018. Hydrophobic networked PbO<sub>2</sub> electrode for electrochemical oxidation of paracetamol drug and degradation mechanism kinetics. *Chemos.*, 193, 89–99.
- HWANG, I. & SCHOLLES, G.D. 2011. Electronic energy transfer and quantum-coherence in  $\pi$ -conjugated polymers. *Chem. Mat.*, 23 (3), 610–620.
- IBRAHIM, R.K., HAYYAN, M., ALSAADI, M.A., HAYYAN, A., & IBRAHIM, S. 2016. Environmental application of nanotechnology: air, soil, and water. *Environ. Sci. Poll. Res.*, 23 (14), 13754–13788.
- ISLAM, M.N., JO, Y.T., & PARK, J.H., 2012. Remediation of PAHs contaminated soil by extraction using subcritical water. *J. Ind. Eng. Chem.*, 18 (5), 1689–1693.

- JIN, Q., WANG, H., HU, C., CHEN, Z., & WANG, X., 2018. Effects of NOM on the degradation of chloramphenicol by UV/H<sub>2</sub>O<sub>2</sub> and the characteristics of degradation products. *Sep. Puri, Tech.*, 191 (March 2017), 108–115.
- KAUR, A., UMAR, A., & KANSAL, S.K. 2016. Heterogeneous photocatalytic studies of analgesic and non-steroidal anti-inflammatory drugs. *Appl. Catal. A: General*, 510, 134–155.
- KIVITY, S., ZAFRIR, Y., LOEBSTEIN, R., PAUZNER, R., MOUALLEM, M., & MAYAN, H. 2014. Autoimmunity Reviews Clinical characteristics and risk factors for low dose methotrexate toxicity : A cohort of 28 patients. *Autoimmunity Reviews*, 13 (11), 1109–1113.
- KLAVARIOTI, M., MANTZAVINOS, D., & KASSINOS, D. 2009. Removal of residual pharmaceuticals from aqueous systems by advanced oxidation processes. *Environ. Int.*, 35 (2), 402–417.
- LIU, Y., WEI, S., & GAO, W., 2015. Ag/ZnO heterostructures and their photocatalytic activity under visible light: Effect of reducing medium. *J. Haz. Mat.*, 287, 59–68.
- LÓPEZ ZAVALA, M.Á. & ESTRADA, E.E. 2016. Degradation of acetaminophen and its transformation products in aqueous solutions by using an electrochemical oxidation cell with stainless steel electrodes. *Water (Switzerland)*, 8 (9), 1–12.
- LUO, Y., CHEN, J., LIU, J., SHAO, Y., LI, X., & LI, D., 2016. Hydroxide SrSn(OH)<sub>6</sub>: A new photocatalyst for degradation of benzene and rhodamine B. *Appl. Catal. B: Environ.*, 182, 533–540.
- MANDLOI, A., 2014. Impact of Industries on Ground Water Quality By Comparison Between Hoshangabad ( Non Industrial Area ) and Mandideep ( Industrial Area ), Bhopal ( India ), *Int.J. Res. Eng. Tech.*, 2319–2321.
- MOHAN, D., SARWAT A., OK, S. Y., & PITTMAN, U. C., 2014. Organic and inorganic contaminants removal from water with biochar, a renewable, low cost and sustainable adsorbent- A critical review. *Biores. tech.*, 160, 191-202.
- NIE, M., YANG, Y., ZHANG, Z., YAN, C., WANG, X., LI, H., & DONG, W., 2014. Degradation of chloramphenicol by thermally activated persulfate in aqueous

- solution. *Chem. Eng. J.*, 246, 373–382.
- RADJENOVIC, J., PETROVIC, M., & BARCELÓ, D. 2007. Analysis of pharmaceuticals in wastewater and removal using a membrane bioreactor. *Anal. Bioanal. Chem.*, 387 (4), 1365–1377.
- RIVERA-UTRILLA, J., SÁNCHEZ-POLO, M., FERRO-GARCÍA, M.Á., PRADOS-JOYA, G., & OCAMPO-PÉREZ, R. 2013. Pharmaceuticals as emerging contaminants and their removal from water. A review. *Chemos.*, 93 (7), 1268–1287.
- SHAHIDI, D., ROY, R., & AZZOUZ, A. 2015. Advances in catalytic oxidation of organic pollutants - Prospects for thorough mineralization by natural clay catalysts. *Appl. Catal. B: Environ.*, 174–175, 277–292.
- TEH, C.Y., WU, T.Y., & JUAN, J.C. 2017. An application of ultrasound technology in synthesis of titania-based photocatalyst for degrading pollutant. *Chem. Eng. J.*, 317, 586–612.
- TREMBLAY, L.A., STEWART, M., PEAKE, B.M., GADD, J.B., & NORTHCOTT, G.L. 2011. Review of the Risks of Emerging Organic Contaminants and Potential Impacts to Hawke's Bay. *Prepared for Hawke's Bay Regional Council. Cawthron Report No. 1973. 39 pp.* Prepared for Hawke's Bay Regional Council. Cawthron Report No. 1973. Hawke's Bay.
- TRIEBSKORN, R., CASPER, H., HEYD, A., EIKEMPER, R., KOHLER, H.-R., & SCHWAIGER, J. 2004. Toxic effects of the non-steroidal anti-inflammatory drug diclofenac: Part II. Cytological effects in liver, kidney, gills and intestine of rainbow trout. *Aqu. Tox.* Elsevier, 68, 151-166.
- VIGNESH, K. SUGANTHI, A., MIN, B., & KANG, M. 2014. Photocatalytic activity of magnetically recoverable solar light irradiation. *J. Mol. Catal. A, Chem.*, 395, 373–383.
- WANG, B., ZHANG, G., LENG, X., SUN, Z., & ZHENG, S. 2015. Characterization and improved solar light activity of vanadium doped TiO<sub>2</sub>/diatomite hybrid catalysts. *J. Haz. Mat.*, 285, 212–220.



- WARKHADE, S.K., GAIKWADB, G.S., SANGESH, P.Z., PRATAPA, U., MALDHUREC, A.V., & WANKHADE, A.V. 2017. Low temperature synthesis of pure anatase carbon doped titanium dioxide: An efficient visible light active photocatalyst. *Mat. Sci. Semic. Proc.*, 6, 18–24.
- WEI, M., WAN, J., HU, Z., PENG, Z., WANG, B., & WANG, H. 2017. Preparation, characterization and visible-light-driven photocatalytic activity of a novel Fe(III) porphyrin-sensitized TiO<sub>2</sub> nanotube photocatalyst. *Appl. Surf. Sci.*, 391, 267–274.
- XU, B., DING, T., ZHANG, Y., WEN, Y., YANG, Z., & ZHANG, M. 2017. A new efficient visible-light-driven composite photocatalyst comprising ZnFe<sub>2</sub>O<sub>4</sub> nanoparticles and conjugated polymer from the dehydrochlorination of polyvinyl chloride. *Mat. Lett.* 187 , 123–125.
- YANG, H., LI, G., AN, T., GAO, Y., & FU, J. 2010. Photocatalytic degradation kinetics and mechanism of environmental pharmaceuticals in aqueous suspension of TiO<sub>2</sub>: A case of sulfa drugs. *Catal. Today*, 153 (3–4), 200–207.
- YANG, L., YU, L.E., & RAY, M.B. 2009. Photocatalytic oxidation of paracetamol: Dominant reactants, intermediates, and reaction mechanisms. *Environ. Sci. Tech.*, 43 (2), 460–465.
- ZHANG, Y., SHAO, Y., GAO, N., GAO, Y., CHU, W., LI, S., WANG, Y., & XU, S. 2018. Kinetics and by-products formation of chloramphenicol (CAP) using chlorination and photocatalytic oxidation. *Chem. Eng. J.*, 333, 85–91.
- ZHANG, Y., ZHANG, F., YANG, Z., XUE, H., & DIONYSIOU, D.D. 2016. Development of a new efficient visible-light-driven photocatalyst from SnS<sub>2</sub> and polyvinyl chloride. *J. Catal.*, 344, 692–700.

## **Chapter 2: Literature review**

This chapter presents the literature survey on the area of the study. It summarises the concepts and the theory of photocatalysis and its application in wastewater decontamination. It identifies some of the studies that have been carried out in heterogeneous photocatalysis using  $\text{TiO}_2$  photocatalysts and the results obtained. The application of polymer molecules in  $\text{TiO}_2$  modification for an effective photocatalysis is also discussed. Some of the intermediates of the selected pharmaceutical compounds used for photocatalytic degradation are listed and reviewed.

## TABLE OF CONTENTS

<b>CHAPTER 2: LITERATURE REVIEW .....</b>	<b>17</b>
2.1 INTRODUCTION .....	19
2.1.1 <i>Pharmaceutical pollutants.....</i>	24
2.1.2 <i>Basis of advanced oxidation process.....</i>	24
2.2 PHOTOCATALYSIS .....	26
2.2.1 <i>Homogeneous photocatalysis.....</i>	27
2.2.2 <i>Heterogeneous photocatalysis.....</i>	28
2.2.2.1 <i>Mechanism and kinetics of heterogeneous process using TiO<sub>2</sub>.....</i>	29
2.3 LIMITATIONS OF TiO <sub>2</sub> PHOTOCATALYST AND IMPROVEMENT WITH POLYMER MODIFICATIONS.....	34
2.3.1 <i>TiO<sub>2</sub> modifications and polymer-TiO<sub>2</sub> photocatalyst.....</i>	35
2.4 PHOTOCATALYTIC APPLICATIONS OF POLYMER-TiO <sub>2</sub> .....	36
2.4.1 <i>Mechanism of polymer-TiO<sub>2</sub> under visible light.....</i>	41
2.5 PHOTOCATALYTIC INTERMEDIATES FOR SELECTED PHARMACEUTICALS USING TiO <sub>2</sub> .....	43
2.5.1 <i>Acetaminophen and its photodegradation intermediate products .....</i>	44
2.5.2 <i>Chloramphenicol and its photodegradation intermediate products.....</i>	46
CONCLUSION.....	48
REFERENCES .....	50

## 2.1 Introduction

Water, being an essential component of life, is vital for the existence of humans. Currently, there are major concerns worldwide on the issues of water pollution as the most critical ecological problem (Kshirsagar *et al.*, 2017). The water contaminants are mostly because of improper treatment of domestic and industrial effluent, as well as inappropriate sewage planning and management (Soon & Hameed, 2011). These pollutants commonly consist of hazardous mixtures of chemicals such as pharmaceuticals, phenols, dyes and endocrine-disrupting compounds that come from chemical and pharmaceutical industries (Al-Hamdi *et al.*, 2017). These mixtures of chemical contaminants have adverse effects, particularly on aquatic life as well as on human health (Boukhatem *et al.*, 2017).

Earlier studies show that more than 25 percent of the total world population suffers from health and hygienic problems associated with water pollution (Pera-Titus *et al.*, 2004; Mezohegyi *et al.*, 2010). Among the numerous pollutants, pharmaceutical products, as emerging micro-pollutants, have been frequently detected in surface water, effluents, as well as in drinking water (Kaur *et al.*, 2016; Zhang *et al.*, 2017; Slamani *et al.*, 2018). Owing to their daily and high consumption rate as animal and human medicine (Yan *et al.*, 2013), pharmaceutical compounds (PCs) are continuously and extensively released into the environment (Chen *et al.*, 2018).

Among various pharmaceuticals used as human and animal medications, antibiotics and non-antibiotic drugs have been commonly studied (Leung *et al.*, 2012; Yang *et al.*, 2013; Liu *et al.*, 2014). Due to antibiotic abuse, their concentration in the environment has steadily increased, which influences bacterial transcription (Liu *et al.*, 2018). Despite many of these pharmaceuticals being categorised as priority pollutants by the US Environmental Protection Agency (USEPA) and European Union of Water Framework Directive (EUWFD) (Dong *et al.*, 2014), the available removal methods are inefficient.

However, continuous efforts have been made to reduce pharmaceutical content in the environment, to forestall further contamination of surface and groundwater. These efforts involve the application of various techniques such as sedimentation, adsorption, flocculation, filtration and reverse osmosis. Most of these drugs are

resistant to degradation offered by conventional methods, due to the presence of aromatic groups combined with several other functional groups (Boreen *et al.*, 2003). Hence, the demand for an efficient and environmentally-benign pollution control and removal technology, has increased worldwide.

In recent years, advanced oxidation processes (AOP) have been widely investigated and considered as viable, environmentally-benign and economical technologies for the removal of toxic and hazardous contaminants (Jyothi *et al.*, 2016). The AOPs are primarily based on the generation of active oxidative agents, largely reactive oxidative species, which can degrade and mineralise a wide range of chemical compounds (Kosera *et al.*, 2017). The end-products of complete organic pollutant treatment are usually carbon dioxide, water and a trace amount of inorganic ions that can easily be removed (Qiao *et al.*, 2014). Other significant advantages of AOPs include relatively mild reaction conditions and proven capability to degrade several toxic refractory pollutants. Based on the reactive phases, AOPs are classified into homogeneous and heterogeneous types, both of which have been successfully used as water purification processes, particularly for the removal of pharmaceutical pollutants (Loaiza-Ambuludi *et al.*, 2014; Kosera *et al.*, 2017).

Considering the current global environmental challenges involving wastewater treatment technologies, heterogeneous photocatalysis has received appreciable consideration, even for industrial applications (Tong *et al.*, 2018). More recently, much attention has been given to heterogeneous photocatalysis as one of the major and promising AOPs (Kosera *et al.*, 2017; Khataee *et al.*, 2017). This keen interest may be due to the simple and environmentally-friendly approach to the technique (Qiu *et al.*, 2018). It also possesses the merit of a rapid recovery and ultimate reuse of the stable chemical reagents applied as a catalyst for the treatment process (Li *et al.*, 2015).

In the heterogeneous process, materials with high photocatalytic activities are used as the catalysts to absorb light radiation from UV or visible light energy source. Hence, the photosensitive property of semiconductors results in their significant roles in heterogeneous photocatalytic processes for environmental pollution control and waste water treatment (Bijanzad *et al.*, 2015). Consequently, a wide range of semiconductor materials such as TiO<sub>2</sub>, SnO<sub>2</sub>, ZnO, CdS, Fe<sub>2</sub>O<sub>3</sub> and WO<sub>2</sub> have been

used in photo-induced degradation of many organic contaminants in aqueous systems (Tong *et al.*, 2018). Among these conventional semiconductor photocatalysts,  $\text{TiO}_2$  is the most researched and applied as an efficient catalyst for photodegradation of organic pollutants (Oseghe & Ofomaja, 2018).

Ideally, semiconductor photocatalysts are applied either in aqueous form or immobilised on a support. However, heterogeneous photocatalytic processes using catalysts as suspended nanoparticles are reported to be more efficient because they offer a highly active catalyst surface area (Díez *et al.*, 2018). Particularly, semiconductors are more photo-active at nano-size level, due to their higher absorption coefficient with an increased reactive surface area (Ghosh *et al.*, 2017).

In recent years, researchers have made significant progress in the field of nanotechnology, particularly as it applies to water purification processes (Al-Hamdi *et al.*, 2015). Different  $\text{TiO}_2$  based nano-materials such as doped and polymer modified  $\text{TiO}_2$  have been prepared using different methods (Xu *et al.*, 2017). These synthetic methods include hydrothermal (Lassoued *et al.*, 2018; Ma & Chen 2018), thermal decomposition (Unni *et al.*, 2017), microwave irradiation (Oseghe & Ofomaja 2018) and sol-gel (Nassar *et al.*, 2014; Hou *et al.*, 2017; Talane *et al.*, 2018) synthetic methods. Some of these methods such as the sol-gel method have advantages such as the possibility of obtaining stable materials with a high purity and compositional homogeneity at moderate temperatures using simple laboratory methods and equipment for their synthesis (Nassar *et al.*, 2014).

Considering the prospect of large-scale industrial applications, heterogeneous photocatalysis using  $\text{TiO}_2$  is a viable technique. However, the apparent limitation of this process is the recombination of generated electrons and holes, as well as the wide band-gap (3.2 eV) of  $\text{TiO}_2$  as a semiconductor (Daghrir *et al.*, 2013). Several attempts have been made to reduce the electron/hole recombination rate in  $\text{TiO}_2$  by modifications, for more extensive photocatalytic applications. Nevertheless, with renewed and progressive efforts to overcome these challenges,  $\text{TiO}_2$  and its modified forms are potential catalysts for eventual large-scale industrial applications (Zhang & Jaroniec, 2018).

Organic polymer molecules (OPM) appear to be a suitable alternative method for effective modification of  $\text{TiO}_2$  due to their properties and improved photocatalytic efficiency (Wang *et al.*, 2017a; Šojić-Merkulov *et al.*, 2018; Li *et al.*, 2018). The modification of  $\text{TiO}_2$  with OPM is basically to enhance its photocatalytic efficiency through an improved adsorption and photosensitisation. They have been recently used as adsorbent/photocatalysts for the removal of several organic pollutants, including some pharmaceutical contaminants (Zhao *et al.* 2017; Jallouli *et al.*, 2017a). These organic polymer molecules range from non-conjugated to conjugated polymers (CP), which are particularly useful to enhance and extend the activity and stability of  $\text{TiO}_2$  photocatalyst into the visible region.

On the other hand, many studies on environmental pollutants are focused on antibiotics and non-antibiotics because they are commonly produced and increasingly used. This continuous application leads to their permanent presence in the environment as they are regarded as "pseudo-persistent" pollutants (Li, 2014). The application of other technologies such as biological technique (Tiwari *et al.*, 2017), plasma treatment (Magureanu *et al.*, 2015) and electrochemical separation (Sirés & Brillas, 2012) techniques for the removal of pharmaceuticals from wastewater have been comprehensively reviewed. Very few reviews (Kaur *et al.*, 2016) with adequate information on the application of polymer conjugated- $\text{TiO}_2$  as photocatalysts for the removal of these pharmaceuticals are in the literature. Consequently, this literature review focuses on the recent studies on the use of polymer- $\text{TiO}_2$  for photo-catalytic removal of pharmaceutical compounds as well as a few other organic pollutants.

In this chapter, we first summarised the general principles of heterogeneous photocatalysis as a form of AOP as compared to other types of AOPs. We then discussed the applications of  $\text{TiO}_2$  and polymer- $\text{TiO}_2$  for the photocatalytic degradation of pharmaceuticals. Various forms of polymer- $\text{TiO}_2$ , their applications and the mechanism of their photodegradation process for pharmaceuticals are discussed. The kinetics of heterogeneous photocatalysis using  $\text{TiO}_2$  semiconductor and the photocatalytic intermediate products of selected pharmaceutical pollutants are also illustrated.

### 2.1.1 Pharmaceutical pollutants

Lately, some emerging unregulated contaminants have become an environmental source of concern. These chemicals mainly originate from products used in large quantities in everyday life, such as pharmaceuticals or therapeutic compounds (TCs) (Liu *et al.*, 2015; Ashfaq *et al.*, 2017). Pharmaceutical compounds, which could be analgesic, anti-inflammatory, or antipyretic in actions (Yu *et al.*, 2011), are an essential group of chemicals, which are useful as drugs for curing various human diseases (Marsoni *et al.*, 2014; Hammad *et al.*, 2018). However, among emerging environmental contaminants, TCs have become one of the most significant and risky groups of pollutants, due to their prolonged half-life in living beings (Kaur *et al.*, 2015; Ahmed, 2017).

Therapeutic compounds used by humans can be toxic to certain organisms in the aquatic environment and their bioaccumulation in living cells usually results in modified character traits especially both in humans and animals (Balakrishna *et al.*, 2017; Hassani *et al.*, 2017). Among other pharmaceuticals, antibiotics and non-steroidal anti-inflammatory drugs (NSAIDs), are the most common water contaminants (Hernández-Uresti *et al.*, 2016) due to their worldwide usages for clinical purposes. Some undesirable human and animal health effects such as genotoxicity, and endocrine disruption, have been attributed to the human and animal exposure to NSAID contaminants (Kaur *et al.*, 2015; Hassani *et al.*, 2017). Moreover, on over usage of analgesics such as acetaminophen had been reported to cause nephrotoxicity, hepatic necrosis and in some cases, death to humans and animals (Olaleye & Rocha, 2008).

Regardless of these adverse environmental and human health effects, a vast number of pharmaceuticals are still widely consumed globally, which makes them prevalent in the environment (Thi & Lee, 2017; Hammad *et al.*, 2018). They make their way to the surroundings through direct dumping of expired and wasted drugs in the household (Hammad *et al.*, 2018), excretion by human and animals (Yu *et al.*, 2011) and the insufficient treatment of industrial and domestic effluents (Ashfaq *et al.*, 2017). The presence of remnant drug molecules in human and animal excreta is as a result of their partial metabolic activities in body systems (Hammad *et al.*, 2018). A large quantity (95%) of administered dose of drugs was reported to be excreted as



parent compounds, (Calamari *et al.*, 2003; Yu *et al.*, 2011), particularly the antibiotics, of which about 30-90% of the administered dosage is excreted through urine (Yu *et al.*, 2011). Due to their hydrophobic nature and structural stability, NSAIDs can persist in effluent for an extended period without disintegration. Consequently, the literature affirms their existence in surface water at significant levels of concentration in the environment (Manzo *et al.*, 2014).

Many antibiotics have also been considered very stable or form harmful intermediates such as halo-nitromethane from chloramphenicol, during the photodegradation process (Dong *et al.*, 2017). The residue, either metabolised or not, results in the development of microbial resistance to antibiotics (Hassani *et al.*, 2017). Untargeted human consumption of PC-contaminated water or food can cause severe liver problems, leading to the damage of vital organs, ultimately, causing death. Therefore, researching for an effective technique to eliminate pharmaceutical pollutants (PP) in the environment and in wastewater is critical. Hence, much attention has been given to advance oxidation processes (AOPs) as a proven viable method for the purification and decontamination of wastewater contaminated with various pharmaceutical compounds (Mirzaei *et al.*, 2016).

### **2.1.2 Basis of advanced oxidation process (AOP)**

AOP, is a water treatment process usually performed at ambient temperature and pressure. AOPs are driven by the in-situ generation of highly reactive transitory oxidising agents i.e., reactive oxidation species (such as hydroxyl radicals ( $\text{OH}^{\bullet}$ ) and others (i.e.,  $\text{H}_2\text{O}_2$ ,  $\text{O}_2^{\bullet-}$ ,  $\text{O}_3$ )). These reactive species are released at sufficient concentrations to effectively decontaminate wastewaters (Oturán & Aaron, 2014; Jin *et al.*, 2018). Advanced oxidation processes have been long useful and are still relevant till date, for water purification, as justified by the number of recent research outputs (He *et al.*, 2016; Fagan *et al.*, 2016; Hassani *et al.*, 2017; Trandafilović *et al.*, 2017; Teh *et al.*, 2017; Zhang & Jaroniec, 2018).

The reactions between the reactive radical ( $\text{OH}^{\bullet}$ ) and organic molecules are uniquely rapid and nonspecific and the reaction rate is ordered by the production of the oxidising species. Most AOP are preferred to the conventional biological process use

for organic matter degradation because they are swift and highly efficient, unlike the biological degradation process, which requires long periods of treatment prior to the observation of sufficient degradation (Eibes *et al.*, 2005). These make AOP a preferred, an effective and reliable water treatment method for wastewaters that are difficult to be handled by conventional methods. AOPs have been successfully applied to decompose many toxic and recalcitrant organic pollutants to a considerable level with little or minimal production of additional hazardous by-products (Kaur *et al.*, 2016).

The generated reactive oxidising agents, such as hydroxyl radical, attack pollutants and degrade them to simpler substances. These OH<sup>•</sup> radicals are characterised by little or no selectivity for water contaminants (Atul *et al.*, 2013). Once they are generated, they can oxidise and mineralise virtually every organic molecule in an aqueous system, yielding environmentally-friendly carbon dioxide (CO<sub>2</sub>), water (H<sub>2</sub>O) and some inorganic ions (Kaur *et al.*, 2016). Many review articles have detailed the efficiency of AOP processes (Akpan & Hameed, 2009; Al-Hamdi *et al.*, 2017). However, in summary, the AOPs can be classified into four broad groups:

- I. Chemical advance oxidation process, which basically involves redox reactions of chemical reagents to produce reactive radicals. Common examples include Fenton reactions (H<sub>2</sub>O<sub>2</sub> + Fe<sup>2+</sup> to generate OH<sup>•</sup>) (Liu *et al.*, 2018) and peroxonation (i.e., coupling H<sub>2</sub>O<sub>2</sub> with ozone O<sub>3</sub> in order to generate OH<sup>•</sup> radicals).
- II. Photochemical advance oxidation which involves a chemical reaction induced by light radiation. This type can be subdivided into homogeneous photo-oxidation and heterogeneous photo-oxidation (Wankhade *et al.*, 2013).
- III. Electrochemical advance oxidation which is based on the application of electrochemistry (involving electron transfer) for in situ generation of hydroxyl radicals (OH<sup>•</sup>) for the destruction of organic pollutants (Oturán & Aaron, 2014)
- IV. Sonochemical advance oxidation which involves the application of ultrasounds in an aqueous medium. The sonochemical process is based on the sonication (direct) and homolytic fragmentation of water and

dioxygen at high frequency (indirect) to produce  $\text{OH}^\bullet$ ,  $\text{HO}_2^\bullet$  and  $\text{O}^\bullet$  radicals (Zhang & Jaroniec, 2018; Oturan & Aaron, 2014)

These general classifications are based on the reagents involved and the reaction mechanisms. **Figure 2.1** presents the summary for the mechanistic classification. However, for this review, attention is focused on photochemical processes (photocatalysis), due to their adaptability for modifications and universal applications as a useful environmental and water remediation method.

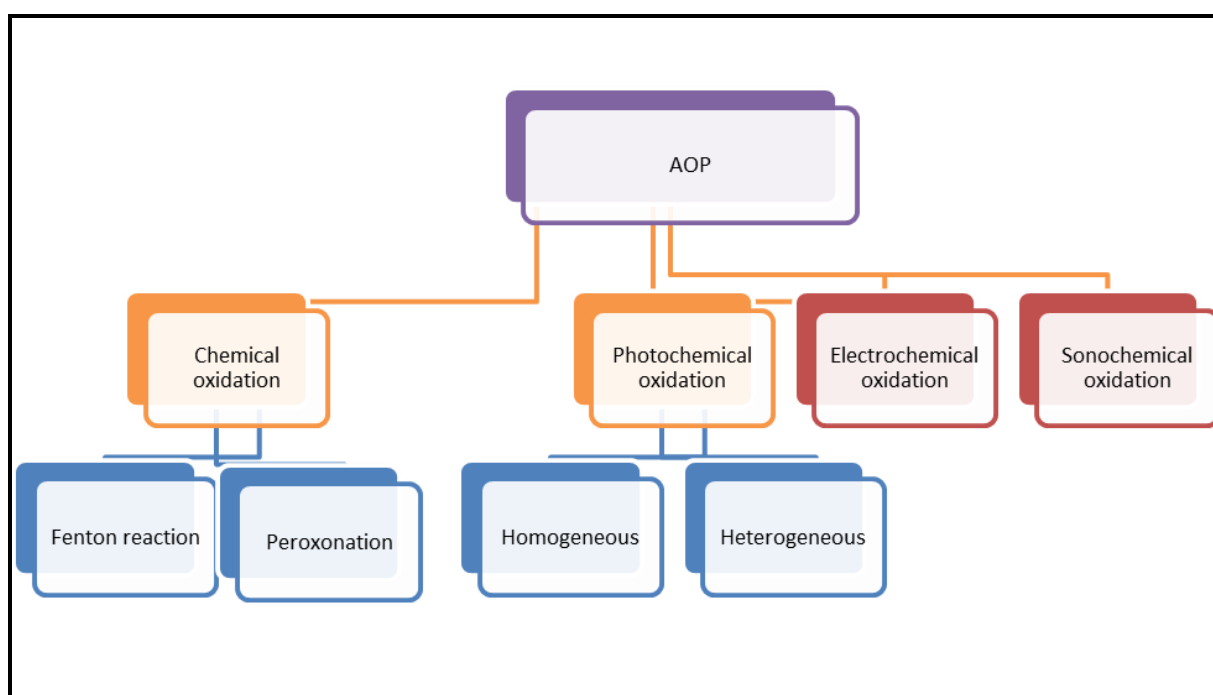


**Figure 2.1:** The proposed classifications of advanced oxidation processes (AOP) based on reaction mechanisms

## 2.2 Photocatalysis

Photochemical oxidation involves the chemical oxidation of pollutants in the presence of light, i.e. visible and ultraviolet light radiation. Photocatalysis is a process in which the rate of photoreaction is accelerated in the presence of a catalyst (Zhang & Jaroniec, 2018). However, photolysis is the degradation or splitting of chemical compounds by light irradiation. Although photolysis itself usually takes place in the presence of light, the addition of chemical reagents (solids or aqueous

solutions) only enhances the process. In other words, the chemical reagents act as catalysts to increase the rate of photolysis. Photocatalysis can be categorised into homogeneous and heterogeneous photocatalysis, based on reaction phases.

### 2.2.1 Homogeneous photocatalysis

Homogeneous photocatalysis refers to photo-oxidative reactions in the same phase. The application in water purification involves the use of a chemical oxidant such as hydrogen peroxide ( $\text{H}_2\text{O}_2$ ) (liquid/liquid) and ozone ( $\text{O}_3$ ) to generate reactive radicals, which attack the pollutants to trigger oxidation. These procedures have found general applications in wastewater purifications and are widely used in several oxidation research studies (Dong *et al.*, 2017; Li *et al.*, 2018; Slamani *et al.*, 2018).

From the literature, many photosensitive chemical materials have been used either individually or in various combinations for homogeneous oxidation reaction processes. These materials include hydrogen peroxide with ultraviolet radiation (UV/ $\text{H}_2\text{O}_2$ ) (Zuorro *et al.*, 2014), ozone in solution with ultraviolet radiation (UV/ $\text{O}_3$ ) (ozonation) (Liu *et al.*, 2014) and the application of a mixture of hydrogen peroxide and ozone in combination with UV or visible light (UV/ $\text{H}_2\text{O}_2/\text{O}_3$ ) (Qin *et al.*, 2015). An improvement in the rate of photo-oxidative degradation of pharmaceuticals has been reported when a combination of  $\text{H}_2\text{O}_2/\text{UV}$  and  $\text{O}_3/\text{UV}$  processes were used (Qin *et al.*, 2015). Furthermore, Fenton reagents ( $\text{Fe}^{3+}$  and  $\text{H}_2\text{O}_2$ ) are used in the presence of light radiations such as Photo-Fenton (PF) (Li *et al.*, 2018) as well as electro Fenton (EF) reactions (Liu *et al.*, 2018). Hydrogen peroxide, due to the ease of splitting to generate OH radicals, is a common oxidising reagent used in most of the homogeneous oxidative processes. Although, the relative oxidising strength of hydrogen peroxide alone is insufficient, nevertheless, the presence of light and other oxidising agents in the oxidation system increases the strength and the rate of oxidation. Consequently, the rate of OH $\cdot$  radicals' production is accelerated.

Homogeneous photocatalysis is known for considerable efficiency especially for the removal of recalcitrant pharmaceuticals (Pourakbar *et al.*, 2016). However, many of these processes have some disadvantages such as the challenge of post-treatment separation of used reagents, the cost of  $\text{H}_2\text{O}_2$ , environmental effects of ozone and

the contamination effects of the treated water with free  $\text{Fe}^{2+}$  in Fenton processes. For the Fenton process, the optimal dosage of  $\text{H}_2\text{O}_2$  is strictly determined by the concentration level of the pollutants to be oxidised. Also, the removal of the total organic carbon (TOC) in waste water is rarely satisfactory (Liu *et al.*, 2018). These issues tend to limit the application of homogeneous oxidation processes. Hence, the introduction of heterogeneous photocatalysis which seems to be a better available alternative to circumvent the challenges associated with homogeneous oxidation system.

### 2.2.2 Heterogeneous photocatalysis

More recently, heterogeneous photocatalysis has emerged as an innovative and effective decontamination technology for the treatment of wastewater and the transformation of hazardous chemicals into non-toxic forms (Zeghioud *et al.*, 2016; Díez *et al.*, 2018). Heterogeneous photocatalysis refer to a system in which the reactants and the applied catalyst are present in two or more different phases. This technique has been generally applied to wastewater purification with the aim of reuse, due to its ability to achieve complete mineralisation of the targeted organic pollutants (Shokri *et al.*, 2016; Koseira *et al.*, 2017). At present, this is the most applicable industrially, because of its efficiency, relative ease of recovery, recycling and adaptability of the material being used which can withstand varying process conditions (Atul *et al.*, 2013). Solid/aqueous catalysis also presents the possibility for various modifications, including alteration with polymeric materials, for improved and sustainable performances.

The basis of hetero-photocatalysis can be explained by photoexcitation of a given semiconductor solid (e.g.,  $\text{TiO}_2$ ) because of its absorption of rays during irradiation (Zhang & Jaroniec, 2018), mostly from the near-ultraviolet region of the light spectrum. Under light illumination, a suitable semiconductor solid material can be excited by sufficient energy photons (Koseira *et al.*, 2017), resulting in the production of conduction band electrons and valence band holes. These charge carriers (electron and hole pairs) can induce reduction or oxidation respectively, while reacting with both water and organic contaminants. The holes are extremely

oxidants, thus are able to react with available oxygen and water (Figure 3), resulting in the formation of hydroxyl radicals including other reactive oxygen species (Alhaji *et al.*, 2017; Díez *et al.*, 2018).

### **2.2.2.1 Mechanism and kinetics of heterogeneous process using semiconductors**

The generation of electron and positive hole pairs ( $e^-/h^+$ ) by UV irradiated semiconductor nanoparticles (e.g.,  $\text{TiO}_2$ ), is a critical and major step in photocatalytic processes (Kosera *et al.*, 2017; Tong *et al.*, 2018). Generally, photon absorption by a semiconductor material results in the promotion of an electron from the valence band (VB) to the conduction band (CB). This process leaves a 'hole' (electron vacancy) in the valence band and an excess of negative charges in the CB (**Figure 2.2**). These charge carriers can either recombine within the particle or move to its surface, where they initiate chemical redox reactions with adsorbed organic molecules (Hoffmann *et al.*, 1995; Díez *et al.*, 2018). These molecules could be an acceptor or a donor of electrons, depending on whether their redox potentials lie within the bandgap of the applied photocatalyst (Zeghioud *et al.*, 2016). Because of this mechanistic process, wastewater could be decontaminated by the reductive or oxidative decomposition of the pollutants by a modified or unmodified semiconductor photocatalyst.

However, various stages are involved in photochemical mechanisms using  $\text{TiO}_2$  and its polymer-modified forms. First, when photon energy ( $h\nu$ ), greater than the bandgap energy ( $E_{bg}$ ) incident on the surface of the catalyst, electron ( $e^-$ ) is excited and transferred from VB to CB. The hole left on VB reacts with water while the excited electron attacks molecular oxygen, hydrogen peroxide or any other oxidising agent available in the solution or on the catalyst surface, to produce reactive radicals (**Figure 2.2**). These reactive radicals serve as the oxidant in the photocatalytic system, majorly responsible for the breakdown of organic pollutants. This process indicates that the mechanisms of photocatalysis are mostly based on the radical attacks on organic pollutants (Turchi & Ollis, 1990; Augugliaro *et al.*, 2012). The  $\text{OH}^\bullet$  radicals have been considered with proven implicating evidence to be the major active species responsible for many photocatalytic oxidation reactions (Turchi &

Ollis, 1990; Xiang *et al.*, 2012). Therefore, the formation rate and the quantity of OH• radicals generated during photocatalysis processes, determine the oxidative and the degradation performances of the photocatalyst. The formation rate of hydroxyl radicals generated and the OH•-index, which is expressed as a percentage of P25 TiO<sub>2</sub>, are presented in **Table 2.1**.

**Table 2.1:** Formation rate of OH• on some metal oxide photocatalysts and their OH•-index values

Photocatalysts	Rate (K (μM/h))	OH•-Index (% of P25)
P25	5.88	100
TiO <sub>2</sub> (anatase)	4.28	72
TiO <sub>2</sub> (rutile)	0.27	4.2
ZnO	0.94	16.3
SnO <sub>2</sub>	0.08	1.4

The photocatalytic oxidation reaction kinetics provides the necessary information about the reaction rates as well as the mechanisms by which the products are formed. This reaction rates can be expressed in a form of a generic reaction rate law as shown in Equation 2.1:

$$\text{Rate} = dC/dt = K[C]^{n-1} \quad \text{Equation 2.1}$$

where k is the rate constant, [C] is the concentration of the pollutant in wastewater and n represents the order of the reaction. This information suggests that the rate of photocatalytic degradation of organic pollutants can fundamentally be treated empirically, which can invariably involve the application of kinetic models.

However, the photocatalytic oxidation kinetics of many organic molecules have been successfully modelled using the Langmuir-Hinshelwood (L-H) equation (Behnajady *et al.*, 2006; Yang *et al.*, 2008) as illustrated in Equation 2.2:

The L-H kinetic model generally becomes an accepted expression in photocatalytic oxidation, relating photocatalytic degradation rate with the initial concentration of the pollutant (Mohapatra & Parida, 2012). The model was developed based on the Langmuir adsorption isotherm with the following set of assumptions:

- (1) The number of adsorption sites on the surface is constant,
- (2) A site can hold only one molecule per time,
- (3) Insignificant interaction takes place between adsorbed molecules, and
- (4) Adsorption equilibrium is always assumed to be established.

$$\text{Rate } (r) = \frac{d[C]}{dt} = \frac{kKC}{1+KC} \quad \text{Equation 2.2}$$

where,  $r$  is the oxidation rate of the reactant (mg/L min),  $C$  the concentration of the reactant (mg/L),  $t$  the irradiation time,  $k$  is the reaction rate constant (mg/L min) and  $K$  the adsorption coefficient of the reactant (L/mg). L-H model represents a mechanism for the surface.

When the concentration ( $C_0$ ) is relatively small or very low, the equation L-H kinetic model can be simplified to an apparent first-order equation (Eqn. 2.3). In this first-order kinetic equation, the logarithm graph of the pollutant concentration with varying catalyst concentrations versus irradiation time should give a linear decomposition profile. This plot is an indication of a pseudo-first order (PFO) reaction (Behnajady *et al.* 2006). Sometimes, first-order kinetics are appropriate for the whole concentration range up to a few mg/L:

$$\ln\left(\frac{C_0}{C}\right) = kK_t = k_{app}t \quad \text{Equation 2.3}$$



In the case of concentration higher than 5 mM, with the  $K_C$  much larger than unity, a zero-order kinetic may be used:

Usually, the photocatalytic process using some semiconductors and their modified form, more often than not are applied to degrade pollutants with low concentrations ranging from ppb to few ppm (Behnajady *et al.*, 2006). Therefore, the first-order kinetics may be applied to simulate the degradation of organic pollutants (Chen & Jenq, 1998) at a low level of concentration, particularly using  $TiO_2$  photocatalyst and its modified forms (Ananpattarachai *et al.*, 2016) such as polymer- $TiO_2$ . The graphical illustration of  $\ln(C_0/C)$  against irradiation time (t) yields a straight line of which the slope is the rate constant describing the rate at which a pollutant is decomposed (Kim Phuong *et al.*, 2016).

Many experimental results indicate that the photocatalytic degradation rates of many organic contaminants over UV-irradiated semiconductors agree with PFO kinetic (Mohapatra & Parida, 2012; Kim Phuong *et al.*, 2016). This model is subject to the light intensity as well as the contaminant concentration. However, according to a reported investigation, the  $OH^\bullet$  radicals formed at the interface of modified  $TiO_2$  are in proportion to the light intensity irrespective of the concentration, obeying zero-order kinetic reaction rate profile (Ananpattarachai *et al.*, 2016) (**Equation 2.4**).

A new concept was recently introduced, which is the application of  $OH^\bullet$ -index, to relate and compare the formation rate kinetics of  $OH^\bullet$  radicals on different photocatalysts (Bubacz *et al.*, 2013). This OH-index value presents the formation rate as the percentage of reference material (P25). The  $OH^\bullet$ -index was expressed as:

$$OH - index = \frac{r}{r_o} \times 100 \quad \text{Equation 2.4}$$

Where  $r$  represents the  $OH^\bullet$  formation rate on a semiconductor photocatalyst and  $r_o$  representing the  $OH^\bullet$  formation rate on the reference material. In general, catalysts with a higher  $OH^\bullet$ -index show higher photocatalytic activity (Ananpattarachai *et al.*,

2016), shown in **Table 2.1**. For the OH<sup>•</sup>-index value determination under visible light irradiation, Degussa P25 was used as a reference material (Bubacz *et al.*, 2013).

The mechanism of photo-oxidation of organic pollutants by semiconductors generally follows a similar scheme (**Figure 2.2**). However, the mechanism and the initial process of the oxidative photocatalytic reactions using TiO<sub>2</sub> are suggested to be based on any one or more of the four possibilities. First, when the reaction occurs while both species are adsorbed on the surface of the photocatalyst. Secondly, when a free radical reacts with an adsorbed organic molecule. Thirdly, when an adsorbed radical reacts with a free organic molecule arriving at the catalyst/solution interface. Lastly, the possibility of when the radicals are released and the reaction occurs while the two species are free in the aqueous solution. Whichever becomes the initial process, the mechanism of photocatalytic reactions using TiO<sub>2</sub> still follows a similar route. The summarised mechanistic route for TiO<sub>2</sub> photocatalytic process is illustrated in **Figure 2.3**.

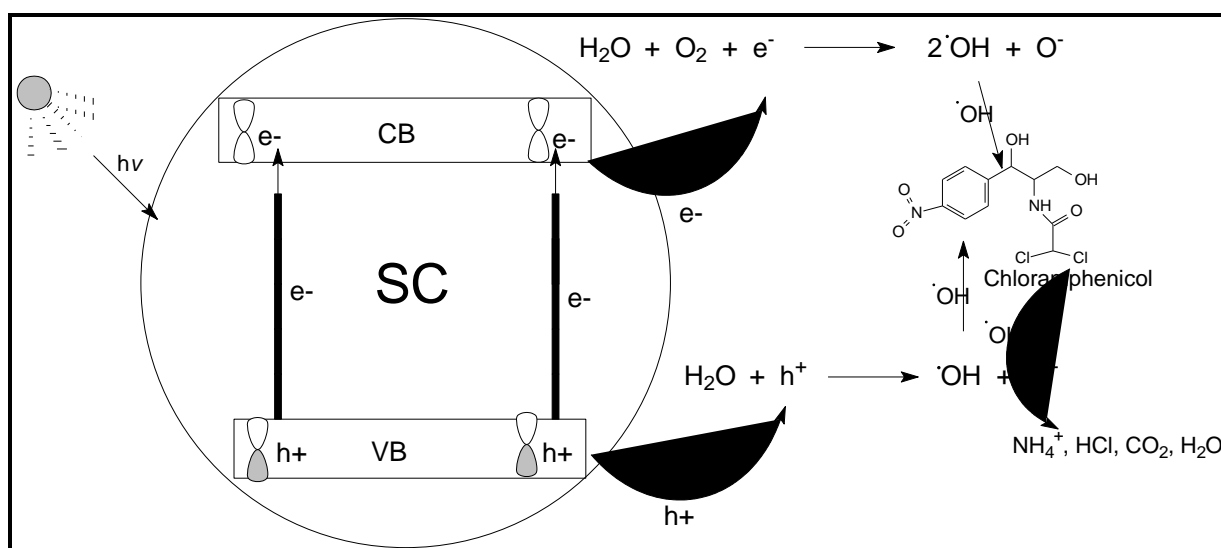


**Figure 2.2:** The scheme of redox process mechanism of semiconductor (SC) photocatalyst in the presence of light.

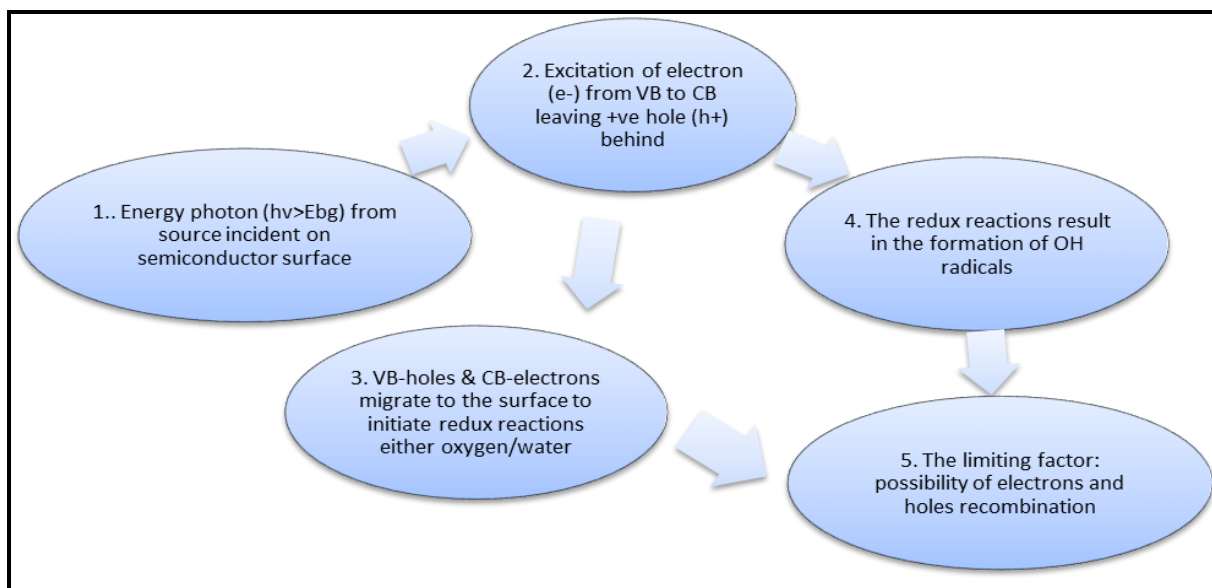


**Figure 2.3:** The flow chart of the mechanistic route for semiconductor ( $\text{TiO}_2$ ) photocatalysis.

Although, the high rate of charge carrier generation and separation should enhance  $\text{TiO}_2$  photocatalyst performance, the system, however, suffers the possibility of electron/hole recombination. This recombination tendency hinders an optimum performance of  $\text{TiO}_2$  photocatalyst for the degradation of pollutants in aqueous solution.

### 2.3 Limitations of $\text{TiO}_2$ photocatalyst and improvement with polymer modifications

The application of  $\text{TiO}_2$  photocatalyst suffers drawbacks because of high photo generated electron-hole recombination rate and wide band-gaps (3.0-3.2 eV) (Daghrir *et al.*, 2013; Oseghe & Ofomaja, 2018). Other conventional photocatalysts with similar band-gaps include  $\text{ZnO}$  and  $\text{SnO}_2$  with 3.2 eV and 3.6 eV, respectively (Al-Odaini *et al.*, 2011). The challenge of wide band-gap makes  $\text{TiO}_2$  inefficient for visible light applications, which is about 45% of naturally available sunlight (Zhang *et al.*, 2014). Considering the overall environmental applicability of  $\text{TiO}_2$  photocatalyst, extending its optical response to the visible region is indispensable.

Various materials have been employed in the modification of TiO<sub>2</sub> for photolytic application (Jia *et al.*, 2017) to improve its visible light absorption properties for an extended photocatalytic performance. Several modification efforts on TiO<sub>2</sub> have been made using different materials, particularly for enhanced degradation of pharmaceutical and other organic pollutants (Abdel-Wahab *et al.*, 2017; Oseghe & Ofomaja, 2018). Among these materials, various polymer organic molecules have been found more useful as efficient TiO<sub>2</sub> photosensitisers for photodegradation of pharmaceutical pollutants (Zhao *et al.*, 2017b; Šojić-Merkulov *et al.*, 2018).

### **2.3.1 TiO<sub>2</sub> modifications and polymer-TiO<sub>2</sub> photocatalysts**

Studies into the development of environmentally-friendly solar and visible light active photocatalysts have significantly increased (Fagan *et al.*, 2016). This growing interest can be attributed to solar energy as a cheap and readily available natural source of irradiation. To improve visible light suitability of TiO<sub>2</sub> photocatalyst, efforts such as doping with metals, non-metals and by functionalising with various materials, have been made (Fagan *et al.*, 2016; Zhang *et al.*, 2012; Jia *et al.*, 2017). The dopants have proven to enhance the photocatalytic efficiency of TiO<sub>2</sub> under visible light through the reduction of the band-gap and serve as electron trapping agents, thereby reducing the recombination rate of electrons and holes (Saud *et al.*, 2015).

For example, Liu *et al.*, (2008) investigated the effect of boron and nitrogen-doping on the visible-light photocatalytic activity of TiO<sub>2</sub> for the degradation of rhodamine B (Liu *et al.*, 2008). The photocatalytic degradation of pollutant shows a considerable enhancement for boron and nitrogen-doped TiO<sub>2</sub> as compared to the undoped TiO<sub>2</sub>. The introduction of extraneous dopants into the lattice structure creates some intermediate energy levels within the band-gap, which allows for visible light absorption through the electronic transition between the band and the impurity level (Zhang *et al.*, 2014). Coupling TiO<sub>2</sub> with other narrow bandgap semiconductors such as CdS, WO<sub>3</sub> and CuO (Zhang *et al.*, 2014) has also been used. However, the effective activity of non-metal doped TiO<sub>2</sub> mostly depends on some other factors such as dopant concentration, dopant energy level, dopant distribution and the oxygen vacancy on the lattice surface (Nasirian *et al.*, 2018).

More recently, organic molecule sensitizers such as organic dyes, which can themselves absorb light, have been used to synthesis composite materials to enhance the visible light absorption capacity of inorganic semiconductors such as TiO<sub>2</sub> (Zhang *et al.*, 2014). The application of a dye sensitizer was able to extend the spectral response of TiO<sub>2</sub> to the visible-light region (Yao *et al.*, 2015). Nevertheless, most dye molecules are toxic, which could aggravate environmental problems thereby, constitute a further threat to aquatic and human lives (Yao *et al.* 2015). On the contrary, many polymer organic molecules are non-toxic, light-sensitive and applicable as a photosensitizer for TiO<sub>2</sub> modification with little or no environmental consequences (Muxika *et al.*, 2017; Zhao *et al.*, 2019) due to their biodegradability.

## 2.4 Photocatalytic applications of polymer-TiO<sub>2</sub>

Polymer-inorganic hybrid materials are attractive because of their relatively high electron mobility and their excellent physical and chemical stability of polymer-inorganic nanocrystals (Lin *et al.*, 2009). In the field of environmental ecotoxicology and management, application of polymer-TiO<sub>2</sub> for enhanced photocatalytic processes have contributed significantly to pollutant degradation. Among the polymer-TiO<sub>2</sub> that have been prepared and used as composite material for both the adsorption and photocatalytic degradation of organic pollutants are cellulose-TiO<sub>2</sub> (Zhao *et al.*, 2019) and polypropylene carbonate-TiO<sub>2</sub> (Li *et al.*, 2018). Others include chitozan-TiO<sub>2</sub> (Zhao *et al.*, 2017b) as well as conjugated polymers, such as polypyrrole-TiO<sub>2</sub> (Sun *et al.*, 2013) and polyaniline-TiO<sub>2</sub> (Šojić-Merkulov *et al.*, 2018). The conjugated pie-bond ( $\pi$ -bond) in conjugated polymer improves light absorption unto the surface of the catalyst. Moreover, the multifunctional groups can provide the pollutants with reaction site on the surface of the photocatalyst, thereby, enhancing the degradation by the polymer-TiO<sub>2</sub> photocatalyst (Zhao *et al.*, 2019).

Cellulose-TiO<sub>2</sub> nanocomposite as a modified TiO<sub>2</sub> photocatalyst is an important adsorptive and photocatalytic material. Cellulose is an organic polysaccharide, which is made of a linear chain of several thousands of  $\beta(1\rightarrow4)$  links through D-glucose units. It contains multiple hydroxyl groups on a chain to form hydrogen bonds, responsible for its adsorptive properties (Tan *et al.*, 2016). Several methods have

been used to synthesise cellulose-TiO<sub>2</sub> nanocomposite, which includes the sol-gel method and polymerisation (Zhao *et al.*, 2019). The well-prepared cellulose-TiO<sub>2</sub> nanocomposite offers a high sorption capacity (2.1 µgcm<sup>-2</sup>) toward a model pollutant (methyl orange) with remarkable photocatalytic degradation under UV and visible light (Zhao *et al.*, 2019). A prepared cellulose-TiO<sub>2</sub>/Ag was also applied as an efficient photocatalyst for the degradation of 4-chlorophenol which was mineralised into small molecules (Zhang *et al.*, 2018).

Polypropylene carbonate-TiO<sub>2</sub> nanocomposite is another useful polymer integrated TiO<sub>2</sub> photocatalyst. The prepared film composite was applied for the photocatalytic removal of methyl orange with a performance of up to 85.06% removal of the dye (Li *et al.*, 2018). Similarly, Chitosan-TiO<sub>2</sub> nanocomposite is also known as a functional material for the removal of organic pollutants from aqueous solutions. Chitosan is a polymer produced from the N-deacetylation of chitin, which is a naturally occurring polysaccharide. It is one of the most abundant biopolymers in nature and has proven to be an efficient adsorbent because of its unique properties such as biocompatibility, biodegradability, non-toxicity and low cost (Igberase and Osifo, 2015; Muxika *et al.*, 2017). Chitosan-TiO<sub>2</sub> is a useful polymer-TiO<sub>2</sub> composite photocatalyst due to its ability to act as a good support for effective dispersion of TiO<sub>2</sub> nano-particles (Wiącek *et al.*, 2018) for the photodegradation of pharmaceutical pollutants. According to a recent study, chitosan-AgO/TiO<sub>2</sub> photocatalyst film demonstrated an enhanced activity for photocatalytic degradation of ampicillin (an antibiotic) with 100% removal from aqueous solution (Zhao *et al.*, 2017b). Metal ion incorporation into the Chitosan-TiO<sub>2</sub> fibre has also been confirmed to be an effective and a way to easily retrieve the catalyst for photocatalytic removal of other organic pollutants (Ali *et al.*, 2018; Zhao *et al.*, 2019) such as methyl orange (Li *et al.*, 2008).

Ali and co-workers (2018) in their investigations, indicated that metal modified Chitosan-TiO<sub>2</sub> composite fibres demonstrated a good photocatalytic ability for various types of organic pollutants (**Figure 2.4**). A report published by Jallouli *et al.* (2017) also indicated an effective photocatalytic property of TiO<sub>2</sub>-cellulosic fibre for the removal of paracetamol i.e acetaminophen (APAP). This material allows for easy separation of the photocatalyst from the treated solution, although, the application of TiO<sub>2</sub> P25 was found more efficient (90% removal) than the use of cellulose-TiO<sub>2</sub>

under UV irradiation of paracetamol (Jallouli *et al.*, 2017). Nevertheless, many of these polymer-modified TiO<sub>2</sub> nanocomposites and nanofibers have proven as good photocatalytic and absorptive materials for the removal of organic pollutants, particularly pharmaceuticals.

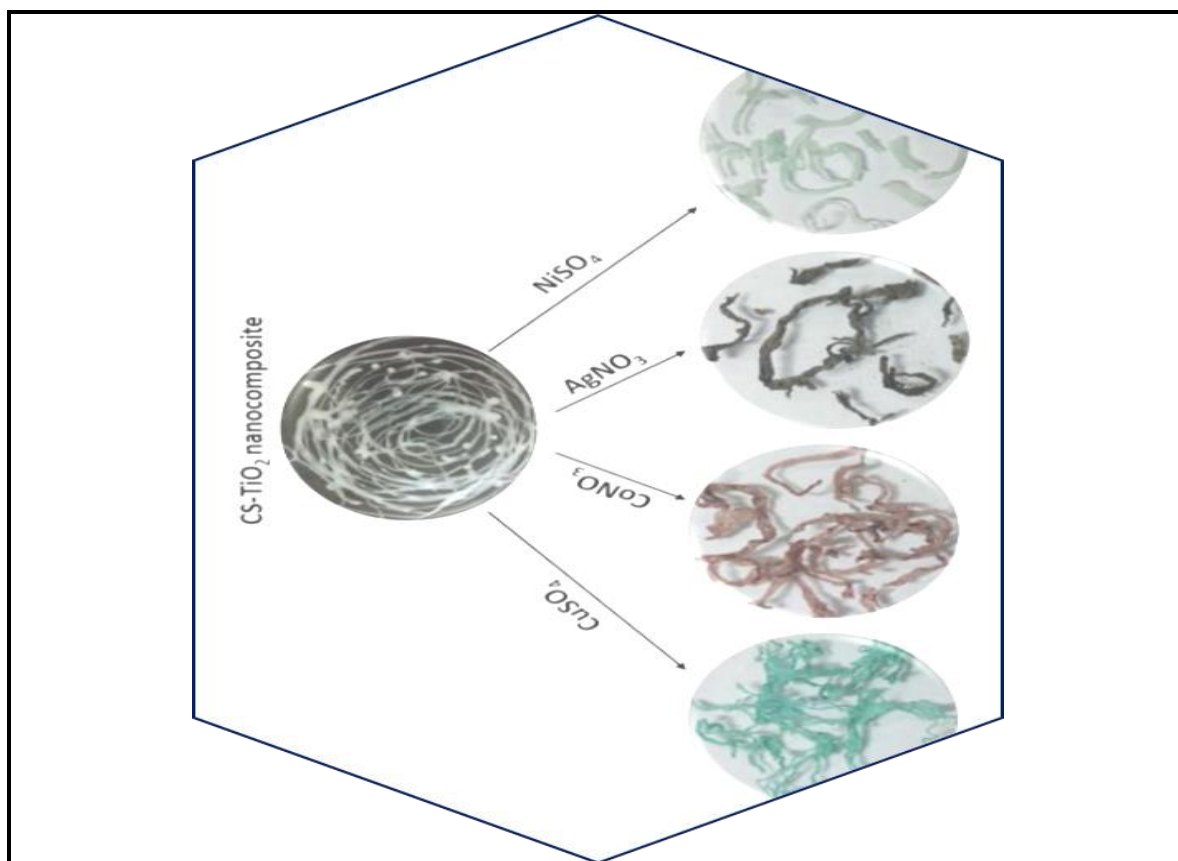


**Figure 2.4:** The scheme of chitosan-TiO<sub>2</sub> composite fibre treated with different metal salt solutions. **Source:** Ali *et al.* (2018)

Currently, there is a growing interest and increasing research focus on using conjugated polymer (CP) as a sensitizer, to stimulate photon absorption and increase electron generation. Various types of CP have been used, which include polyaniline (Li *et al.*, 2004), polypyrrole (Sun *et al.*, 2013; Scharrel *et al.*, 2015), polythiophene (Xu *et al.*, 2012), to enhance the photocatalytic activity of TiO<sub>2</sub>. The efficiency of polythiophene polymer as a visible light absorbent is due to its short band-gap (2.02 eV) (Lan *et al.*, 2011), between the lowest unoccupied molecular orbital (LUMO) and the highest occupied molecular orbital (HOMO). The proposed

mechanistic scheme for CP modified  $\text{TiO}_2$  for an enhanced visible-light photodegradation of chloramphenicol is presented in Figure 2.5. Although CP- $\text{TiO}_2$  hybrid materials are mostly used to produce solar cell for power conversion due to enhanced electron mobility, this property is also useful in photocatalysis.

Recent studies conducted by Šojić-Merkulov *et al.* (2018) on the photocatalytic decomposition of both propranolol (a drug for high blood pressure) and amitriptyline (a tricyclic antidepressant) using polyaniline- $\text{TiO}_2$ , show an enhanced decomposition compared to bare  $\text{TiO}_2$ . The result indicates that 34% of propranolol and 45.4% of amitriptyline were degraded after an hour (Šojić-Merkulov *et al.*, 2018).

According to the literature, hetero-junction plays a significant role in an enhanced photodegradation capacity of  $\text{TiO}_2$  nanocomposite. A silver oxide/titania modified chitosan polymer (Chitosan- $\text{Ag}_2\text{O}/\text{TiO}_2$ ) shows a wide visible light adsorption band with lower band-gap (2.4 eV), due to the synergistic effect of the nano-components (Zhao *et al.*, 2017b). Therefore, the synergetic behaviour due to strong interfacial interaction between the two components in polymer- $\text{TiO}_2$  nanocomposite is an important factor for enhanced photocatalytic ability of the material. The applications of  $\text{TiO}_2$  and polymer- $\text{TiO}_2$  as photocatalysts for some pharmaceuticals and other organic pollutants from past research work are presented in

**Table 2.2** and **Table 2.3** respectively.

**Table 2.2:** Application of  $\text{TiO}_2$  photocatalyst for pharmaceutical degradation in solution

Photocatalyst	Contaminant	Light source	Removal efficiency	% Removal	Reference
$\text{TiO}_2$ (Three forms)	Ibuprofen	UV	Increase in degradation efficiency as Anatase>Brookite>Rutile	97	(Tran <i>et al.</i> , 2017)
$\text{TiO}_2/\text{Fe}_2\text{O}_3/\text{Vis}$	Paracetamol	Visible	Shows degradation efficiency of 99%	99	(Abdel-Wahab <i>et al.</i> , 2017)



Photocatalyst	Contaminant	Light source	Removal efficiency	% Removal	Reference
Pure TiO <sub>2</sub>	Ibuprofen	UV/LED	It was efficient to remove IBU and the acute toxicity reduced by 40%	100	(Jallouli <i>et al.</i> , 2018)
Doped TiO <sub>2</sub> /Vis	Tetracycline	Visible	83% performance	83	(Oseghe & Ofomaja, 2018)
Pure TiO <sub>2</sub>	Ciprofloxacin	UV	Rapid release of OH with reaction rate constant $8.04 \times 10^9 \text{ M}^{-1}\text{S}^{-1}$ and efficient degradation of in aqueous solution	-	(An <i>et al.</i> , 2010)
Pure TiO <sub>2</sub>	Acetaminophen	UV	95% of 2.0mM degraded in 1hr: 20min	95	(Yang <i>et al.</i> , 2008)
Immobilised TiO <sub>2</sub>	Diclofenac	UV	100% degradation in 96 hrs	100	(He <i>et al.</i> , 2016)

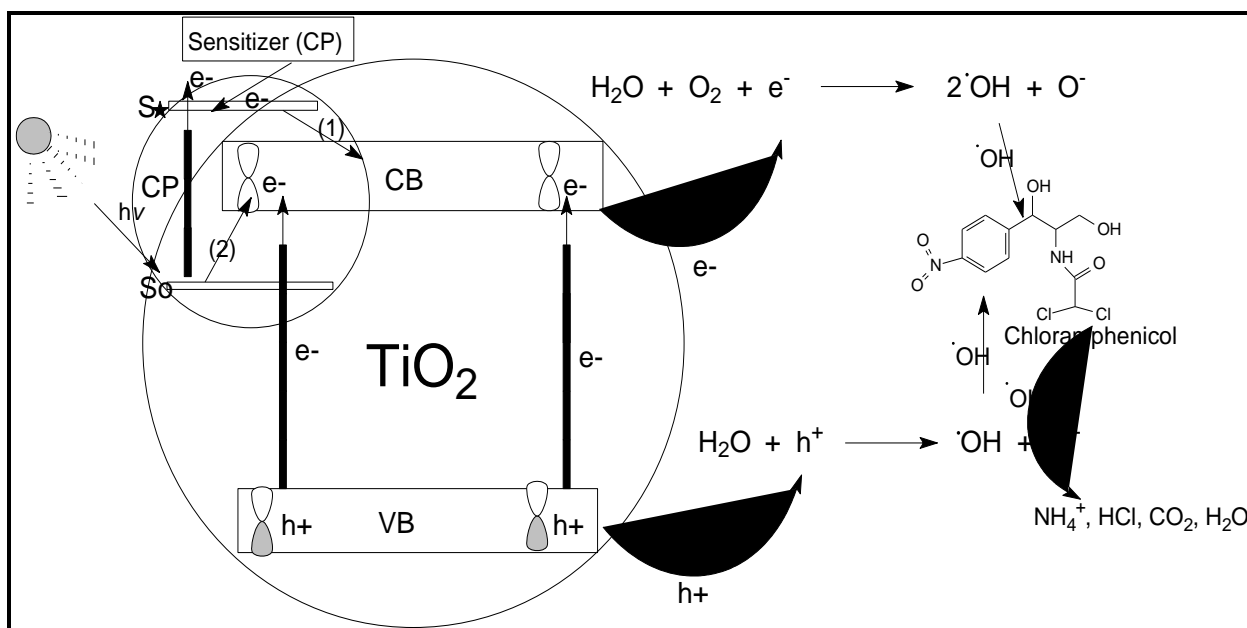
**Table 2.3:** Photodegradation of pharmaceuticals and other pollutants using polymer-TiO<sub>2</sub> catalysts

Photocatalyst	Contaminant	Light source	Removal Efficiency	Removal (%)	Reference
Chitosan-TiO <sub>2</sub> /Ag <sub>2</sub> O	Ampicillin	Visible-light	Efficient in the reduction of the concentration	100 in 3 hrs	(Zhao <i>et al.</i> , 2017b)
Polyaniline-TiO <sub>2</sub>	Amitriptyline	UV	Better degradation efficiency than bare TiO <sub>2</sub>	45.4% In 1 hr	(Šojić-Merkulov <i>et al.</i> , 2018)
Celulose-TiO <sub>2</sub> (C-TiO <sub>2</sub> ) fibre And TiO <sub>2</sub> P25	Paracetamol	UV	TiO <sub>2</sub> P25 shows greater efficiency than C-TiO <sub>2</sub>	90%	(Jallouli <i>et al.</i> , 2017b)
Polyaniline-TiO <sub>2</sub>	Propranolol	UV	Better degradation efficiency than bare	34% After	(Šojić-Merkulov <i>et al.</i> , 2018)

Photocatalyst	Contaminant	Light source	Removal Efficiency	Removal (%)	Reference
			TiO <sub>2</sub>	60min	
Chitosan-TiO <sub>2</sub>	Methyl Orange	UV	Excellent removal rate	85.06	(Li <i>et al.</i> , 2008)
Polypyridazine-TiO <sub>2</sub>	MO	Sunlight	The degradation efficiency is 4.39 times more than that of pure TiO <sub>2</sub>	94.8	(Wang <i>et al.</i> , 2017b)
Celulose-TiO <sub>2</sub> @Ag	4-Chlorophenol	UV	Efficiently mineralised	-	(Zhang <i>et al.</i> , 2018)

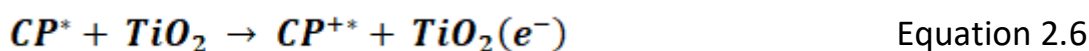
#### 2.4.1 Electron generation mechanism of polymer-TiO<sub>2</sub> composite under visible light

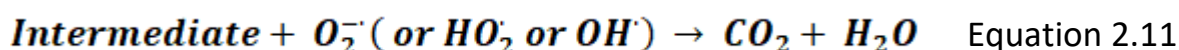
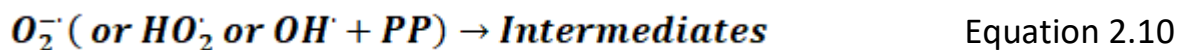
The mechanism of the electron generation process, in polymer sensitised TiO<sub>2</sub> under visible light irradiation, is different from the pathway obtainable under UV light illumination (Kumar & Devi, 2011). Although the fate of the generated electrons was suggested to be the same for both modified and unmodified TiO<sub>2</sub>, however, the number of electrons increased since there are other sources of electron generation in polymer sensitised TiO<sub>2</sub>. Considering the conjugated polymer (CP) modified TiO<sub>2</sub> (CP-TiO<sub>2</sub>) nanocomposite for example, extra electrons can be produced from the photosensitive CP. **Figure 2.5** illustrates the photodegradation mechanism scheme for polymer (CP) sensitised TiO<sub>2</sub> catalyst in the presence of light: (1) electron transfer to the CB of the semiconductor and the acceptor (oxidants) after CP excitation. (2) the excitation of the CP sensitizer by visible light generates electrons.



**Figure 2.5:** The mechanism of CP modified TiO<sub>2</sub> photocatalyst under light irradiation.

The sensitisation process is suggested to involve indirect electron addition, from the polymer sensitizer, through the intermediate of TiO<sub>2</sub> conduction band (CB). Under the visible light irradiation, conjugated polymer gets excited and electrons are released and transferred to CB energy level of TiO<sub>2</sub>, which then reacts with adsorbed O<sub>2</sub> molecules (Daghrir *et al.*, 2013). The O<sub>2</sub> molecule on the TiO<sub>2</sub> surface, acts as an electron scavenger, takes up an electron to produce highly reactive oxidising species such as OH<sup>•</sup>, O<sub>2</sub><sup>•-</sup> and HO<sub>2</sub><sup>•</sup>. Thus, the generated species are involved in oxidative degradation of the pharmaceutical organic pollutants. The proposed photodegradation mechanism of pharmaceutical pollutants (PP) using conjugated polymer-modified TiO<sub>2</sub> (CP-TiO<sub>2</sub>) under visible light irradiation is as presented (Equations 2.5 to Equation 2.11):





## 2.5 Photocatalytic intermediates for selected pharmaceuticals using TiO<sub>2</sub>

Usually, photolysis involves the breaking down of a target molecule by the absorption of light, leading to its decomposition into intermediate products, which is further degraded, ultimately, to give mineralised end products (Kaur *et al.*, 2015; Kaur *et al.*, 2016; Thi & Lee, 2017). Limited studies have reported the behaviour of pharmaceuticals and their photochemistry in aquatic environments (Kaur *et al.*, 2016), for clear identification of their common photolytic by-products. However, the photochemistry of pharmaceutical compounds in aqueous solution has revealed the formation of new compounds (Gao *et al.*, 2017), which may also be harmful.

Some investigations have identified few intermediates that are produced during photocatalytic degradation of some pharmaceuticals and have established their concentrations during the time (Boreen *et al.*, 2003; Kaur *et al.*, 2015; Thi & Lee, 2017). For example, the potential intermediates of paracetamol photocatalytic degradation under visible light irradiation were identified to include aliphatic butyric acid and Oxamic acid (Thi & Lee, 2017). It was also reported that the photodegradation of paracetamol using TiO<sub>2</sub> catalyst under UV irradiation, shows several other intermediates, which include aromatic benzoquinone and phenols, as monitored by HPLC and GC-MS, (Moctezuma *et al.*, 2012).

Kaur *et al.*, (2015), in their review article, summarised the mineralisation process of various pharmaceutical compounds during heterogeneous photocatalysis. The study revealed that ibuprofen under UV irradiation and TiO<sub>2</sub> catalyst, produces formic acid

and acetic acid, among other intermediates, as identified by LC-MS (Kaur *et al.*, 2015). The study also reported the formation of four transitional compounds, which were identified as the intermediate formed from the photocatalytic degradation of diclofenac under simulated solar light irradiation using  $\text{TiO}_2$  catalyst.

In summary, the whole process of pharmaceutical photodegradation may be simplified as the conversion of the primary compounds into  $\text{CO}_2$  and  $\text{H}_2\text{O}$ , through three major stages. First, the formation of aromatic intermediates; secondly, the production of aliphatic intermediates; lastly, the formation of the final products (i.e.  $\text{CO}_2$  and  $\text{H}_2\text{O}$ ). These stages are clearly illustrated in **Figure 2.6**, showing the pathway and the general intermediate products for photo degraded pharmaceuticals. For further illustration, paracetamol (APAP) and chloramphenicol (CAP) are used as models in this discussion, representing analgesics and antibiotics pharmaceuticals, respectively.

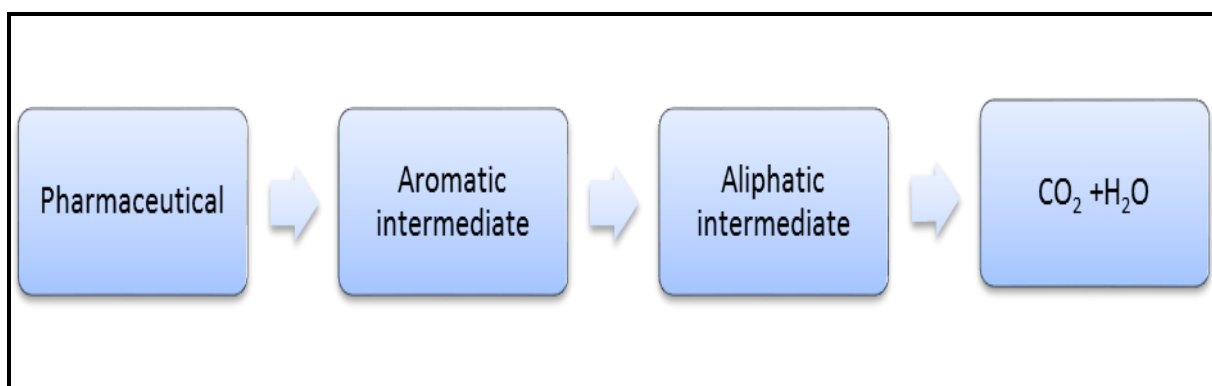


**Figure 2.6:** The summary of intermediates and final degradation products of pharmaceuticals

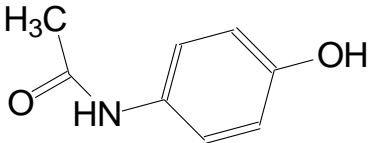
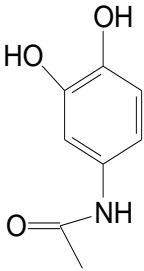
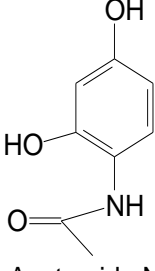
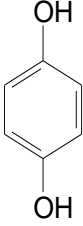
### 2.5.1 Acetaminophen and its photodegradation intermediate products

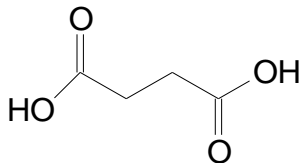
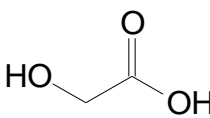
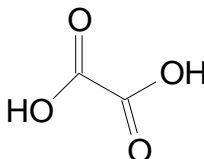
Acetaminophen (N-4-hydroxyphenyl-acetamide) (APAP) is a conventional anti-inflammatory pharmaceutical that is widely used, without the necessity of prescription, for the relief of headache, migraine, neuralgia, backache and rheumatic pains (Ziylan-Yavaş & Ince, 2018). Consequently, APAP and its harmful metabolites have been detected in surface waters and drinking water (Slamani *et al.*, 2018). Its toxic effects on aquatic organisms have also been reported (Antunes *et al.*, 2013;

López-Zavala & Estrada, 2016; Slamani *et al.*, 2018). APAP is one of the PCs that are normally resistant to biodegradation (Cheshme *et al.*, 2018). However, advanced oxidation processes (AOPs) have been used to degrade such recalcitrant contaminants (Cheshme *et al.*, 2018; (Tobajas *et al.*, 2017), including APAP (Moctezuma *et al.*, 2012). During the process of photocatalytic degradation, some intermediate compounds have been identified for APAP (Autónoma *et al.*, 2011; Moctezuma *et al.*, 2012). These intermediate compounds, such as succinic and oxamic acids are suggested to evolve from the cleavage of the benzene ring present in their structure (Thi & Lee, 2017; Kaur *et al.*, 2016).

To date, several other intermediate molecules have been identified and reported for the photocatalytic oxidation of APAP (Moctezuma *et al.*, 2012; Gao *et al.*, 2017) using TiO<sub>2</sub> catalyst. **Table 2.4** presents a summarised proposed scheme and the intermediate compounds for APAP photodegradation.

**Table 2.4:** Paracetamol photodegradation intermediates and products

<p><b>Acetaminophen</b></p> <p>(Before OH<sup>•</sup> radical attack on APAP)</p>			
<p><b>Primary intermediates</b></p> <p>(After OH<sup>•</sup> radical attack on APAP)</p>	 <p>Acetamide N-(3,4hydroxyphenyl)</p>	 <p>Acetamide N-(2,4-hydroxyphenyl)</p>	 <p>4-HydroxyPhenol</p>

<b>Secondary intermediate</b>  (After OH <sup>•</sup> radical attack on benzene ring)	 Succinic acid	 Hydroxy-acetic acid	 Oxamic acid	
<b>End Products</b>	NH <sub>4</sub> <sup>+</sup> , NO <sub>3</sub> <sup>-</sup> , CO <sub>2</sub> , H <sub>2</sub> O			

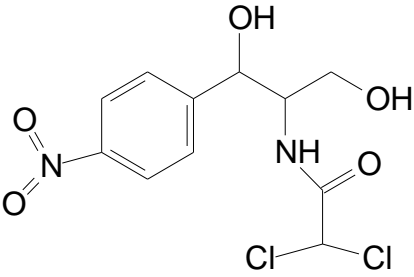
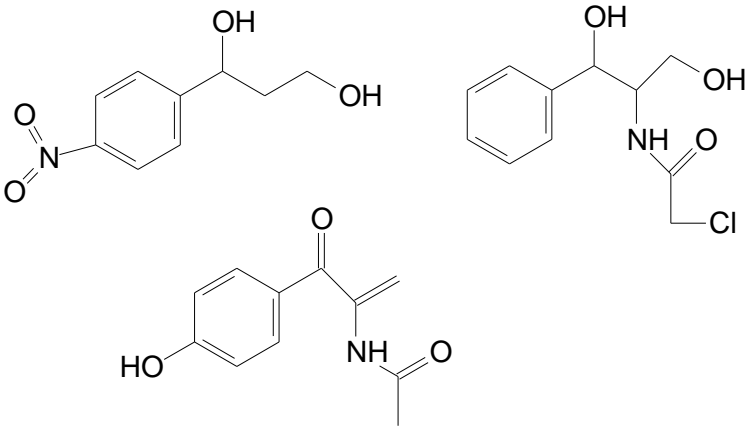
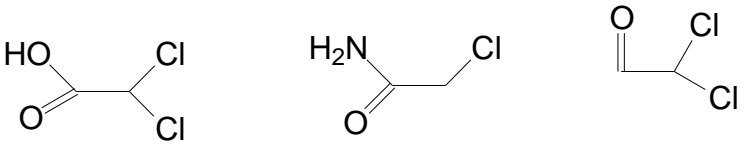
## 2.5.2 Chloramphenicol and its photodegradation intermediate products

Chloramphenicol (CAP) is a chlorinated nitro-aromatic antibiotic. The IUPAC nomenclature of CAP is (2,2-dichloro-N-[(1R,2R)-2-hydroxy-1-(hydroxymethyl)-2-(4-nitrophenyl) ethyl] acetamide). This drug was the first synthetic antibiotic to be applied on a large scale (Liang *et al.*, 2013; Martelli *et al.*, 1991), as an effective antimicrobial. However, owing to the fatal toxicity of CAP and its potential carcinogenicity to humans (Feder & Osier, 2016), the US Food and Drug Administration (USFDA) banned its use in food-producing animals (Martelli *et al.*, 1991). Despite this restriction, CAP is still used in low-income countries due to its low production cost and wide availability (Liang *et al.*, 2013). In Asian countries including China, CAP concentrations ranging 26–2430 ngL<sup>-1</sup> in the influent and 3–1050 ngL<sup>-1</sup> in the effluent of sewage treatment plants were noted (Peng *et al.*, 2006; Xu *et al.*, 2007; Minh *et al.*, 2009; Leung *et al.*, 2012). On exposure, CAP resistant bacteria/genes have been found in numerous water streams (Xi *et al.*, 2009; Zhang *et al.*, 2009; Parsley *et al.*, 2010). However, photocatalytic degradation has been applied as a remediation method to remove CAP from aqueous medium.

The chemistry of photodegradation products using TiO<sub>2</sub> photocatalyst suggests that CAP in water under irradiation undergoes oxidation, reduction and condensation reactions (Shih, 1971). The common identified intermediates of CAP photodegradation are illustrated in **Table 2.5**. These intermediates include aromatic compounds such as p-nitro benzaldehyde, p-nitrobenzoic acid, 4,4-azoxybenzoic acid and p-aminophenyl-2-acetamido-1,3-propnediol. Identified intermediates also include aliphatic acids such as hydrochloric acid and the final products (CO<sub>2</sub> and H<sub>2</sub>O).

The mechanism of the photo-degradation of pharmaceutical using  $\text{TiO}_2$  catalysts shows that  $\text{OH}^{\bullet}$  radicals attack the phenyl ring to yield aromatic intermediates (Kaur *et al.*, 2016; Thi & Lee, 2017). In the case of chloramphenicol, it breaks down to form intermediate molecules such as Indole-3-lactic acid ( $\text{C}_{11}\text{H}_{11}\text{NO}_3$ ) and Dihydroxylphenylalanine ( $\text{C}_9\text{H}_{11}\text{NO}_4$ ) (Gao *et al.*, 2017). The phenyl rings in these compounds subsequently break up to give malonic acid and other short-chain aliphatic molecules such as chloroacetamide ( $\text{C}_2\text{H}_4\text{ClNO}$ ) as presented in Table 2.5.

**Table 2.5:** Chloramphenicol photodegradation intermediates and products

<b>Chloramphenicol</b>  (Before $\text{OH}^{\bullet}$ radicals attack)	
<b>Primary intermediate</b>  (After $\text{OH}^{\bullet}$ radicals attack on CAP)	
<b>Secondary intermediate</b>  (After $\text{OH}^{\bullet}$ radical attack on a benzene ring)	
<b>End products</b>	$\text{NH}_4$ , $\text{HCl}$ , $\text{CO}_2$ , $\text{H}_2\text{O}$



## Conclusion

Chapter 2 discussed the significance of modified TiO<sub>2</sub> photocatalyst with a focus on polymer-TiO<sub>2</sub> nanocomposite for water purification and remediation. Quite many other studies have focused on the development of a new TiO<sub>2</sub> based photocatalyst that can utilise visible light. The limitations of bare TiO<sub>2</sub> to UV light absorption ability and its high recombination rate of photo-generated electron and hole, necessitated this development of polymer-TiO<sub>2</sub> composites. It is of great interest to discover a new technique, which utilises the optical and electronic properties of polymer-TiO<sub>2</sub> materials to overcome the prevailing limitation of TiO<sub>2</sub>, by forming a composite with a polymer-TiO<sub>2</sub> interface. The coupling of TiO<sub>2</sub> with various polymer materials has significantly enhanced the visible light absorption of TiO<sub>2</sub> photocatalysts. This technique has also improved the concentration of organic pollutants TiO<sub>2</sub> interactions at the surface for a faster reaction, as discussed in the review.

The application of modified TiO<sub>2</sub> photocatalysts, from reported researches, was demonstrated to significantly reduced the occurrence of pharmaceuticals in wastewater, particularly wastewater for reuse. Although, several of these harmful compounds are not immediately converted into final harmless products since other potentially harmful intermediates are formed during catalysis. However, continuous irradiation in the presence of the photocatalysts under steady state conditions used, has been reported to result in complete mineralisation of the by-products of the pharmaceutical organic pollutants in the aqueous phase. Hence, three distinctive stages were identified during photocatalytic degradation of pharmaceuticals, using paracetamol and chloramphenicol as models. These stages include the formation of primary intermediates, which mostly are aromatic organic compounds. The second stage is the formation of secondary intermediates, which are basically aliphatic organic compounds. The final stage is the formation of the end products such as CO<sub>2</sub>, H<sub>2</sub>O and other ionic inorganic by-products. However, little or no studies have been carried out on the modification of TiO<sub>2</sub> and other photocatalysts by coupling them with poly-conjugated molecules (Polyene) and their application in the removal of pharmaceutical contaminants, hence, this study.

## References

- ABDEL-WAHAB, A.M., AL-SHIRBINI, A.S., MOHAMED, O., & NASR, O. 2017. Photocatalytic degradation of paracetamol over magnetic flower-like  $\text{TiO}_2/\text{Fe}_2\text{O}_3$  core-shell nanostructures. *J. Photochem. Photobio. A: Chemistry*, 347, 186–198.
- AHMED, M.J. 2017. Adsorption of non-steroidal anti-inflammatory drugs from aqueous solution using activated carbons: Review. *J.f Environ. Man.*, 190, 274–282.
- AKPAN, U.G. & HAMEED, B.H. 2009. Parameters affecting the photocatalytic degradation of dyes using  $\text{TiO}_2$ -based photocatalysts: A review. *J. Haz. Mat.*, 170 (2–3), 520–529.
- AL-HAMDI, A.M., RINNER, U., & SILLANPÄÄ, M. 2017. Tin dioxide as a photocatalyst for water treatment: A review. *Proc. Saf. Environ. Prot.*, 107, 190–205.
- AL-HAMDI, A.M., SILLANPÄÄ, M., & DUTTA, J. 2015. Photocatalytic degradation of phenol by iodine doped tin oxide nanoparticles under UV and sunlight irradiation. *J. All. Comp.*, 618, 366–371.
- AL-ODAINI, N.A., ZAKARIA, M.P., YAZIZ, M.I., SURIF, S. & ABDULGHANI, M. 2011. The occurrence of human pharmaceuticals in wastewater effluents and surface water of Langat River and its tributaries, Malaysia. *International J. Environ. Anal. Chem.*, 7319 (February 2015), 1–20.
- ALHAJI, M.H., SANAULLAH, K., KHAN, A., HAMZA, A., MUHAMMAD, A., ISHOLA, M.S., RIGIT, A.R.H., & BHAWANI, S.A. 2017. Recent developments in immobilizing titanium dioxide on supports for degradation of organic pollutants in wastewater- A review. *International J. Environ. Sci. Tech.* 14 (9), 2039–2052.
- ALI, F., KHAN, S.B., KAMAL, T., ALAMRY, K.A., & ASIRI, A.M. 2018. Chitosan-titanium oxide fibers supported zero-valent nanoparticles: Highly efficient and easily retrievable catalyst for the removal of organic pollutants. *Sci. Rep.* 8 (1), 1–18.

- An, T., Yang, H., Li, G., Song, W., Cooper, W.J., & Nie, X. 2010. Kinetics and mechanism of advanced oxidation processes (AOPs) in degradation of ciprofloxacin in water. *Appl. Catal. B: Environ.*, 94 (3–4), 288–294.
- ANANPATTARACHAI, J., SERAPHIN, S., & KAJITVICHYANUKUL, P. 2016. Formation of hydroxyl radicals and kinetic study of 2-chlorophenol photocatalytic oxidation using C-doped TiO<sub>2</sub>, N-doped TiO<sub>2</sub>, and C,N Co-doped TiO<sub>2</sub> under visible light. *Environ. Sci. Poll. Res.*, 23 (4), 3884–3896.
- ANTUNES, S.C., FREITAS, R., FIGUEIRA, E., GONÇALVES, F., AND NUNES, B., 2013. Biochemical effects of acetaminophen in aquatic species: Edible clams *Venerupis decussata* and *Venerupis philippinarum*. *Environ.Sci. Poll. Res.*, 20 (9), 6658–6666.
- ASHFAQ, M., NAWAZ KHAN, K., SAIF UR REHMAN, M., MUSTAFA, G., FAIZAN NAZAR, M., SUN, Q., IQBAL, J., MULLA, S.I., & YU, C.P. 2017. Ecological risk assessment of pharmaceuticals in the receiving environment of pharmaceutical wastewater in Pakistan. *Ecotox. Environ. Saf.* 136 (November 2016), 31–39.
- ATUL, W., GAIKWARD, G., DONDHE, M., & KHATY, N. 2013. Removal of organic pollutant from water by heterogeneous photocatalysis: a review. *Res. J. Chem. Environ.*, 17 (September), 84–94.
- AUGUGLIARO, V., BELLARDITA, M., LODDO, V., PALMISANO, G., PALMISANO, L., & YURDAKAL, S. 2012. Overview on oxidation mechanisms of organic compounds by TiO<sub>2</sub> in heterogeneous photocatalysis. *J. Photochem. Photobio. C: Photochemistry Reviews*, 13 (3), 224–245.
- AUTÓNOMA, U., QUÍMICA, F. DE, CONCORDIA, C.A., & CARMEN, C. 2011. Photocatalytic Degradation of Acetaminophen. *International J. Environ. Res.*, 5 (4), 1071–1078.
- BALAKRISHNA, K., RATH, A., PRAVEENKUMARREDDY, Y., GURUGE, K.S., & SUBEDI, B. 2017. A review of the occurrence of pharmaceuticals and personal care products in Indian water bodies. *Ecotox. Environ. Saf.*, 137, 113–120.
- BEHNAJADY, M.A., MODIRSHAHLA, N., & HAMZAVI, R. 2006. Kinetic study on

- photocatalytic degradation of C.I. Acid Yellow 23 by ZnO photocatalyst. *J. Haz. Mat.*, 133 (1–3), 226–232.
- BIJANZAD, K., TADJARODI, A., MOGHADDASI KHIAMI, M., & AKHAVAN, O. 2015. Microwave-assisted synthesis of bismuth oxybromochloride nanoflakes for visible light photodegradation of pollutants. *Phy. B: Cond. Mat.*, 475, 14–20.
- BOREEN, A.L., ARNOLD, W.A., & MCNEILL, K. 2003. Photodegradation of pharmaceuticals in the aquatic environment: A review. *Aq. Sci.*, 65 (4), 320–341.
- BOUKHATEM, H., KHALAF, H., DJOUADI, L., GONZALEZ, F. V., NAVARRO, R.M., SANTABALLA, J.A., & CANLE, M. 2017. Photocatalytic activity of mont-La (6%)-Cu<sub>0.6</sub>Cd<sub>0.4</sub>S catalyst for phenol degradation under near UV visible light irradiation. *Appl. Catal. B: Environ.*, 211, 114–125.
- BUBACZ, K., KUSIAK-NEJMAN, E., TRYBA, B., & MORAWSKI, A.W. 2013. Investigation of OH radicals formation on the surface of TiO<sub>2</sub>/N photocatalyst at the presence of terephthalic acid solution. Estimation of optimal conditions. *J. Photochem. Photobio. A: Chem.*, 261, 7–11.
- CALAMARI, D., ZUCCATO, E., CASTIGLIONI, S., BAGNATI, R., & FANELLI, R. 2003. Strategic survey of therapeutic drugs in the rivers Po and Lambro in Northern Italy. *Environ. Sci. Tech.* 37 (7), 1241–1248.
- CHEN, P.H. & JENQ, C.H. 1998. Kinetics of photocatalytic oxidation of trace organic compounds over titanium dioxide. *Environ. Int.*, 24 (8), 871–879.
- CHEN, T., ZHANG, Q., XIE, Z., TAN, C., CHEN, P., ZENG, Y., WANG, F., LIU, H., LIU, Y., LIU, G., & LV, W. 2018. Carbon nitride modified hexagonal boron nitride interface as highly efficient blue LED light-driven photocatalyst. *Appl. Catal. B: Environ.*, 238 (100), 410–421.
- CHESHME KHAVAR, A.H., MOUSSAVI, G., & MAHJOUR, A.R. 2018. The preparation of TiO<sub>2</sub>/rGO nanocomposite efficiently activated with UVA/LED and H<sub>2</sub>O<sub>2</sub> for high rate oxidation of acetaminophen: Catalyst characterization and acetaminophen degradation and mineralization. *Appl. Surf. Sci.*, 440, 963–973.

- DAGHRIR, R., DROGUI, P., & ROBERT, D. 2013. Modified TiO<sub>2</sub> for environmental photocatalytic applications: A review. *Ind. Eng. Chem. Res.*, 52 (10), 3581–3599.
- DÍEZ, A.M., MOREIRA, F.C., MARINHO, B.A., ESPÍNDOLA, J.C.A., PAULISTA, L.O., SANROMÁN, M.A., PAZOS, M., BOAVENTURA, R.A.R., & VILAR, V.J.P. 2018. A step forward in heterogeneous photocatalysis: Process intensification by using a static mixer as catalyst support. *Chem. Eng. J.*, 343 (March), 597–606.
- DONG, H., QIANG, Z., HU, J., & QU, J., 2017. Degradation of chloramphenicol by UV/chlorine treatment: Kinetics, mechanism and enhanced formation of halonitromethanes. *Water Res*, 121, 178–185.
- DONG, S., LI, Y., SUN, J., SUN, J., YU, C., & LI, Y. 2014. Facile synthesis of novel ZnO/RGO hybrid nanocomposites with enhanced catalytic performance for visible-light-driven photodegradation of metronidazole. *Mat. Chem. Phys.*, 145 (3), 357–365.
- EIBES, G., LÚ-CHAU, T., FEIJOO, G., MOREIRA, M.T., & LEMA, J.M. 2005. Complete degradation of anthracene by Manganese Peroxidase in organic solvent mixtures. *Enz. Micr. Tech.*, 37 (4), 365–372.
- FAGAN, R., MCCORMACK, D.E., DIONYSIOU, D.D., & PILLAI, S.C. 2016. A review of solar and visible light active TiO<sub>2</sub> photocatalysis for treating bacteria, cyanotoxins and contaminants of emerging concern. *Mat. Sci. Semicon. Pro.*, 42, 2–14.
- FEDER, H.M. & OSIER, C. 2016. Chloramphenicol : A Review of Its Use in Clinical Practice. *Reviews of Infectious Diseases*, 3, (3) 479-491.
- GAO, B., CHEN, W., DONG, S., LIU, J., LIU, T., WANG, L., & SILLANPÄÄ, M. 2017. Polypyrrole/ZnIn<sub>2</sub>S<sub>4</sub> composite photocatalyst for enhanced mineralization of chloramphenicol under visible light. *J. Photochem. Photobio. A: Chem.*, 349, 115–123.
- GHOSH, A., NAYAK, A.K., & PAL, A. 2017. Nano-Particle-Mediated Wastewater

- Treatment: a Review. *Curr. Poll. Rep.*, 3 (1), 17–30.
- HAMMAD, H.M., ZIA, F., BAKHAT, H.F., FAHAD, S., ASHRAF, M.R., WILKERSON, C.J., SHAH, G.M., NASIM, W., KHOSA, I., & SHAHID, M. 2018. Uptake and toxicological effects of pharmaceutical active compounds on maize. *Agric., Ecos. Environ.*, 258, 143–148.
- HASSANI, A., KHATAEE, A., KARACA, S., & FATHINIA, M. 2017. Degradation of mixture of three pharmaceuticals by photocatalytic ozonation in the presence of TiO<sub>2</sub>/montmorillonite nanocomposite: Simultaneous determination and intermediates identification. *J. Environ. Chem. Eng.*, 5 (2), 1964–1976.
- HE, Y., SUTTON, N.B., RIJNAARTS, H.H.H., & LANGENHOFF, A.A.M. 2016. Degradation of pharmaceuticals in wastewater using immobilized TiO<sub>2</sub> photocatalysis under simulated solar irradiation. *Appl. Catal. B: Environ.*, 182, 132–141.
- HERNÁNDEZ-URESTI, D.B., VÁZQUEZ, A., SANCHEZ-MARTINEZ, D., & OBREGÓN, S. 2016. Performance of the polymeric g-C<sub>3</sub>N<sub>4</sub> photocatalyst through the degradation of pharmaceutical pollutants under UV-vis irradiation. *J. Photochem. Photobiol. A: Chem.*, 324, 47–52.
- HOFFMANN, M.R., HOFFMANN, M.R., MARTIN, S.T., CHOI, W., & BAHNEMANN, D.W. 1995. Environmental Applications of Semiconductor Photocatalysis Environmental Applic. Semic. Photocat., 69–96.
- HOU, H., XU, G., TAN, S., & ZHU, Y. 2017. A facile sol-gel strategy for the scalable synthesis of CuFe<sub>2</sub>O<sub>4</sub> nanoparticles with enhanced infrared radiation property: Influence of the synthesis conditions. *Infr. Phy. Tech.*, 85, 261–265.
- IGBERASE, E. & OSIFO, P. 2015. Equilibrium, kinetic, thermodynamic and desorption studies of cadmium and lead by polyaniline grafted cross-linked chitosan beads from aqueous solution. *J. Ind. Eng. Chem.*, 26, 340–347.
- JALLOULI, N., ELGHNIJI, K., TRABELSI, H., & KSIBI, M. 2017. Photocatalytic degradation of paracetamol on TiO<sub>2</sub> nanoparticles and TiO<sub>2</sub>/cellulosic fiber under UV and sunlight irradiation. *Arab. J. Chem.*, 10, S3640–S3645.

- JALLOULI, N., PASTRANA-MARTÍNEZ, L.M., RIBEIRO, A.R., MOREIRA, N.F.F., FARIA, J.L., HENTATI, O., SILVA, A.M.T., & KSIBI, M. 2018. Heterogeneous photocatalytic degradation of ibuprofen in ultrapure water, municipal and pharmaceutical industry wastewaters using a TiO<sub>2</sub>/UV-LED system. *Chem. Eng. J.*, 334 (October 2017), 976–984.
- JIA, Q., WANG, W., ZHAO, J., XIAO, J., LU, L., & FAN, H. 2017. Synthesis and characterization of TiO<sub>2</sub>/polyaniline/graphene oxide bouquet-like composites for enhanced microwave absorption performance. *J. All. Comp.*, 710, 717–724.
- JIN, Q., WANG, H., HU, C., CHEN, Z., & WANG, X. 2018. Effects of NOM on the degradation of chloramphenicol by UV/H<sub>2</sub>O<sub>2</sub> and the characteristics of degradation products. *Separ. Puri. Tech.* 191 (March 2017), 108–115.
- JYOTHI, K.P., YESODHARAN, S., & YESODHARAN, E.P. 2016. Contaminant salts as enhancers of sonocatalytic degradation of organic water pollutants: Effect of concentration, reaction time and adsorption on the efficiency of enhancement and the fate of concurrently formed H<sub>2</sub>O<sub>2</sub>. *J. Environ. Chem. Eng.*, 6 (3), 3574–3589.
- KAUR, A., UMAR, A., & KANSAL, S.K. 2015. Sunlight-driven photocatalytic degradation of non-steroidal anti-inflammatory drug based on TiO<sub>2</sub> quantum dots. *J. Coll. Interf. Sci.*, 459, 257–263.
- KAUR, A., UMAR, A., & KANSAL, S.K. 2016. Heterogeneous photocatalytic studies of analgesic and non-steroidal anti-inflammatory drugs. *Appl. Catal. A: General*, 510, 134–155.
- KHATAEE, A., KIRANŞAN, M., KARACA, S., & SHEYDAEI, M. 2017. Photocatalytic ozonation of metronidazole by synthesized zinc oxide nanoparticles immobilized on montmorillonite. *J. Taiw. Inst. Chem. Eng.* 74, 196–204.
- KIM PHUONG, N.T., BEAK, M. WOOK, HUY, B.T., & LEE, Y.I. 2016. Adsorption and photodegradation kinetics of herbicide 2,4,5-trichlorophenoxyacetic acid with MgFeTi layered double hydroxides. *Chemos.*, 146, 51–59.
- KOSERA, V.S., CRUZ, T.M., CHAVES, E.S., & TIBURTIUS, E.R.L. 2017. Triclosan

- degradation by heterogeneous photocatalysis using ZnO immobilized in biopolymer as catalyst. *J. Photochem. Photobio. A: Chem.*, 344, 184–191.
- KSHIRSAGAR, A.S., GAUTAM, A., & KHANNA, P.K. 2017. Efficient photo-catalytic oxidative degradation of organic dyes using CuInSe<sub>2</sub>/TiO<sub>2</sub> hybrid hetero-nanostructures. *Journal of Photochem. Photobio. A: Chem.*, 349, 73–90.
- KUMAR, S.G. & DEVI, L.G. 2011. Review on modified TiO<sub>2</sub> photocatalysis under UV/visible light: Selected results and related mechanisms on interfacial charge carrier transfer dynamics. *J. Phy./ Chem. A*, 115 (46), 13211–13241.
- LAN, Y., ZHOU, L., TONG, Z., PANG, Q., WANG, F., & GONG, F. 2011. Synthesis and characterization of polythiophene-modified TiO<sub>2</sub> nanotube arrays. *Bull. Mat. Sci.*, 34 (6), 1173–1177.
- LASSOUED, A., LASSOUED, M.S., DKHIL, B., AMMAR, S., & GADRI, A. 2018. Synthesis, photoluminescence and Magnetic properties of iron oxide ( $\alpha$ -Fe<sub>2</sub>O<sub>3</sub>) nanoparticles through precipitation or hydrothermal methods. *Phy. E: Low-Dime. Sys. Nanostr.*, 101, 212–219.
- LEUNG, H.W., MINH, T.B., MURPHY, M.B., LAM, J.C.W., SO, M.K., MARTIN, M., LAM, P.K.S., & RICHARDSON, B.J. 2012. Distribution, fate and risk assessment of antibiotics in sewage treatment plants in Hong Kong, South China. *Environ. Int.*, 42, 1–9.
- LI, H., LI, Y., XIANG, L., HUANG, Q., QIU, J., ZHANG, H., SIVIAIAH, M.V., BARON, F., BARRAULT, J., PETIT, S., & VALANGE, S. 2015. Heterogeneous photo-Fenton decolorization of Orange II over Al-pillared Fe-smectite: Response surface approach, degradation pathway, and toxicity evaluation. *J. Haz. Mat.*, 287, 32–41.
- LI, Q., SU, H., & TAN, T. 2008. Synthesis of ion-imprinted chitosan-TiO<sub>2</sub> adsorbent and its multi-functional performances. *Biochem. Eng. J.*, 38 (2), 212–218.
- LI, S., ZHAO, S., QIANG, S., CHEN, G., CHEN, Y., & CHEN, Y. 2018. A novel zein/poly (propylene carbonate)/nano-TiO<sub>2</sub> composite films with enhanced photocatalytic and antibacterial activity. *Proc. Biochem.*, 70, 198–205.



- LI, W.C. 2014. Occurrence, sources, and fate of pharmaceuticals in aquatic environment and soil. *Environ. Poll.*, 187, 193–201.
- LI, X., WANG, G., LI, X., & LU, D. 2004. Surface properties of polyaniline/nano-TiO<sub>2</sub>composites. *Appl.Surf. Sci.*, 229 (1–4), 395–401.
- LIANG, B., CHENG, H.Y., KONG, D.Y., GAO, S.H., SUN, F., CUI, D., KONG, F.Y., ZHOU, A.J., LIU, W.Z., REN, N.Q., WU, W.M., WANG, A.J., & LEE, D.J. 2013. Accelerated reduction of chlorinated nitroaromatic antibiotic chloramphenicol by biocathode. *Environ. Sci. Tech.*, 47 (10), 5353–5361.
- LIN, Y.-Y., CHU, T.-H., LI, S.-S., CHUANG, C.-H., CHANG, C.-H., SU, W.-F., CHANG, C.-P., CHU, M.-W., & CHEN, C.-W. 2009. Interfacial Nanostructuring on the Performance of Polymer / TiO<sub>2</sub> Nanorod Bulk Heterojunction Solar Cells. *J. Am. Chem. Soc.*, 131 (13), 3644–3649.
- LIU, P., ZHANG, H., FENG, Y., YANG, F., & ZHANG, J. 2014. Removal of trace antibiotics from wastewater: A systematic study of nanofiltration combined with ozone-based advanced oxidation processes. *Chem. Eng. J.*, 240, 211–220.
- LIU, X., ZHOU, Y., ZHANG, J., LUO, L., YANG, Y., HUANG, H., PENG, H., TANG, L., & MU, Y. 2018. Insight into electro-Fenton and photo-Fenton for the degradation of antibiotics: Mechanism study and research gaps. *Chem. Eng. J.*, 347, 379–397.
- LIU, Y., WEI, S., & GAO, W. 2015. Ag/ZnO heterostructures and their photocatalytic activity under visible light: Effect of reducing medium. *J. Haz. Mat.*, 287, 59–68.
- LOAIZA-AMBULUDI, S., PANIZZA, M., OTURAN, N., AND OTURAN, M.A. 2014. Removal of the anti-inflammatory drug ibuprofen from water using homogeneous photocatalysis. *Catal. Today*, 224, 29–33.
- LÓPEZ ZAVALA, M.Á. & ESTRADA, E.E. 2016. Degradation of acetaminophen and its transformation products in aqueous solutions by using an electrochemical oxidation cell with stainless steel electrodes. *Water (Switzerland)*, 8 (9), 1–12.
- MA, J. & CHEN, K. 2018. Silica-free hydrothermal synthesis of  $\epsilon$ -Fe<sub>2</sub>O<sub>3</sub> nanoparticles

- and their oriented attachment to nanoflakes with unique magnetism evolution. *Ceram. Int.*, 44 (16), 19338–19344.
- MAGUREANU, M., MANDACHE, N.B., & PARVULESCU, V.I. 2015. Degradation of pharmaceutical compounds in water by non-thermal plasma treatment. *Water Res.*, 81, 124–136.
- MANZO, V., HONDA, L., NAVARRO, O., ASCAR, L., & RICHTER, P. 2014. Microextraction of non-steroidal anti-inflammatory drugs from waste water samples by rotating-disk sorptive extraction. *Talan.* 128, 486–492.
- MARSONI, M., DE MATTIA, F., LABRA, M., BRUNO, A., BRACALE, M., & VANNINI, C. 2014. Uptake and effects of a mixture of widely used therapeutic drugs in *Eruca sativa* L. and *Zea mays* L. plants. *Ecotox. Environ. Saf.*, 108, 52–57.
- MARTELLI, A., MATTIOLI, F., PASTORINO, G., ROBBIANO, L., ALLAVENA, A., & BRAMBILLA, G. 1991. Genotoxicity testing of chloramphenicol in rodent and human cells. *Mut. Res./Genet. Tox.*, 260 (1), 65–72.
- MEZOHEGYI, G., GONÇALVES, F., ÓRFÃO, J.J.M., FABREGAT, A., FORTUNY, A., FONT, J., BENGIOA, C., & STUBER, F. 2010. Tailored activated carbons as catalysts in biodecolourisation of textile azo dyes. *Appl. Catal. B: Environ.*, 94 (1–2), 179–185.
- MINH, T.B., LEUNG, H.W., LOI, I.H., CHAN, W.H., SO, M.K., MAO, J.Q., CHOI, D., LAM, J.C.W., ZHENG, G., MARTIN, M., LEE, J.H.W., LAM, P.K.S., & RICHARDSON, B.J. 2009. Antibiotics in the Hong Kong metropolitan area: Ubiquitous distribution and fate in Victoria Harbour. *Mar. Poll. Bull.*, 58 (7), 1052–1062.
- MIRZAEI, A., CHEN, Z., HAGHIGHAT, F., & YERUSHALMI, L., 2016. Removal of pharmaceuticals and endocrine disrupting compounds from water by zinc oxide-based photocatalytic degradation: A review. *Sust. Cities Soc.*, 27, 407–418.
- MOCTEZUMA, E., LEYVA, E., AGUILAR, C.A., LUNA, R.A., & MONTALVO, C., 2012. Photocatalytic degradation of paracetamol: Intermediates and total reaction mechanism. *J. Haz. Mat.*, 243, 130–138.

- MOHAPATRA, L. & PARIDA, K.M., 2012. Zn–Cr layered double hydroxide: Visible light responsive photocatalyst for photocatalytic degradation of organic pollutants. *Sep Purif Te. Separ. Puri. Tech.*, 91, 73–80.
- MUXIKA, A., ETXABIDE, A., URANGA, J., GUERRERO, P., & DE LA CABA, K. 2017. Chitosan as a bioactive polymer: Processing, properties and applications. *Int. J. Bio. Macro.*, 105, 1358–1368.
- NASIRIAN, M., LIN, Y.P., BUSTILLO-LECOMPTE, C.F., & MEHRVAR, M. 2018. Enhancement of photocatalytic activity of titanium dioxide using non-metal doping methods under visible light: a review. *Int. J. Environ. Sci. Tech.*, 15 (9), 2009–2032.
- NASSAR, M.Y., AHMED, I.S., & SAMIR, I. 2014. A novel synthetic route for magnesium aluminate ( $\text{MgAl}_2\text{O}_4$ ) nanoparticles using sol-gel auto combustion method and their photocatalytic properties. *Spectrochimica Acta - Part A: Molec. Biomol. Spec.*, 131, 329–334.
- OLALEYE, M.T. & ROCHA, B.T.J. 2008. Acetaminophen-induced liver damage in mice: Effects of some medicinal plants on the oxidative defense system. *Experi. Toxi.Path.*, 59 (5), 319–327.
- OSEGHE, E.O. & OFOMAJA, A.E. 2018. Facile microwave synthesis of pine cone derived C-doped  $\text{TiO}_2$  for the photodegradation of tetracycline hydrochloride under visible-LED light. *J. Environ. Manag.*, 223, 860–867.
- OTURAN, M.A. & AARON, J.J. 2014. Advanced oxidation processes in water/wastewater treatment: Principles and applications. A review. *Critical Reviews in Environ. Sci. Tech.*, 44 (23), 2577–2641.
- PARSLEY, L.C., CONSUEGRA, E.J., KAKIRDE, K.S., LAND, A.M., HARPER, W.F., & LILES, M.R. 2010. Identification of diverse antimicrobial resistance determinants carried on bacterial, plasmid, or viral metagenomes from an activated sludge microbial assemblage. *Appl. Environ. Microbio.*, 76 (11), 3753–3757.
- PENG, X., WANG, Z., KUANG, W., TAN, J., & LI, K. 2006. A preliminary study on

- the occurrence and behavior of sulfonamides, ofloxacin and chloramphenicol antimicrobials in wastewaters of two sewage treatment plants in Guangzhou, China. *Science of The Total Environ.* 371 (1–3), 314–322.
- PERA-TITUS, M., GARCÍA-MOLINA, V., BAÑOS, M.A., GIMÉNEZ, J., & ESPLUGAS, S. 2004. Degradation of chlorophenols by means of advanced oxidation processes: a general review. *Appl. Catal. B: Environ.*, 47 (4), 219–256.
- QIAO, X., ZHENG, X., XIE, Q., YANG, X., XIAO, J., XUE, W., & CHEN, J. 2014. Faster photodegradation rate and higher dioxin yield of triclosan induced by cationic surfactant CTAB. *J. Haz. Mat.*, 275, 210–214.
- QIN, W., SONG, Y., DAI, Y., QIU, G., REN, M., & ZENG, P. 2015. Treatment of berberine hydrochloride pharmaceutical wastewater by O<sub>3</sub>/UV/H<sub>2</sub>O<sub>2</sub> advanced oxidation process. *Environ. Ear. Sci.*, 73 (9), 4939–4946.
- QIU, J., ZHANG, X., FENG, Y., ZHANG, X., WANG, H., & YAO, J. 2018. Modified metal-organic frameworks as photocatalysts. *Appl. Catal. B: Environ.*, 231, 317–342.
- SAUD, P.S., PANT, B., ALAM, A.-M., GHOURI, Z.K., PARK, M., & KIM, H.-Y. 2015. Carbon quantum dots anchored TiO<sub>2</sub> nanofibers: Effective photocatalyst for waste water treatment. *Ceram. Int.*, 41 (9), 11953–11959.
- SCHARTEL, B., DITTRICH, B., WARTIG, K., HOFMANN, D., & ROLF, M. 2015. The influence of layered, spherical, and tubular carbon nanomaterials' concentration on the flame retardancy of polypropylene. *Polym. Compos.*, 2 (36), 1230–1241.
- SHIH, I.K. 1971. Photodegradation products of chloramphenicol in aqueous solution. *J. Pharm. Sci.* 60 (12), 1889–1890.
- SHOKRI, A., MAHANPOOR, K., & SOODBAR, D. 2016. Evaluation of a modified TiO<sub>2</sub>(GO-B-TiO<sub>2</sub>) photo catalyst for degradation of 4-nitrophenol in petrochemical wastewater by response surface methodology based on the central composite design. *J. Environ. Chem. Eng.*, 4 (1), 585–598.
- SIRÉS, I. & BRILLAS, E. 2012. Remediation of water pollution caused by

- pharmaceutical residues based on electrochemical separation and degradation technologies: A review. *Environ. Int.* 40 (1), 212–229.
- SLAMANI, S., ABDELMALEK, F., GHEZZAR, M.R., & ADDOU, A. 2018. Initiation of Fenton process by plasma gliding arc discharge for the degradation of paracetamol in water. *J. Photochem. Photobio. A: Chem.*, 359, 1–10.
- ŠOJIĆ-MERKULOV, D. V., DESPOTOVIĆ, V.N., BANIĆ, N.D., ARMAKOVIĆ, S.J., FINČUR, N.L., LAZAREVIĆ, M.J., ČETOJEVIĆ-SIMIN, D.D., ORČIĆ, D.Z., RADOIČIĆ, M.B., ŠAPONJIĆ, Z. V., ČOMOR, M.I., & ABRAMOVIĆ, B.F. 2018. Photocatalytic decomposition of selected biologically active compounds in environmental waters using TiO<sub>2</sub>/polyaniline nanocomposites: Kinetics, toxicity and intermediates assessment. *Environ. Pollu.*, 239, 457–465.
- SOON, A.N. & HAMEED, B.H. 2011. Heterogeneous catalytic treatment of synthetic dyes in aqueous media using Fenton and photo-assisted Fenton process. *Desalination*, 269 (1–3), 1–16.
- SUN, L., SHI, Y., LI, B., LI, X., & WANG, Y. 2013. Preparation and Characterization of Polypyrrole / TiO<sub>2</sub> nanocomposites by reverse microemulsion polymerization and its photocatalytic activity for the degradation of methyl orange under natural Light. *Polym. compo.*, 34 (7); 1076-1080.
- TALANE, T.E., MBULE, P.S., NOTO, L.L., SHINGANGE, K., MHLONGO, G.H., MOTHUDI, B.M., & DHLAMINI, M.S. 2018. Sol-gel preparation and characterization of Er<sup>3+</sup>doped TiO<sub>2</sub> luminescent nanoparticles. *Mat. Res. Bull.*, 108, 234–241.
- TAN, K.B., ABDULLAH, A.Z., HORRI, B.A., & SALAMATINIA, B. 2016. Adsorption mechanism of microcrystalline cellulose as green adsorbent for the removal of cationic methylene blue dye. *J. Chem. Soc. Pak*, 38 (04), 651-659.
- TEH, C.Y., WU, T.Y., & JUAN, J.C., 2017. An application of ultrasound technology in synthesis of titania-based photocatalyst for degrading pollutant. *Chem. Eng. J.*, 317, 586–612.
- THI, V.H.T. & LEE, B.K. 2017. Effective photocatalytic degradation of paracetamol

- using La-doped ZnO photocatalyst under visible light irradiation. *Mat. Res. Bull.*, 96, 171–182.
- TIWARI, B., SELLAMUTHU, B., OUARDA, Y., DROGUI, P., TYAGI, R.D., & BUELNA, G. 2017. Review on fate and mechanism of removal of pharmaceutical pollutants from wastewater using biological approach. *Biores. Tech.*, 224, 1–12.
- TOBAJAS, M., BELVER, C., & RODRIGUEZ, J.J. 2017. Degradation of emerging pollutants in water under solar irradiation using novel TiO<sub>2</sub>-ZnO/clay nanoarchitectures. *Chem. Eng. J.*, 309, 596–606.
- TONG, H., ZHAN, X., TIAN, X., LI, J., QIAN, D., & WU, D. 2018. Understanding the energy level matching relationships between semiconductor photocatalysts and organic pollutants for effective photocatalytic degradations. *J. Coll. Interf. Sci.*, 526, 384–391.
- TRANDAFILOVIĆ, L.V., JOVANOVIĆ, D.J., ZHANG, X., PTASIŃSKA, S., & DRAMIĆANIN, M.D. 2017. Enhanced photocatalytic degradation of methylene blue and methyl orange by ZnO: Eu nanoparticles. *Appl. Catal. B: Environ.*, 203, 740–752.
- TURCHI, C.S. & OLLIS, D.F. 1990. Photocatalytic degradation of organic water contaminants: Mechanisms involving hydroxyl radical attack. *J. Catal.*, 122 (1), 178–192.
- UNNI, M., UHL, A.M., SAVLIWALA, S., SAVITZKY, B.H., DHAVALIKAR, R., GARRAUD, N., ARNOLD, D.P., KOURKOUTIS, L.F., ANDREW, J.S., & RINALDI, C. 2017. Thermal Decomposition Synthesis of Iron Oxide Nanoparticles with Diminished Magnetic Dead Layer by Controlled Addition of Oxygen. *ACS Nano.*, 11 (2), 2284–2303.
- WANG, J., LI, J., LI, H., DUAN, S., MENG, S., FU, X., & CHEN, S. 2017a. Crystal phase-controlled synthesis of BiPO<sub>4</sub> and the effect of phase structure on the photocatalytic degradation of gaseous benzene. *Chem. Eng. J.*, 330, 433–441.
- WANG, Y., JAMAL, R., WANG, M., YANG, L., LIU, F., & ABDIRYIM, T. 2017b. A

- donor–acceptor–donor-type conjugated polymer-modified TiO<sub>2</sub> with enhanced photocatalytic activity under simulated sunlight and natural sunlight. *J. Mat. Sci.*, 52 (9), 4820–4832.
- WANKHADE ATUL, V., GAIKWAD, G.S., DHONDE, M.G., KHATY, N.T., & THAKARE, S.R. 2013. Removal of organic pollutant from water by heterogenous photocatalysis: A review. *Research J. Chem. Environ.*, 17 (1), 84–94.
- WIĄCEK, A.E., GOZDECKA, A., & JURAK, M. 2018. Physicochemical Characteristics of Chitosan-TiO<sub>2</sub> Biomaterial. 1. Stability and Swelling Properties. *Ind. Eng. Chem. Res.*, 57 (6), 1859–1870.
- XI, C., ZHANG, Y., MARRS, C.F., YE, W., SIMON, C., FOXMAN, B., & NRIAGU, J. 2009. Prevalence of antibiotic resistance in drinking water treatment and distribution systems. *Appl. Environ. Microbio.*, 75 (17), 5714–5718.
- XIANG, Q., YU, J., & JARONIEC, M. 2012. Synergetic effect of MoS<sub>2</sub> and graphene as cocatalysts for enhanced photocatalytic H<sub>2</sub> production activity of TiO<sub>2</sub> nanoparticles. *J. Ame. Chem. Soc.*, 134 (15), 6575–6578.
- XU, B., DING, T., ZHANG, Y., WEN, Y., YANG, Z., & ZHANG, M. 2017. A new efficient visible-light-driven composite photocatalyst comprising ZnFe<sub>2</sub>O<sub>4</sub> nanoparticles and conjugated polymer from the dehydrochlorination of polyvinyl chloride. *Mat. Lett.*, 187, 123–125.
- XU, S., GU, L., WU, K., YANG, H., SONG, Y., JIANG, L., & DAN, Y. 2012. The influence of the oxidation degree of poly(3-hexylthiophene) on the photocatalytic activity of poly(3-hexylthiophene)/TiO<sub>2</sub> composites. *Sol. Ener. Mat. Sol. Cells*, 96, 286–291.
- XU, W., ZHANG, G., ZOU, S., LI, X., & LIU, Y. 2007. Determination of selected antibiotics in the Victoria Harbour and the Pearl River, South China using high-performance liquid chromatography-electrospray ionization tandem mass spectrometry. *Environ. Poll.*, 145 (3), 672–679.
- YAN, C., YANG, Y., ZHOU, J., LIU, M., NIE, M., SHI, H., & GU, L. 2013. Antibiotics

- in the surface water of the Yangtze Estuary: Occurrence, distribution and risk assessment. *Environ. Poll.*, 175, 22–29.
- YANG, H., CHEN, F., JIAO, Y., & ZHANG, J. 2013. The role of interfacial lattice Ag<sup>+</sup> on titania based photocatalysis. *Appl. Catal. B: Environ.*, 130–131, 218–223.
- YANG, L., YU, L.E., & RAY, M.B. 2008. Degradation of paracetamol in aqueous solutions by TiO<sub>2</sub> photocatalysis. *Water res.* 42, 3480–3488.
- YAO, B., PENG, C., ZHANG, W., ZHANG, Q., NIU, J., & ZHAO, J. 2015. A novel Fe(III) porphyrin-conjugated TiO<sub>2</sub> visible-light photocatalyst. *Appl. Catal. B: Environ.*, 174–175, 77–84.
- YU, T.H., LIN, A.Y.C., PANCHANGAM, S.C., HONG, P.K.A., YANG, P.Y., & LIN, C.F. 2011. Biodegradation and bio-sorption of antibiotics and non-steroidal anti-inflammatory drugs using immobilized cell process. *Chemos.*, 84 (9), 1216–1222.
- ZEGHIOUD, H., KHELLAF, N., DJELAL, H., AMRANE, A., & BOUHELASSA, M. 2016. Photocatalytic Reactors Dedicated to the Degradation of Hazardous Organic Pollutants: Kinetics, Mechanistic Aspects, and Design – A Review. *Chem. Eng. Comm.*, 203 (11), 1415–1431.
- ZHANG, G., CHEN, L., FU, X., & WANG, H. 2018. Cellulose Microfiber-Supported TiO<sub>2</sub>@Ag Nanocomposites: A Dual-Functional Platform for Photocatalysis and in Situ Reaction Monitoring. *Industrial and Eng. Chem. Res.*, 57 (12), 4277–4286.
- ZHANG, G., KIM, G., & CHOI, W. 2014. Visible light driven photocatalysis mediated via ligand-to-metal charge transfer (LMCT): an alternative approach to solar activation of titania. *Ener. Environ. Sci.*, 7 (3), 954.
- ZHANG, L. & JARONIEC, M. 2018. Toward designing semiconductor-semiconductor heterojunctions for photocatalytic applications. *Appl. Surf. Sci.*, 430, 2–17.
- ZHANG, L., LI, L., MOU, Z., & LI, X. 2012. Study on microstructure and catalytic performance of B, C, N co-doped TiO<sub>2</sub>. *Procedia Eng.*, 27, 552–556.



- ZHANG, X.X., ZHANG, T., & FANG, H.H.P. 2009. Antibiotic resistance genes in water environment. *Appl. Microbio. Biotech.*, 82 (3), 397–414.
- ZHANG, Y., CHEN, J., HUA, L., LI, S., ZHANG, X., SHENG, W., & CAO, S. 2017. High photocatalytic activity of hierarchical  $\text{SiO}_2$  @C-doped  $\text{TiO}_2$  hollow spheres in UV and visible light towards degradation of rhodamine B. *J. Haz. Mat.*, 340, 309–318.
- ZHAO, J., JI, M., DI, J., GE, Y., ZHANG, P., XIA, J., & LI, H. 2017a. Synthesis of g- $\text{C}_3\text{N}_4/\text{Bi}_4\text{O}_5\text{Br}_2$  via reactable ionic liquid and its cooperation effect for the enhanced photocatalytic behavior towards ciprofloxacin degradation. *J. Photochem. Photobio. A: Chem.*, 347, 168–176.
- ZHAO, Y., TAO, C., XIAO, G., & SU, H. 2017b. Controlled synthesis and wastewater treatment of  $\text{Ag}_2\text{O}/\text{TiO}_2$  modified chitosan-based photocatalytic film. *RSC Advances*, 7 (18), 11211–11221.
- ZHAO, Y., WANG, Y., XIAO, G., & SU, H. 2019. Fabrication of biomaterial/ $\text{TiO}_2$  composite photocatalysts for the selective removal of trace environmental pollutants. *Chin. J. Chem. Eng.*, 27(6):1416-1428.
- ZIYLAN-YAVAŞ, A. & INCE, N.H. 2018. Catalytic ozonation of paracetamol using commercial and Pt-supported nanocomposites of  $\text{Al}_2\text{O}_3$ : The impact of ultrasound. *Ultraso. Sonochem*, 40, 175–182.
- ZUORRO, A., FIDALEO, M., FIDALEO, M., & LAVECCHIA, R. 2014. Degradation and antibiotic activity reduction of chloramphenicol in aqueous solution by UV/ $\text{H}_2\text{O}_2$  process. *J. Environ. Manag.*, 133, 302–308.

### **Chapter 3: Materials and methods**

This chapter presents materials and methods, the list and properties of the materials used, including the pharmaceutical (model) pollutants and the materials used for the synthesis of the catalysts. The overview of all the experimental methodologies is clearly stated. The synthetic methods, different analytical techniques used for the characterisation of the catalytic materials and the analysis of sample solutions are detailed. Finally, the various experimental designs and set-ups in the study are described and their operational parameters are detailed.

## TABLE OF CONTENTS

<b>CHAPTER 3: MATERIALS AND METHODS.....</b>	<b>65</b>
3.1 PHOTOCATALYTIC MATERIALS AND MODEL PHARMACEUTICALS.....	69
3.1.1 Acetaminophen (paracetamol).....	67
3.1.2 Chloramphenicol .....	67
3.2 MATERIALS AND METHODS FOR EXPERIMENTAL STUDIES.....	69
3.2.1 Synthesis of titania (TiO <sub>2</sub> ) nanoparticles .....	69
3.2.2 Thermal dehydration of polyvinyl alcohol (PVA).....	70
3.2.3 Preparation of polyene from polyvinyl alcohol (PVA).....	71
3.2.4 Synthesis of conjugated polyene/titania (CPE-TiO <sub>2</sub> ) nanoparticles.....	72
3.3 ANALYTICAL TECHNIQUES AND EQUIPMENT .....	72
3.3.1 Characterisation of synthesised materials.....	72
3.3.2 Analytical monitoring techniques for solutions .....	75
3.3.2.1 UV-Vis spectroscopy.....	75
3.3.2.2 High-performance liquid chromatography (HPLC).....	75
3.4 PHOTOCATALYTIC DEGRADATION EXPERIMENTS.....	77
3.4.1 Photoreactor.....	77
3.4.2 Photocatalytic procedures.....	77
3.4.3 Preparation of solutions .....	79
3.4.4 Optimisation of photocatalysis parameters .....	79
3.4.5 Preliminary experimental design .....	80
3.4.5.1 Investigation of effects of pH.....	80
3.4.5.2 Investigating the effects of initial concentrations.....	81
3.4.5.3 Investigation of catalyst loading .....	81
3.4.6 Photocatalytic activities of modified and unmodified TiO <sub>2</sub> catalysts compared.....	81
3.4.7 Total organic carbon (TOC) measurement during photodegradation .....	81
3.4.8 The reusability test for the catalyst.....	82
REFERENCES .....	83

### 3.1 Photocatalytic materials and model pharmaceuticals

The study was carried-out with two pharmaceutical pollutants, namely an antibiotic drug, chloramphenicol, and a non-antibiotic drug, acetaminophen (paracetamol).

Visible light was applied for the photodegradation and two different catalytic materials were used to treat these pollutants in an aqueous system via the photocatalytic process. The list of the materials is as follows:

- Titanium IV oxide (TiO<sub>2</sub>),
- Conjugated polyene (CPE) as a modifier and
- CPE-TiO<sub>2</sub>, nanocomposite for photodegradation.

The characteristics, properties and justifications of selecting the two organic compounds as model pollutants used for this study, are presented below.

#### 3.1.1 Acetaminophen (paracetamol)

Acetaminophen, known as paracetamol (APAP), is an analgesic non-antibiotic compound with a unique aromatic structure, selected in this work to represent the family of non-antibiotic pharmaceuticals. Acetaminophen is a common antipyretic drug, which is widely used worldwide in many branded medicine (Thi & Lee, 2017).

The selection of this compound was motivated by its potential health effects from long-term ingestion and overdose as reported in the literature (Slamani *et al.*, 2018). It is one of the most consumed therapeutic compounds around the world, which results in its widespread presence in the environment. However, its overdose can result in fatal liver damage and its toxic effects on microorganisms have been reported elsewhere (Ayanda *et al.*, 2017; López Zavala & Estrada, 2016).

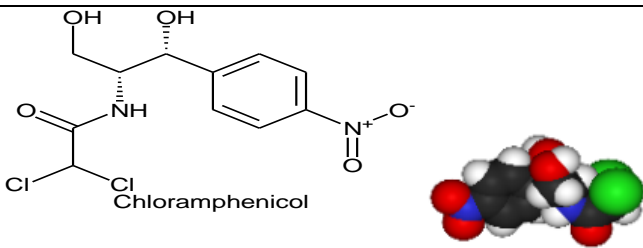
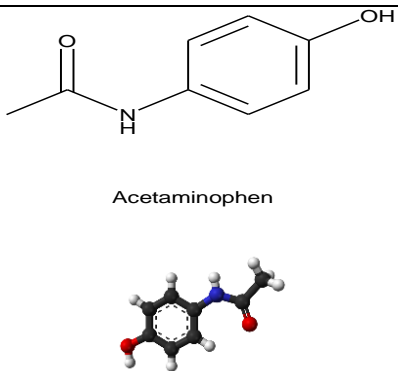
#### 3.1.2 Chloramphenicol

Chloramphenicol is a therapeutic antibiotic compound. It is a phenolic compound that consists of an aromatic ring with various functional groups such as OH (Hydroxyl), Cl (chloro), NO<sub>2</sub>, (nitro) C=O (amide) and NH (secondary amine group).

Due to aquatic toxicity, development of bacteria strains and antimicrobial resistance, antibiotics are problematic emerging pollutants frequently found in the environment (Agarwal *et al.*, 2017). Chloramphenicol, as a model antibiotic organic pollutant, results from its occurrence in the residual waters coming from different pharmaceutical industries and hospital wastewater. It is also one of the most commonly prescribed thus used aromatic antibiotic drugs (Zhang *et al.*, 2010) representing the phenolic group type pharmaceutical. The physicochemical properties of chloramphenicol and paracetamol are summarised in

Table 3.1.

**Table 3.1:** Physicochemical properties of chloramphenicol and acetaminophen

Properties	Chloramphenicol	Acetaminophen (Paracetamol)
IUPAC name	2,2-dichloro-N-[(1R,2R,3-dihydroxyl-1-(4-nitrophenyl) propan-2-yl] acetamide	N-(4-hydroxyphenyl) acetamide
Symbol	CAP	APAP
Molecular formula	$C_{11}H_{12}Cl_2N_2O_5$	$C_8H_9NO_2$
Molecular Weight (g/mol)	323.1320	151.165
Chemical structure	 <p>Chloramphenicol</p>	 <p>Acetaminophen</p>
Water solubility at 25°C (g/L)	2.5	14
Density (g/cm <sup>3</sup> )	1.5	1.3
Elimination	4.0	2.5

Properties	Chloramphenicol	Acetaminophen (Paracetamol)
half-life (h)		
UV-max (nm)	275	250
Boiling point (°C)	Sublimes in high vacuum	>500
Melting point (°C)	105.5	170
Log K <sub>w</sub>	1.14	0.46
PKa	7.49	9.38
Heat stability	Stable (Emits toxic NO <sub>x</sub> when decomposed)	Stable (only under recommended condition)
% Excretion	15% as whole and 75% as metabolites (in Urine)	5% as whole (in Urine)

### 3.2 Materials and methods for experimental studies

All chemicals used in the study were of analytical grade standard, purchased from Sigma Aldrich chemical company in South Africa and applied without further purifications. These include chloramphenicol (>99% purity), paracetamol (>99% purity), 99% hydrolysed polyvinyl chloride (PVA), 98% methanol (CH<sub>3</sub>OH), titanium (IV) isopropoxide (97%), acetonitrile and hydrochloric acid (32%). All reagents were prepared in solutions using milli-Q water from a milliporemilli-Q ultrapure gradient A10 purification system.

#### 3.2.1 Synthesis of titania (TiO<sub>2</sub>) nanoparticles

The sol-gel method was used to obtain pure crystal nanoparticles of titania (TiO<sub>2</sub>) from isopropoxide precursor according to a modified procedure adopted from the literature (Xu *et al.*, 2017).

A 50 ml mixture of methanol and isopropoxide in a ratio of 3:2 was transferred into a 250 ml two necked, round bottom flask fixed with a condenser. The mixture (the sol) is refluxed at about 80°C under rigorous stirring with a magnetic bar stirrer and 10 ml of distilled water was introduced dropwise into the mixture with continuous refluxing and stirring for 8 h to obtain whitish dispersed particles called a gel. The mixture (sol and gel), was transferred into a 400 mL beaker and then set under a homogeniser

stirrer working at 2000 rpm for 20 min and the resulting solution was allowed to seed for 30 min before being taken for centrifugation at 4000 rpm for 10 min. The wet particles were removed and washed three times with ultrapure water and ethanol sequentially and then centrifuged before drying in an oven at 110°C for 2 h to obtain a dried powder. This was further subjected to calcination at 400°C for 3 h. The experimental setup is illustrated in Figure 3.1.

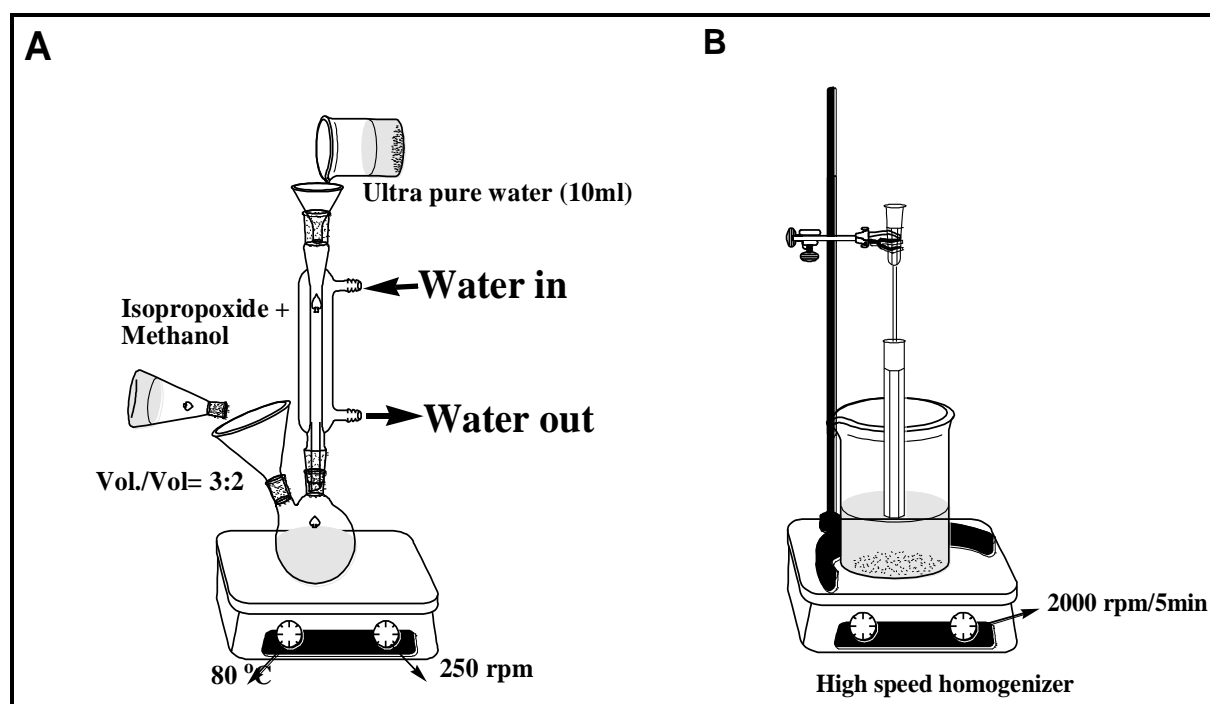
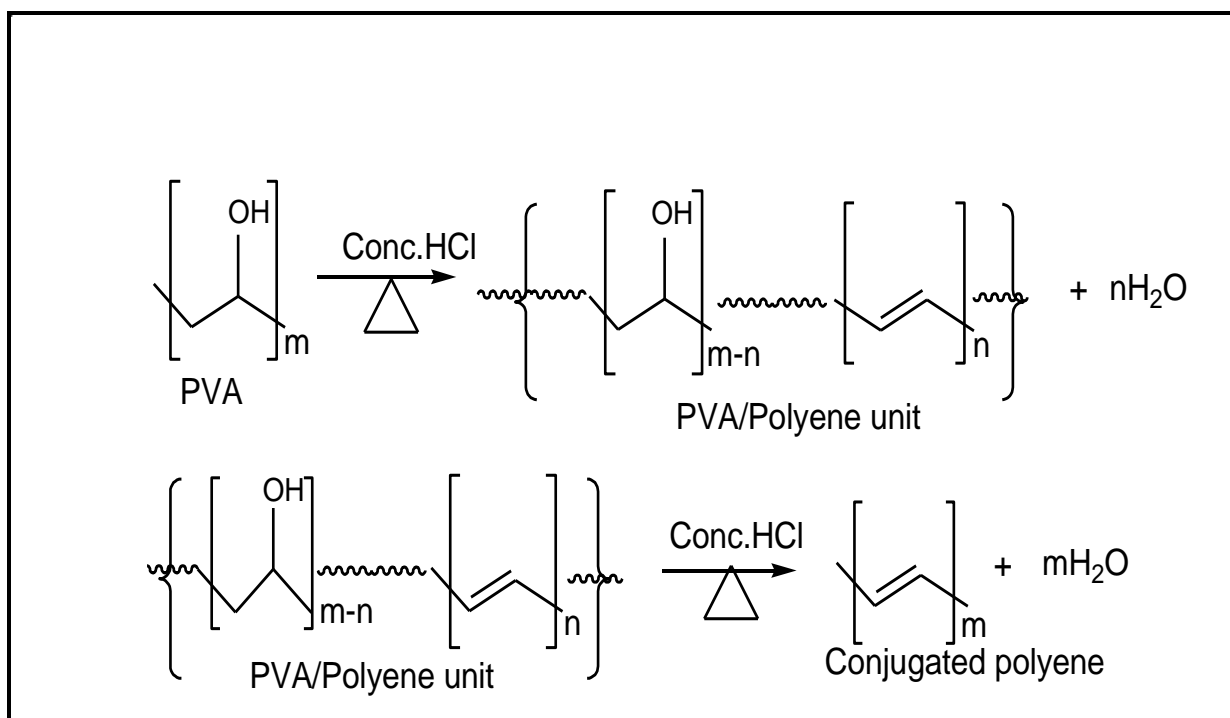


**Figure 3.1:** Homogenised sol-gel synthesis set up; (A) Refluxing (B) Homogenising

### 3.2.2 Thermal dehydration of polyvinyl alcohol (PVA)

The initial stage of thermal dehydration of polyvinyl alcohol (PVA) is the removal of water molecules, which involves the cleavage of hydroxyl groups and hydrogen atoms from the polymer in an elimination reaction. This elimination process results in the formation of a PVA/polyethylene copolymer and water is liberated as illustrated in Scheme 3.1.



**Scheme 3.1:** Proposed reaction mechanism for the formation of conjugated polyene from PVA

The polyvinyl alcohol and polyene units are represented by  $\{\dots(\text{CH}_2\text{-CHOH})_{m-n} \dots (\text{CH=CH})_n \dots\}$  units. The added HCl acts as catalysts to enhance thermal dehydration of PVA and  $\text{H}_2\text{O}$  is a by-product.

### 3.2.3 Preparation of polyene from polyvinyl alcohol (PVA)

About 0.2%, 0.4%, 0.6% and 0.8% (g/v) solutions of PVA were prepared by dissolving exactly 0.2 g, 0.4 g, 0.6 g and 0.8 g of PVA respectively in 100 mL ultrapure water. 2% conc. Hydrochloric acid (HCl) was added to the PVA solutions to obtain PVA (polymer unit) to HCL ratio 50:1, with stirring on a magnetic stirrer. The solutions were heated at  $110^\circ\text{C}$  for 45 min for thermal dehydration to obtain linear conjugated polyene (CPE) molecule as illustrated in Scheme 3.1.



### **3.2.4 Synthesis of conjugated polyene/titania (CPE-TiO<sub>2</sub>) nanoparticles**

The procedure used is the same as described above for the homogenised sol-gel synthesis of TiO<sub>2</sub>. However, 10 ml of the PVA derived conjugated polyene was added dropwise during the process instead of ultrapure water to form the CPE-TiO<sub>2</sub> particles. The solution was centrifuged and decanted. The obtained particles were then dried in an oven at 110°C for 2 h and calcined at much lower temperature of 250°C for 2 h compared to pure TiO<sub>2</sub> (400°C) to avoid the thermal decomposition of the polyene modifier.

## **3.3 Analytical techniques and equipment**

### **3.3.1 Characterisation of synthesised materials**

Characterisations of the prepared catalysts were carried out using different analytical techniques, which include powder X-ray diffraction (PXRD) analysis, transmission electron microscopy (TEM), scanning electron microscopy (SEM) and Fourier transform infrared spectroscopy (FT-IR). Others include UV-vis diffuse reflectance spectrophotometer (UV-Vis DRS), photoluminescence spectroscopy (PLS), cyclic voltammetry (CV), electrochemical impedance spectroscopy (EIS), energy dispersive X-ray spectroscopy (EDX) as well as thermal gravimetric analysis (TGA-DSC). The TGA was applied to estimate the mass degradation and water/volatile material evolution.

The crystalline nature of the as-prepared samples of TiO<sub>2</sub> nanoparticles and CPE-TiO<sub>2</sub> nanocomposites were obtained using X-ray diffraction (XRD). The XRD patterns were recorded in the 2 $\theta$  range of 5-90° with a scan rate of 0.02° s<sup>-1</sup> using a Bruker-D8-AXS diffractometer system equipped with a Cu K $\alpha$  radiation ( $\lambda$  = 0.15406 Å) (Bruker Co., Germany). Fourier transforms infrared (FT-IR) spectra were recorded using an FTIR analyser (Perkin-Elmer, Spectrum 400), where KBr served as the reference sample. The morphologies of the obtained product materials were inspected by a JEM-2100 plus transmission electron microscopy (TEM) operating at 10 kV. Optical absorption properties of the samples were assessed by an ultraviolet and visible (UV-Vis DRS) spectrophotometer (Lambda 17, Perkin-Elmer) and UV-Vis

spectrophotometer (UV- 1700, Shimadzu). The photoluminescence spectroscopy (PLS) spectra of photocatalysts were recorded using a fluorescence spectrophotometer (FP-6500, Japan) equipped with a xenon lamp using an excitation wavelength of 240 nm with an emission wavelength range from 220 to 800 nm.

About 1.0 g of the prepared materials, pure titania ( $\text{TiO}_2$ ), conjugated polyene modified titania (0.2% CPE- $\text{TiO}_2$ , 0.4% CPE- $\text{TiO}_2$ , 0.6% CPE- $\text{TiO}_2$  and 0.8% CPE- $\text{TiO}_2$ ) were separately weighed.

#### *Scanning electron microscopy (SEM) and energy dispersive X-ray (EDX)*

The scanning electron microscopy (SEM) is an electronic-microscopy technique based on the interactions of electrons and materials to produce images of the material surface. The principle of SEM is based on the re-emission of a certain particle when an electron beam bombards the surface of the sample to be analysed. These particles are analysed by the detector, which gives a three-dimensional image of the surface. Due to the excited state of the atoms in the sample through interaction with the incident electrons, photons are emitted (de-excitation process). The emission volume of the photon X ( $\mu\text{m}^3$ ) depends on the energy of the incidental electrons, the atomic number of the elements in the sample and their initial energy levels.

The EDX (energy dispersive X-ray) chemical analysis involves the detection of the emitted photons with the aid of solid detector Si-Li (detection by energy dispersion). The energy of this photon X is a characteristic of its atoms, thus makes it possible to achieve the elemental analysis of the sample. A spectrum consists of various lines (peaks) that will be obtained, each representing a photon X of a given energy, thus corresponds to a given element. This analysis is also quantitative in the sense that the intensity of with each peak in the spectra obtained gives the relative amount of the corresponding element in the material volume. The instrument has detection limit of about 0.1-1% concentration. This limit is for elements having relatively light atomic weight. However, the detector permits the detection of light elements such as carbon (C), oxygen (O), nitrogen (N) and boron (B), but to a limited degree.

### *Thermogravimetric analysis (TGA)*

The thermogravimetric analysis (TGA) was carried out to determine the heat stability of the material. The TGA response gives the weight change under heat treatment and the amount of the volatilised species as the samples are heated. Samples (about 20 .mg) were subjected to heat set at 100°C to 900°C under nitrogen flow at a heating rate of 10°C min<sup>-1</sup> in an SDT Q600 (TA Instruments) thermobalance.

### *Cyclic voltammetry (CV) and electrochemical impedance spectrometry (EIS)*

Cyclic voltammetry (CV) was applied to measure current flow as a function of electron transfer in the synthesised materials (TiO<sub>2</sub> and CPE-TiO<sub>2</sub>). The cyclic voltammograms were recorded at room temperature on a potentiostat (SP 240) with a glassy carbon working electrode (WE), Ag/AgCl reference electrode (RE) and platinum-wire counter electrode (CE). The experiments were carried out in ferrocyanide solution and measurements were taken at the scan rate of 50 mVs<sup>-1</sup> in the potential region between -0.8 and 1V. As the potential is scanned across a specified potential range, the resulting current from each of the materials (TiO<sub>2</sub> and CPE-TiO<sub>2</sub>) at the WE were measured. The current generated is then plotted against potential to produce a CV graph that provides insights on the materials based on the anodic peak current ( $I_{pa}$ ) from oxidation process and cathodic peak current ( $I_{pc}$ ) from reduction process that occurs on the WE. The potentials at which the peak currents occur are known as peak potentials ( $E_p$ ). These peak potentials allow us to analyse the electrochemical reversibility of the reaction at the electrode surface by increasing the rate of scanning during experiments.

Electrochemical impedance spectroscopy (EIS) was measured in the frequency range of 0.5 Hz-105 KHz, with AC voltage amplitude of 10 mV in a 0.5 M ferrocyanide solution. For photocurrent density against potential curve, the WE with an area of 1 x 1 cm<sup>2</sup> was immersed in 0.5 M ferrocyanide solution and illuminated using a 300 W Xe-lamp with a light density of 100 mWcm<sup>-2</sup>.

### 3.3.2 Analytical monitoring techniques for solutions

#### 3.3.2.1 UV-Vis spectroscopy

Ultraviolet-visible (UV-Vis) spectroscopy is one of the most common analytical techniques in the chemical laboratory. It was used in the study for both qualitative and quantitative purposes. It is a preferred technique because of its fast quantitative determination of various organic compounds in solution.

UV-Vis spectroscopy works based on the Beer-Lambert Law. This law states that when a beam of monochromatic light is passed through a solution containing an absorbing substance, the rate of decrease in the light intensity along with the path-length of the solution is proportional to the concentration of the solution. The mathematical expression is as follows (Equation 3.1):

$$A = \log\left(\frac{I_0}{I}\right) = ECL \quad \text{Equation 3.1}$$

where A is the absorbance,  $I_0$  is the intensity of incident light, I is the intensity of light leaving the solution, L is the length of the sample cell and E is the molar absorptivity.

UV spectroscopy technique was used to monitor change (decrease) in the concentration of the pollutants during the degradation process. A Shimadzu UV-3600 spectrophotometer was used at a specified wave-maximum ( $\lambda_{\max}$ ) for each of the pollutants (chloramphenicol at  $\lambda_{\max} = 275$  nm and 250 nm for acetaminophen (paracetamol)). Carefully prepared standard solutions (5, 10, 15, 20, 25, 30, 35, 40 and 50ppm) of the pollutants were used for calibration curves.

#### 3.3.2.2 High-performance liquid chromatography (HPLC)

The high-performance liquid chromatography (HPLC) is an analytical technique for the separation, identification as well as quantification of constituents in a liquid sample. HPLC was used in the study to monitor the degradation by-products as well to observe the continuous decrease in the concentration of the pollutants with irradiation time.

The HPLC analysis was performed using phenomenex C<sub>18</sub> (100 mm x 4.6 mm x 5 µm) column with a UV detector. The mobile phase consists of a mixture of 98% methanol and 0.1 M ammonium acetate solution (prepared with 5% acetic acid) for chloramphenicol and a mixture of acetonitrile and water for acetaminophen. The instrument was operated in isocratic mode with methanol: ammonium acetate (40% 60%) and water acetonitrile ratio for chloramphenicol and acetaminophen respectively. The column temperature condition was 25°C with 10µL injection volume at a flow rate of 0.5 ml min<sup>-1</sup>. The UV detector was set at 275 nm for one analyte (chloramphenicol) and at 250 nm for the other analyte (acetaminophen).

Figure 3.2 presents the schematic diagram for the HPLC instrument. Prior to the running, the instrument was purged for 30 min for proper column equilibration. The method and the instrument operating conditions are summarised in Table 3.2.

**Table 3.2:** Summarized methods of separation by HPLC for the pollutants during photocatalytic process

Condition	Analyte measured	
	Chloramphenicol	Acetaminophen
Column	Phenomenex C <sub>18</sub> column (100 mm x 4.6mm x 5µm)	
Detector	UV	
Mobile phase	Methanol and ammonium acetate (40:60% v/v)	Water and acetonitrile (40:60% v/v)
Method applied	Isocratic elution	Isocratic elution
Column temperature(°C)	25	
Injection volume (µL)	10	
Flow rate (ml min <sup>-1</sup> )	0.1	
Wavelength (nm)	275	250

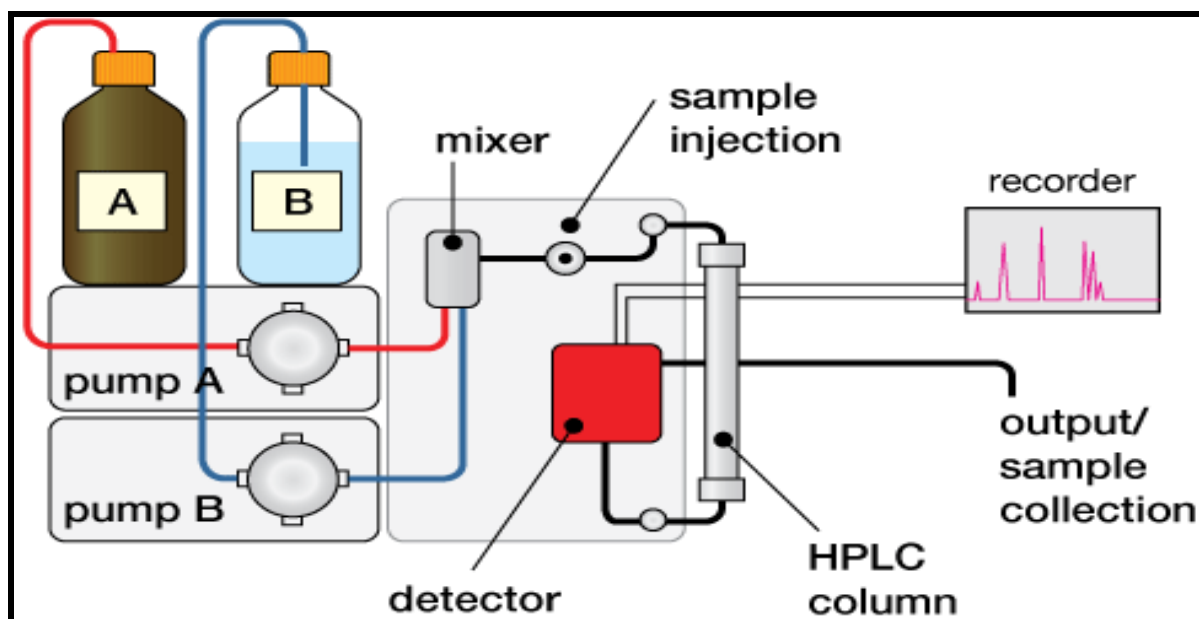


**Figure 3.2:** The schematic diagram for HPLC analytical technique: Source; Cruzan, (2012)

### 3.4 Photocatalytic degradation experiments

#### 3.4.1 Photoreactor

All photocatalytic oxidation reactions of the pollutants were carried out under visible light source irradiation set up, equipped with 72 W LED lamp (rated voltage was DC 12 V,  $\lambda > 400$  nm), with the lampshade, beaker reaction vessel with a magnetic stirrer.

#### 3.4.2 Photocatalytic procedures

Batch experiments were carried-out using 400 mL glass beakers at room temperature ( $25 \pm 1^\circ\text{C}$ ). Before each test, the lamp was turned on and warmed up for 10 min to establish a constant light output. Batch tests were performed as follows: known masses (5 mg, 10 mg, 15 mg and 20 mg) of the catalysts were weighed and used for 200 mL solution of the pharmaceuticals of varying concentrations. Just before irradiation, the mixture (solution and catalyst) was magnetically stirred for 40 min in the dark to allow for adsorption equilibrium of the pharmaceuticals on the catalyst surfaces. The solution was subsequently exposed to visible light irradiation

under magnetic stirring at 450 rpm, which marks the starting point of photodegradation test. An air diffuser pump was connected to the reactor to uniformly disperse air into the solution mixture, with a low rate of  $0.2 \text{ m}^3\text{h}^{-1}$ . At regular intervals, 3 mL samples were withdrawn, filtered using an acrodisc premium 25 mm syringe (APS) filter with GxP/0.45  $\mu\text{m}$  GHP membrane, to separate the photocatalyst suspensions. The filtrate was then taken for further analysis.

The concentration of the filtrate was determined by measuring the absorption intensity at a predetermined maximum absorbance wavelength of 275 nm (for chloramphenicol) and 254 nm (for acetaminophen) using a UV-Vis spectrophotometer (UV- 1700, SHIMADZU) with a 1 cm path length spectrometric quartz cell. The corresponding concentration of the measured absorbance was determined using the calibration curve ( $R^2 = 0.999$  for chloramphenicol and 0.998 for acetaminophen). The degradation efficiency for the two pharmaceuticals was determined according to Equation 3.2.

$$\text{Degradation Efficiency (\%)} = \frac{C_0 - C_t}{C_t} \times 100 \quad \text{Equation 3.2}$$

where  $C_0$  was the initial concentration of chloramphenicol before the degradation experiment and  $C_t$  was the concentration of chloramphenicol at certain degradation time  $t$  (min) during irradiation. The summary of the experimental set-up and conditions is given in Table 3.3.

**Table 3.3:** Experimental set-up and conditions for the photocatalytic process

Set - up	Batch experiment under visible light
Light source	LED
Catalyst material	TiO <sub>2</sub> and CPE-TiO <sub>2</sub>
Mass of catalyst (mg)	5, 10, 15, and 20
pollutants	Chloramphenicol and acetaminophen

<b>Set - up</b>	<b>Batch experiment under visible light</b>
Solution concentrations (ppm)	25, 30, 35, 40 and 45
Volume of solution (mL)	200
Stirring	Magnetic
Temperature	Ambient
Pressure	Atmospheric

### 3.4.3 Preparation of solutions

The stock solutions used in separate photocatalysis experiments were prepared by dissolving an accurately weighed amount of each of the analytes in ultrapure water. Further dilution was made from the stock solutions, with ultrapure water to obtain the required initial and standard concentrations ranging from 5 ppm to 60 ppm for calibrations. Although further analysis was not carried out on the prepared solution, however, the calibration curve with  $R^2 = 0.9995$  confirms the accuracy. The photocatalytic degradation efficiency of the modified and pure unmodified catalysts was investigated under visible light.

### 3.4.4 Optimisation of photocatalysis parameters

Some of the operational experimental-parameters that were optimised for the photocatalytic degradation experiment (Table 3.4) include the catalyst loading (i.e. the relative amount of the catalyst used in the experiment), the pH of the aqueous solution, concentration of the organic pollutant and percentage of the modifier.

**Table 3.4: Variable experimental parameters**

<b>PARAMETERS</b>	<b>VARIABLES</b>
Amount of catalyst (loading) (mg/200ml)	5, 10, 15, 20
Concentration of organic pollutants (ppm)	25, 30, 35, 40, 45.
pH	4, 7, 8, 9, 10.
Percentage modifier (%)	0.2, 0.4, 0.6, 0.8.



### 3.4.5 Preliminary experimental design

Several experiments were carried out to set the background for the photocatalytic process and the optimisation of experimental conditions, based on the design (generated by central composite design method (CCD)) as presented in

**Table 3.5.** All experimental setups follow the procedure earlier described above.

**Table 3.5:** Preliminary experimental design for condition optimisation

Experimental runs	Initial concentration (mg/L)	Catalyst dosage (mg 200 m/L)	Catalyst dosage (mg/L)	Solution Initial pH
1	25	15	75	7
2	30	15	75	7
3	35	15	75	7
4	40	15	75	7
5	45	15	75	7
6	25	5	25	7
7	25	10	50	7
8	25	15	75	7
9	25	20	100	7
10	25	15	75	4
11	25	15	75	7
12	25	15	75	8
13	25	15	75	10

#### 3.4.5.1 Investigation of effects of pH

Five different solutions with the same concentration of 25 mg/L were prepared from the stock solution (100 mg/L). The pH of the sample solutions was adjusted with 0.2 M HCL and 0.2 M NaOH to various pH values ranging from 4 to 10 while keeping other parameters (catalyst dosage and initial concentration) constant. Each solution

(200 mL), in turn, was transferred into 400 mL capacity photoreactor equipped with visible light source for irradiation. 15 mg of the catalyst was weighed and transferred into the solution, then the irradiation and sampling at time intervals were carried out following the procedures described earlier for photocatalysis.

#### **3.4.5.2 Investigating the effects of initial concentrations**

Various concentrations were prepared in the range of 5 ppm – 50 ppm to investigate the effect of initial concentrations on the degradation percentage, to select the optimum initial concentration, while other parameters were kept constant. 200 mL of each solution of varying concentrations were taken for irradiation, using 15 mg of catalysts and pH of 7 (CAP) and 8 (APAP).

#### **3.4.5.3 Investigation of catalyst loading**

The investigation on the effect of mass:volume ratio (catalyst:solution) on degradation percentage was carried out by weighing varying masses (5, 10, 15 and 20 mg) of the catalysts into 200 mL of 25 mg/L solution. The pH of the solutions was kept constant.

#### **3.4.6 Photocatalytic activities of modified and unmodified TiO<sub>2</sub> catalysts compared**

Following the photocatalytic procedure described earlier, 15 mg of each of modified and unmodified catalyst was separately applied for photocatalytic degradation of the pharmaceuticals. The irradiation was allowed for 210 min, during which samples were taken 10 times at different time intervals to compare the photocatalytic degradation efficiency for the two catalysts (TiO<sub>2</sub> and CPE-TiO<sub>2</sub>).

#### **3.4.7 Total organic carbon (TOC) measurement during photodegradation**

The concentration of total organic carbons (TOC) in the solutions was measured using a TOC analyser (Shimadzu TOC-V<sub>CSH</sub>). The TOC is a measure of the carbon content present in an aqueous solution. As a precautionary measure, it is necessary to eliminate any inorganic carbon sources, such as CO<sub>3</sub><sup>2-</sup>, HCO<sub>3</sub> and H<sub>2</sub>CO<sub>3</sub>, present in the solution to assess the TOC. Therefore, some drops of concentrated hydrochloric acid could be added to samples, to release CO<sub>2</sub> and then followed by

degassing by a current of nitrogen gas. However, since the standard solutions were prepared for the organic pollutants using ultrapure water, this precautionary step was not necessary. During photodegradation process, sampling was carried out at time intervals and was taken for TOC analysis.

#### **3.4.8 The reusability test for the catalyst**

The recyclability test was carried out for the synthesised catalyst (CPE-TiO<sub>2</sub>) to assess its photochemical stability. The photocatalytic experiments were repeated with the used catalyst for many cycles of oxidation, to evaluate its transformations due to use. After the initial 210 min of irradiation in the solution, the composite was washed with ultrapure water to be cleansed of any adsorbed pharmaceutical on the surface, which permits for more adaptability in its use without cross-contamination. The washed composite was then filled with fresh pharmaceutical solutions.

## References

- AGARWAL, S., TYAGI, I., GUPTA, V.K., SOHRABI, M., MOHAMMADI, S., GOLIKAND, A.N., & FAKHRI, A. 2017. Iron doped SnO<sub>2</sub>/Co<sub>3</sub>O<sub>4</sub> nanocomposites synthesized by sol-gel and precipitation method for metronidazole antibiotic degradation. *Mater. Sci. Eng.*, 70, 178–183.
- AYANDA, O.S., NELANA, S.M., PETRIK, L.F., & NAIDOO, E.B. 2017. Nano-TiO<sub>2</sub>, ultrasound and sequential nano-TiO<sub>2</sub>/ultrasonic degradation of N-acetyl-para-aminophenol from aqueous solution. *J. Water Health.*, 15 (6), 1015–1027.
- CRUZAN, J. 2012. The concept of chromatography. Chemistry @.com.
- LÓPEZ ZAVALA, M.Á. & ESTRADA, E.E. 2016. Degradation of acetaminophen and its transformation products in aqueous solutions by using an electrochemical oxidation cell with stainless steel electrodes. *Water (Switzerland)*, 8 (9), 1–12.
- SLAMANI, S., ABDELMALEK, F., GHEZZAR, M.R., & ADDOU, A. 2018. Initiation of Fenton process by plasma gliding arc discharge for the degradation of paracetamol in water. *J. Photochem. Photobiol., A: Chemistry*, 359, 1–10.
- THI, V.H.T. & LEE, B.K. 2017. Effective photocatalytic degradation of paracetamol using La-doped ZnO photocatalyst under visible light irradiation. *Mater. Res. Bull.*, 96, 171–182.
- TRETINNIKOV, O.N. & SUSHKO, N.I. 2015. Formation of Linear Polyenes in Thermal Dehydration of Polyvinyl Alcohol, Catalyzed by Phosphotungstic Acid. *J. Appl. Spectrosc.*, 81 (6), 1044–1047.
- XU, B., DING, T., ZHANG, Y., WEN, Y., YANG, Z., & ZHANG, M. 2017. A new efficient visible-light-driven composite photocatalyst comprising ZnFe<sub>2</sub>O<sub>4</sub> nanoparticles and conjugated polymer from the dehydrochlorination of polyvinyl chloride. *Mater. Lett.*, 187, 123–125.
- ZHANG, J., FU, D., XU, Y., & LIU, C. 2010. Optimization of parameters on photocatalytic degradation of chloramphenicol using TiO<sub>2</sub> as photocatalyst by response surface methodology. *J. Environ. Sci.*, 22 (8), 1281–1289.

## Chapter 4: Result and Discussion

This chapter presents the results obtained from the study and the discussion. It is divided into four sections of different parts of the results with an independent conclusion for each:

**Section A:** The structural and morphological characterisation.

**Section B:** The electrochemical and optical characterisation.

**Section C:** The photocatalytic parameters investigation for the degradation of APAP, CAP and the durability test of the catalyst materials.

**Section D:** The kinetics and mechanisms of APAP and CAP photocatalytic degradations.

## TABLE OF CONTENTS

<b>CHAPTER 4: RESULT AND DISCUSSIONS .....</b>	<b>84</b>
<b>SECTION A: STRUCTURAL AND MORPHOLOGICAL CHARACTERISATION .....</b>	<b>87</b>
INTRODUCTION .....	87
4.1 STRUCTURAL CHARACTERISATION.....	87
4.1.1 <i>Fourier transforms infrared (FTIR) analysis .....</i>	<i>87</i>
4.1.2 <i>Powder X-ray diffraction (PXRD) analysis.....</i>	<i>89</i>
4.1.3 <i>Thermogravimetric analysis (TGA).....</i>	<i>92</i>
4.2 MORPHOLOGICAL AND COMPOSITIONAL CHARACTERISATION.....	94
4.2.1 <i>Scanning electron microscopy (SEM) Images .....</i>	<i>94</i>
4.2.2 <i>Transmission electron microscopy (TEM) images .....</i>	<i>95</i>
4.2.3 <i>Energy-dispersive X-ray spectroscopy (EDS/EDX) analysis .....</i>	<i>96</i>
4.2.4 <i>Particle size, shape and composition of the materials .....</i>	<i>98</i>
CONCLUSION.....	101
<b>SECTION B: OPTICAL AND ELECTROCHEMICAL CHARACTERISATION .....</b>	<b>102</b>
INTRODUCTION .....	102
4.3 OPTICAL CHARACTERISATION.....	102
4.3.1 <i>UV-Vis electronic absorption of PVA and CPE.....</i>	<i>102</i>
4.3.2 <i>UV-Vis, UV-Vis DRS electronic absorption and Tauc plots of bare TiO<sub>2</sub> and CPE-TiO<sub>2</sub> composites .....</i>	<i>103</i>
4.3.3 <i>Photoluminescence (PL) measurement of bareTiO<sub>2</sub> and CPE-TiO<sub>2</sub>.....</i>	<i>106</i>
4.4 ELECTROCHEMICAL CHARACTERISATION.....	108
4.4.1 <i>Cyclic voltammetry analysis.....</i>	<i>108</i>
4.4.2 <i>Electrochemical impedance spectroscopy .....</i>	<i>109</i>
CONCLUSION.....	110
<b>SECTION C: THE PHOTOCATALYTIC PARAMETERS INVESTIGATION FOR THE DEGRADATION OF APAP, CAP AND DURABILITY TEST OF THE CATALYST MATERIALS .....</b>	<b>112</b>
INTRODUCTION .....	112
4.5 EFFECTS OF CATALYST DOSAGE.....	112

4.6 EFFECTS OF INITIAL CONCENTRATION .....	115
4.7 EFFECT OF THE SOLUTION PH .....	118
4.8 EFFECT OF IRRADIATION TIME .....	121
4.9 PHOTOCATALYTIC DEGRADATION AT OPTIMUM CONDITIONS .....	123
4.10 THE TOTAL ORGANIC CARBON (TOC) REMOVAL FOR THE PHARMACEUTICALS .....	127
4.11 THE DURABILITY AND REUSABILITY TEST FOR THE CATALYST .....	129
CONCLUSION.....	130
 SECTION D: THE KINETICS AND MECHANISMS OF APAP AND CAP PHOTOCATALYTIC DEGRADATIONS .....	 <b>131</b>
INTRODUCTION .....	131
4.12 KINETICS OF PHOTODEGRADATION .....	131
<i>4.12.1 Kinetics based on various pollutants concentrations .....</i>	<i>135</i>
<i>4.12.2 Kinetics based on varying catalyst dosages.....</i>	<i>137</i>
<i>4.12.3 Kinetics based on various solution pH .....</i>	<i>139</i>
<i>4.12.4 Degradation kinetics at optimised conditions .....</i>	<i>141</i>
4.13 POSSIBLE PHOTODEGRADATION MECHANISM AND INTERMEDIATE IDENTIFICATIONS.....	143
<i>4.13.1 Evaluation of reactive species contributions and mechanism .....</i>	<i>143</i>
<i>4.13.2 High performance liquid chromatography (HPLC) analysis and intermediate identification</i>	<i>145</i>
REFERENCES .....	150

## Section A: Structural and morphological characterisation

### Introduction

This section presents the results obtained from the characterisation in terms of the structural and morphological properties of the synthesised materials. The methods used for the preparation of the materials were discussed in Chapter 3. Usually, materials for an efficient photocatalytic degradation of organic pollutants in aqueous solution must possess a good balance of properties, such as structural, morphological and compositional characteristics. The most commonly useful TiO<sub>2</sub> morphology is that of mono-dispersed nanoparticles in which the shape and the diameter are well controlled. The controlled shapes and sizes enable to maximise the benefits of the small crystallite size such as high reactive surface area and reduced bulk recombination (Wang *et al.*, 2015).

### 4.1 Structural characterisation

#### 4.1.1 Fourier transforms infrared (FTIR) analysis

Surface functional groups and chemical states Fourier transform-infrared (FTIR) analysis were carried out to identify the functional groups on the surface of the materials. **Figure 4.1A and 4.1B** presents the FTIR spectra of the synthesised materials. The FTIR spectra of PVA and CPE, as shown in **Figure 4.1A**, present the percentage transmittance at varying wavelengths for the materials. A sharp peak between 1600 cm<sup>-1</sup> and 1640 cm<sup>-1</sup> was observed on the CPE spectrum. This prominent peak at around 1630 cm<sup>-1</sup> represents C=C stretching vibration, an indication of the presence of the polyene group (Merah *et al.*, 2013). The linear polyene with C=C conjugated bonds (formed from thermal dehydration of PVA) is a conductive polymer that possesses electrical and optical abilities (Sun *et al.*, 2013). The conjugated system could serve as an electron carrier for TiO<sub>2</sub> for better photocatalytic performance.



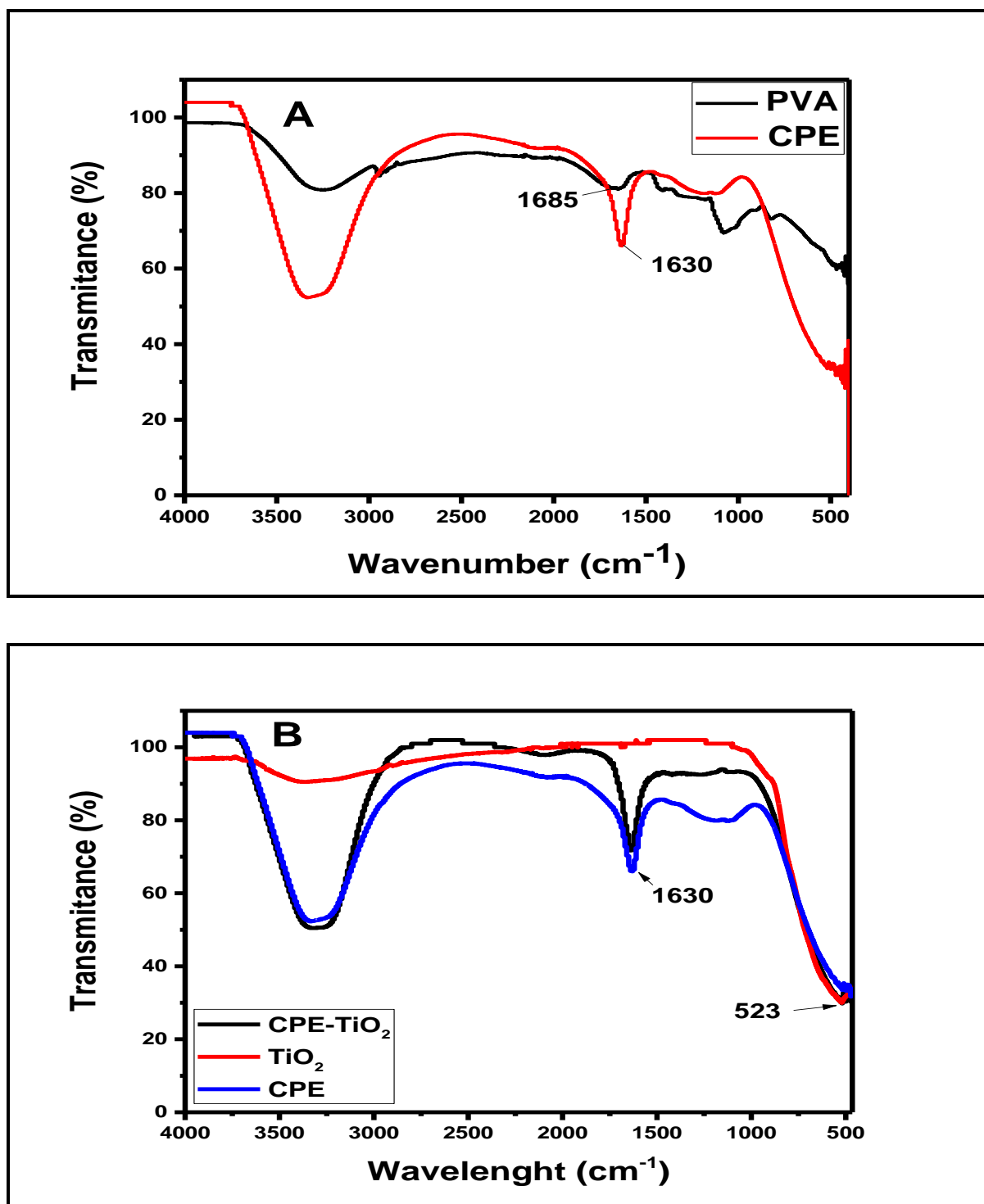


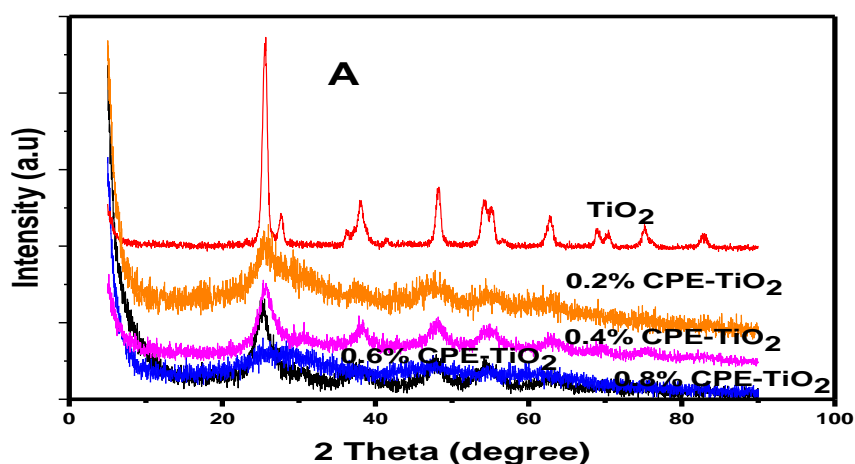
**Figure 4.1:** The FTIR spectra of (A) conjugated polyene (CPE) and PVA and (B) CPE, TiO<sub>2</sub> and CPE-TiO<sub>2</sub> materials

To understand the functional impact of CPE on TiO<sub>2</sub>, the FT-IR spectra of TiO<sub>2</sub> and CPE-TiO<sub>2</sub> nanocomposite were taken in the range of wavenumber 500-3900  $\text{cm}^{-1}$

(Figure 4.1B). The appearance of a strong absorption band on  $\text{TiO}_2$  spectrum, with no shoulder peaks at around  $460\text{--}900\text{ cm}^{-1}$ , is attributed to stretching vibration of T-O and T-O-T and confirms the presence of titanium oxide (Zhang *et al.*, 2010). A distinguished bonding peak located around  $1620\text{ cm}^{-1}$  -  $1640\text{ cm}^{-1}$  attributed to conjugated C=C was observed on the CPE spectrum (Tretinnikov and Sushko, 2015). A similar peak at  $1630\text{ cm}^{-1}$  was observed on CPE- $\text{TiO}_2$ , which was not present on bare  $\text{TiO}_2$  spectrum. This implies that the conjugated (C=C) bonds from CPE were well integrated onto  $\text{TiO}_2$ . It is therefore, anticipated that the CPE on  $\text{TiO}_2$  should improve the optical property of the catalyst.

#### 4.1.2 Powder X-ray diffraction (PXRD) analysis

To obtain information on the phases and crystallite sizes, powder X-ray diffraction (PXRD) analysis was carried out on the material samples. The diffractograms of the samples are presented in Figure 4.2A and 4.2B. It was observed from the diffractogram that all the materials possess peaks typical for polycrystalline materials. However, the crystalline nature of the peaks for CPE modified materials was observed to decrease with an increase in CPE percentage (%) modifications following  $0.8\% \text{ CPE-TiO}_2 < 0.6\% \text{ CPE-TiO}_2 < 0.4\% \text{ CPE-TiO}_2 < 0.2\% \text{ CPE-TiO}_2$ . This could be due to an increase in the amount of organic carbon in the composite material that resulted in a more amorphous end-products.



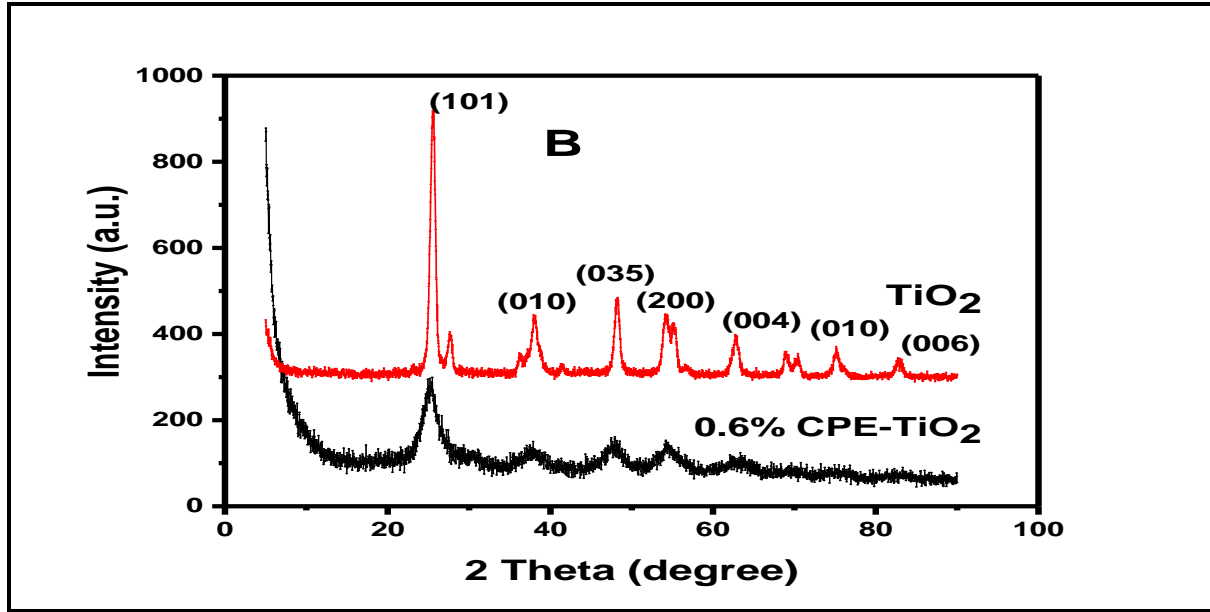


**Figure 4.2:** Powder X-ray diffraction (PXRD) of (A)  $\text{TiO}_2$  and CPE- $\text{TiO}_2$  at varying CPE modifications and (B) synthesised  $\text{TiO}_2$  and 0.6% CPE- $\text{TiO}_2$ .

The PXRD patterns diffractogram of  $\text{TiO}_2$  and CPE- $\text{TiO}_2$  samples at varying CPE percentages are as shown in **Figure 4.2A**. The sharp diffraction lines appearance can be related to the crystalline anatase phase of  $\text{TiO}_2$ , according to the JCPDS database 00-021-1272 peaks reflection annotation (Oseghe *et al.*, 2019). Similar set of peaks are observed on the CPE modified  $\text{TiO}_2$  nanocomposites. The crystalline sizes of all the materials were calculated using Debye-Scherrer's equation, from the [101] diffraction peak, as shown in Equation 4.1:

$$D = \frac{K\lambda}{\beta \cos \theta}$$

**Equation 4.1**

where  $D$  is the crystalline size,  $\lambda$  represents the Cuka 1 radiation wavelength ( $\lambda$ ) = 1.54060 Å,  $K$  is the crystalline shape factor with an approximate value ( $K$ ) = 0.9.  $\beta$  is equal to the full width of the peak at an intensity equal to half of the maximum peak (FWHM), measured in radians and  $2\theta$  is the diffracted angle at the maximum peak

intensity. **Figure 4.2B** compares the X-ray diffraction patterns for both the prepared pure TiO<sub>2</sub> and 0.6% CPE-TiO<sub>2</sub> (optimal modification). It indicates that there are several crystalline reflection peaks particularly for pure TiO<sub>2</sub> at  $2\theta$  values of 25° (101), 38° (004) and 48° (200). Since these peaks, at various  $2\theta$  and the corresponding reflections, match the anatase phase (Abdullah *et al.*, 2016), it then implies that only anatase existed in the synthesised materials. It was noticed that the composite material (0.6% CPE-TiO<sub>2</sub>) shows less crystalline peaks, however, this does not affect the original phase (anatase) of the material as indicated by the peaks represented at various  $2\theta$ . Hence, it is envisaged that the catalyst performance may not in any way be undesirably affected. The crystallite sizes were calculated and were found to be in the range 3 - 3.5 nm for bare TiO<sub>2</sub> and 7 - 9.16 nm for CPE modified TiO<sub>2</sub> materials. The calculated crystallite particle sizes for the synthesised materials are presented in **Table 4.1**.

**Table 4.1:** The estimated crystallite sizes of the materials from PXRD plots

Materials	FWHM ( $\beta$ )	2theta ( $2\theta$ )	Theta ( $\theta$ )	Theta ( $\theta$ ) in radians	$\beta$ (in radians)	Crystallite size (D) (nm)
TiO <sub>2</sub>	2.2757	25.5059	12.753	0.22258	0.3972	3.41
0.2% CPE-TiO <sub>2</sub>	10.7509	25.2166	12.753	0.22258	0.1876	7.51
0.4% CPE-TiO <sub>2</sub>	11.5723	25.2166	12.753	0.22258	0.1241	8.37
<b>0.6% CPE-TiO<sub>2</sub></b>	<b>11.8259</b>	<b>25.2166</b>	<b>12.753</b>	<b>0.22258</b>	<b>0.1221</b>	<b>8.39</b>
0.8% CPE-TiO <sub>2</sub>	12.6718	25.2166	12.753	0.22258	0.0975	9.16

#### *Optimisation of material modifications*

For further applications, optimisation experiments were carried out to identify the material of best performance among the modified TiO<sub>2</sub> at varying CPE percentages. It was observed that photocatalytic performances increase with an increase in percentage modification until 0.6%. Further increases in CPE percentage resulted in decreasing performance. This trend could be because of an increase in agglomerations as the amount of CPE further increases leading to a drastic

reduction in the reactive surface area thus blockage of reactive sites of the nanoparticles. Since the surface area is an important factor that affects the photocatalytic performance of materials (Wang *et al.*, 2015; Wang *et al.*, 2016). The photocatalytic degradation of the tested pharmaceuticals (acetaminophen and chloramphenicol) indicated that 0.6% CPE-TiO<sub>2</sub> gave the highest degradation percentage (**Figure 4.3**). Consequently, 0.6% CPE-TiO<sub>2</sub> was chosen as an optimal synthesised catalyst for further photocatalytic experiments.

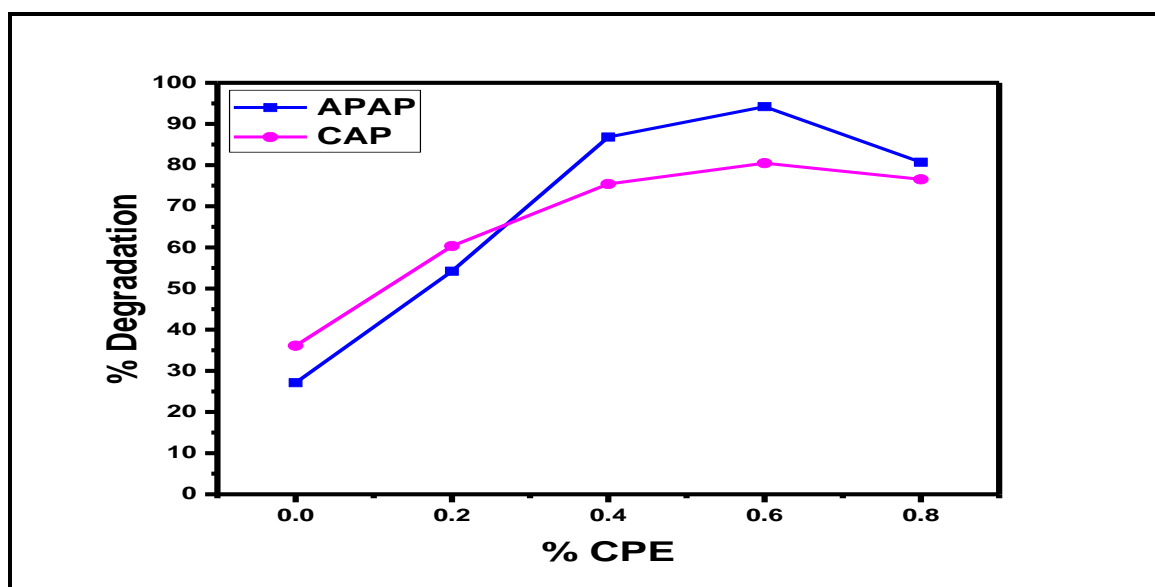


**Figure 4.3:** Optimisation of CPE modified TiO<sub>2</sub> for photodegradation of acetaminophen and chloramphenicol

#### 4.1.3 Thermogravimetric analysis (TGA)

Thermogravimetric analysis was carried out to determine the weight loss for both the bare TiO<sub>2</sub> and the optimised CPE-TiO<sub>2</sub> (0.6% CPE-TiO<sub>2</sub>) materials, to compare their percentage loss in weight at varying heating temperatures. The gravimetric analysis was also necessary to evaluate the stability temperature for the prepared material and to determine the calcination temperatures, particularly for CPE-TiO<sub>2</sub>. The TGA and DTA curves obtained for both materials are given in **Figure 4.4A and 4.4B**, respectively.

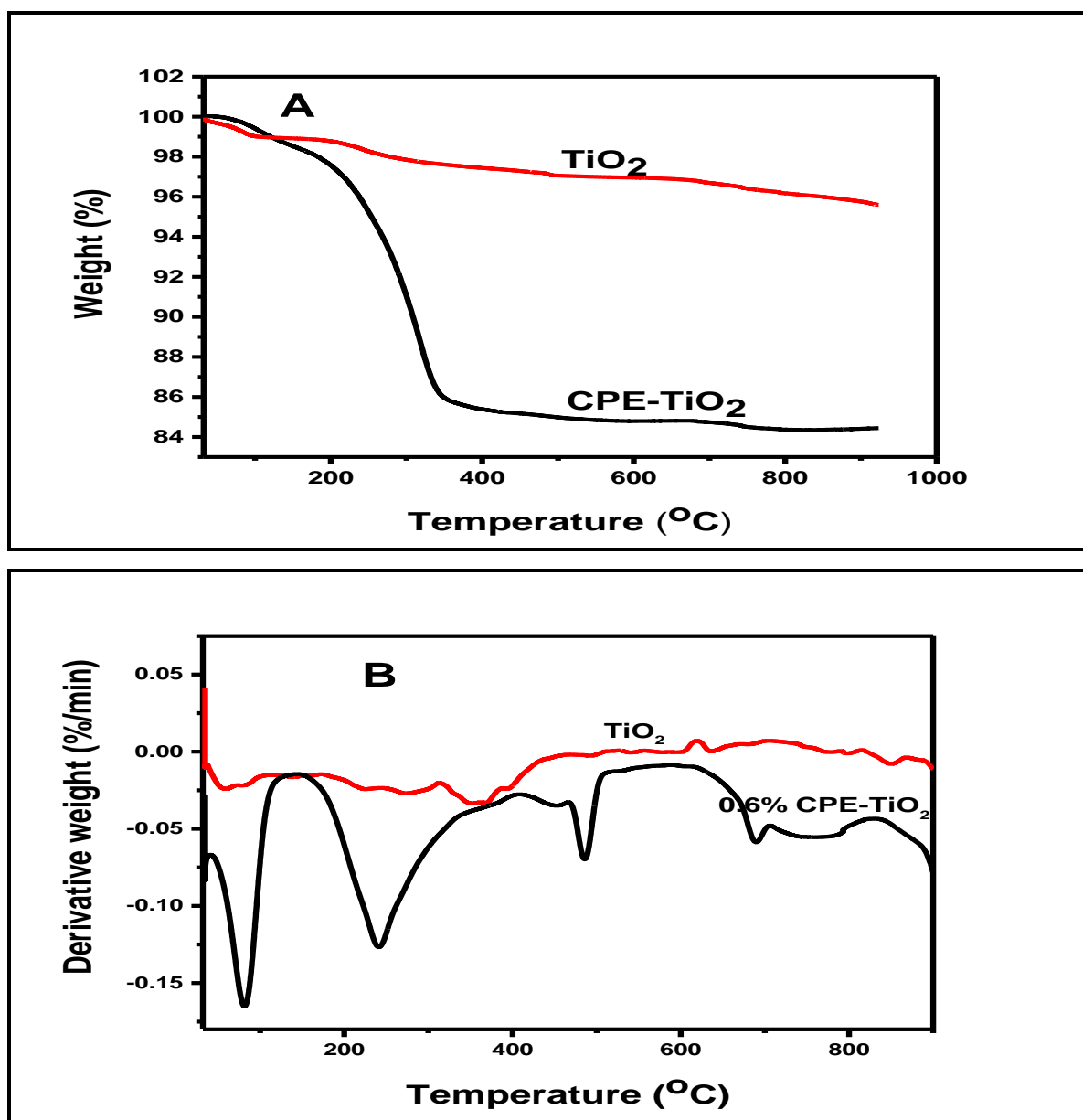


**Figure 4.4:** (A) The thermal gravimetric analysis (TGA) (B) the derivative thermal analysis (DTA) of  $\text{TiO}_2$  and  $\text{CPE-TiO}_2$ .

Four distinct temperature regions are identified for  $\text{CPE-TiO}_2$ , while three regions were for  $\text{TiO}_2$ . The first region between 45 $^{\circ}\text{C}$  and 85 $^{\circ}\text{C}$  characterised by low weight loss (between 1-5% for both materials), may be attributed to the loss of some physically adsorbed volatile impurities on the surface of the materials. In the temperature range of 110 $^{\circ}\text{C}$  to 230 $^{\circ}\text{C}$ , was the second weight loss phase due to the liberation of chemically bonded water molecules as often reported in the literature (Audichon *et al.*, 2017). This very low (<1%) loss in weight is accompanied by a clearly defined endothermic peak at about 110 $^{\circ}\text{C}$  on the DTA spectral **Figure 4.4B**.

After this, at the range of 280°C to 350°C, the combustion of hydrocarbon polymer takes place, leading to a weight loss of approximately 25% for CPE-TiO<sub>2</sub> and about just 2% for the pure TiO<sub>2</sub>. The loss in weight due to the combustion of hydrocarbon implies that at a temperature above 280°C, the CPE-TiO<sub>2</sub> becomes unstable. The broad exothermic peak observed from 450°C to 620°C can be attributed to the combustion of remnant carbon atoms on the surface of CPE-TiO<sub>2</sub>, while such was not observed on the DTA of pure TiO<sub>2</sub>. Finally, above 620°C the TGA for both catalysts remain unchanged, indicating a constant weight.

## 4.2 Morphological and compositional characterisation

### 4.2.1 Scanning electron microscopy (SEM) Images

The morphology of the materials was examined using scanning electron microscopy (SEM). **Figure 4.5** presents the SEM micrograph confirming the spherically shaped particles of regular size. Pure TiO<sub>2</sub> indicates a more separated circularly shaped nanoparticles, which appear more distinct with increase CPE percentage modification. However, slight agglomeration of the nanoparticle was observed at 0.6% CPE and more pronounced as the percentage CPE modification further increases. The slight clustering observed is understandable to be a result of the amount of polymer organic molecule modification, which may lead to an increase in particle aggregation. This observation is well supported in the literature, which confirms that organic molecules play an important role in the agglomeration of nanoparticles (Li *et al.*, 2016).

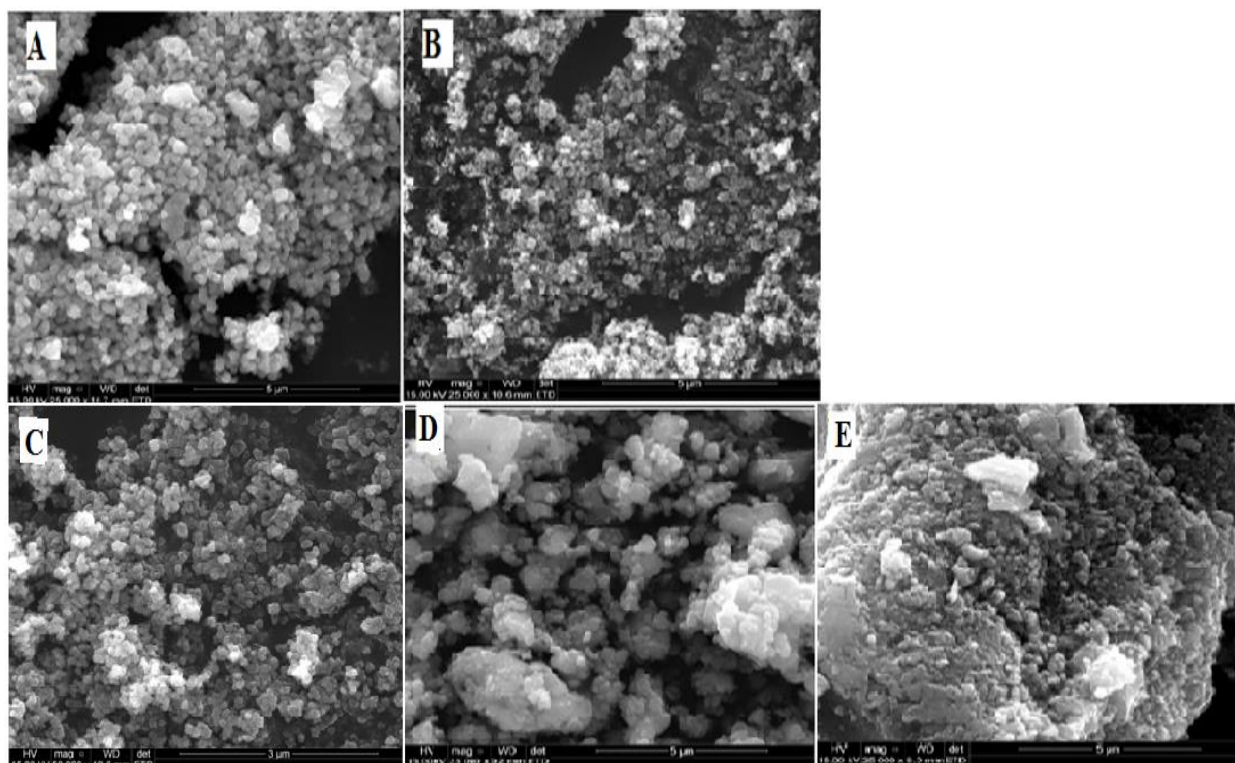


**Figure 4.5:** Scanning electron microscopy (SEM) images of (A)  $\text{TiO}_2$  (B) 0.2% CPE- $\text{TiO}_2$  (C) 0.4% CPE- $\text{TiO}_2$  (D) 0.6% CPE- $\text{TiO}_2$  (E) 0.8% CPE- $\text{TiO}_2$

#### 4.2.2 Transmission electron microscopy (TEM) images

The morphology of the materials was further confirmed using transmission electron microscopy (TEM) and the images obtained are presented in **Figure 4.6**. The TEM micrograph further confirms that the particles are mostly circular in shapes with few other irregularly shaped particles. Pure  $\text{TiO}_2$  indicates a more separated circularly shaped nanoparticles, while for the CPE- $\text{TiO}_2$  nanocomposite, a few agglomerated particles were observed as was observed with SEM image. This slight clustering, is due to the presence of organic polymer in the composite material, as indicated by the presence of carbon atoms in the EDS spectrum.



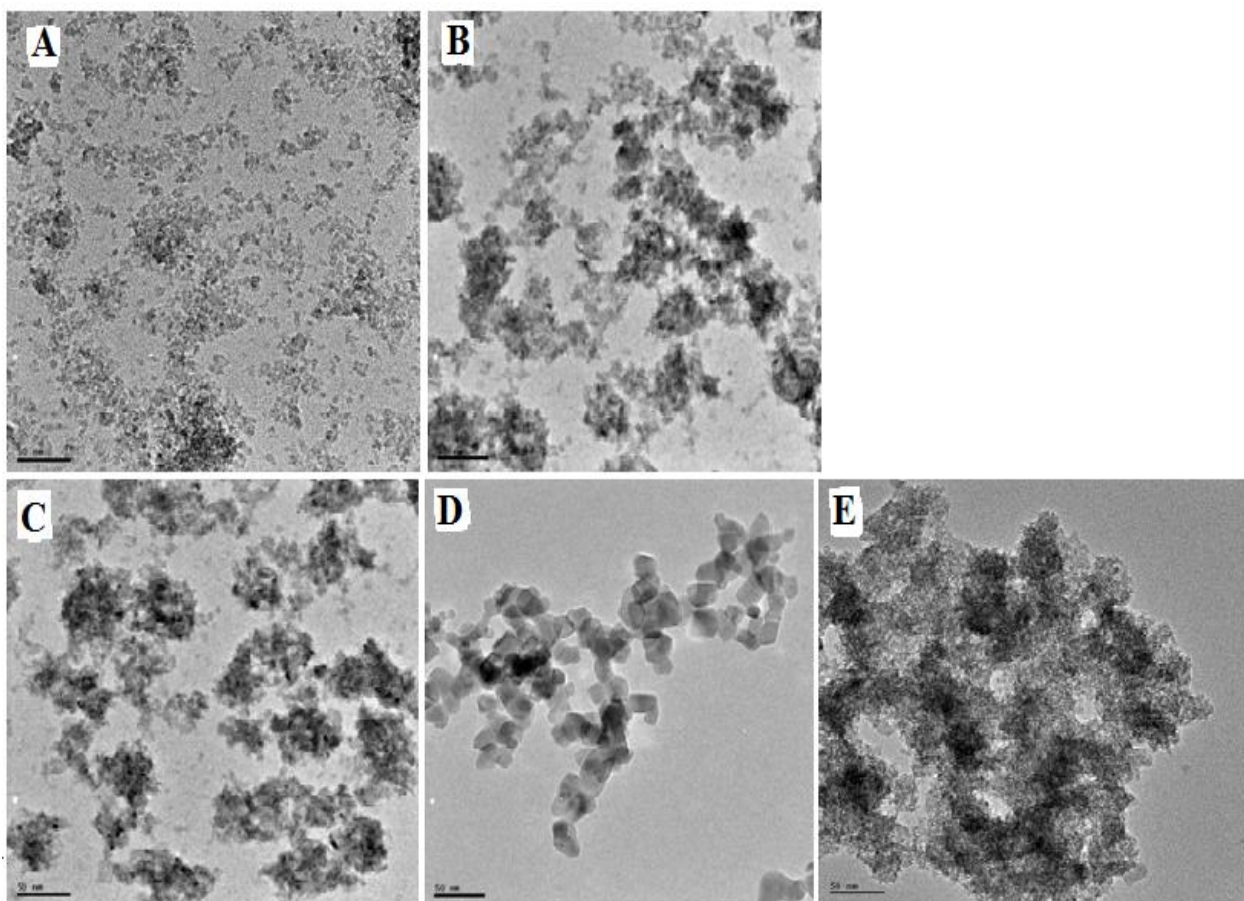


**Figure 4.6:** Transmission electron microscopy (TEM) analysis for (A)  $\text{TiO}_2$  (B) 0.2% CPE- $\text{TiO}_2$  (C) 0.4% CPE- $\text{TiO}_2$  (D) 0.6% CPE- $\text{TiO}_2$  and (E) 0.8% CPE- $\text{TiO}_2$

#### 4.2.3 Energy-dispersive X-ray spectroscopy (EDS/EDX) analysis

For the identification of the atomic compositions in the synthesised materials, the EDX chemical analysis was performed. The analysis involves the detection of the excitation photons from the composite elements with the aid of solid detector Si-Li (detection by energy dispersion). The energy of photons is a characteristic of its atoms, which is a mean to achieve the elemental analysis of the samples. A spectrum consisting of various lines (peaks) was obtained (**Figure 4.7**); each corresponds to a photon of given energy (KeV), thus represents a given element. The analysis was also done quantitatively to illustrate percentage compositions.

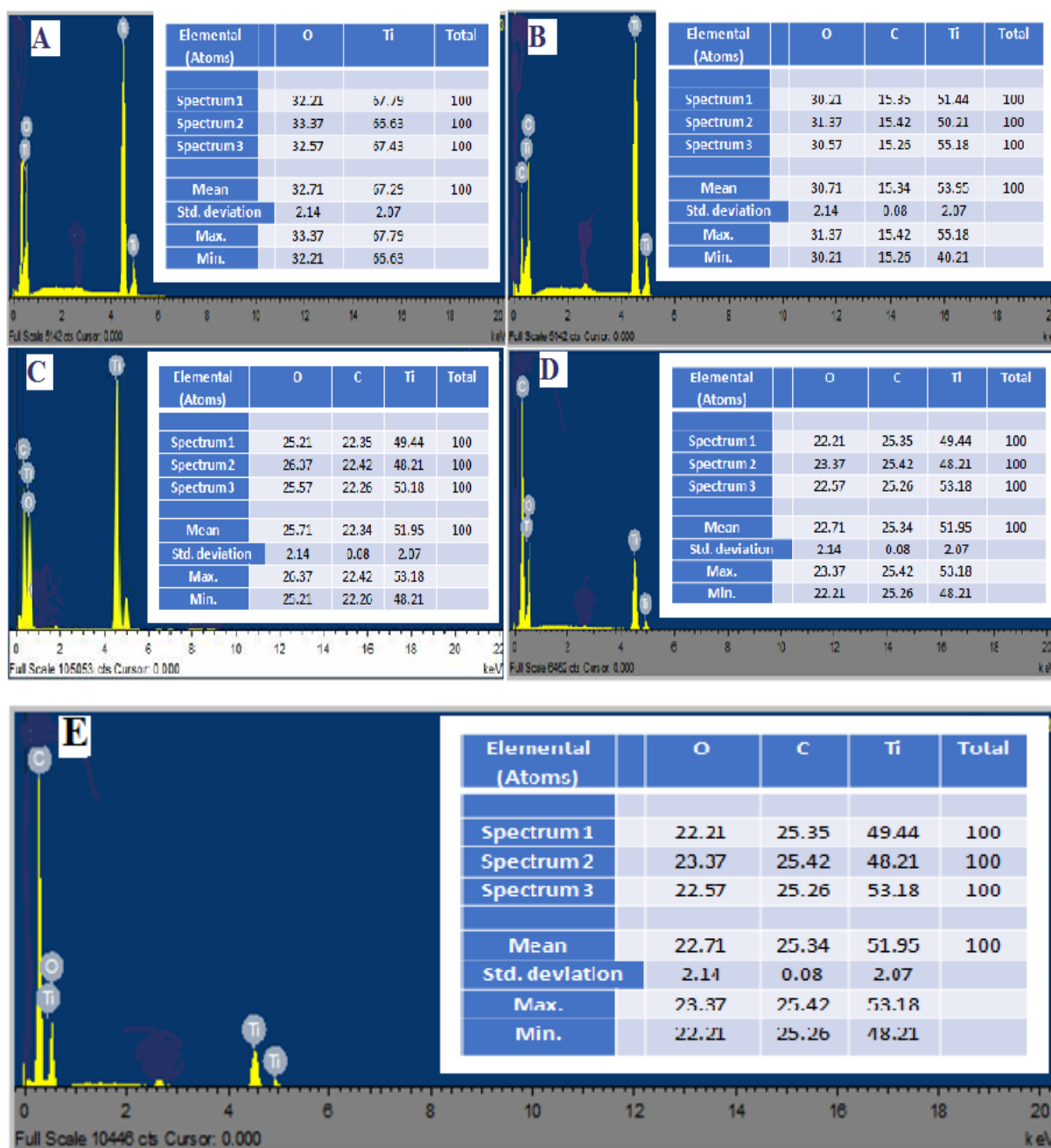


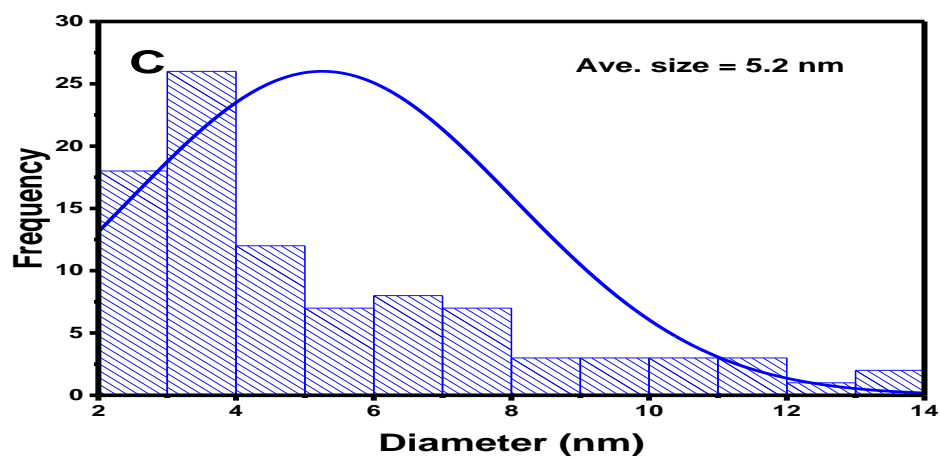
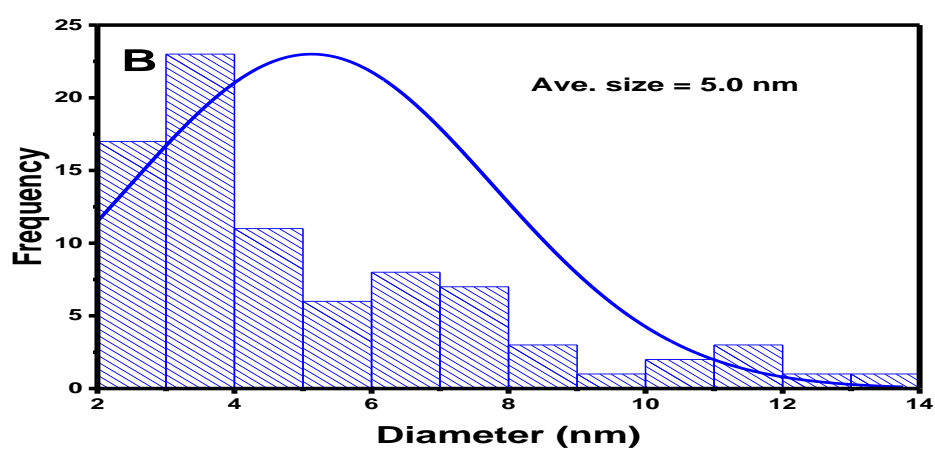
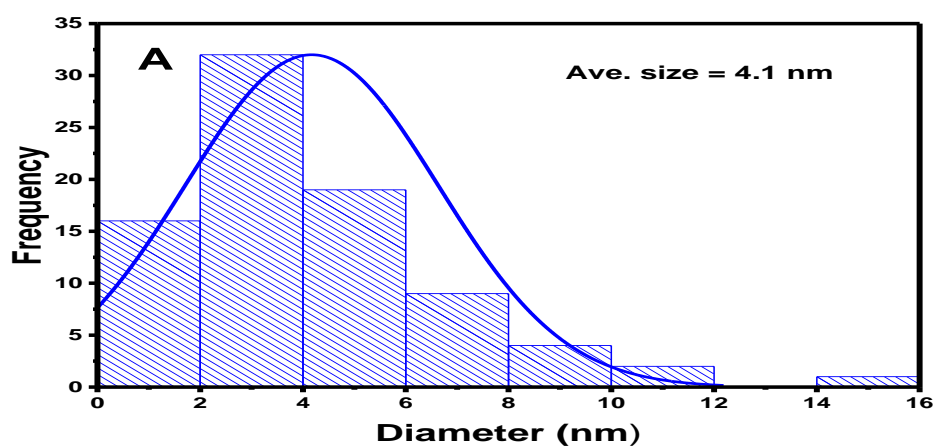
**Figure 4.7:** Energy dispersive X-ray spectroscopy (EDS) analysis of (A) TiO<sub>2</sub> (B) 0.2% CPE-TiO<sub>2</sub> (C) 0.4% CPE-TiO<sub>2</sub> (D) 0.6% CPE-TiO

The intensity of each peak in the spectra obtained is proportional to the concentration of the corresponding element in the material volume. **Figure 4.7** presents the EDX results for pure TiO<sub>2</sub> and CPE-TiO<sub>2</sub> at varying polyene percentages. It was observed that the materials composed of Ti and O for pure TiO<sub>2</sub> (**Figure 4.7A**), and Ti, O and C for the composite materials (**Figure 4.7B-D**). This

observation shows the purity of the sample as an indication of the suitability of the method used in the preparation.

#### 4.2.4 Particle size, shape and composition of the materials

It was suggested that when particle's surface area increases by reducing the particle size, especially down to a nano-size range, photocatalytic characteristics could be considerably improved (Kim *et al.*, 2004). It then implies that the size and the shape of photocatalyst have a direct influence on its performances. Gaussian fit particle size distribution from TEM micrographs images was used to estimate the average particle size and size count distribution of the materials. **Figure 4.8** illustrates the average particle sizes and size count distributions for bare and modified TiO<sub>2</sub>. The average particle sizes obtained for the materials were in the nanosized range, indicating a high reactive surface area, which is beneficial to improve photocatalytic activity. As reported, a high surface to volume ratio of photocatalysts would increase surface oxygen content defect, which prevents electron/hole recombination and improves visible light photocatalytic activity (Wang *et al.*, 2016).



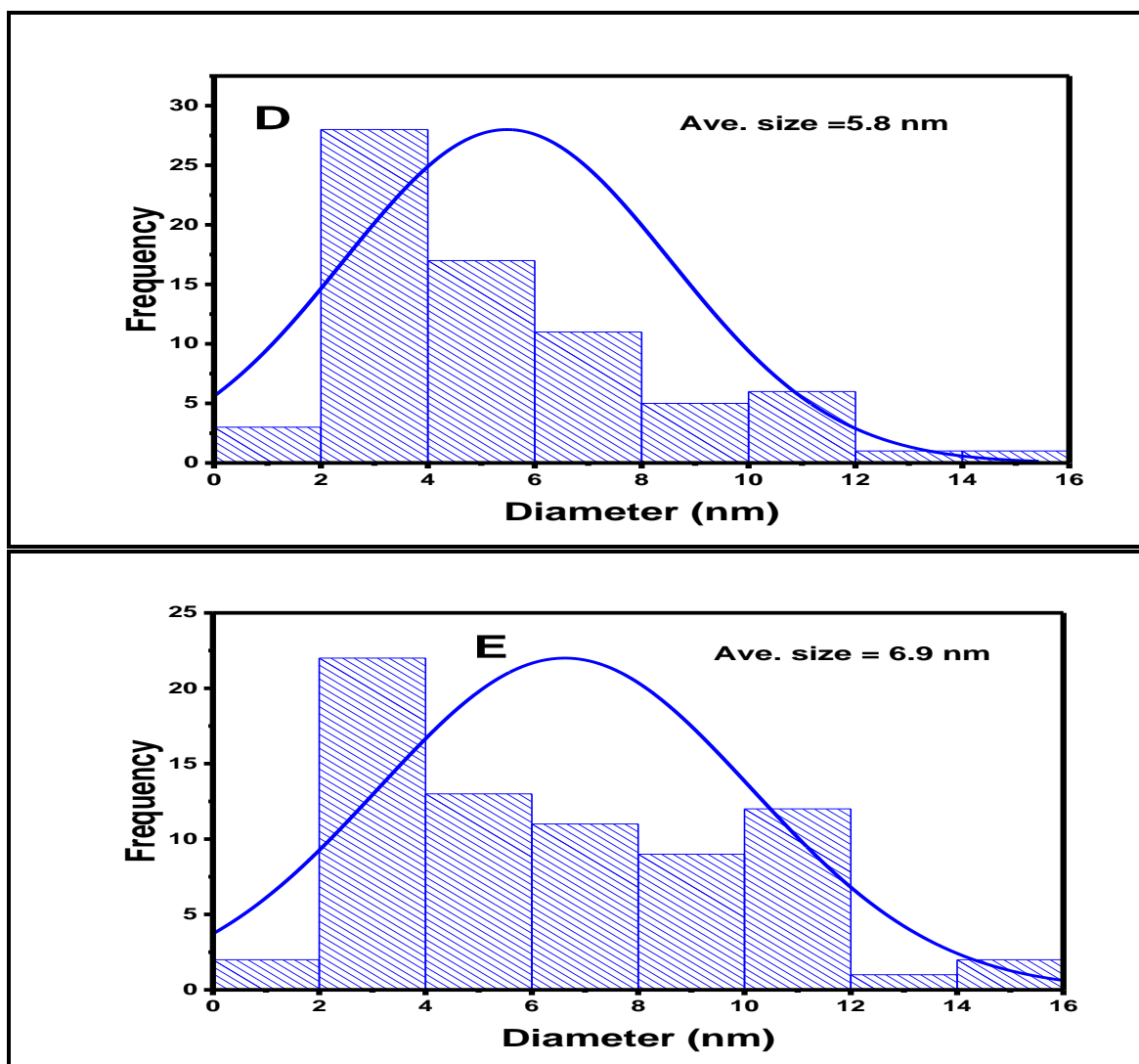


**Figure 4.8:** Gaussian fit particle size distribution plots from TEM micrograph for (A)  $\text{TiO}_2$ , (B) 0.2% CPE- $\text{TiO}_2$ , (C) 0.4% CPE- $\text{TiO}_2$ , (D) 0.6% CPE- $\text{TiO}_2$ , (E) 0.6% CPE- $\text{TiO}_2$ .

It was observed that  $\text{TiO}_2$  gave the smallest average or mean particle size, which was measured to be 4.1 nm (**Figure 4.8A**) with a standard deviation ( $W/2$ ) of 0.43, giving an average particle size of  $4.10 \pm 0.43$  nm and that the particle sizes increase with CPE- $\text{TiO}_2$  as the polyene percentage modifications increases (**Figure 4.8B-E**), giving average particle sizes of 5.0 nm, 5.2 nm, 5.8 nm and 6.9 nm for 0.2% CPE- $\text{TiO}_2$ , 0.4% CPE- $\text{TiO}_2$ , 0.6% CPE- $\text{TiO}_2$  and 0.8% CPE- $\text{TiO}_2$  respectively. This observed trend agrees with SEM and TEM results and is due to polymer capping on

the TiO<sub>2</sub> nanoparticles, which grow in layers as the quantity of CPE increase and lead to increase in the particle size.

## **Conclusion**

Pure TiO<sub>2</sub> and CPE-TiO<sub>2</sub> composite nanoparticles were synthesised using a facile homogenised sol-gel synthesis procedure. The materials were appropriately characterised for structural and morphological properties using various analytical techniques. The powder X-ray diffraction studies showed that the TiO<sub>2</sub> nanoparticles are in anatase phase with an average crystallite size of 3.41 nm and 7.51 nm for the modified form (CPE-TiO<sub>2</sub>). Scanning electron micrographs (SEM) and transmission electron micrographs with energy dispersion spectroscopy (TEM-EDS) results showed a well interactive polymer/TiO<sub>2</sub> nanocomposite material. The SEM showed that the particles are mostly circularly shaped of an average size of 4.1 nm for bare TiO<sub>2</sub> and 5.8 nm for CPE-TiO<sub>2</sub> composite. The EDS spectra show a well dispersed elemental composition with three different peaks, representing Ti, O and C, which is an indication of the degree of purity of the materials. The height of carbon peak in the composite was observed to increase as the CPE percentage modification increased. The synthesised materials showed a good structural and morphological properties suitable for efficient photocatalysis. However, there is a need to check the electronic properties of the materials in order to investigate their electron/hole pair generation efficiency.

## Section B: Optical and electrochemical characterisation

### Introduction

In this section of the work, we present the results obtained and the discussion on the characterisation in terms of the optical and electrochemical properties of the synthesised materials. The optical and electronic properties of a photocatalyst play a crucial role in its photocatalytic activity. Hence, different materials such as metals and non-metal and organic polymers have been employed to tune the electronic structure of photocatalysts to enhance the photocatalytic performance of  $\text{TiO}_2$  (Yu *et al.*, 2009).

### 4.3 Optical characterisation

#### 4.3.1 UV-Vis electronic absorption of PVA and CPE

Since the conjugated polyene (CPE) material was derived from polyvinyl alcohol (PVA), following the scheme illustrated in Chapter 3, the UV-vis absorption spectra of polyene and PVA were then compared at the visible light region of absorption. The first stage of thermal degradation of polyvinyl alcohol (PVA) usually involves the cleavage of the hydroxyl group and hydrogen atoms from the polymer in an elimination kind of reaction. This elimination process results in the formation of polyene and water molecules (Tretinnikov and Sushko, 2015). **Figure 4.89** presents the UV-Vis absorption spectra of PVA and CPE over a range of 900 to 350 nm.

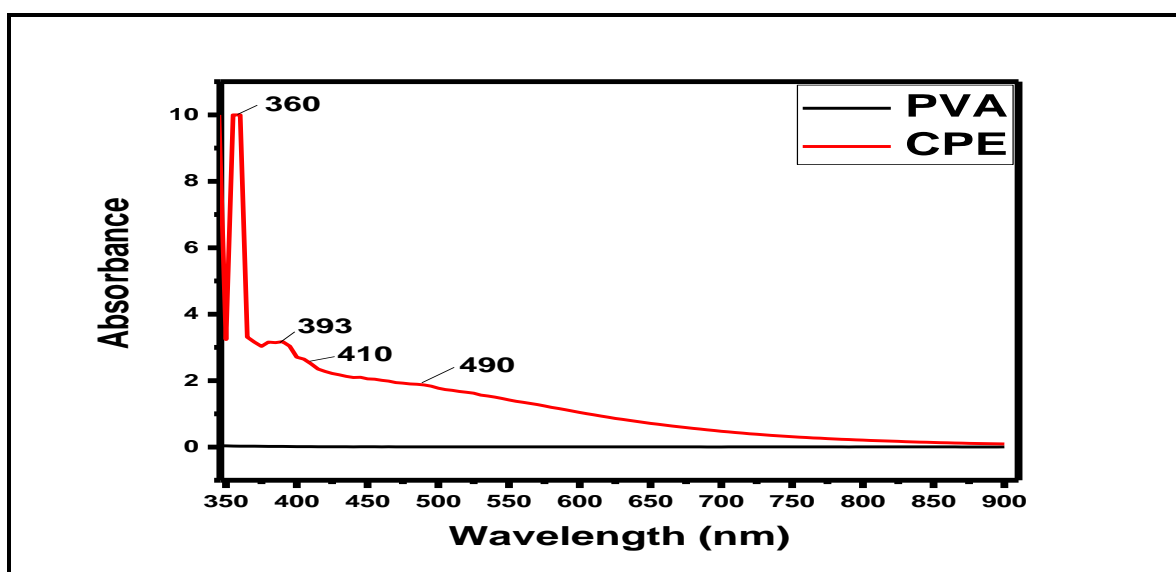
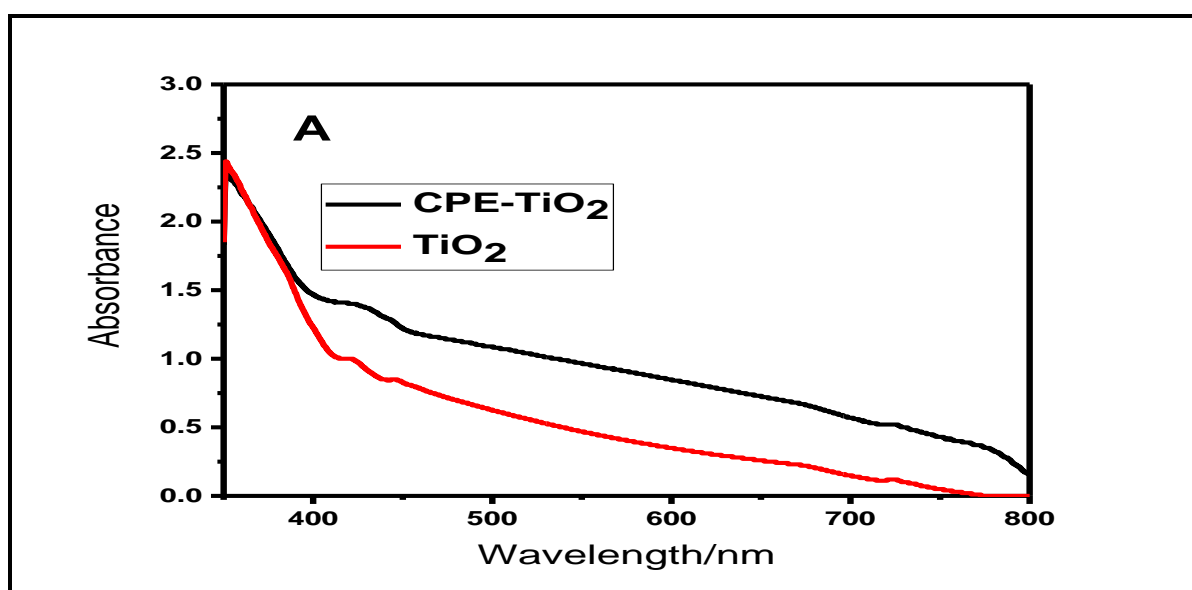


**Figure 4.9:** UV-Vis electronic absorption spectra of PVA and CPE

It was observed that PVA has no absorption peaks at the visible light region while the prepared CPE shows intense peaks, particularly at 393, 410 and 490 nm. These visible absorption peaks indicate a new chromophore (C=C), which is expected in the polyene molecule as supported by the FTIR spectra. Linear polyene with greater or equivalent to eight conjugated double bonds ( $C=C \geq 8$ ) is characterised by intense electronic absorption bands (EAB) that lie in the visible region of the light spectrum (Tretinnikov and Sushko, 2015).

#### 4.3.2 UV-Vis, UV-Vis DRS electronic absorption and Tauc plots of bare $TiO_2$ and CPE- $TiO_2$ composites

The light absorption capacity of semiconductors is an important characteristic for the evaluation of its optical property and photocatalytic performance (Dong *et al.*, 2014). Consequently, ultraviolet-visible diffused reflectance and fluorescence spectroscopic studies were carried out to investigate the optical characteristics of the synthesised materials. The UV-Vis DRS spectra and the Tauc plot for the materials are presented in **Figure 4.10A** and **4.10B**.





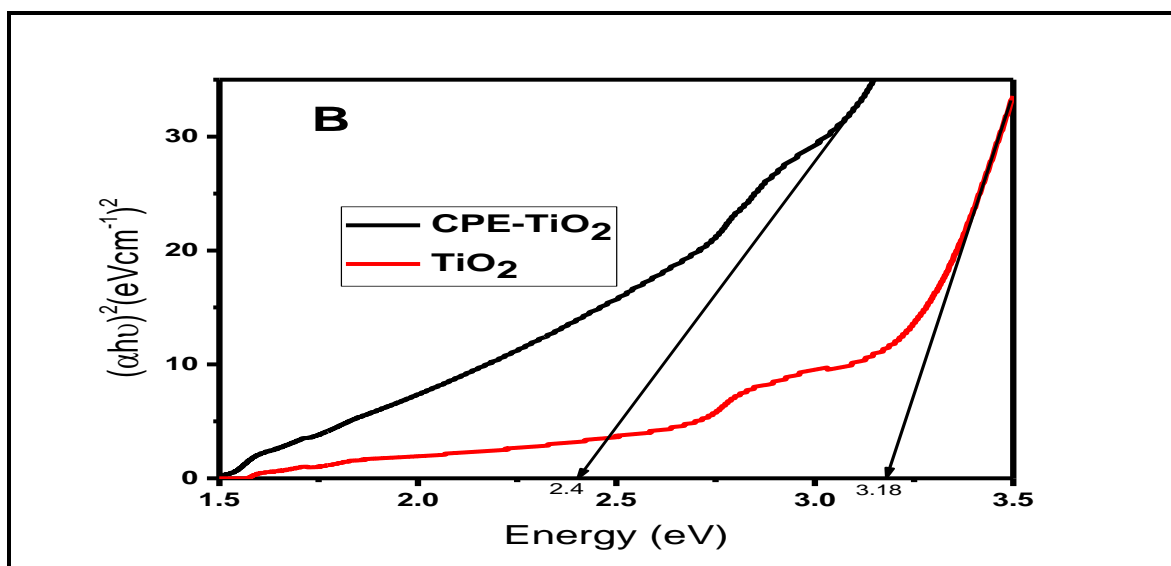


**Figure 4.10:** (A) Uv-vis DRS spectra of bare TiO<sub>2</sub> and 0.6% CPE-TiO<sub>2</sub> and (B) Tauc plot for bare TiO<sub>2</sub> and 0.6% CPE-TiO<sub>2</sub>

A redshift in the absorption edge was observed for all the materials in the sequence of 0.2% CPE-TiO<sub>2</sub> < 0.4% CPE-TiO<sub>2</sub> < 0.6% CPE-TiO<sub>2</sub>. It is well known that pure TiO<sub>2</sub> lacks effective visible light (>400 nm) absorption. However, the composite presents a significant increase in light absorption within a wide range of wavelengths (400 nm – 700 nm) at the visible region. This increase in absorption indicates that CPE-TiO<sub>2</sub> has a better UV-Vis light absorption capacity as compared to that of bare TiO<sub>2</sub>, which also implies that at the visible light region, CPE-TiO<sub>2</sub> composite possesses a better photon absorption, thus better ability to maintain pollutant degradation in wastewater after treatment systems.

Tauc plot was constructed from the UV- Vis DRS spectra and used in estimating the direct bandgap energy of the materials. Tauc's relationship for estimating the bandgap energy of the materials is presented in Equation 4.2.

$$(\alpha h\nu)^2 = A(h\nu - E_{bg}) \quad \text{Equation 4.2}$$

Where  $\alpha$ ,  $h\nu$ ,  $A$  and  $E_{bg}$  represent the absorption coefficient, photon energy, relationship constant and energy band-gap, respectively. If the straight line for equation 5.1 is extrapolated (**Figure 4.10B**), the band-gap energy can be obtained. The estimated band-gap energies for the materials obtained from the Tauc plot is given in **Table 5.1**. The absorbance and bandgap energy of materials are subject to factors such as particle size, oxygen deficiency and crystallite sizes (Huang *et al.*, 2000; Soitah *et al.*, 2010). These properties are often determined and influenced by synthetic methods.

**Table 4.2:** The crystallite sizes and bandgaps for bare TiO<sub>2</sub> and CPE-TiO<sub>2</sub>

Materials	Crystallite size (D) (nm)	Bandgap Energy (eV)
TiO <sub>2</sub>	3.41	3.18
0.2% CPE-TiO <sub>2</sub>	7.51	3.02
0.4% CPE-TiO <sub>2</sub>	8.37	2.80
0.6% CPE-TiO <sub>2</sub>	8.39	2.40

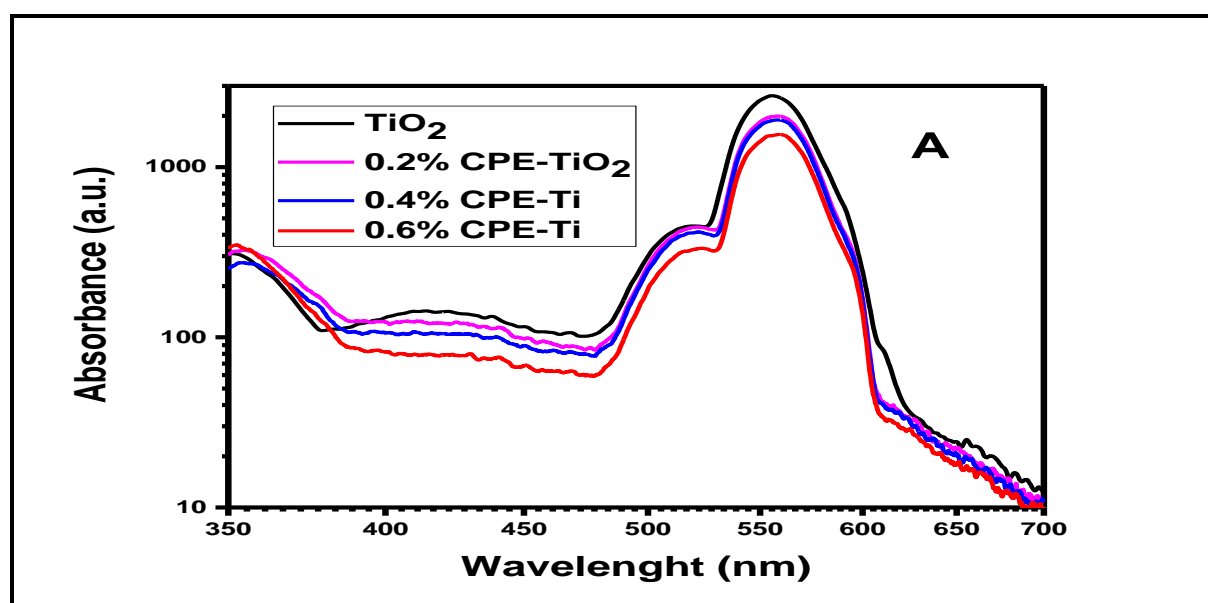
A correlation was observed between the crystallite size of the materials and the bandgap energy. Though the crystallite sizes increase with percentage modification, the bandgap was observed to decrease. Theoretically, the redshift in absorption as a result of decreased bandgap energy of CPE-TiO<sub>2</sub> implies that it will absorb more photons under visible light compared to bare TiO<sub>2</sub>. This observation agrees with a report that stated; coupling TiO<sub>2</sub> with a conjugated molecule resulted in a redshift (decrease in bandgap) in absorption value due to the formation of new energy state levels (Yang *et al.*, 2018). In this case, the coupling of CPE with TiO<sub>2</sub> showed a decrease in bandgap value of bare TiO<sub>2</sub> by 0.78 eV (**Figure 4.10B**), which corroborates a better performance of CPE-TiO<sub>2</sub> catalysts under visible light.

The photodegradation efficiency of a semiconductor was established to largely depend on good light absorption and rapid transfer of charge carriers to the surface for redox reaction (Yang *et al.*, 2013; Yi *et al.*, 2017). It then implies that CPE-TiO<sub>2</sub>

has a better visible light absorption capacity and more rapid electron transfer. This fact is also well supported by a reduced electron-hole recombination rate as presented in photoluminescence spectra measured.

#### 4.3.3 Photoluminescence (PL) measurement of bareTiO<sub>2</sub> and CPE-TiO<sub>2</sub>

Application of photoluminescence (PL) is an efficient method to study the migration, separation and recombination activities of photogenerated electron-hole pairs in semiconductor photocatalysts (Guo *et al.*, 2018; Mou *et al.*, 2018). The emission signal in PL is established to have originated from the recombination of the induced charge carrier. Hence, the charge generation, separation and recombination properties of bare TiO<sub>2</sub> and CPE-TiO<sub>2</sub> composite were explored by the PL measurement of the materials. **Figure 4.11A and 4.11B** illustrate the PL spectra of TiO<sub>2</sub> and CPE-TiO<sub>2</sub> with two emission peaks of both centred at shorter wavelength 520 nm and longer wavelength around 560nm measured at room temperature.



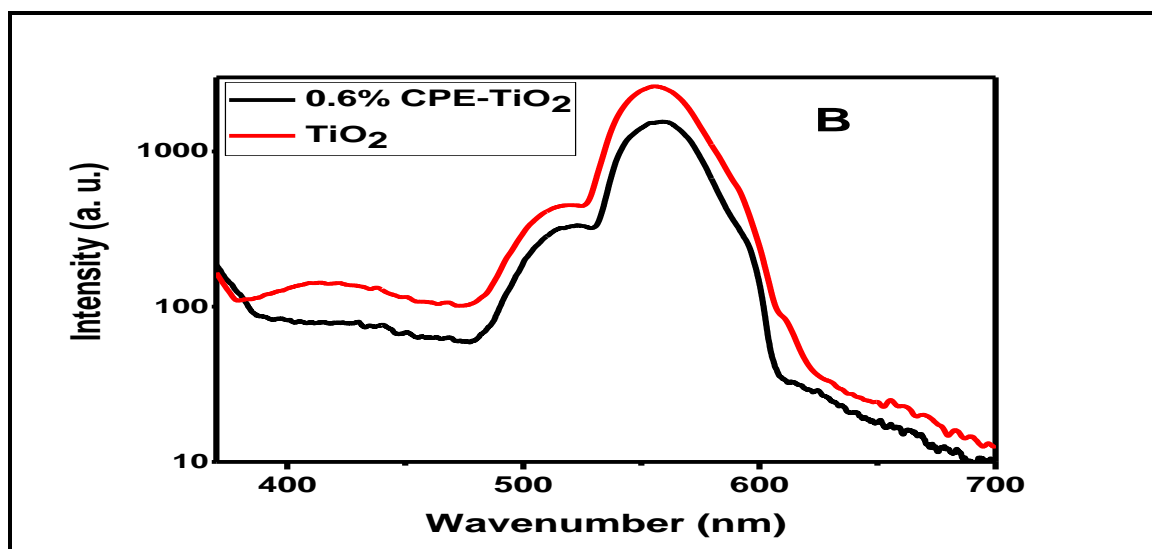


**Figure 4.11:** The photoluminescence (PL) spectra of (A)  $\text{TiO}_2$  and CPE- $\text{TiO}_2$  at varying polyene percentage modification (B)  $\text{TiO}_2$  and 0.6% CPE- $\text{TiO}_2$

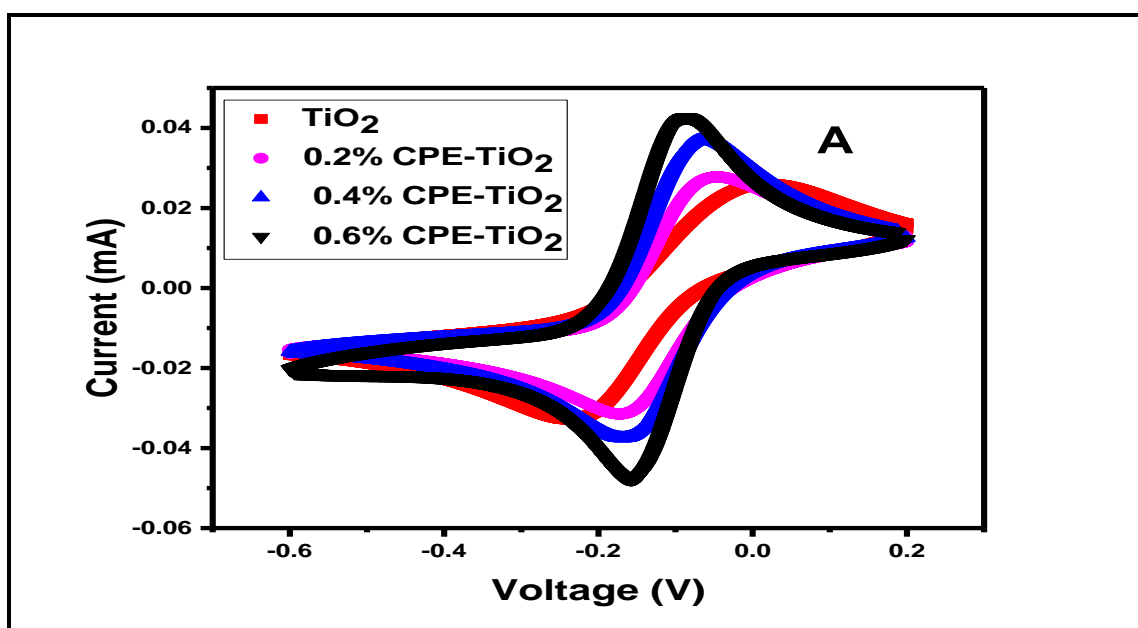
The bands originated from the recombination transition of free electrons and holes. However, the emission maximum at about 560 nm is relatively stronger than other emission peaks with CPE- $\text{TiO}_2$  composite presenting a lower emission peak. The relative peak heights of the spectra are usually compared to examine a change in the recombination rate. When the PL intensity is higher, it indicates a higher electron-hole recombination rate. The reverse is the case when the intensity is lower (Parayil *et al.*, 2012). Carbon, particularly in a conjugated molecule has been reported to reduce the electron-hole recombination rate in  $\text{TiO}_2$  by acting as electron sinks and promotes the formation of oxygen vacancies, which also supports electron sinks (Shao *et al.*, 2015). From the literature, the lower photoluminescence signal intensity shows a more efficient charge separation in the photocatalyst (Yi *et al.*, 2017; Hou *et al.*, 2014).

For the CPE- $\text{TiO}_2$  composite, the PL emission intensity at longer wavelength is lower compared to that of  $\text{TiO}_2$ , indicating that the incorporation of CPE favours the separation of photogenerated charge carrier, which then prevents the recombination of electron-hole pairs. This increase in electron transfer can be attributed to the pie-conjugated unit provided by CPE (Hwang & Scholes 2011).

## 4.4 Electrochemical characterisation

### 4.4.1 Cyclic voltammetry analysis

To further investigate the electrochemical property of the materials, cyclic voltammetry (CV) was applied to measure current flow as a function of electron transfer. **Figure 4.12A and 4.12B** illustrate the cyclic voltammograms recorded on a potentiostat with a glassy carbon working electrode (WE), Ag/AgCl reference electrode (RE) and Pt.-wire counter electrode (CE). The redox-peak potentials enable us to analyse the electrochemical reversibility of the reaction at the electrode surface by increasing the scan rates during experiments. It was observed that the CPE modified materials gave higher current (0.04 mA) flow as compared to bare  $\text{TiO}_2$ . (0.026 mA). The higher current flow is an indication of better electron transfer in CPE- $\text{TiO}_2$ , which is essential in photocatalytic processes.



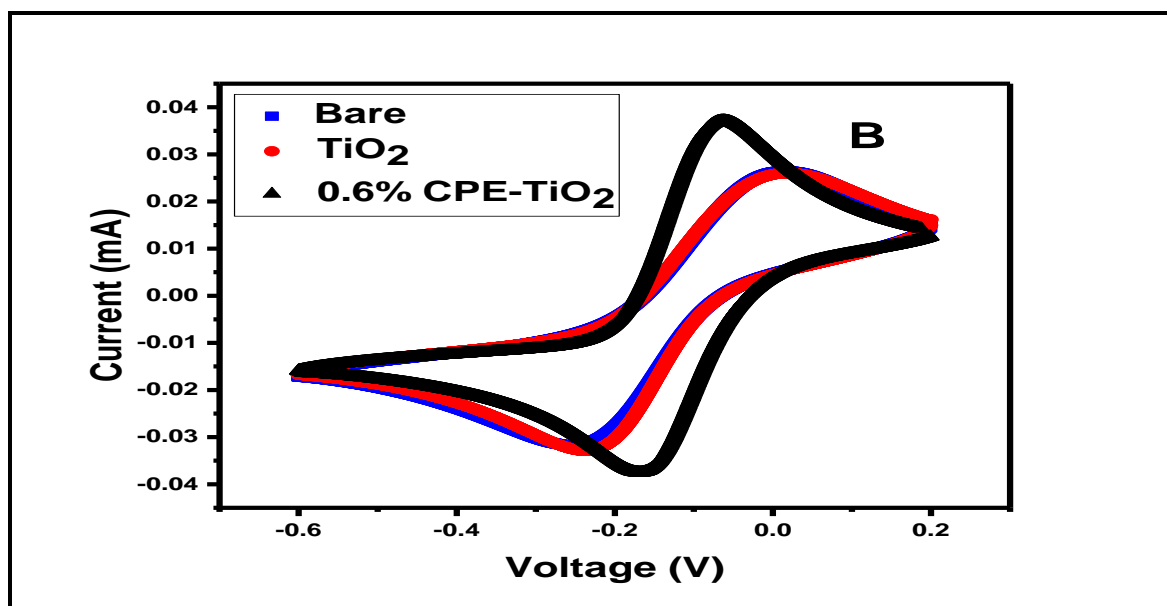


**Figure 4.12:** CV curve for (A)  $\text{TiO}_2$  and CPE- $\text{TiO}_2$  at varying polyene percentage modification (B) bare-electrode,  $\text{TiO}_2$  and 0.6% CPE- $\text{TiO}_2$

#### 4.4.2 Electrochemical impedance spectroscopy

The electrochemical impedance spectroscopy (EIS) Nyquist plots were also employed to provide an insight, regarding the available distinctive electronic properties of the CPE- $\text{TiO}_2$  as compared to the bare  $\text{TiO}_2$ . The charge generation and transfer properties of the materials were evaluated. **Figure 4.13A and 4.13B** present the Nyquist plots for the transport process of photogenerated electron/hole pairs. The comparative sizes of the arc radius correspond to the interface layer resistance at the surface of the electrode, thus smaller radius usually represents lower charge transfer resistance (Deng *et al.*, 2015). A much smaller arc was observed for CPE- $\text{TiO}_2$  as compared to that of pure  $\text{TiO}_2$  (inset of **Figure 4.13B**). This indicates less impedance or resistance to the flow and transfer of generated electrons in CPE- $\text{TiO}_2$  during the photo-excitation process (Zhang *et al.*, 2014). This smaller arc further confirms the fast charge transfer and more effective charge separation in CPE- $\text{TiO}_2$  composite compared to that which occurs in bare  $\text{TiO}_2$  (Han *et al.*, 2015; Chen *et al.*, 2018).

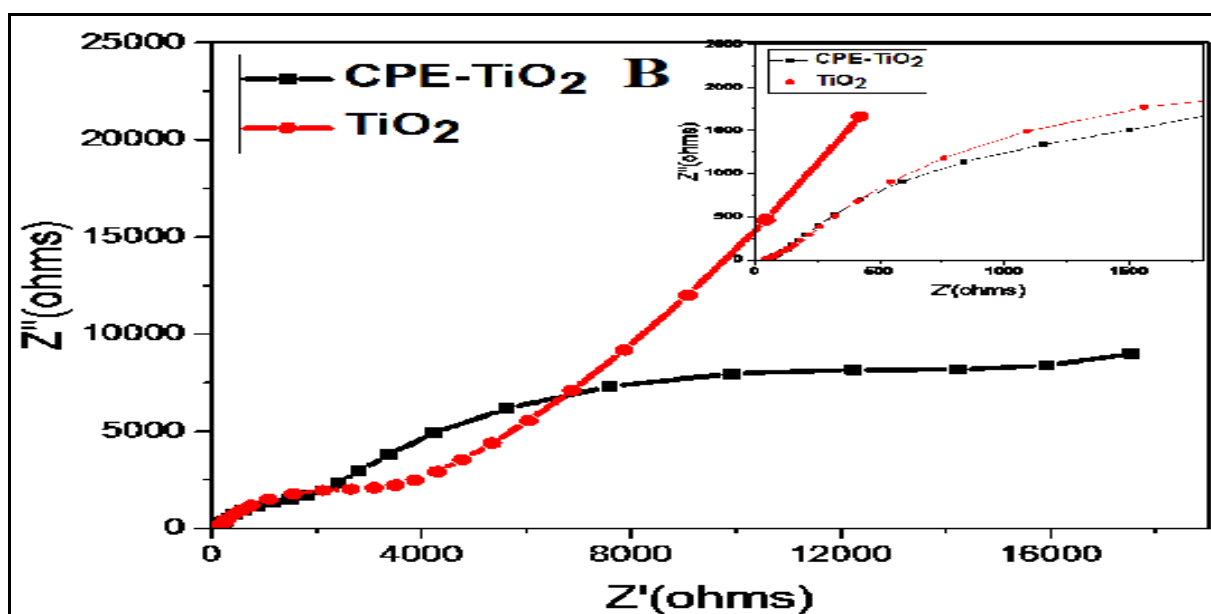
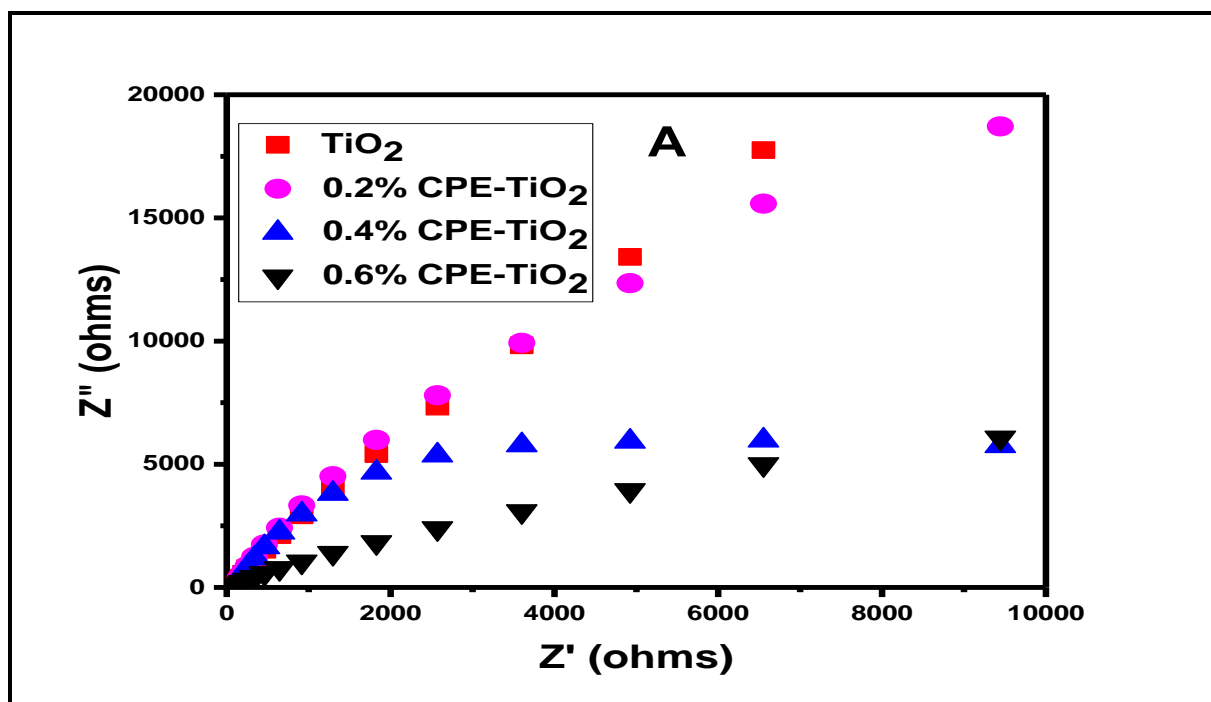


**Figure 4.13:** The EIS Nyquist plots of (A)  $\text{TiO}_2$  and CPE- $\text{TiO}_2$  at varying polyene percentage modification and (B)  $\text{TiO}_2$  and 0.6% CPE- $\text{TiO}_2$

## Conclusion

The optical property revealed an improvement in the visible light absorption capacity of the polyene sensitised  $\text{TiO}_2$  over bare  $\text{TiO}_2$  with an excellent enhancement of

electron-hole separation, as indicated by UV-Vis DRS and photoluminescence results respectively. A significant reduction in the synthesised  $\text{TiO}_2$  band gap (3.18 eV) was observed with the CPE- $\text{TiO}_2$  band gap (2.4 eV) as estimated from Tauc plot, which implies a better light absorption at the visible region of the light spectrum. The cyclic voltammetry and electrochemical impedance spectroscopy measurement for the materials show a good electronic property that is appropriate for the photocatalytic process. The observed optical and the electrochemical properties of the synthesised materials indicate an effective electron release, thus can serve as a good photocatalyst for the degradation of organic pollutants in wastewater. Hence, the following chapter discussed the photocatalytic ability of the materials for the degradation of APAP and CAP at varying experimental conditions.



## Section C: The photocatalytic parameters investigation for the degradation of APAP, CAP and durability test of the photocatalyst

### Introduction

This section presents the results obtained and the discussion on the studies on the effects of operating parameters on the photocatalytic degradation of acetaminophen (APA) and chloramphenicol (CAP) using the catalysts prepared in Chapter 3. Various factors have been identified to influence the photodegradation of organic pollutants in aqueous solution. Among these factors, pH of the solution to be remediated, catalyst dosage (loading) and the initial concentration of the pollutants are essential, which are usually set as environmental parameters for effective photocatalytic degradation process.

### 4.5 Effects of catalyst dosage

**Figure 4.14 and 4.15** present the results obtained for the investigation of catalyst dosage effects on the degradation efficiency. Based on the preliminary experimental results, 25 mgL<sup>-1</sup> initial concentration was used to investigate the effect of the catalysts (CPE-TiO<sub>2</sub> and TiO<sub>2</sub>) dosage on the removal efficiency of APAP and CAP in aqueous solutions. As shown in **Figure 4.14A**, it was observed that APAP removal percentage increased from 80% to 94.21% for CPE-TiO<sub>2</sub> and from 20% to 27.12% for TiO<sub>2</sub>, when the catalysts dose was increased from 5 mg to 15 mg per 200 mL solution. Further increase of the catalysts dose (from 15 mg to 20 mg per 200 mL of the solution) did not improve APAP removal (94.21%) after the 210 min of photocatalytic degradation. By contrast, the removal dropped to 92.13% when the catalyst dose was further increased from 15 mg. The same trend of catalysts dose effects was observed for the removal of CAP by the two photocatalysts.

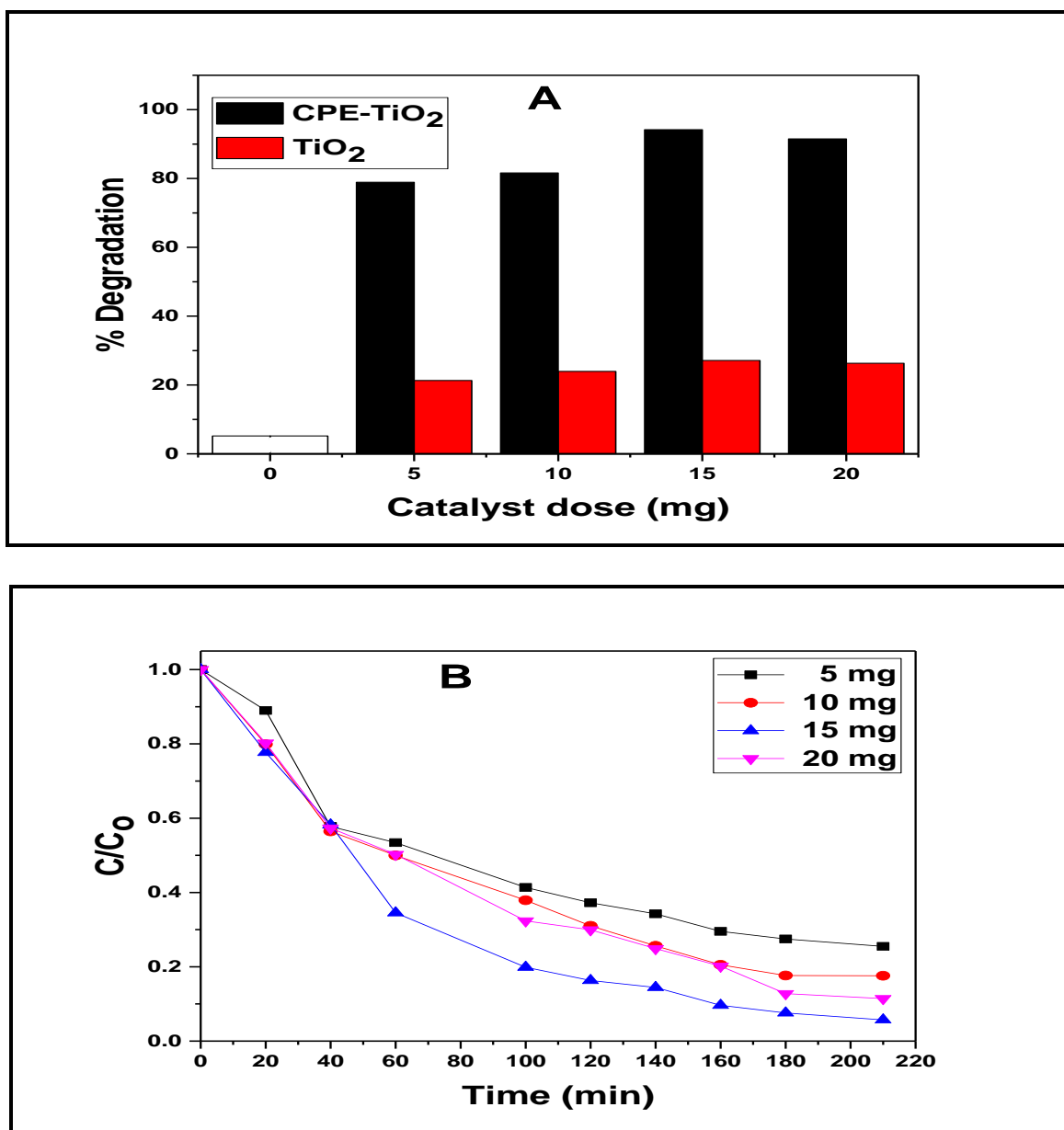


**Figure 4.14:** Visible light degradation of APAP by(A) bare TiO<sub>2</sub> and CPE-TiO<sub>2</sub> at various catalysts dosages (pH 8) and (B) the corresponding degradation rate (using CPE-TiO<sub>2</sub>) with respect to time

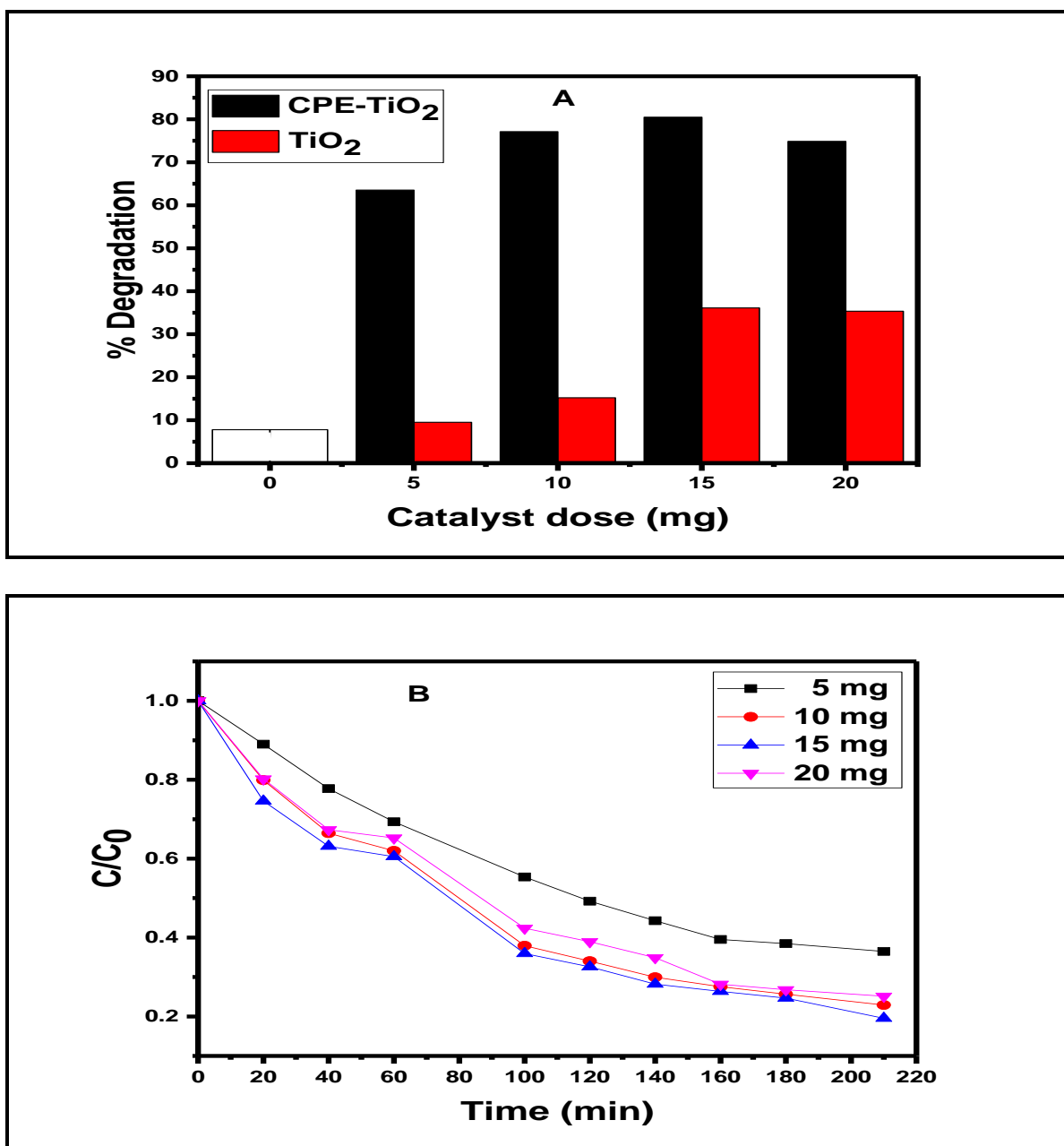


**Figure 4.15:** Visible light degradation of CAP by (A) pure TiO<sub>2</sub> and CPE-TiO<sub>2</sub> at various catalysts dosages (pH 8) and (B) the corresponding degradation rate (using CPE-TiO<sub>2</sub>) with respect to time

The drop in the removal percentage, when excess catalyst (>15 mg) was added to the system might have resulted in decrease of light penetration. Although higher catalyst dose was useful to provide more available active sites, shielding effects of the suspended catalysts could reduce photocatalytic degradation rates (Chiou *et al.*,

2008). Also, agglomeration and aggregation of nanoparticles may occur if a high catalyst to solution ratio is used, which could reduce its photocatalytic ability. Past studies showed that aggregation of nanoparticles does influence the optical properties of materials, consequently, their absorption ability and photocatalytic activity (Park *et al.*, 2013; Pap *et al.*, 2011; Pellegrino *et al.*, 2017).

Also, aggregation may decrease the available surface sites for photon absorption. The photolysis of the two pollutants under visible light irradiation without catalyst was used as a control, which gave 5.32% APAP removal and 7.78% CAP removal. The comparison of the degradation results, in the presence of catalysts and without catalyst indicates that a small amount (5 mg) of the catalyst used gave a considerable removal of the pollutants. The instantaneous concentrations of the two pollutants over their initial concentrations ( $C/C_0$ ) were also monitored and plotted against the time as presented in **Figure 4.14B and 4.15B**. Decreasing trends of the concentration can be clearly seen with different catalysts (CPE-TiO<sub>2</sub>) dosages, however, the lowest final concentration is achieved with the application of 15 mg catalyst dosage in 200 mL of the pollutant concentration.

#### 4.6 Effects of initial concentration

The effects of varying initial concentrations on degradation efficiency were also investigated using 50, 40, 30 and 25 mgL<sup>-1</sup> solutions of APAP and CAP. **Figure 4.16 and 4.17** present the decreasing trends of the four initial concentrations for APAP and CAP respectively. The highest removal percentage was achieved for both pollutants when the lowest initial concentration of 25 mgL<sup>-1</sup> was applied. This observation may be due to the fact that a high concentration of the pollutants can result in competition for active reaction sites and photons on the surface of the catalyst. At high initial concentrations, the pollutants would occupy a greater number of catalyst surface reactive sites, which could inhibit reactive oxidant generation.

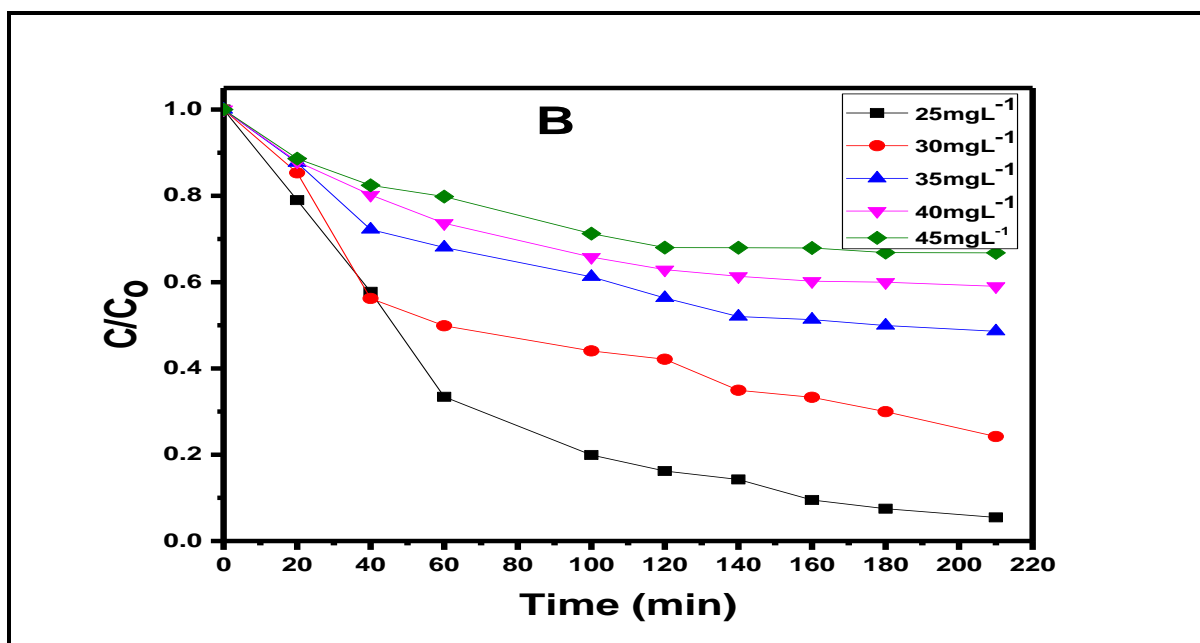
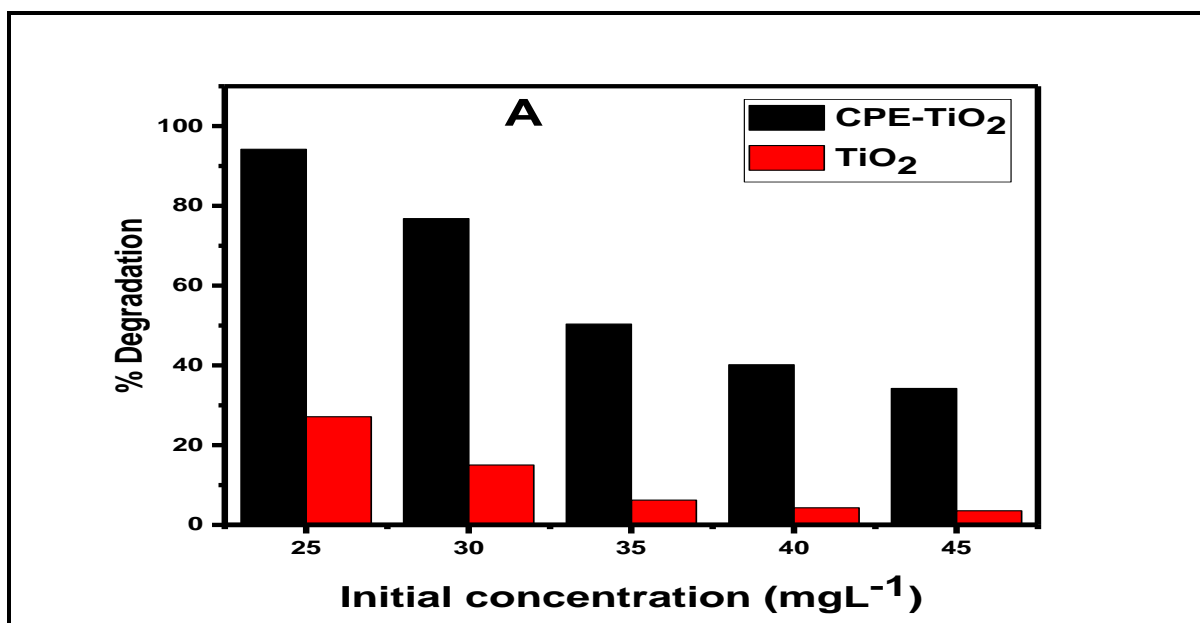


**Figure 4.16:** Visible light degradation of APAP by (A) bare TiO<sub>2</sub> and CPE-TiO<sub>2</sub> at various initial concentrations and (B) the corresponding degradation rate (using CPE-TiO<sub>2</sub>) with respect to time

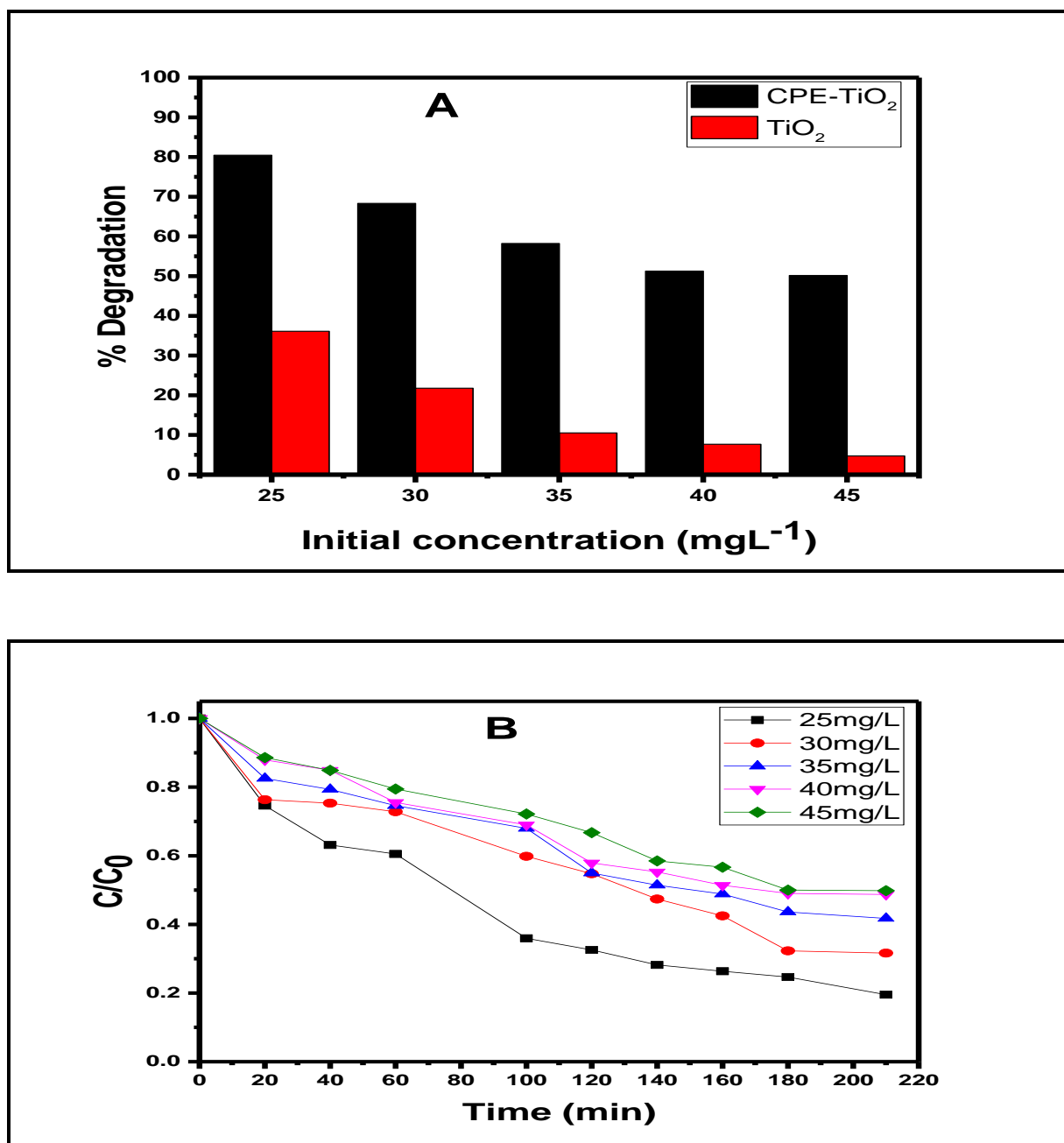


**Figure 4.17:** Visible light degradation of CAP by (A) bare TiO<sub>2</sub> and CPE-TiO<sub>2</sub> at various initial concentrations and (B) the corresponding degradation rate (using CPE-TiO<sub>2</sub>) with respect to time

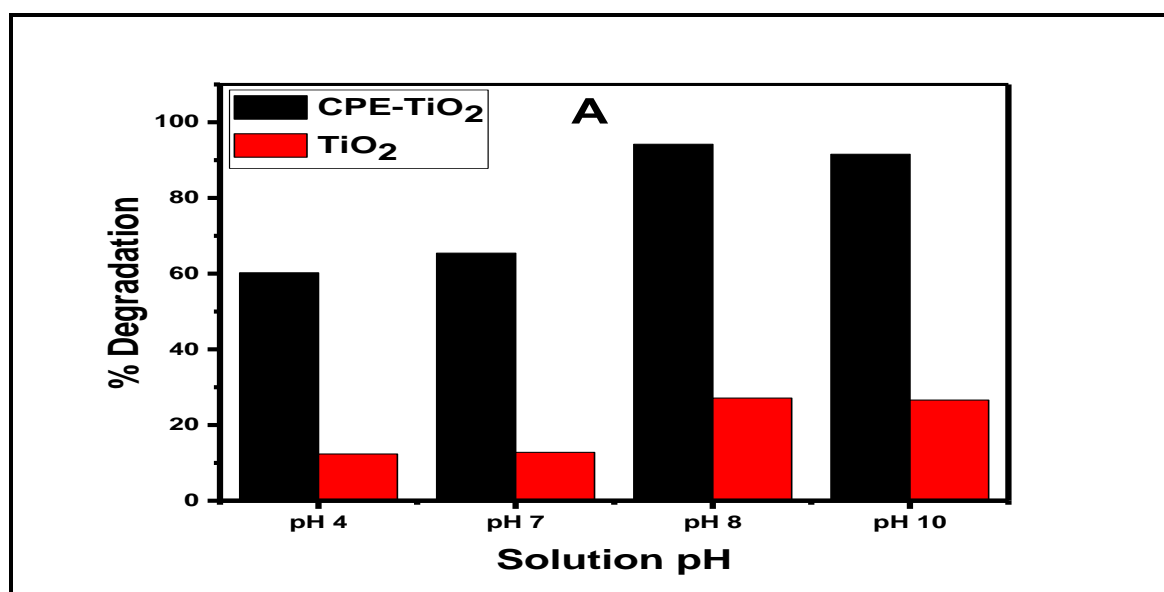
Since the pollutant molecules are capable of photon absorption, the higher initial concentration would likely absorb more photons. The more photons that are absorbed by the pollutants, the less available photons to activate the catalysts. An

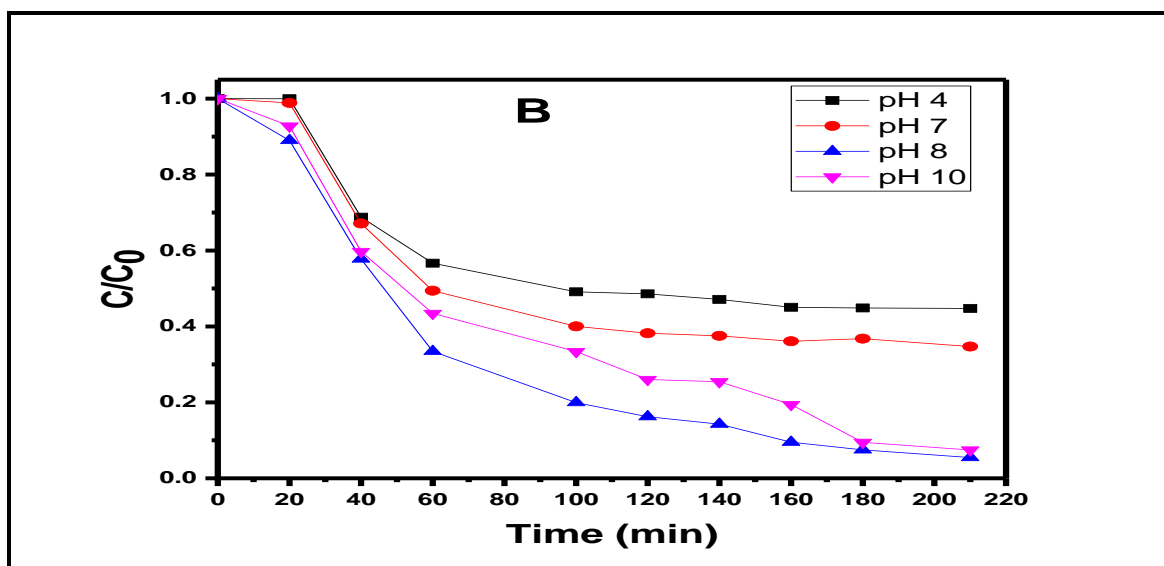
activated catalyst is required for the conversion of the photon energy into chemical energy by redox reaction for pollutant degradation (Yasmina *et al.*, 2014). Therefore, the inability to activate the surface of the catalyst due to insufficient photons would result in hindered pollutant degradation at higher concentrations.

**Figure 4.16B and 4.17B** illustrate the plots of the instantaneous concentrations over the initial concentrations ( $C/C_0$ ) of the pollutants. The five initial concentrations were observed to show decreasing trends and the highest pollutant removal was achieved at the end of the monitoring (after 210 min) when the lowest initial concentration ( $25 \text{ mgL}^{-1}$ ) was used for the two pollutants.

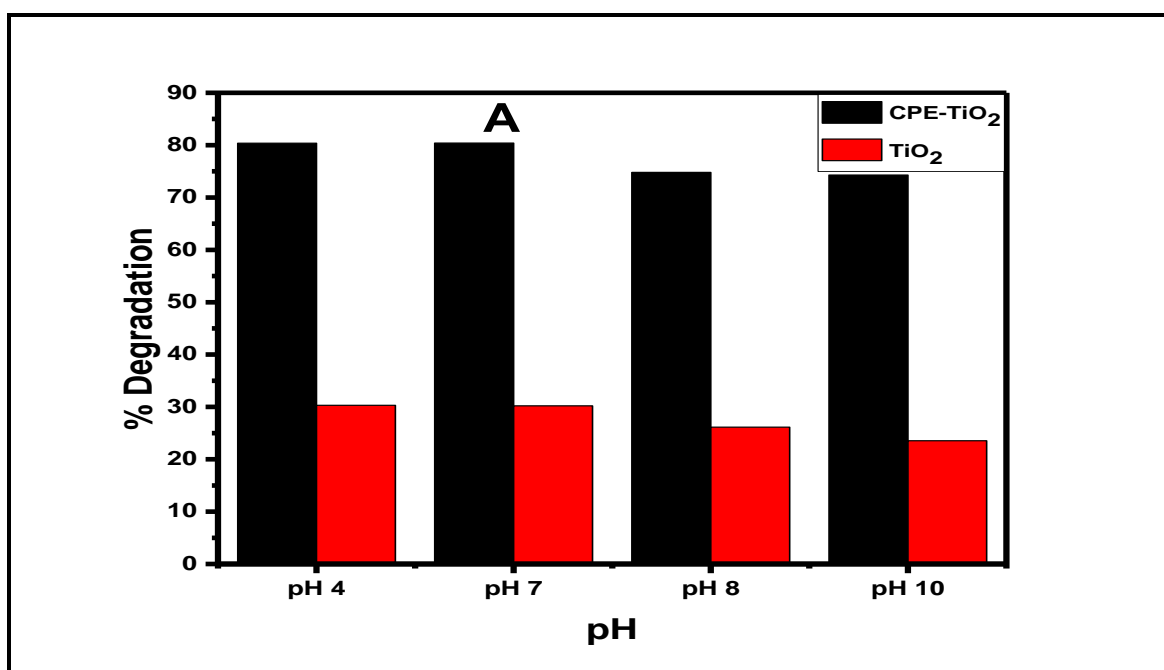
#### 4.7 Effect of the solution pH

Studies showed that the solution pH is an important factor that influences the formation of hydroxyl radicals during photodegradation of organic molecules in wastewater treatment (Jeong & Yoon, 2005; Moussavi *et al.*, 2017). Also, the pH of solution determines the surface charge properties of  $\text{TiO}_2$  photocatalyst, the charge of organic molecules and adsorption of organic molecules onto  $\text{TiO}_2$  surface (Jallouli *et al.*, 2017). Thus, the photodegradation of APAP and CAP was studied in the pH ranging from 4 to 10 and the results are as presented in **Figure 4.18 and 4.19** respectively. The results indicated that acidic medium does not favour the photodegradation of APAP, as the degradation efficiency is lower at lower pH value.





**Figure 4.18:** Visible light degradation of APAP by (A) bare  $\text{TiO}_2$  and CPE- $\text{TiO}_2$  at various pH and (B) the corresponding degradation rate (using CPE- $\text{TiO}_2$ ) with respect to time





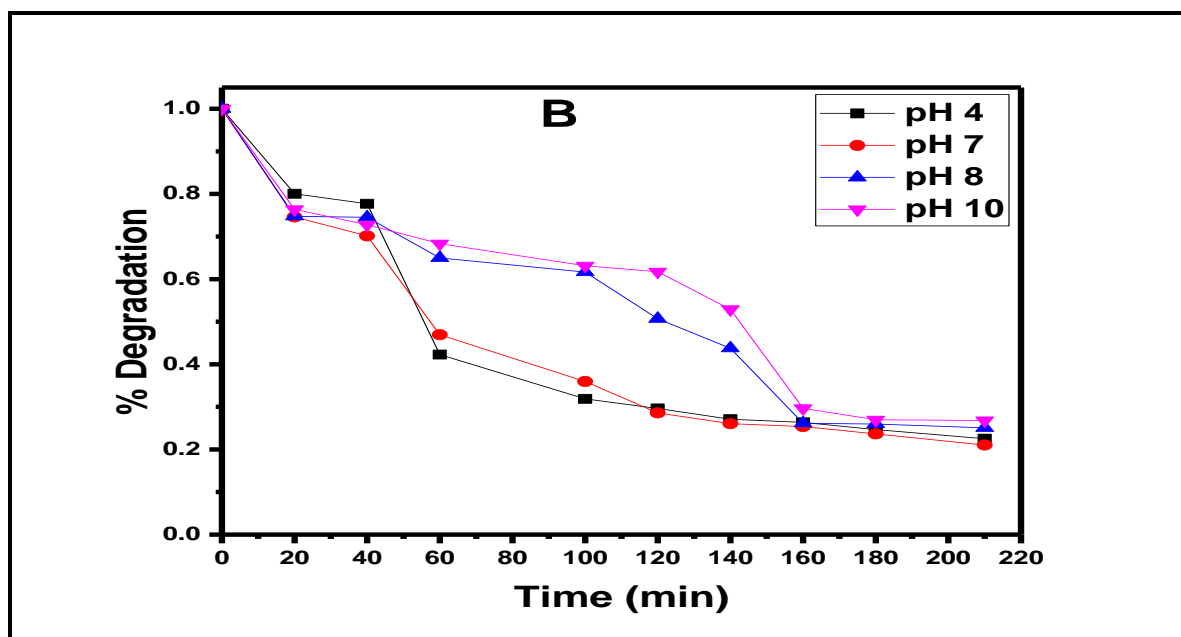


**Figure 4.19:** Visible light degradation of CAP by (A) bare TiO<sub>2</sub> and CPE-TiO<sub>2</sub> at various pH and (B) the corresponding degradation rate (using CPE-TiO<sub>2</sub>) with respect to time

Studies established that photodegradation efficiency is associated with the charge on the TiO<sub>2</sub> surface based on the pH of the solution medium (Jallouli *et al.*, 2017). In the acidic media (pH<7), the APAP is in its no charge form and at this state, its water solubility is reduced and the adsorption onto catalyst surface is maximised. As shown in **Figure 4.18A**, an increase in the pH of the solution enhanced the photodegradation efficiency until pH 8.0, when the degradation reaches the maximum. This observation can be attributed to enhanced formation of hydroxyl radicals (OH<sup>•</sup>), since at high pH, more OH groups are available on the TiO<sub>2</sub> surface, which can then be easily oxidised to form more OH<sup>•</sup> radicals (Galindo *et al.*, 2000). Thus, the efficiency of APAP degradation is increased in the process.

However, a decrease in the photodegradation was observed as the pH further increased to 10. This could be attributed to charge attraction between negatively charged APAP molecules and positively charged TiO<sub>2</sub> particles, which enhances the adhesion of APAP molecules to TiO<sub>2</sub> particles surface. On the other hand, paracetamol tends to carry a negative charge (anions form) when pH>pK<sub>APAP</sub>. Such

anions have extremely high solubility in solution and will not be adsorbed significantly. Thus, increasing pH ( $\text{pH} > 8$ ) gradually increases the electrostatic repulsion between  $\text{TiO}_2$  surface and APAP (Yang *et al.*, 2008). As such, it is anticipated that the degradation rate of APAP would decrease at pH higher than 8 (**Figure 4.18B**).

The results obtained for the effect of pH on the photocatalytic degradation of CAP are presented in **Figure 4.19A** and **4.19B**. It can be clearly seen that the pH of the solution has a significant effect on the removal of CAP from solution. At pH 4 and 7, the removal percentage was maintained at 80.39% and 80.47%, respectively. It reduced to 74.81% at pH of 8 and further to 74.29% at a pH of 10. The previous study showed that the degradation rate of CAP is highly dependent on solution pH and that the degradation rate constants in acidic medium are higher than that in alkaline medium (Nie *et al.*, 2014). This observation may be due to the electrostatic interactions between the charged  $\text{TiO}_2$  particles and pollutants, since  $\text{TiO}_2$  is positively charged below 6.5 (point of zero charges for  $\text{TiO}_2$ ) and negatively charged above pH 6.5 (Friedmann *et al.*, 2010).

#### 4.8 Effect of irradiation time

As presented in **Figure 4.20A** and **4.21A** for APAP and CAP respectively, the mineralisation efficiency in terms of percentage degradation for the two pharmaceuticals obviously improved with the increase in irradiation time. The percentage of degradation increases from 10.8% at 20 min to 94.21% at 210 min for APAP using CPE- $\text{TiO}_2$  and 2.1% at 20 min to 27.12% at 210 min using bare  $\text{TiO}_2$ . The instantaneous concentration over the initial concentration ( $C/C_0$ ) of the pharmaceuticals was also monitored with respect to time, as presented in **Figure 4.20B** and **4.21B** for APAP and CAP respectively. A decreasing trend of  $C/C_0$  can be seen and the maximum removal was attained for the two pollutants at the end of the monitoring period.

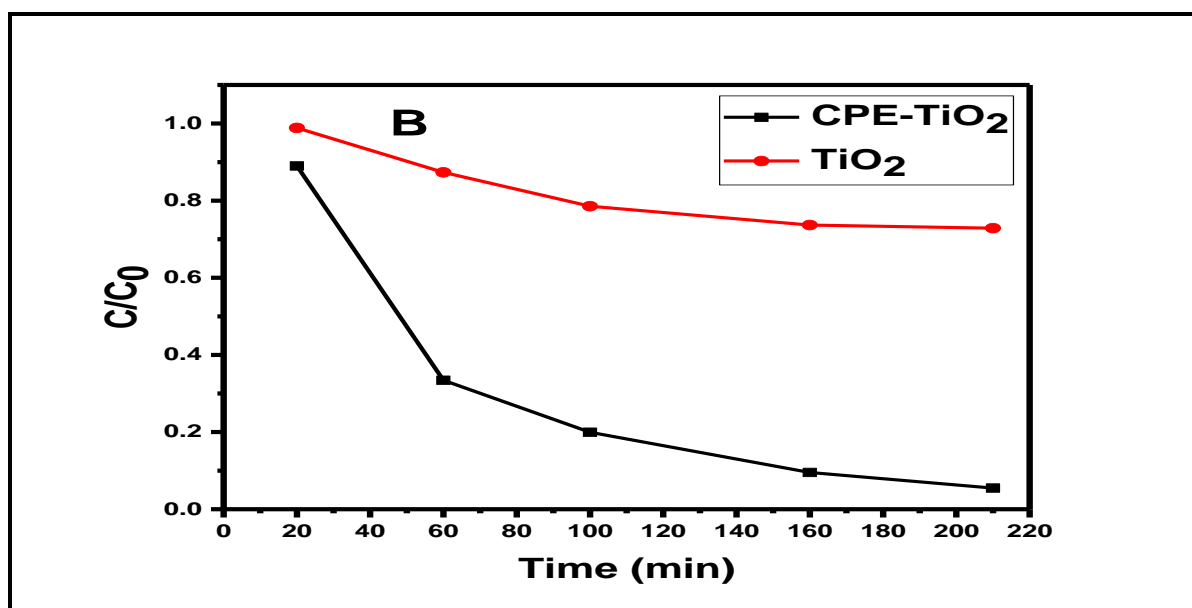
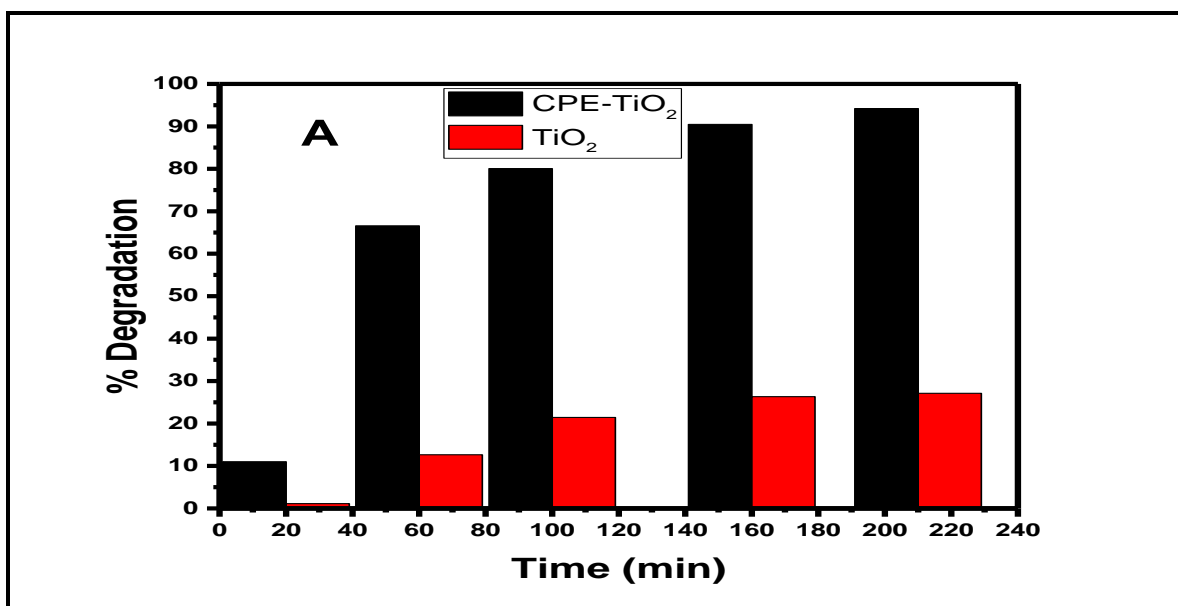


**Figure 4.20:** Visible light degradation of paracetamol by (A) pure TiO<sub>2</sub> and CPE-TiO<sub>2</sub> at different irradiation time and (B) the corresponding degradation rate

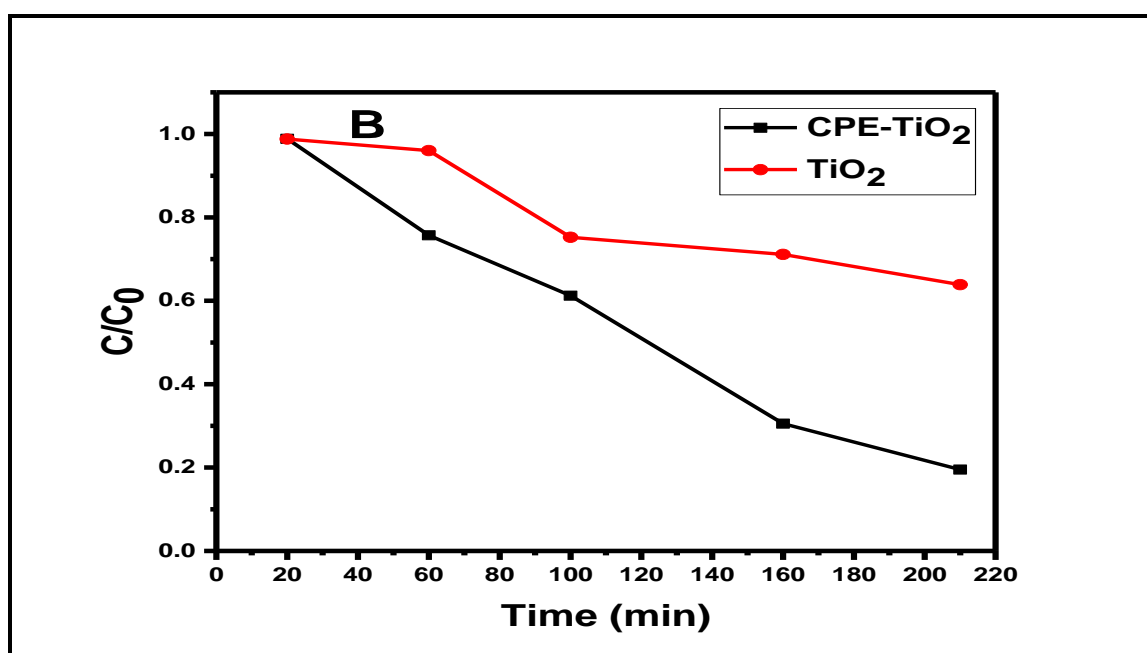
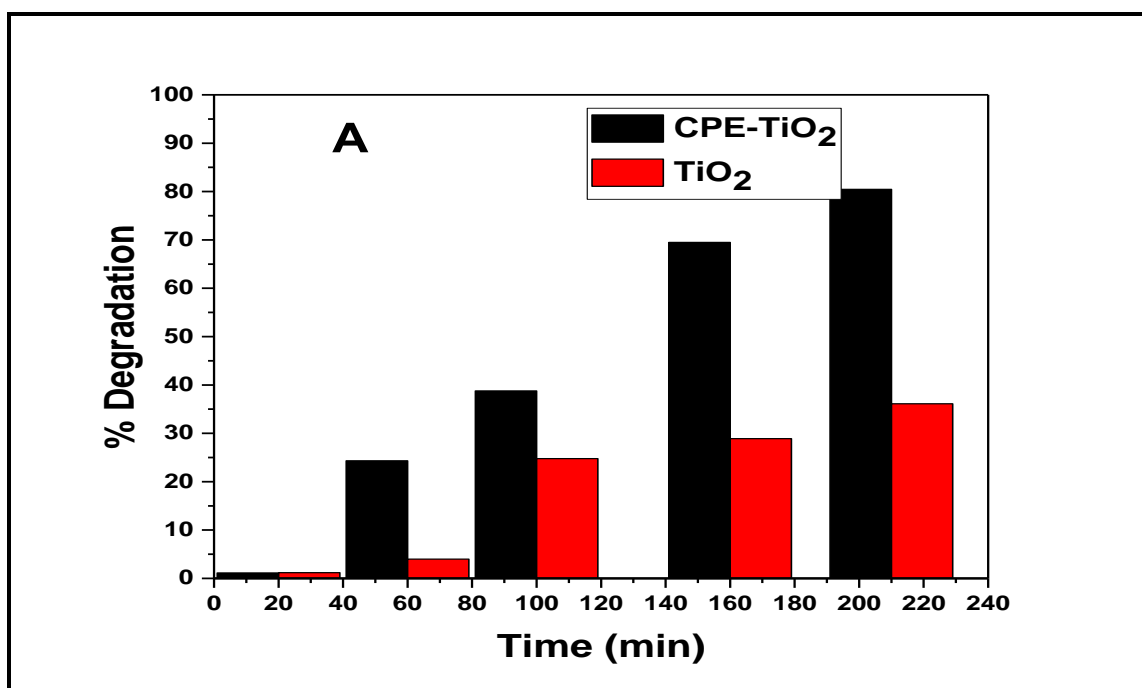


**Figure 4.21:** Visible light degradation of chloramphenicol by (A) pure TiO<sub>2</sub> and CPE-TiO<sub>2</sub> at different irradiation time and (B) the corresponding degradation rate

#### 4.9 Photocatalytic degradation at optimum conditions

The evaluation of photocatalytic performance was carried out at optimum conditions of 25 mgL<sup>-1</sup> initial concentration, 15 mg catalyst dosage, pH 8 for APAP and pH 7 for

CAP. **Figure 4.22A and 4.22B** present the absorption spectra of APAP and CAP respectively, during the photocatalytic degradation in aqueous solution. The maximum absorbance ( $\lambda_{\max}$ ) at around 250 nm for APAP is attributed to the electronic transition of C=O functional group found on acetaminophen structure (Jallouli *et al.*, 2017). This peak was observed to have gradually reduced with time as photocatalysis continued. A similar trend was observed during the photocatalytic degradation of CAP, where the intensity of the peak around 275 nm ( $\lambda_{\max}$ ) was observed to diminish with time of visible light irradiation.

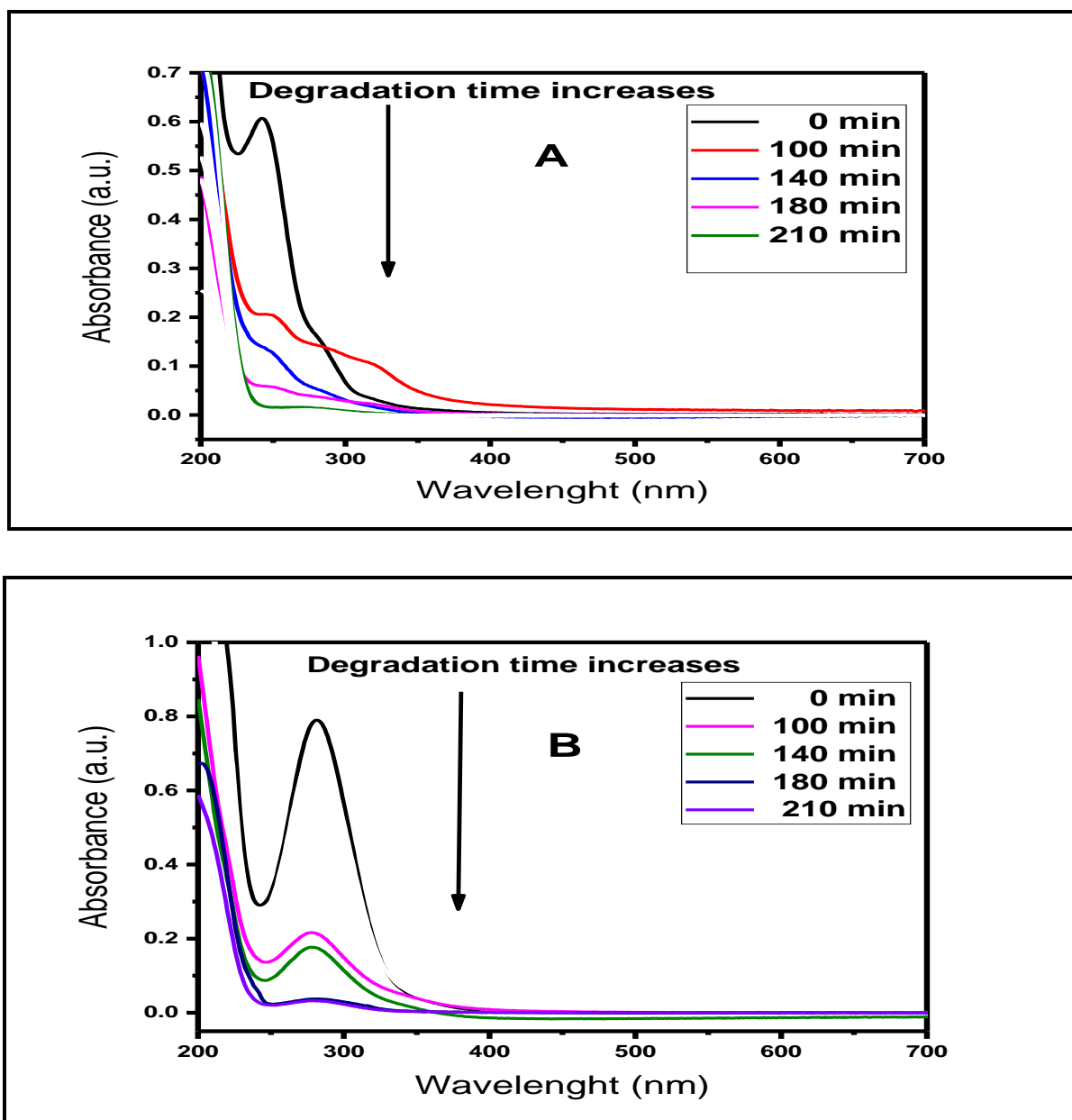


**Figure 4.22:** UV-Vis absorption spectra during photocatalytic degradation monitoring of (A) APAP (B) CAP using CPE-TiO<sub>2</sub> as a catalyst

A similar experiment was performed and under identical conditions using both  $\text{TiO}_2$  and CPE- $\text{TiO}_2$  as catalysts, for comparison purposes. **Figure 4.23A and 4.24A** present the photocatalytic degradation kinetics of APA and CAP respectively, at the optimum conditions. Direct photolysis without catalyst in the control experiment shows insignificant reduction in the initial concentration of the acetaminophen solution. This observation demonstrates the photostability of acetaminophen under visible light (Lin & Yang, 2014), within the irradiation period. A noticeable, though very low, removal (7.78%) of CAP was observed after 210 min during photolysis (visible light without catalyst).

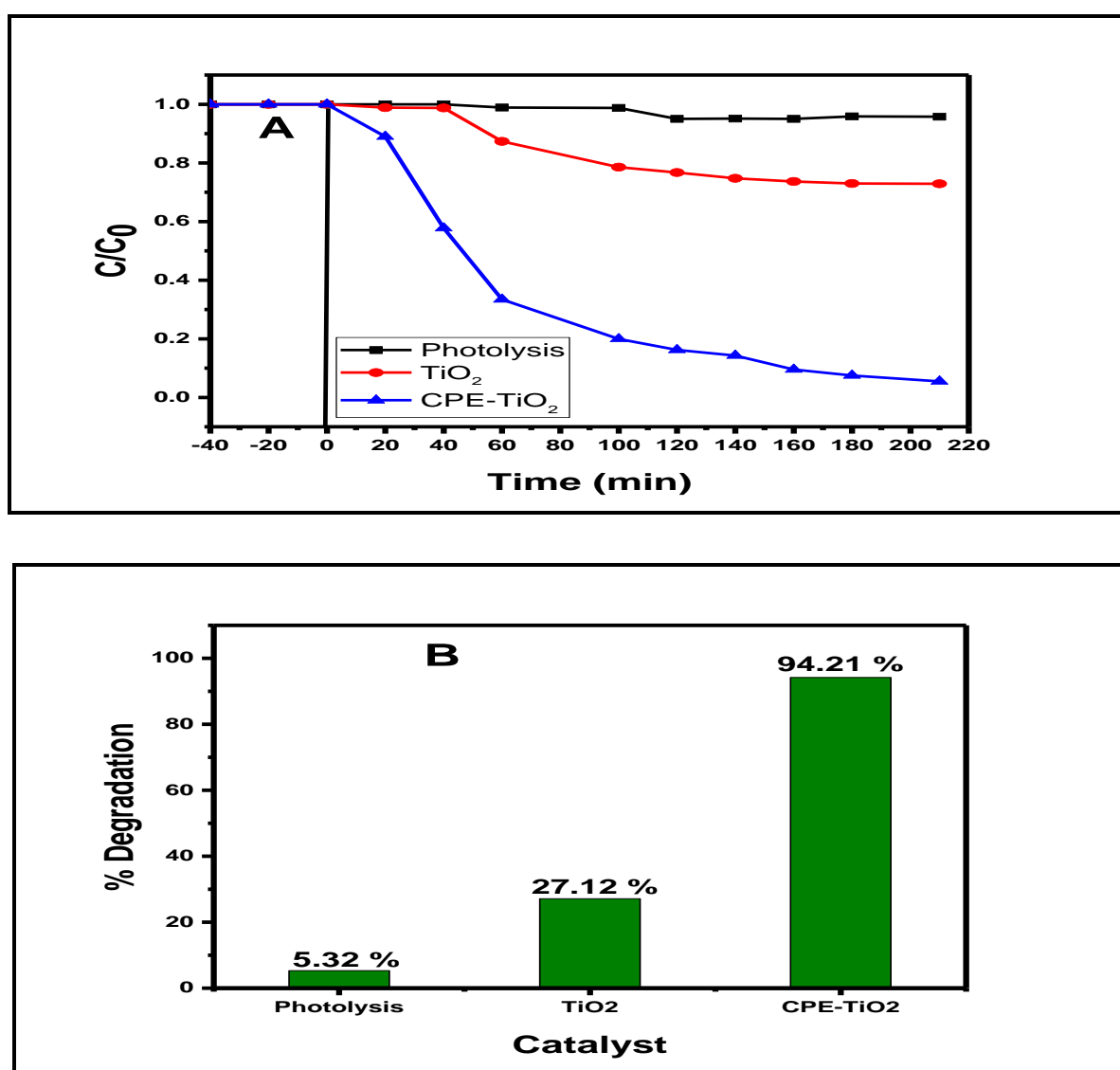


**Figure 4.23:** Visible light photodegradation of APAP; (A) degradation rate with respect to time and (B) Relative % degradations (with no catalyst, pure  $\text{TiO}_2$  and CPE- $\text{TiO}_2$ ) at optimum conditions

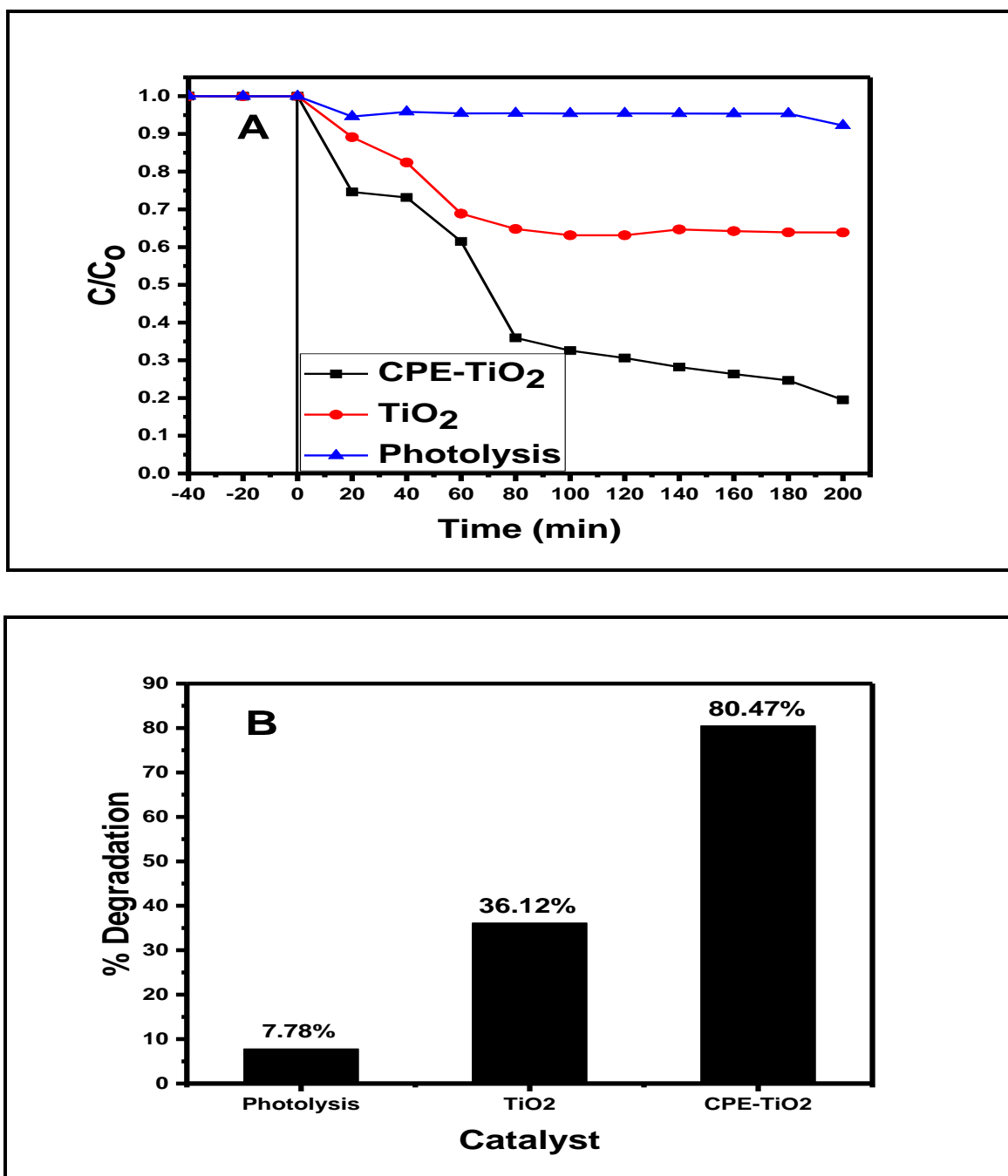


**Figure 4.24:** Visible light photodegradation of CAP; (A) degradation rate with respect to time and (B) Relative % degradations (with no catalyst, bare TiO<sub>2</sub> and CPE-TiO<sub>2</sub>) at optimum conditions

This slight decrease in the concentration after irradiation without the catalyst might be due to the presence of a light-absorbing chromophore (C=C), in the structure of CAP. The adsorption experiment of the catalysts in 25 mgL<sup>-1</sup> solutions of the

pollutants was then conducted in the dark after adding 15 mg of the catalyst. No significant amount of the pharmaceuticals adsorbed was observed after 40 min of the equilibration experiments. It could be clearly seen that CPE-TiO<sub>2</sub> is more efficient in the photodegradation of the pharmaceuticals as compared to bare TiO<sub>2</sub> under visible light. A better photocatalytic activity of CPE-TiO<sub>2</sub> over bare TiO<sub>2</sub> is anticipated, since it possesses a relatively lower band-gap (2.4eV), resulting in a high activation of the catalyst under visible light irradiation.

**Figure 4.23B and 4.24B** present the relative percentage degradation of APAP and CAP, respectively, after 210 min of irradiation. The photocatalytic activity of CPE-TiO<sub>2</sub> was 94.21%, and much higher than of bare TiO<sub>2</sub>, which was 27.12% for APAP photocatalytic degradation. But for CAP photocatalytic degradation, CPE-TiO<sub>2</sub> gave 80.47% removal, which was also higher than 36.12% removal was observed for the bare TiO<sub>2</sub>. This observed improvement in the photocatalytic degradation efficiency under visible light, was suggested to be due to the presence of the conjugated system in the CPE-TiO<sub>2</sub> structure.

#### **4.10 The total organic carbon (TOC) removal for the pharmaceuticals**

The total organic carbons (TOCs) is a common indicator for the assessment of the degree of organic pollutant mineralisation and its measurement could be a demonstration of the elimination of the pollutants (Barhoumi *et al.*, 2016). **Figure 4.25** illustrates the relative percentage TOC removal by CPE-TiO<sub>2</sub> and bare TiO<sub>2</sub> during photocatalytic degradation monitoring of the pharmaceuticals. A significant reduction in percentage TOC was achieved for both APAP (80.31%) and CAP (64.45%) within 210 min of photocatalytic degradation.



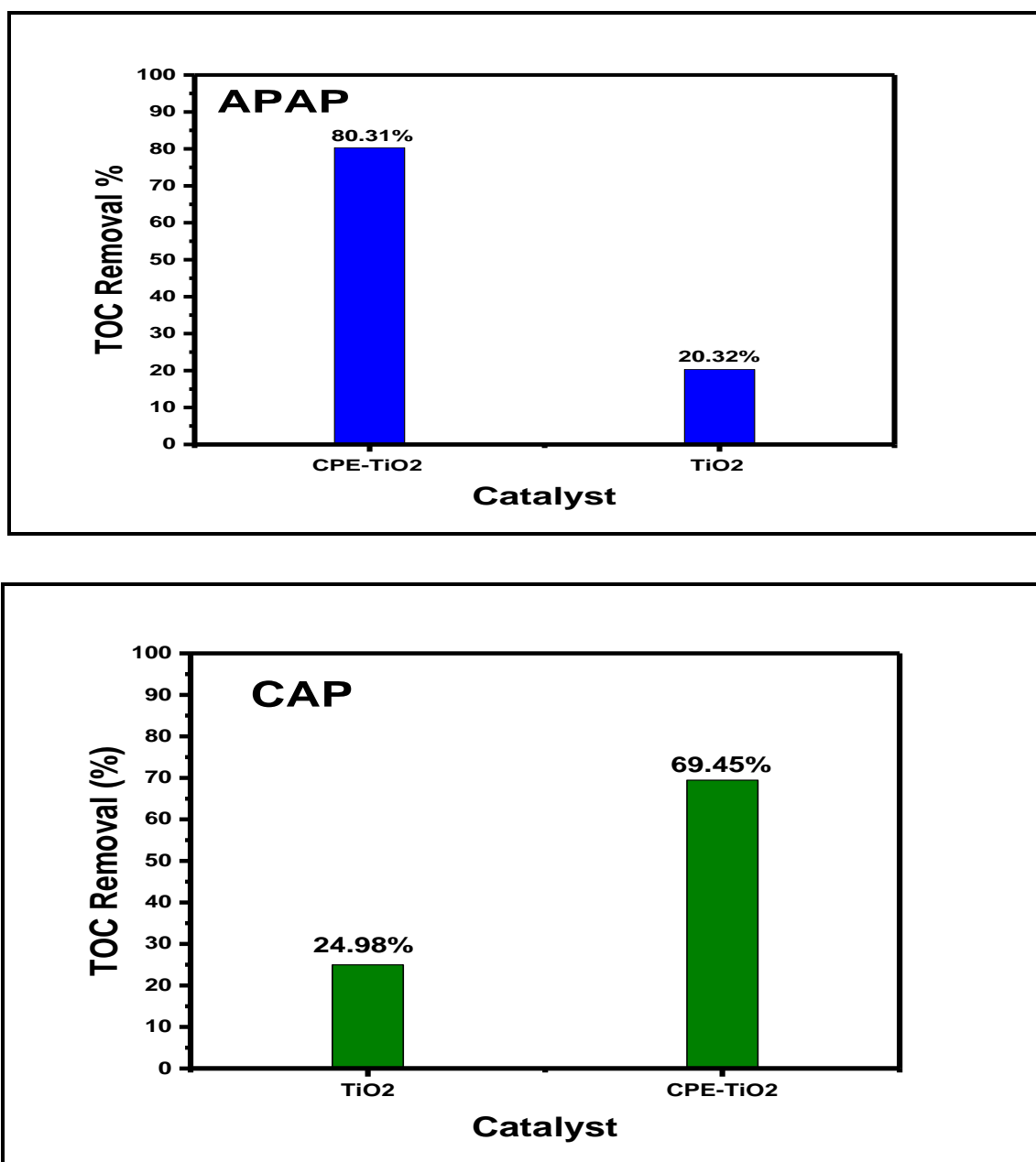


**Figure 4.25:** Total organic carbon (TOC) removal percentage for (A) CAP and (B) APAP photocatalytic degradation after 210 min of visible light irradiation

However, since the TOC removal percentage was less than 100%, it then suggests that some organic intermediates that are difficult to mineralise might have been formed in the process. Recent studies reported that the degradation of pharmaceuticals such as APAP and CAP is accompanied by the production of some aromatic organic intermediates (Jallouli *et al.*, 2017; Gao *et al.*, 2017; Gao *et al.*,

2017). This generated intermediate takes a longer time (possibly beyond the set irradiation time) to degrade.

#### 4.11 The durability and reusability test for the catalyst

Since the application of solar energy in water purification processes has become the trend of scientific research in the field of photocatalysis, reusability without depreciation then should be the central feature of TiO<sub>2</sub> based photocatalysts. The photodegradation of APAP was used (having a higher removal percentage of 94.21%) for the usability test of the composite material catalyst. After the initial 210 min of irradiation in the pharmaceutical solution, the CPE-TiO<sub>2</sub> composites were washed with ultrapure water to be cleansed of any adsorbed pharmaceutical on the surface. The thorough washing of the photocatalysts permits for more adaptability in their use without cross-contamination. The composites were then filled with fresh pharmaceutical solutions.

As illustrated in **Figure 4.26**, each attempt at photocatalytic degradation only resulted in a slightly lower percentage removal of the organic pollutants. However, after three attempts the CPE-TiO<sub>2</sub> composites were performing slightly worse than in the original state. A similar result was reported after four attempts with cellulose-polymer modified TiO<sub>2</sub> nanomaterial in the degradation of methylene blue (Snyder *et al.*, 2013). The first degradation run for APAP gave 94.31% removal and that of the third time gave 91.21%, indicating that CPE-TiO<sub>2</sub> composite had good stability and could be reused several times.

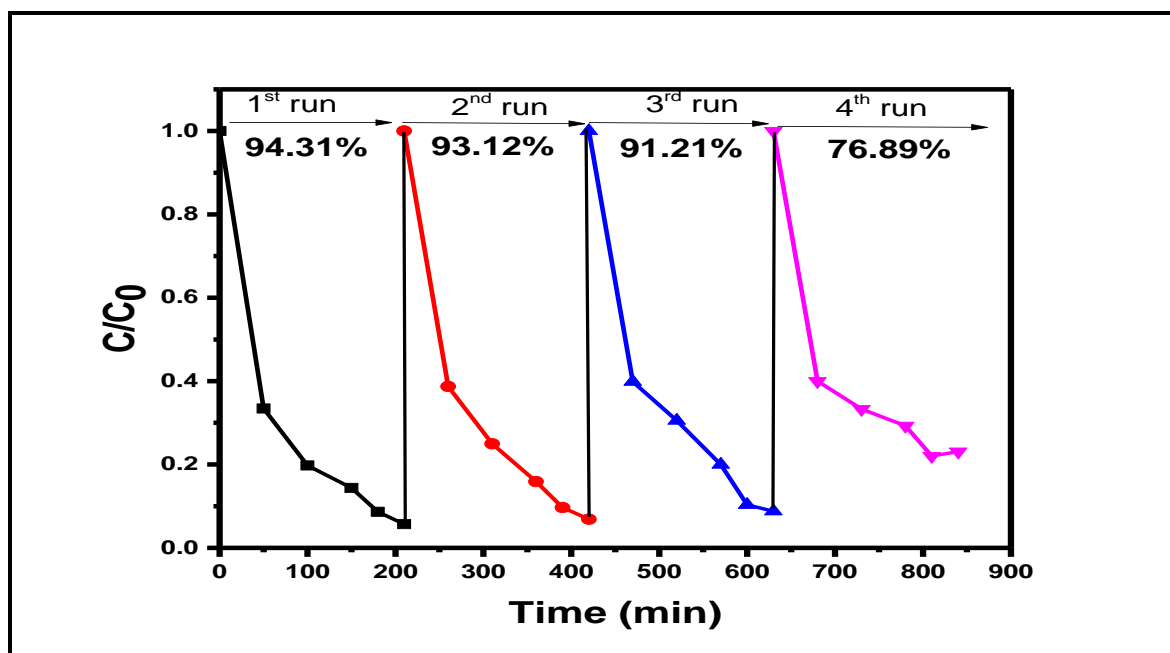


**Figure 4.26:** Recycled photocatalytic degradation of acetaminophen in aqueous solution using CPE-TiO<sub>2</sub> nanocomposite

## Conclusion

Integration of conjugated polyene with TiO<sub>2</sub> exhibited an enhancement in the photocatalytic degradation of acetaminophen and chloramphenicol under visible light irradiation due to high surface area, small crystallite size and reduced bandgap. The highest degradation efficiency of the CPE-TiO<sub>2</sub> catalyst was observed with an optimum dosage of 15 mg, at the lowest possible initial concentration of 25 mgL<sup>-1</sup> and pH 8 for acetaminophen and pH7 for chloramphenicol. The reusability test for the material catalyst shows that it is durable for three to four photocatalytic cycles before any observable drop in the performance.

## Section D: The kinetics and mechanisms of APAP and CAP photocatalytic degradations

### Introduction

A clear understanding of the kinetics and mechanism of photocatalytic oxidation of pharmaceutical pollutants such as acetaminophen (APAP) and chloramphenicol (CAP) is a crucial aspect of environmental risk assessment. The kinetics and mechanism can enable us to clarify the photocatalytic process efficiency. However, the trend of kinetic data from photoreactors is frequently concealed by the fact that light distribution is not always homogenous in the reaction solution. Unlike the concentration gradient that normally levels out by simple mixing, the field of local volumetric rate of photon absorption ( $e_a$ ) is non-homogeneous (Motegh *et al.*, 2012). This is because of the gradient in photon adsorption in many photoreactors, from high rate close to the lamp side to low rate far from the lamp and deep into the solution. Hence, evaluating the kinetics of the overall degradation of the pollutants becomes necessary.

### 4.12 Kinetics of photodegradation

Photocatalytic degradation kinetics of the chosen pharmaceuticals were modelled under different conditions of pH, initial concentrations and CPE-TiO<sub>2</sub> composite dosages, for photo reactor operation. Two reaction kinetic models, PFO and pseudo second order (PSO) were tested.

Since the degradation of many organic pollutants in heterogeneous photocatalysis is surface controlled, the reaction on the catalyst surface then plays a significant role in the determination of the degradation rate. L-H kinetic model has been successfully used for the interpretation of photocatalytic degradation of many organic compounds (Rizzo *et al.*, 2009; Lee *et al.*, 2016; Lee *et al.*, 2016; Falah *et al.*, 2016; Ling *et al.*, 2018; Sun *et al.*, 2018).

Generally, heterogeneous photo reactions involve two consecutive steps, first, the adsorption of the reactants on the surface of the photocatalysts and secondly, the commencement of the photocatalytic reaction. The rate of the first step involving

adsorption is generally slower than the photocatalytic second step. So, the overall photocatalytic reaction rate is mainly dominated by the second step. Furthermore, the adsorption rate can be consistently expressed using the coverage ratio of the absorbed reactants on the surface of the photocatalyst (Chen *et al.*, 2017; Dong *et al.*, 2010). Therefore, the photocatalytic reaction rate  $r$  can be expressed as given in Equation 4.3 (Golshan *et al.*, 2017; Deng *et al.*, 2017), which is widely known as the original L-H model.

$$r = -\frac{dc}{dt} = k(p)\theta \quad \text{Equation 4.3}$$

where  $c$  is the concentration of the reactant,  $t$  is photocatalytic reaction time,  $\theta$  is the coverage ratio of pollutants on the CPE-TiO<sub>2</sub> surface,  $k_p$  is the photoreaction coefficient.

According to Langmuir adsorption theory, the coverage ratio is related to adsorption capacity and the concentration of the reactants.  $K_L$  was defined as the adsorption equilibrium constant to measure the adsorption capacity of CPE-TiO<sub>2</sub> and coverage ratio  $\theta$  can be expressed as in Equation 4.4 according to adsorption theory (Langmuir, 1916).

$$\theta = \frac{K_L c}{1 + K_L c} \quad \text{Equation 4.4}$$

input  $\theta$  from Equation 4.4 to Equation 4.3, the photoreaction rate  $r$  can then be expressed as Equation 4.5.

$$r = K_p \frac{K_L c}{1 + K_L c} \quad \text{Equation 4.5}$$

equation 3 is a much-known expression of L-H model and has been widely used in investigating the kinetics of photocatalytic reactions, representing the PSO reaction model (Sun *et al.*, 2018).

However, the PFO rate equation can be derived from Equation 4.6 (Lin *et al.*, 2016)

$$r = \frac{dc}{dt} = \frac{k_r K_{ads} c}{1 - K_{ads} c} \quad \text{Equation 4.6}$$

where  $k_r$  is the intrinsic rate constant and  $k_{ads}$  is the adsorption equilibrium constant. equation 7.4 may be rearranged as follows (Equation 4.7):

$$\frac{1}{K_{ads}} = \frac{1}{k_r c} + \frac{1}{k_r K_{ads}} \quad \text{Equation 4.7}$$

Provided that the concentration of targeted pollutant is relatively low (between 0.1-0.5 M as in this work) or the adsorption is relatively weak, the two constants ( $k_r$  and  $K_{ads}$ ) may be incorporated (Lin *et al.*, 2016) as one ( $K_{app}$ ) as presented in Equation 4.8:

$$\ln\left(\frac{c}{c_0}\right) = -k_r K_{ads} t = k_{app} t \quad \text{Equation 4.8}$$

This allows equation 4.7 to be expressed in a simplified form of PFO kinetics (equation 4.8), which then clarified why it fits well and better than the other type.

These kinetic models were used to describe the photocatalytic degradation rate of APAP and CAP by plotting the graph of  $\ln(C/C_0)$  against time for varying (I) Initial

concentrations, (II) catalyst dosage and (II) pH of the solutions. In addition, the observed rates of the degradation using CPE-TiO<sub>2</sub> catalyst were estimated from Equation 4.9 (Moussavi et al., 2017). The photocatalytic half-life of each of the pollutants was calculated using Equation 4.10.

$$r_{app} = -k_{app}t \quad \text{Equation 4.9}$$

$$t_{\frac{1}{2}} = \ln 2 \frac{\ln 2}{k_{app}} = \frac{0.69309}{k_{app}} \quad \text{Equation 4.10}$$

The results of the kinetic studies are presented in Table 4.3 and Table 4.4 for acetaminophen and chloramphenicol respectively.

**Table 4.3:** Acetaminophen % removal, half-life, rate constants ( $k_{app}$ ) and  $R^2$  values for pseudo first order (PFO) kinetic model in the photocatalytic experiments using CPE-TiO<sub>2</sub>

Initial concentration (mgL <sup>-1</sup> )	Catalyst dosage (mg )	Solution pH	Removal Efficiency (%)	$k_{app}$ (× 10 <sup>-2</sup> min <sup>-1</sup> )	$r_{app}$ (mgL <sup>-1</sup> min <sup>-1</sup> )	Half life (t <sub>1/2</sub> ) (min)	$R^2$	
							PFO	PSO
<b>Optimum 25</b>	<b>15</b>	<b>8</b>	<b>94.21</b>	<b>2.61</b>	<b>0.653</b>	<b>26.55</b>	<b>0.989</b>	<b>0.884</b>
<b>30</b>	15	8	76.81	2.31	0.693	32.85	0.935	0.876
<b>35</b>	15	8	50.36	2.01	0.704	34.48	0.855	0.697
<b>40</b>	15	8	40.16	1.78	0.712	55..89	0.917	0.847
<b>45</b>	15	8	34.22	1.61	0.726	57.28	0.918	0.799
25	<b>5</b>	8	78.91	2.12	0.531	32.69	0.946	0.784
25	<b>10</b>	8	81.64	2.42	0.605	28.64	0.976	0.852
25	<b>15</b>	8	94.21	2.61	0.653	26.55	0.988	0.883
25	<b>20</b>	8	91.53	2.43	0.608	28.52	0.986	0.694
25	15	<b>4</b>	60.23	2.09	0.523	33.16	0.798	0.877
25	15	<b>7</b>	65.42	2.09	0.523	33.16	0.818	0.865
25	15	<b>8</b>	94.21	2.58	0.645	26.86	0.989	0.784
25	15	<b>10</b>	91.56	2.46	0.615	28.17	0.936	0.856

**Table 4.4:** Chloramphenicol % removal, rate constants ( $k_{app}$ ) and  $R^2$  values for pseudo first order (PFO) kinetic model in the photocatalytic experiments using CPE-TiO<sub>2</sub> bear

Initial concentration (mgL <sup>-1</sup> )	Catalyst dosage (mg )	Solution pH	Removal Efficiency (%)	$k_{app}$ ( $\times 10^{-2}$ min <sup>-1</sup> )	$r_{app}$ (mgL <sup>-1</sup> min <sup>-1</sup> )	Half-life ( $t_{1/2}$ ) (min)	$R^2$	
							PFO	PSO
<b>Optimum: 25</b>	<b>15</b>	<b>7</b>	<b>80.47</b>	<b>2.41</b>	<b>0.603</b>	<b>28.76</b>	<b>0.973</b>	<b>0.779</b>
<b>30</b>	15	7	68.32	2.10	0.631	33.004	0.963	0.874
<b>35</b>	15	7	58.23	1.99	0.696	34.83	0.976	0.784
<b>40</b>	15	7	51.28	1.98	0.792	35.01	0.969	0.659
<b>45</b>	15	7	50.18	1.96	0.882	35.36	0.982	0.877
25	<b>5</b>	7	63.52	2.01	0.503	34.48	0.979	0.894
25	<b>10</b>	7	77.11	2.12	0.531	32.69	0.968	0.873
25	<b>15</b>	7	80.47	2.28	0.571	30.40	0.974	0.798
25	<b>20</b>	7	74.85	2.12	0.531	32.69	0.977	0.768
25	15	<b>4</b>	80.39	2.41	0.603	28.52	0.893	0.876
25	15	<b>7</b>	80.41	2.23	0.558	31.08	0.847	0.798
25	15	<b>8</b>	74.81	2.12	0.532	32.69	0.921	0.864
25	15	<b>10</b>	74.29	2.12	0.532	32.69	0.870	0.785

From the kinetic model tested, the photocatalytic data for the two pollutants does not fit well into PSO kinetic model. However, PFO kinetic, as noted from the  $R^2$  and the kinetic rate constant values, found to fit well the experimental data with  $R^2$  values close to 1.

#### 4.12.1 Kinetics based on various pollutants concentrations

**Figure 4.27 and Figure 4.28** are the kinetics plots based on various initial concentrations of pollutants in the photocatalytic degradation experiments at pH 8, catalyst dose 15 mg and room temperature. When the initial concentration was reduced from 45 mgL<sup>-1</sup> to 25 mgL<sup>-1</sup>, the degradation efficiency of APAP increased from 34.22% to 94.21%, while that of CAP increased from 50.18% to 80.47% in 210



min of irradiation. The PFO rate constant was obtained from the slope of the straight-line plot of  $\ln(C/C_0)$  against time. It is worth noting that the lowest concentration (25 mg) for both APAP and CAP exhibits the highest rate constant of  $0.061 \text{ min}^{-1}$  and  $0.041 \text{ min}^{-1}$  respectively.

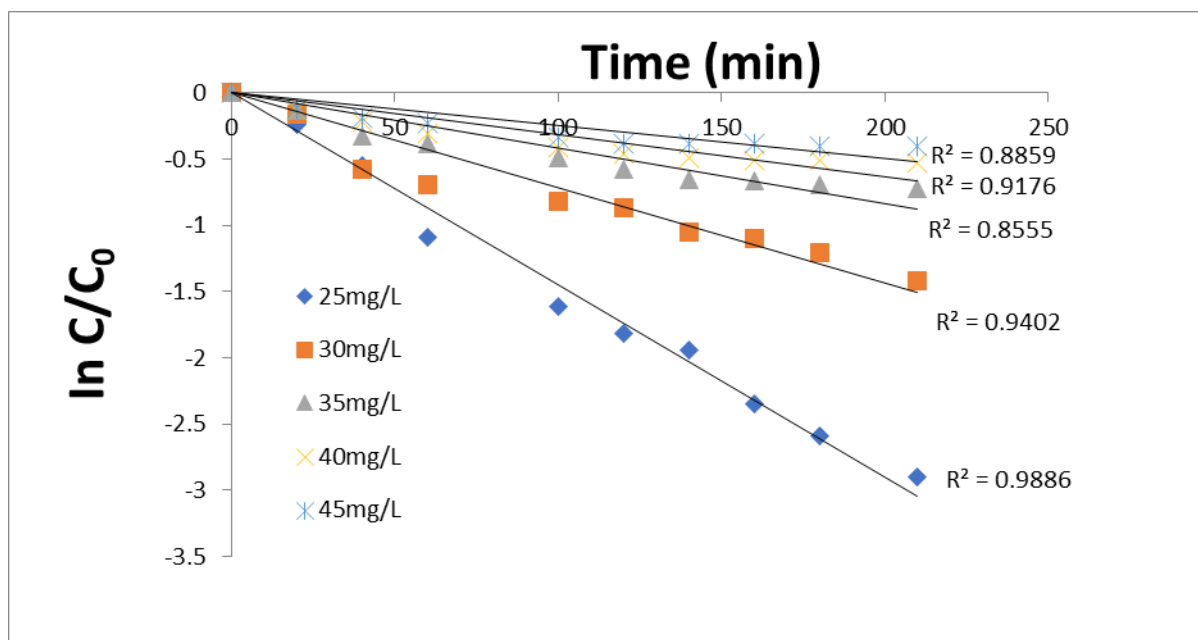


**Figure 4.27:** The rate plot for photocatalytic degradation of APAP with respect to time at varying initial concentrations

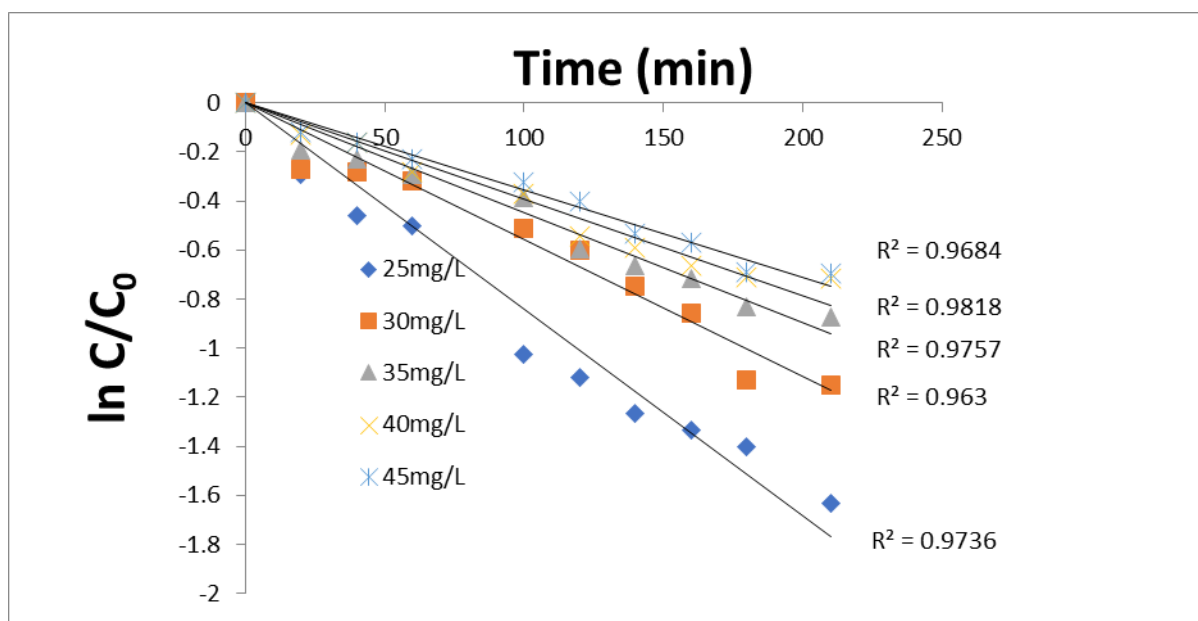


**Figure 4.28:** The rate plot for photocatalytic degradation of CAP with respect to time at varying initial concentrations

These values are about three times higher than what was obtained for the highest concentration ( $45 \text{ mgL}^{-1}$ ) for both pollutants. This indicates that the rate constant decreases at higher concentration of the pollutants. A similar result was reported for other pharmaceuticals, where the degradation rate constant was found to decrease with increase in the concentrations of metoprolol and propranolol (Yang *et al.*, 2010). However, based on the information provided in **Tables 4.3 and 4.4**, the observed degradation rate ( $r_{\text{app}}$ ) of both pollutants calculated from **Equation 4.17** increases with increase in the initial concentrations.

This observation is contrary to the results obtained for the percentage degradation, where the highest removal (94.21% for APAP and 80.12% for CAP) was achieved at the lowest initial concentration ( $25 \text{ mgL}^{-1}$ ) of the pollutants after the irradiation time. As it was explained in the previous chapter, increased amounts of the pharmaceuticals may occupy a greater number of the CPE-TiO<sub>2</sub> active sites, at higher concentration. The covering of the catalyst active sites could subsequently suppress the generation of oxidants and result in lower percentage degradation (Yang *et al.*, 2008) after a long period of irradiation.

#### 4.12.2 Kinetics based on varying catalyst dosages

Based on the preliminary experimental results,  $25 \text{ mgL}^{-1}$  initial concentration was used to investigate the effect of catalysts as was mentioned previously. To further give an insight on degradation trend and rate during the monitoring periods,  $\ln(C/C_0)$  was plotted against time for various catalyst dosages (**Figure 4.29 and Figure 4.30**). It was observed that as the catalyst dose was increased from 5 mg to 15 mg, the degradation efficiency of APAP increased from 78.91% to 94.21%, while that of CAP increased from 63.52% to 80.47% in 210 min of irradiation. A CPE-TiO<sub>2</sub> dosage over 15 mg could not further increase the degradation efficiency (**Tables 4.3 and 4.4**).

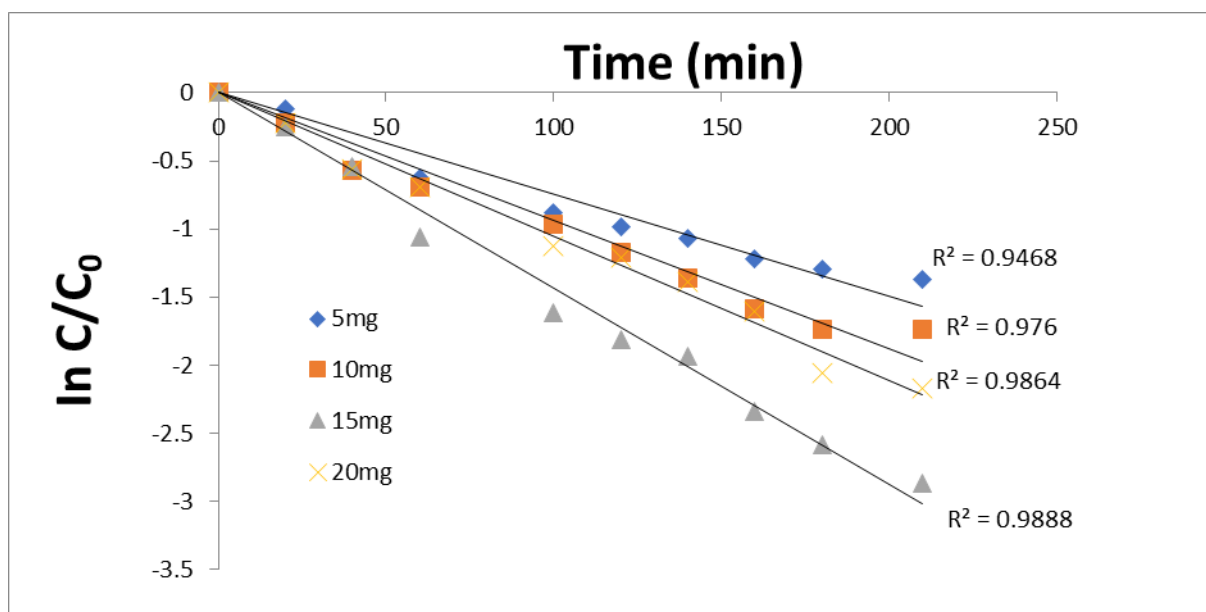


**Figure 4.29:** The rate plot for photocatalytic degradation of APAP with respect to time at varying catalyst dosages

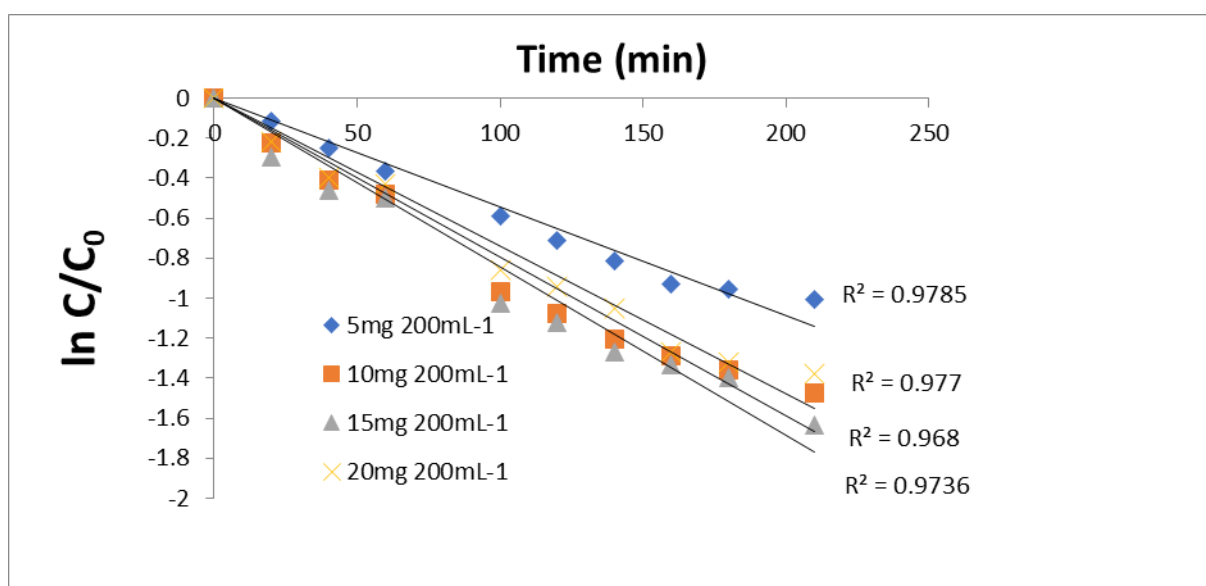


**Figure 4.30:** The rate plot for photocatalytic degradation of CAP with respect to time at varying catalyst dosages

In terms of linearity of the plots, PFO kinetic model is more fitted with the highest  $R^2$  values, for the same reason given earlier. The reaction rate increased with increasing catalyst dosage and the fastest rate was for 15 mg ( $r_{app} = 0.988 \text{ mgL}^{-1}\text{min}^{-1}$ )

<sup>1</sup> for APAP and 0.973 mgL<sup>-1</sup>min<sup>-1</sup> for CAP), further increase to 20 mg leads to decrease in degradation rate ( $r_{app}$  = 0.961 mgL<sup>-1</sup>min<sup>-1</sup> for APAP and 0.957 mgL<sup>-1</sup>min<sup>-1</sup> for CAP).

The digression coefficients of the results obtained for the kinetic of degradation for various catalyst dosages are provided in **Tables 4.3 and 4.4**. Expectedly, increasing catalyst loading resulted in an increase in the photodegradation efficiency and rate of both the APAP and CAP. This result could be attributed to an increase in the number of CPE-TiO<sub>2</sub> active sites that are available for photocatalytic reactions. This trend continues up to a point (at 15 mg dosage per 200 mL) where all the catalysts particles are fully illuminated (Yang *et al.*, 2008; Hapeshi *et al.*, 2010). At higher catalyst dosage (20 mg dosage per 200 mL), screening effect of excess particles occurs, which tends to mask part of the photosensitive area of the surface (Hapeshi *et al.*, 2010). Consequently, the penetrating photons are blocked or reflected away from the surface of the catalyst. As a result, a drop in the photocatalyst performance was observed at higher dosage for APAP and CAP degradation.

#### 4.12.3 Kinetics based on various solution pH

The initial pH of a solution is an important parameter that can affect photocatalytic reaction rate. In this view, the photocatalytic degradation of APAP and CAP was investigated at different pH and the kinetics of the photodegradation at various pH was evaluated. The initial pH of APAP and CAP was adjusted to alkaline or acidic conditions by the addition of NaOH or HCl solutions respectively. **Figure 4.31 and Figure 4.32** illustrate the plots of  $\ln(C/C_0)$  against degradation time at different initial pH for APAP and CAP respectively. The better linear relationship model obtained was still PFO. Therefore, for investigating the kinetics at various pH of solution, the experimental data generated was fitted into PFO model and the results are illustrated in **Tables 4.3 and 4.4**.

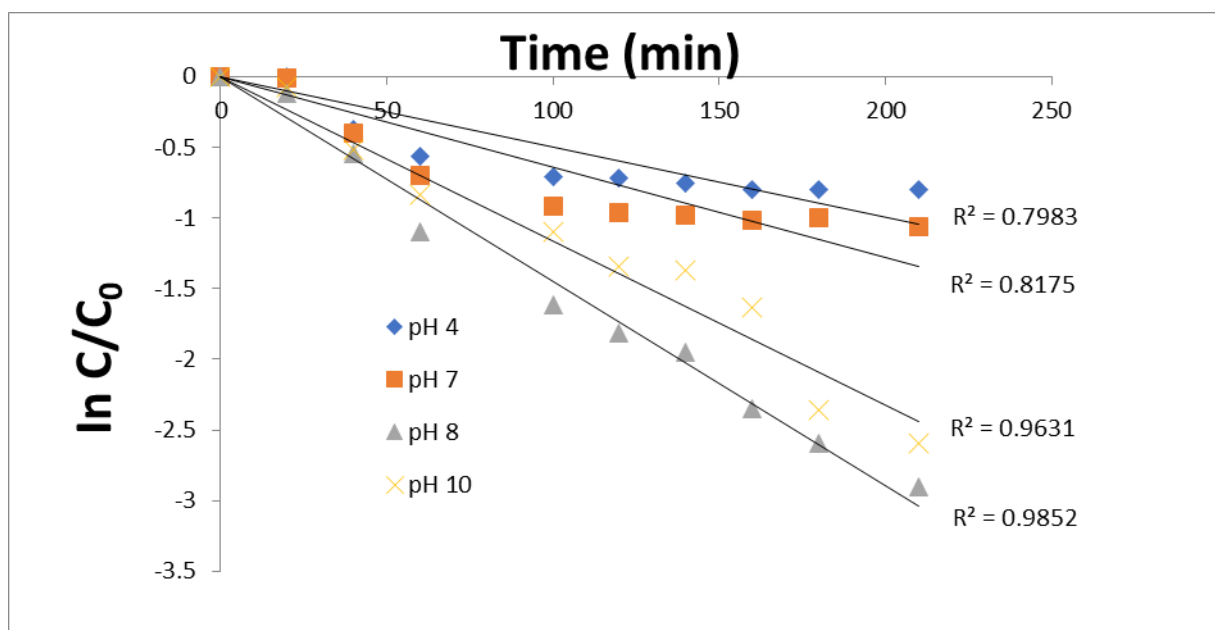


**Figure 4.31:** The rate plot for photocatalytic degradation of APAP with respect to time at varying pH.

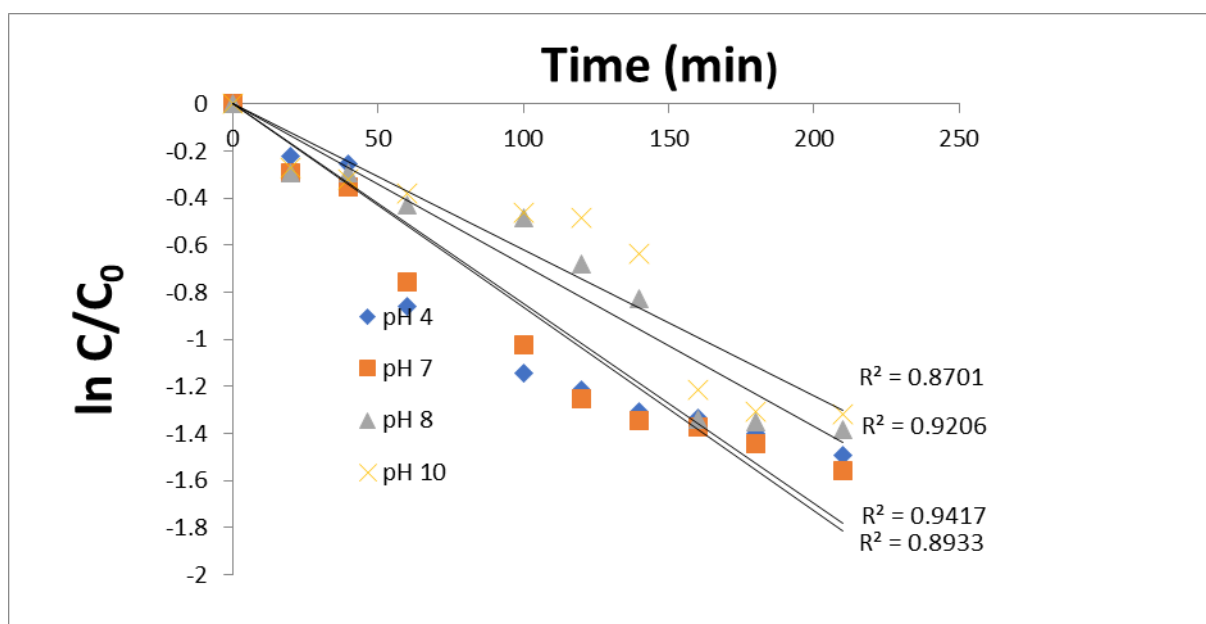


**Figure 4.32:** The rate plot for photocatalytic degradation of CAP with respect to time at varying pH.

From the evaluated percentage degradation as was discoursed in the previous chapter, the degradation efficiency changes with pH and is different for each of the

pollutants. For APAP, the degradation efficiency increased from 60.23% at pH 4 to 94.21% at pH 8, further increase in the initial pH led to reduction in the degradation efficiency after 210 min of irradiation.

However, the observed influence of initial pH on degradation efficiency of CAP is different. The degradation efficiency of CAP remains approximately constant as the initial solution pH was increased from 4 up to 7. A drop in the degradation efficiency was observed as the initial pH was further increased to 10. For the removal kinetics, the  $r_{app}$  values for both APAP and CAP vary for different solution pH. The fastest removal rate at the maximum  $r_{app} = 0.985 \text{ mgL}^{-1}\text{min}^{-1}$  was observed for APAP at pH 8 and  $r_{app} = 0.0893 \text{ mgL}^{-1}\text{min}^{-1}$  was observed for CAP at pH 4. An increase in pH from 4 shows continuous increase in  $r_{app}$  value until the pH of 8, it then decreases as the pH further increased to 10. Change in  $r_{app}$  values at varying solution pH can be attributed to the effect of electronic interaction between the reactants and the catalyst surface (Jallouli *et al.*, 2017). Decrease in the solubility of (no charge state) APAP enhances its adsorption onto the surface of CPE-TiO<sub>2</sub>, leading to a faster rate of oxidation at lower pH.

Acetaminophen (APAP) tends to carry a negative charge when  $\text{pH} > \text{pK}_{\text{APAP}}$ . Thus, increasing pH ( $\text{pH} > 8$ ) gradually increases the electrostatic repulsion between TiO<sub>2</sub> surface and APAP (Yang *et al.*, 2008). For CAP, as the pH increased continuously to 10, the  $r_{app}$  further decreased to the minimum value of  $0.870 \text{ mgL}^{-1}\text{min}^{-1}$  at pH 10, indicating lower rate of degradation at a high solution pH. The surface ionisation of CPE-TiO<sub>2</sub> could be responsible for the decrease in  $r_{app}$ , since TiO<sub>2</sub> is negatively charged at alkaline medium (Friedmann *et al.*, 2010), leading to repulsion of negatively charged chloramphenicol at high pH.

#### 4.12.4 Degradation kinetics at optimised conditions

After all the influencing parameters were optimised, the photodegradation was carried out at optimum conditions and the degradation kinetics was evaluated for APAP and CAP. The kinetics for visible light photocatalytic degradation using CPE-TiO<sub>2</sub> at optimum conditions of pH, catalyst dosage and initial concentrations were studied. From the plot of  $\ln C/C_0$  versus irradiation time in **Figure 4.33** and **Figure**

4.34, the photocatalytic degradation data for both the pollutants fitted well into the first-order rate model. The degradation rate constant was at highest ( $K_{app} = 2.61 \times 10^{-2}$  for APAP and  $2.41 \times 10^{-2}$  for CAP) at the optimum conditions. The corresponding reaction rate are listed in **Tables 4.3 and 4.4**. PFO kinetics gave  $R^2$  values of 0.989 for APAP and .0.973 for CAP. The half-life ( $t_{1/2}$ ) of the photocatalytic degradation of the pharmaceuticals were calculated and the values at the optimum conditions are 26.55 min for APAP and 28.76 min for CAP for  $25 \text{ mgL}^{-1}$  solutions.

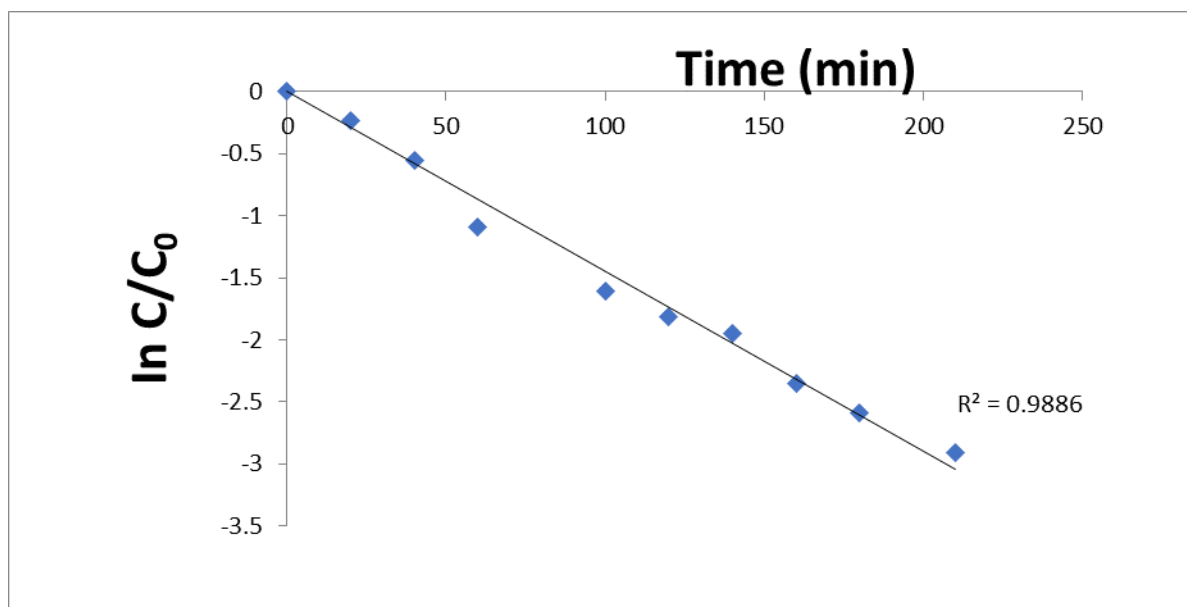


**Figure 4.33:** The rate plot for photocatalytic degradation of APAP with respect to time at optimum conditions (pH = 8, Initial conc. =  $25 \text{ mgL}^{-1}$ , catalyst dosage =  $15 \text{ mg } 200\text{mgL}^{-1}$  ).

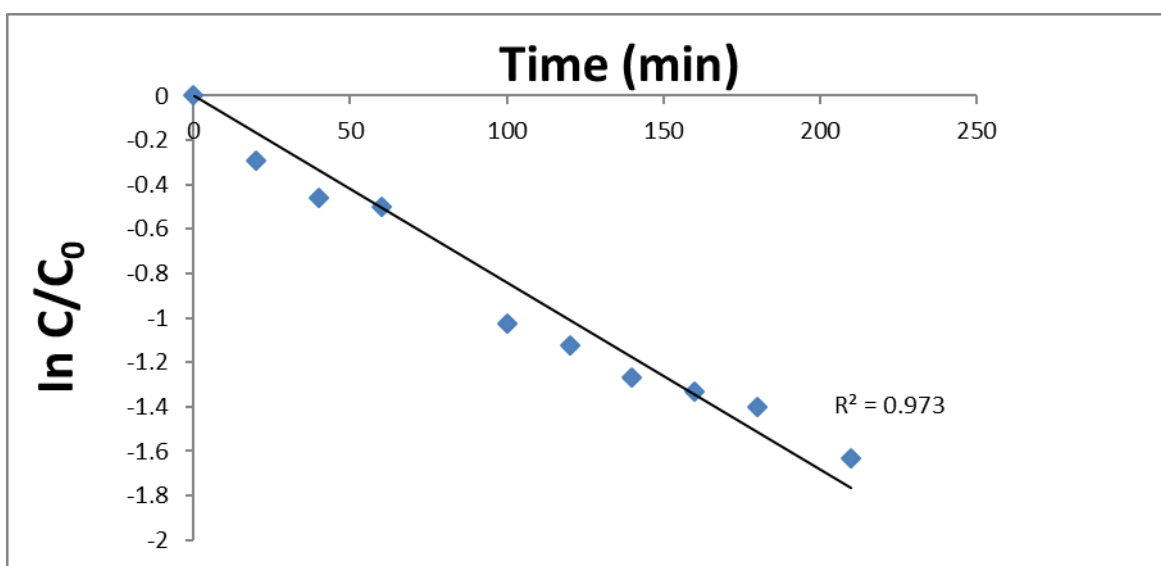


**Figure 4.34:** The rate plot for photocatalytic degradation of CAP with respect to time at optimum conditions (pH = 8, Initial conc. = 25 mgL<sup>-1</sup>, catalyst dosage = 15 mg 200 mgL<sup>-1</sup>) .

#### 4.13 Possible photodegradation mechanism and intermediate identifications

Generally, there are many reactive species that could be responsible for an effective photo oxidation of organic molecules in aqueous solution. These reactive species contribute at various levels of degradation and influence the product of photocatalytic degradation. To investigate the degradation mechanism involved in the photocatalytic oxidation process for the degradation of APAP and CAP, as well as to detect the presence of any intermediate product, chromatographic techniques were employed.

##### 4.13.1 Evaluation of reactive species contributions and mechanism

The degradation of many organic compounds is considered to proceed through ionic or free radical mechanism (Skoumal *et al.*, 2006). To find out the underlying contributions of different reactive species such as h<sup>+</sup>, e<sup>-</sup>, O<sub>2</sub><sup>•-</sup> and OH<sup>•</sup>, that are involved during the photocatalytic degradation process, several reactive radical trapping experiments were carried out. Different scavenging reagents such as



potassium iodide (KI), tert-butanol (TB), benzoquinone (BQ) and isopropanol (IPA) were employed to trap  $h^+$ ,  $e^-$ ,  $O_2^{\cdot-}$  and  $OH^{\cdot}$  respectively, in the presence and absence of scavenging reagents (**Table 4.5**).

**Table 4.5:** The photo-oxidation reactive species and the scavenging reagents

Reactive species	Scavenger
$OH^{\cdot}$	Isopropanol (ISP)
$H^+$	Potassium iodide (KI)
$e^-$	Tert-butanol (TB)
$O^{\cdot-}$	Benzoquinone (BQ)

**Figure 4.35** illustrates the degradation percentages of APAP and CAP with or without the addition of different scavengers using the CPE-TiO<sub>2</sub> catalyst. The percentage degradation for both pollutants was observed to be at maximum (APAP =94.12% and CAP= 80.47%) in the absence of scavenger after 210 min. A drop in the percentage degradation was noticeable for both pollutants in the presence of different scavengers. This observation indicates that all the reactive species play a role in the oxidation of APAP and CAP using CPE-TiO<sub>2</sub>. However, a significant decrease in percentage degradation (APAP =20.2% and CAP = 19.4%) was observed with the use of ISP as the scavenger, indicating that  $OH^{\cdot}$  played a major role in the photocatalytic degradation of both APAP and CAP pollutants. This experimental result agrees with the study reported in the literature (Oseghe et al., 2019).

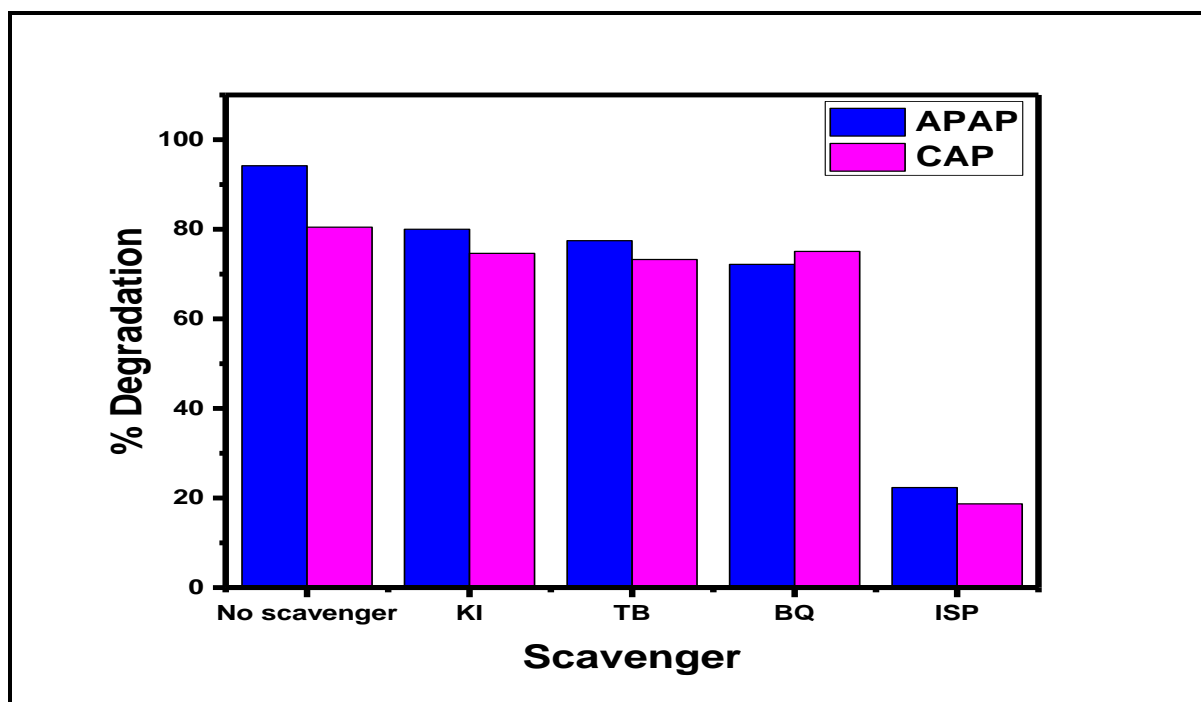


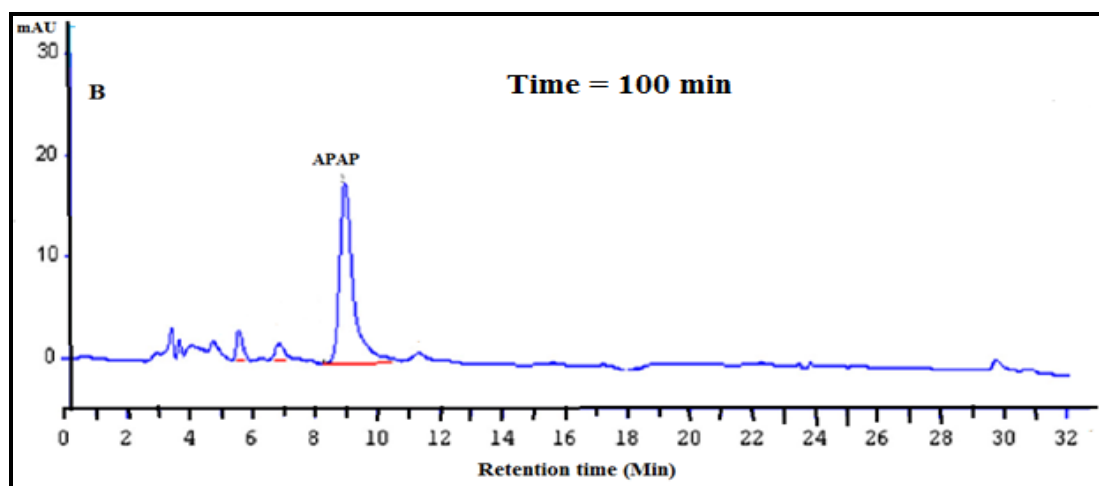
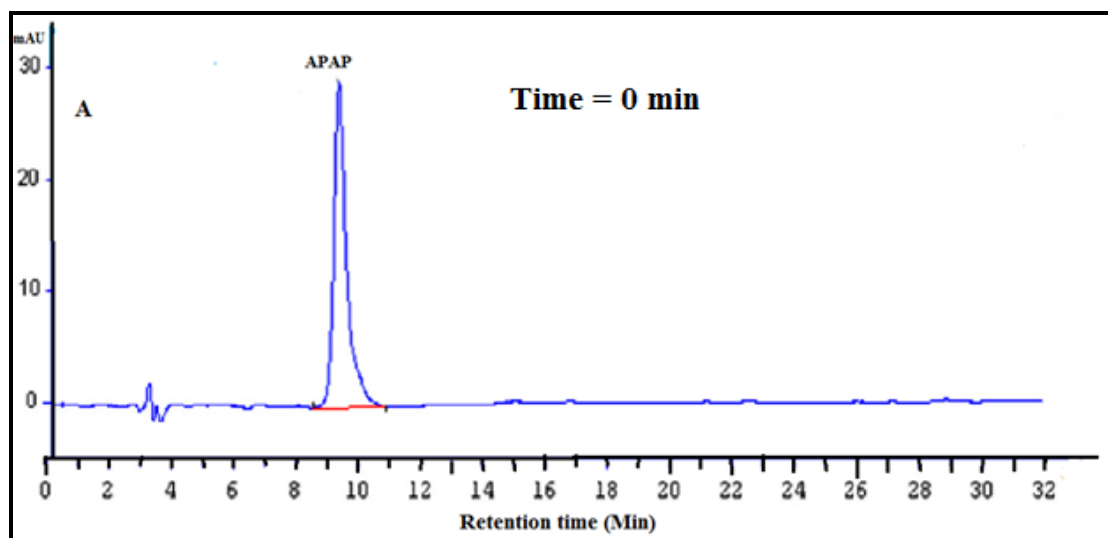
**Figure 4.35:** Effect of scavengers on the photocatalytic degradation of paracetamol and chloramphenicol using CPE-TiO<sub>2</sub>

#### 4.13.2 High performance liquid chromatography (HPLC) analysis and intermediate identification

It was noted in the results of the total organic carbon measurement that the TOC removal for APAP and CAP is lower compared to the removal efficiency recorded. This then indicates that intermediates may be generated during degradation. Consequently, a high-performance liquid chromatography (HPLC) was employed to monitor and identify the likely intermediates that may be formed during photochemical degradation. It also allowed for the probing of the likely degradation mechanism for the pharmaceutical oxidation. Photodegradation experiments were carried out at the optimum operating conditions of pH. Concentration and CPE-TiO<sub>2</sub> catalyst dosage. Samples were taken just before the start of the experiment at 100 min and 210 min of irradiation for HPLC analysis.

**Figure 4.36** presents the HPLC chromatograms obtained for the separations of APAP sampled solutions during photocatalytic degradation experiments. It is clearly shown that the main peak at the retention time  $t_R = 9.24$  min, due to APAP

separation, decreases gradually and reduced to the minimum intensity after 210 min of irradiation. The observed gradual reduction in APAP is as indicated in **Figure 4.36A, B and C**, which represent the chromatograms at 0 min, 100 min and 210 min irradiation time respectively. Besides APAP, other peaks were observed emanating at various retention times.



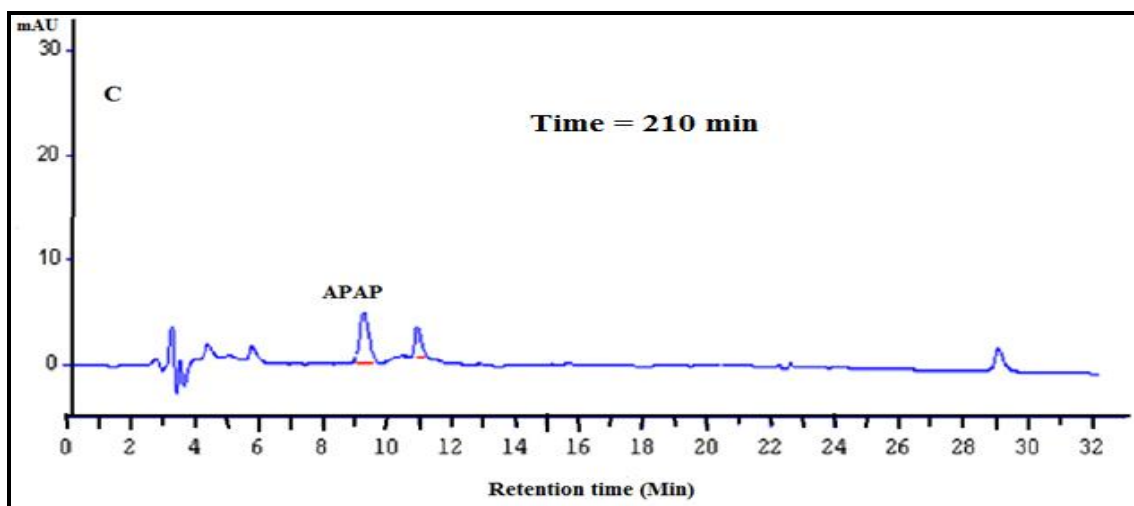


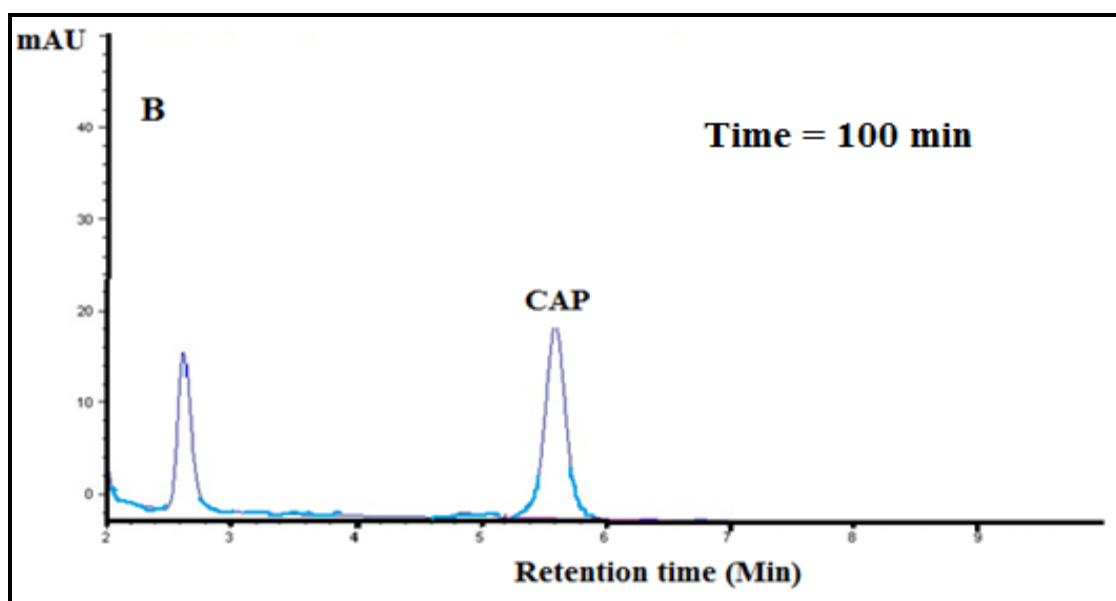
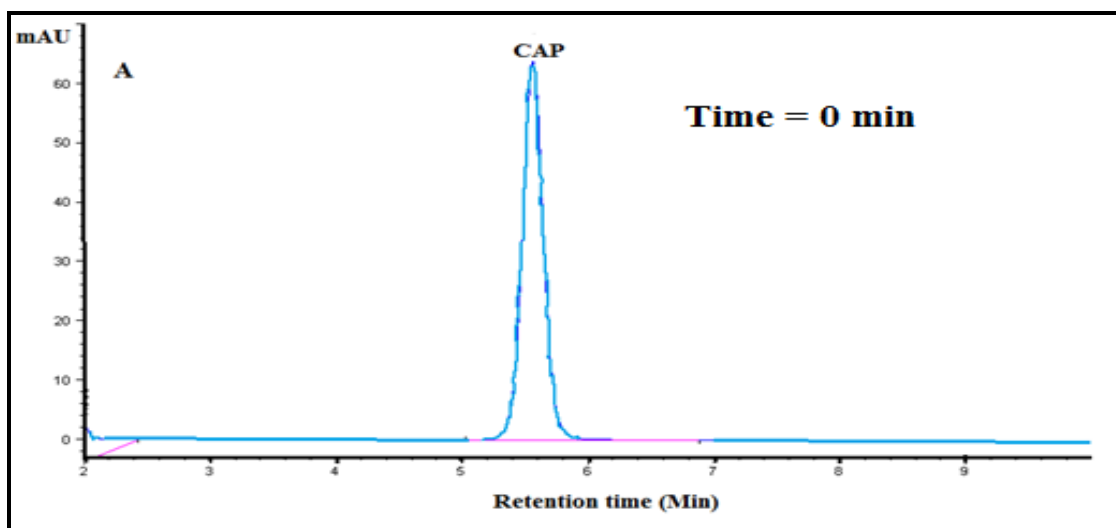
**Figure 4.36:** HPLC of APAP solution during photocatalytic degradation of  $25\text{mgL}^{-1}$  initial concentration at different irradiation times (min): at (A) 0, (B) 100 and (C) 210

These emerging peaks observed particularly after 100 min of irradiation can be ascribed to the formation of organic intermediates from APAP degradation. The intermediates are most like to be benzoquinone, hydroquinone p-nitrophenol and 124-trihydroxybenzen, as compared with the standards form HPLC peaks. These sets of intermediates are already identified in similar studies (Andreozzi *et al.*, 2003; Skoumal *et al.*, 2006; Moctezuma *et al.*, 2012). Other intermediates from APAP photodegradation are as shown in table 2.4.

In the case of CAP as shown in **Figure 4.37**, gradual reduction in the peak intensity was also noticed at the retention time  $t_R = 5.5$  min due to chloramphenicol elution. Similar to what was observed for APAP degradation monitoring. At 100 min of sample analysis, other peaks were observed appearing, indicating the formation of intermediate compounds. The peaks at the retention time  $t_R = 2.65$  min and 2.21 min are suspected to be due to the formation of oxamic acid and succinic acid respectively. From the literature, other intermediates from CAP photodegradation are shown in table 2.5.

Notably, as the original peak at  $t_R = 5.5$  for CAP decreases, the height of new emerged peak was drastically reduced after 210 min of photocatalytic degradation. This peak reduction indicates a further degradation of the intermediate during the

process. All the peaks that appeared on the chromatogram were identified by comparison of their retention time with the standard HPLC peaks (Table C 1: Detected Intermediate products and their retention time during photocatalytic degradation. Appendix C)



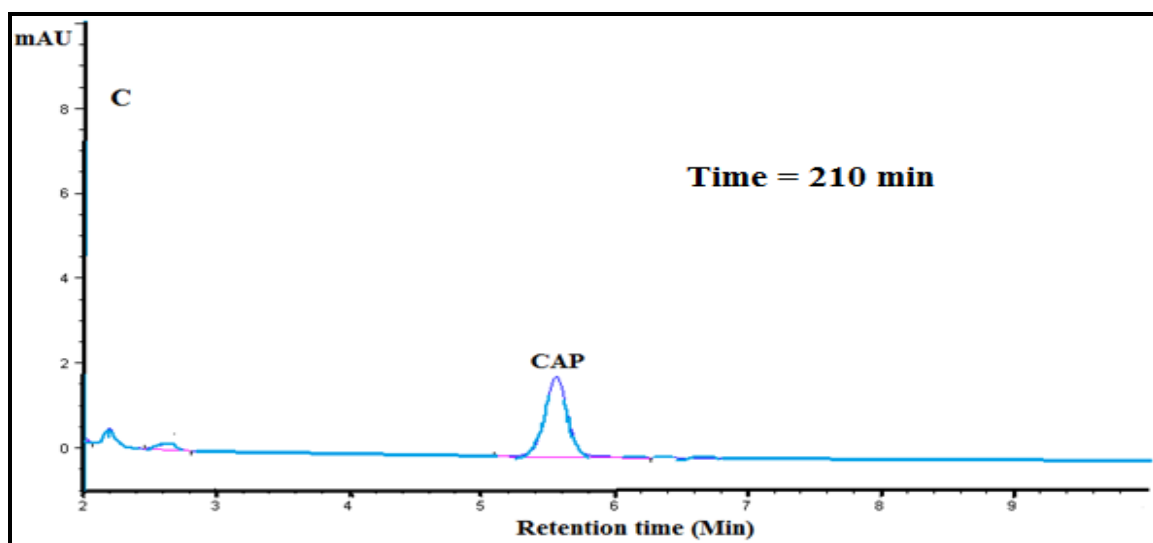


**Figure 4.37:** HPLC of APAP solution during photocatalytic degradation of  $25\text{mgL}^{-1}$  initial concentration at different irradiation times (min): at (A) 0, (B) 120 and (C) 210

## Conclusion

In this section, the L-H model has been used to investigate the kinetics of photocatalytic degradation of acetaminophen and chloramphenicol under visible light at varying conditions of pH, concentration and catalyst dosage. Experimental result data showed that the PFO rate model fitted better between the two tested models. The observed degradation rates increased with increase in initial concentrations. However, the photoreaction coefficient  $K_{\text{app}}$  (rate constant) was observed to increase with the decrease in the concentration and increase in the mass of catalyst dosage for both reactants. Also, the effect of the solution pH on  $K_{\text{app}}$  was found to depend on the nature of electronic charge interaction between the solution and the reactant. The half-life ( $t_{1/2}$ ) of the photodegradation for the pharmaceuticals, as calculated from the PFO rate model, was 26.55 min and 28.76 min for acetaminophen and chloramphenicol respectively, at the optimum conditions. The mechanism of photocatalytic degradation showed that OH free radicals are mostly responsible for the oxidation of the reactants. The HPLC monitoring of photocatalytic degradation showed the production of some intermediates during the process.

## References

- ABDULLAH, A.M., AL-THANI, N.J., TAWBI, K., & AL-KANDARI, H., 2016. Carbon/nitrogen-doped TiO<sub>2</sub>: New synthesis route, characterization and application for phenol degradation. *Arab. J. Chem.*, 9 (2), 229–237.
- ANDREOZZI, R., CAPRIO, V., MAROTTA, R., & VOGNA, D. 2003. Paracetamol oxidation from aqueous solutions by means of ozonation and H<sub>2</sub>O<sub>2</sub>/UV system. *Water Res.*, 37, 993–1004.
- AUDICHON, T., GUENOT, B., BARANTON, S., CRETIN, M., LAMY, C., & COUTANCEAU, C., 2017. Preparation and characterization of supported Ru<sub>x</sub>Ir<sub>(1-x)</sub>O<sub>2</sub> nano-oxides using a modified polyol synthesis assisted by microwave activation for energy storage applications. *Appl. Catal. B Environ.*, 200, 493–502.
- BARHOUMI, N., OTURAN, N., OLVERA-VARGAS, H., BRILLAS, E., GADRI, A., AMMAR, S., & OTURAN, M.A. 2016. Pyrite as a sustainable catalyst in electro-Fenton process for improving oxidation of sulfamethazine. Kinetics, mechanism and toxicity assessment. *Water Res.*, 94, 52–61.
- CHEN, M., BAO, C., CUN, T., & HUANG, Q. 2017. One-pot synthesis of ZnO/oligoaniline nanocomposites with improved removal of organic dyes in water: Effect of adsorption on photocatalytic degradation. *Mater. Res. Bull.*, 95, 459–467.
- CHEN, T., ZHANG, Q., XIE, Z., TAN, C., CHEN, P., ZENG, Y., WANG, F., LIU, H., LIU, Y., LIU, G., & LV, W. 2018. Carbon nitride modified hexagonal boron nitride interface as highly efficient blue LED light-driven photocatalyst. *Appl. Catal. B Environ.*, 238 (100), 410–421.
- CHIOU, C.-H., WU, C.-Y., & JUANG, R.-S. 2008. Influence of operating parameters on photocatalytic degradation of phenol in UV/TiO<sub>2</sub> process. *Cheml. Eng J.*, 139 (2), 322–329.
- DENG, Q., TANG, H., LIU, G., SONG, X., XU, G., LI, Q., NG, D.H.L., & WANG, G. 2015. The fabrication and photocatalytic performances of flower-like Ag

- nanoparticles/ZnO nanosheets-assembled microspheres. *Appl. Surf. Sci.*, 331, 50–57.
- DENG, X.-Q., LIU, J.-L., LI, X.-S., ZHU, B., ZHU, X., & ZHU, A.-M. 2017. Kinetic study on visible-light photocatalytic removal of formaldehyde from air over plasmonic Au/TiO<sub>2</sub>. *Catal. Today*, 281, 630–635.
- DONG, S., LI, Y., SUN, J., SUN, J., YU, C., & LI, Y. 2014. Facile synthesis of novel ZnO/RGO hybrid nanocomposites with enhanced catalytic performance for visible-light-driven photodegradation of metronidazole. *Mater. Chem. Phys.*, 145 (3), 357–365.
- DONG, W., LEE, C.W., LU, X., SUN, Y., HUA, W., ZHUANG, G., ZHANG, S., CHEN, J., HOU, H., & ZHAO, D. 2010. Synchronous role of coupled adsorption and photocatalytic oxidation on ordered mesoporous anatase TiO<sub>2</sub>–SiO<sub>2</sub> nanocomposites generating excellent degradation activity of RhB dye. *Appl. Catal. B: Environ.*, 95 (3–4), 197–207.
- FALAH, M., MACKENZIE, K.J.D., KNIBBE, R., PAGE, S.J., & HANNA, J. V. 2016. New composites of nanoparticle Cu (I) oxide and titania in a novel inorganic polymer (geopolymer) matrix for destruction of dyes and hazardous organic pollutants. *J. Hazard. Mater.*, 318, 772–782.
- FRIEDMANN, D., MENDIVE, C., & BAHNEMANN, D. 2010. TiO<sub>2</sub> for water treatment: Parameters affecting the kinetics and mechanisms of photocatalysis. *Appl. Catal. B Environ.*, 99 (3–4), 398–406.
- GALINDO, C., JACQUES, P., & KALT, A. 2000. Photodegradation of the aminoazobenzene acid orange 52 by three advanced oxidation processes: UV/H<sub>2</sub>O<sub>2</sub>, UV/TiO<sub>2</sub> and VIS/TiO<sub>2</sub>: Comparative mechanistic and kinetic investigations. *J. Photochem. Photobio. A Chem.*, 130 (1), 35–47.
- GAO, B., CHEN, W., DONG, S., LIU, J., LIU, T., WANG, L., & SILLANPÄÄ, M. 2017. Polypyrrole/ZnIn<sub>2</sub>S<sub>4</sub> composite photocatalyst for enhanced mineralization of chloramphenicol under visible light. *J. Photochem. Photobio. A Chem.*, 349, 115–123.



- GOLSHAN, M., ZARE, M., GOUDARZI, G., ABTAHI, M., & BABAEI, A.A. 2017. Fe<sub>3</sub>O<sub>4</sub>@HAP-enhanced photocatalytic degradation of Acid Red 73 in aqueous suspension: Optimization, kinetic, and mechanism studies. *Mater Res. Bull.*, 91, 59–67.
- GUO, H., NIU, C.G., WEN, X.J., ZHANG, L., LIANG, C., ZHANG, X.G., GUAN, D.L., TANG, N., & ZENG, G.M. 2018. Construction of highly efficient and stable ternary AgBr/Ag/PbBiO<sub>2</sub>Br Z-scheme photocatalyst under visible light irradiation: Performance and mechanism insight. *J. Colloid Interface Sci.*, 513, 852–865.
- HAN, C., CHEN, Z., ZHANG, N., COLMENARES, J.C., & XU, Y.J. 2015. Hierarchically CdS decorated 1D ZnO nanorods-2D graphene hybrids: Low temperature synthesis and enhanced photocatalytic performance. *Adv. Funct. Mater.*, 25 (2), 221–229.
- HAPESHI, E., ACHILLEOS, A., VASQUEZ, M.I., MICHAEL, C., XEKOUKOULOTAKIS, N.P., MANTZAVINOS, D., & KASSINOS, D. 2010. Drugs degrading photocatalytically: Kinetics and mechanisms of ofloxacin and atenolol removal on titania suspensions. *Water Res.*, 44 (6), 1737–1746.
- HOU, Y., ZUO, F., DAGG, A.P., LIU, J., & FENG, P. 2014. Branched WO<sub>3</sub> nanosheet array with layered C<sub>3</sub>N<sub>4</sub> heterojunctions and CoOx nanoparticles as a flexible photoanode for efficient photoelectrochemical water oxidation. *Adv. Mater.*, 26 (29), 5043–5049.
- HUANG, W., TANG, X., WANG, Y., KOLTYPIN, Y., GEDANKEN, A. 2000. Selective synthesis of anatase and rutile via ultrasound irradiation. *Chem. Comm.*, 1415–1416.
- HWANG, I. & SCHOLLES, G.D. 2011. Electronic energy transfer and quantum-coherence in  $\pi$ -conjugated polymers. *Chem. Mater.*, 23 (3), 610–620.
- JALLOULI, N., ELGHNIJI, K., TRABELSI, H., & KSIBI, M. 2017. Photocatalytic degradation of paracetamol on TiO<sub>2</sub> nanoparticles and TiO<sub>2</sub>/cellulosic fiber under UV and sunlight irradiation. *Arab. J. Chem.*, 10, S3640–S3645.
- JEONG, J. & YOON, J. 2005. pH effect on OH radical production in

- photo/ferrioxalate system. *Water Res.*, 39 (13), 2893–2900.
- LANGMUIR, I. 1916. The constitution and fundamental properties of solids and liquids. Part I . Solids. *J. Am. Chem. Soc.*, 38, 2221-2229.
- LEE, K.M., LAI, C.W., NGAI, K.S., & JUAN, J.C. 2016. Recent developments of zinc oxide based photocatalyst in water treatment technology: A review. *Water Res.*, 88, 428–448.
- LI, S., MA, H., WALLIS, L.K., ETTERSON, M.A., RILEY, B., HOFF, D.J., & DIAMOND, S.A., 2016. Impact of natural organic matter on particle behavior and phototoxicity of titanium dioxide nanoparticles. *Sci. Total Environ.*, 542, 324–333.
- LIN, C. & YANG, W. 2014. Ordered mesostructured Cu-doped TiO<sub>2</sub> spheres as active visible-light-driven photocatalysts for degradation of paracetamol. *Chem. Eng. J.*, 237, 131–137.
- LIN, J.C.-T., DE LUNA, M.D.G., ARANZAMENDEZ, G.L., & LU, M.-C. 2016. Degradations of acetaminophen via a K<sub>2</sub>S<sub>2</sub>O<sub>8</sub>-doped TiO<sub>2</sub> photocatalyst under visible light irradiation. *Chemos.*, 155, 388–394.
- LING, R., CHEN, J.P., SHAO, J., & REINHARD, M. 2018. Degradation of organic compounds during the corrosion of ZVI by hydrogen peroxide at neutral pH: Kinetics, mechanisms and effect of corrosion promoting and inhibiting ions. *Water Res.*, 134, 44–53.
- MERAH, N., BAZOUNE, A., FAZAL, A., & KHAN, Z., 2013. Weathering degradation mechanisms of chlorinated PVC. *Int. J. Plast. Technol.*, 17 (2), 111–122.
- MOCTEZUMA, E., LEYVA, E., AGUILAR, C.A., LUNA, R.A., & MONTALVO, C. 2012. Photocatalytic degradation of paracetamol: Intermediates and total reaction mechanism. *J. Hazard. Mater.*, 243, 130–138.
- MOTEGH, M., CEN, J., APPEL, P.W., VAN OMMEN, J.R., & KREUTZER, M.T. 2012. Photocatalytic-reactor efficiencies and simplified expressions to assess their relevance in kinetic experiments. *Chem. Eng. J.*, 207–208, 607–615.
- MOU, H., SONG, C., ZHOU, Y., ZHANG, B., & WANG, D. 2018. Design and

- synthesis of porous Ag/ZnO nanosheets assemblies as super photocatalysts for enhanced visible-light degradation of 4-nitrophenol and hydrogen evolution. *Appl. Catal. B Environ.*, 221, 565–573.
- MOUSSAVI, G., MOMENINEJAD, H., SHEKOOHIYAN, S., & BARATPOUR, P. 2017. Oxidation of acetaminophen in the contaminated water using UVC/8 process in a cylindrical photoreactor : Efficiency and kinetics of degradation and mineralization. *Sep. Purif. Technol.*, 181, 132–138.
- NIE, M., YANG, Y., ZHANG, Z., YAN, C., WANG, X., LI, H., & DONG, W. 2014. Degradation of chloramphenicol by thermally activated persulfate in aqueous solution. *Chem. Eng. J.*, 246, 373–382.
- OSEGHE, E.O., MSAGATI, T.A.M., MAMBA, B.B., & OFOMAJA, A.E., 2019. An efficient and stable narrow bandgap carbon dot-brookite composite over other CD-TiO<sub>2</sub> polymorphs in rhodamine B degradation under LED light. *Ceram. Int.*, Apr. 2019.
- PARAYIL, S.K., KIBOMBO, H.S., WU, C.-M., PENG, R. BALTRUSAITIS, J., & KOODALI, R.T., 2012. Enhanced photocatalytic water splitting activity of carbon-modified TiO<sub>2</sub> composite materials synthesized by a green synthetic approach. *Int. J. Hydrogen Energy*, 37 (10), 8257–8267.
- PAP, Z., DANCIU, V., CEGLÉD, Z., KUKOVECZ, Á., OSZKÓ, A., DOMBI, A., & MOGYORÓSI, K. 2011. The influence of rapid heat treatment in still air on the photocatalytic activity of titania photocatalysts for phenol and monuron degradation. *Appl. Catal. B Environ.*, 101 (3–4), 461–470.
- PARK, Y., KIM, W., MONLLOR-SATOCA, D., TACHIKAWA, T., MAJIMA, T., & CHOI, W. 2013. Role of interparticle charge transfers in agglomerated photocatalyst nanoparticles: Demonstration in aqueous suspension of dye-sensitized TiO<sub>2</sub>. *J. Phys. Chem. Lett.*, 4 (1), 189–194.
- PELLEGRINO, F., PELLUTIÈ, L., SORDELLO, F., MINERO, C., ORTEL, E., HODOROABA, V.-D., & MAURINO, V. 2017. Influence of agglomeration and aggregation on the photocatalytic activity of TiO<sub>2</sub> nanoparticles. *Appl. Catal. B*

*Environ.*, 216, 80–87.

RIZZO, L., MERIC, S., GUIDA, M., KASSINOS, D., & BELGIORNO, V. 2009.

Heterogenous photocatalytic degradation kinetics and detoxification of an urban wastewater treatment plant effluent contaminated with pharmaceuticals. *Water Res.*, 43 (16), 4070–4078.

SHAO, P., TIAN, J., ZHAO, Z., SHI, W., GAO, S., & CUI, F. 2015. Amorphous TiO<sub>2</sub> doped with carbon for visible light photodegradation of rhodamine B and 4-chlorophenol. *Appl. Surf. Sci.*, 324, 35–43.

SKOUMAL, M., CABOT, P.-L., CENTELLAS, F., ARIAS, C., RODRÍGUEZ, R.M., GARRIDO, J.A., & BRILLAS, E. 2006. Mineralization of paracetamol by ozonation catalyzed with Fe<sup>2+</sup>, Cu<sup>2+</sup> and UVA light. *Appl. Catal. B: Environ.*, 66 (3–4), 228–240.

SOITAH, T.N., CHUNHUI, Y., & LIANG, S. 2010. Effect of Fe doping on structural and electrical properties of nanocrystalline ZnO thin films prepared by sol-gel dip coating technique. *Sci. Adv. Mater.*, 2, 534-538.

SNYDER, A., BO, Z., MOON, R., ROCHET, J.-C., & STANCIU, L. 2013. Reusable photocatalytic titanium dioxide–cellulose nanofiber films. *J. Colloid Interface Sci.*, 399, 92–98.

SUN, L., SHI, Y., LI, B., LI, X., & WANG, Y., 2013. Preparation and Characterization of Polypyrrole / TiO<sub>2</sub> Nanocomposites by Reverse Microemulsion Polymerization and its Photocatalytic Activity for the Degradation of Methyl Orange Under Natural Light. *Polymer composition*, 2013 .

SUN, P., ZHANG, J., LIU, W., WANG, Q., & CAO, W. 2018. Modification to L-H kinetics model and its application in the investigation on photodegradation of gaseous benzene by nitrogen-doped TiO<sub>2</sub>. *Catal.*, 8 (8).

TRETINNIKOV, O.N. & SUSHKO, N.I., 2015. Formation of Linear Polyenes in Thermal Dehydration of Polyvinyl Alcohol, Catalyzed by Phosphotungstic Acid. *J. Appl. Spectrosc.*, 81 (6), 1044–1047.

- WANG, B., ZHANG, G., LENG, X., SUN, Z., & ZHENG, S., 2015. Characterization and improved solar light activity of vanadium doped TiO<sub>2</sub>/diatomite hybrid catalysts. *J. Hazard. Mater.*, 285, 212–220.
- WANG, J., XIA, Y., DONG, Y., CHEN, R., XIANG, L., & KOMARNENI, S., 2016. Defect-rich ZnO nanosheets of high surface area as an efficient visible-light photocatalyst. *Appl. Catal. B Environ.*, 192, 8–16.
- YANG, H., CHEN, F., JIAO, Y., & ZHANG, J. 2013. The role of interfacial lattice Ag<sup>+</sup> on titania based photocatalysis. *Appl. Catal. B Environ.*, 130–131, 218–223.
- YANG, H., LI, G., AN, T., GAO, Y., & FU, J., 2010. Photocatalytic degradation kinetics and mechanism of environmental pharmaceuticals in aqueous suspension of TiO<sub>2</sub>: A case of sulfa drugs. *Catal. Today*, 153 (3–4), 200–207.
- YANG, L., YU, L.E., & RAY, M.B., 2008. Degradation of paracetamol in aqueous solutions by TiO<sub>2</sub> photocatalysis. *Water Res.*, 42 (13), 3480–3488.
- YANG, L., YU, Y., ZHANG, J., CHEN, F., MENG, X., QIU, Y., DAN, Y., & JIANG, L. 2018. In-situ fabrication of pyrrolopyrrole-carbazole-based conjugated polymer/TiO<sub>2</sub> heterojunction for enhanced visible-light photocatalysis. *Appl. Surf. Sci.*, 434, 796–805.
- YASMINA, M., MOURAD, K., MOHAMMED, S.H., & KHAOULA, C. 2014. Treatment Heterogeneous Photocatalysis; Factors Influencing the Photocatalytic Degradation by TiO<sub>2</sub>. *Energy Procedia*, 50, 559–566.
- YI, S.S., YAN, J.M., WULAN, B.R., LI, S.J., LIU, K.H., & JIANG, Q. 2017. Noble-metal-free cobalt phosphide modified carbon nitride: An efficient photocatalyst for hydrogen generation. *Appl. Catal. B Environ.*, 200, 477–483.
- YU, J., XIANG, Q., & ZHOU, M. 2009. Preparation, characterization and visible-light-driven photocatalytic activity of Fe-doped titania nanorods and first-principles study for electronic structures. *Appl. Catal. B Environ.*, 90 (3–4), 595–602.
- ZHANG, G., KIM, G., & CHOI, W. 2014. Visible light-driven photocatalysis mediated via ligand-to-metal charge transfer (LMCT): an alternative approach to solar

activation of titania. *Energy Environ. Sci.*, 7 (3), 954.

ZHANG, W., WANG, K., YU, Y., & HE, H., 2010. TiO<sub>2</sub> / HZSM-5 nano-composite photocatalyst : HCl treatment of NaZSM-5 promotes photocatalytic degradation of methyl orange. *Chem. Eng. J.*, 163 (1–2), 62–67.

## **Chapter 5: General conclusion and recommendations**

This is the final chapter, which summarises the work done and the findings from each phase of the research project. It highlights the contribution of the project to the body of knowledge in photocatalysis and water purification. The chapter presents recommendations for further studies in this area of research.

## TABLE OF CONTENTS

<b>CHAPTER 5: GENERAL CONCLUSION AND RECOMMENDATIONS .....</b>	<b>158</b>
5.1 GENERAL CONCLUSION .....	160
5.2 RECOMMENDATIONS .....	162



## 5.1 General conclusion

This research work aimed at synthesising and characterising pure titania and a hybrid material, in the form of conjugated-polyene modified titania photocatalysts. In addition, the prepared catalysts were to be evaluated for the photodegradation of acetaminophen and chloramphenicol as chosen non-antibiotic and antibiotic pharmaceuticals under visible light irradiation. An intricate technique has been applied to synthesise both  $\text{TiO}_2$  nanoparticles and polyene/ $\text{TiO}_2$  nanocomposites, which possess conjugated polymer chains covalently grafted onto the ceramic nanoparticle. The polyene was cheaply prepared from polyvinyl alcohol using a facile acid dehydration process and the synthesis of the bare  $\text{TiO}_2$  and polyene/ $\text{TiO}_2$  nanocomposites was achieved by sol-gel coupled with homogenisation techniques.

To monitor the morphological properties, structural architecture, particle sizes, electronic and optical properties, several characterisation techniques were employed. Among these techniques are powder X-ray diffraction (PXRD) analysis, transmission electron microscopy (TEM), scanning electron microscopy (SEM), Fourier transform infrared spectroscopy (FT-IR) and thermal gravimetric analysis (TGA-DSC). Others include UV-vis diffuse reflectance spectrophotometer (UV-Vis DRS), photoluminescence spectroscopy (PLS), cyclic voltammetry (CV), electrochemical impedance spectroscopy (EIS), as well as energy-dispersive X-ray spectroscopy (EDX).

The FTIR revealed the presence of a C=C conjugated surface functional group on both the polyene and polyene modified  $\text{TiO}_2$ , which is an indication of a successful grafting of polyene into  $\text{TiO}_2$  nanoparticles. The PXRD flaunted the presence of sharp diffraction peaks, which are typical of the crystalline anatase phase of  $\text{TiO}_2$  for both the modified and unmodified materials with calculated crystallite sizes of 3.41 nm and 7.5 nm respectively. In addition, the SEM images displayed circularly shaped particles at nano-size level with a well interactive polymer/ $\text{TiO}_2$  structural morphology for the composite. The particle sizes, which were calculated from TEM images, revealed particle distribution of average sizes within nano-range. However, the

particle sizes for the composites were observed to increase with an increase in polyene percentage modifications due to polymer layers grafted on nanoparticles. The nano-size anatase phase of  $\text{TiO}_2$  is well known as an efficient photocatalyst. The EDS spectra presented the presence of Ti and O in the unmodified and Ti, O and C in the composite materials for elemental composition.

Regarding the problem of the lack of effective activation of  $\text{TiO}_2$  by visible light, the optical property revealed a great improvement in the visible light absorption capacity of the hybrid composite material. The composite material provides an excellent enhancement of electron-hole separation over bare  $\text{TiO}_2$ . A significant reduction in the synthesised  $\text{TiO}_2$  band gap (3.18eV) was achieved with the CPE- $\text{TiO}_2$  hybrid material bandgap (2.4eV), which implies a better light absorption at the visible region of the light spectrum. The cyclic voltammetry and electrochemical impedance spectroscopy measurement for the materials exhibited a good electronic property that is appropriate for the photocatalytic process. Therefore, the coexistence of multiple bonds in the poly-conjugate carbon chain with a reduced bandgap and  $\text{TiO}_2$  in the hybrid materials enhanced charge separation and migration.

The results from the photocatalytic degradation under visible light revealed that conjugated polyene/ $\text{TiO}_2$  structure exhibits excellent mineralisation of acetaminophen at 94.21% removal and chloramphenicol at 84.12% removal. This performance could be due to a reduction in the bandgap energy value, which enables the composite to be readily activated under visible light irradiation. It was demonstrated that the hybrid materials could act as efficient photocatalysts under visible light irradiation and it is thermally stable for a certain degree of temperature rise during the process of irradiation.

Experimental studies were performed on both materials using one-factor-at-a-time experimental design to investigate and evaluate the removal performance at varying experimental conditions. The kinetics and reaction mechanistic studies show the fitness of the degradation data into PFO rate kinetics with the highest rate constant and the lowest half-life obtained at the lowest concentration of the pollutants. The mechanism of the photodegradation indicated that  $\text{OH}^\cdot$  radical species are mostly responsible for the oxidation of both pollutants and that the degradation process involves the production of some intermediate organic compounds. Hydroquinone,

benzoquinone p-nitrophenol and 2,4-trihydroxy-benzene are some of the intermediate compounds identified during acetaminophen degradation. While oxamic acid and succinic acid were identified for chloramphenicol. Photocatalytic degradation experiments revealed that the modified titania achieved higher mineralisation of acetaminophen compared to chloramphenicol.

In summary, the following milestones were achieved in this work as a contribution to the body of knowledge:

- ❖ For the first time, a linear polyene material was applied to alter and improve the bandgap reduction of titania photocatalyst with up to 76% percent reduction. This is a huge improvement compared to what has been reported and available in the literature.
- ❖ By conjugating polyenes to the surface of  $\text{TiO}_2$ , the achievement of a 75% reduction in bandgap ultimately led to an increase of 71.2% and 55.5% in the conversion of acetaminophen and chloramphenicol respectively. This feat is commendable as compared to many past works on  $\text{TiO}_2$  application in photocatalysis.
- ❖ Polyene/ $\text{TiO}_2$  hybrid material was found to be highly effective in visible light absorption, a good initiative for low-cost solar light application in water purification technology, particularly at industrial scale.

## 5.2 Recommendations

All the objectives set for this research work were accomplished. However, more advances could have been made during this research work, particularly to resolve some of the challenges encountered, but for the constraints of time and resources. Therefore, future work in this area of study should include the following:

- ❖ Because of the improvement that was observed in the electrochemical and optical properties of the material, we suggest that other conjugated polymers like polypropylene and monomer organic molecules such as porphyrin could be explored.
- ❖ The mechanistic of the chemical interaction between conjugated polymers and  $\text{TiO}_2$  to adjust the band structure to improve its visible light activation and the transfer of the generated charge carriers should be innovative.

- ❖ Further research should be carried out to explore other synthesis techniques yielding different structures and to fully understand the structural relationship in polymer/TiO<sub>2</sub>nanocomposite.
- ❖ For future research, we recommend that LC-MS should be used to confirm the identity of the intermediate products for photocatalytic degradation of the pharmaceuticals.
- ❖ The design of experimental methods such as central composite design (CCD), factorial and Box-Behnken should be considered to investigate further the interactive effects of the variable parameters on the mineralisation efficiency of pharmaceutical pollutants.
- ❖ Future research should be focused on a novel modification for large-scale industrial applications. The achievement in this respect will provide for broader applications of polymer/TiO<sub>2</sub> composites in water remediation technology.

## Appendices

**APPENDIX A:** The electrochemical behaviour of bare  $\text{TiO}_2$  and the modified  $\text{TiO}_2$  at varying polyene percentages

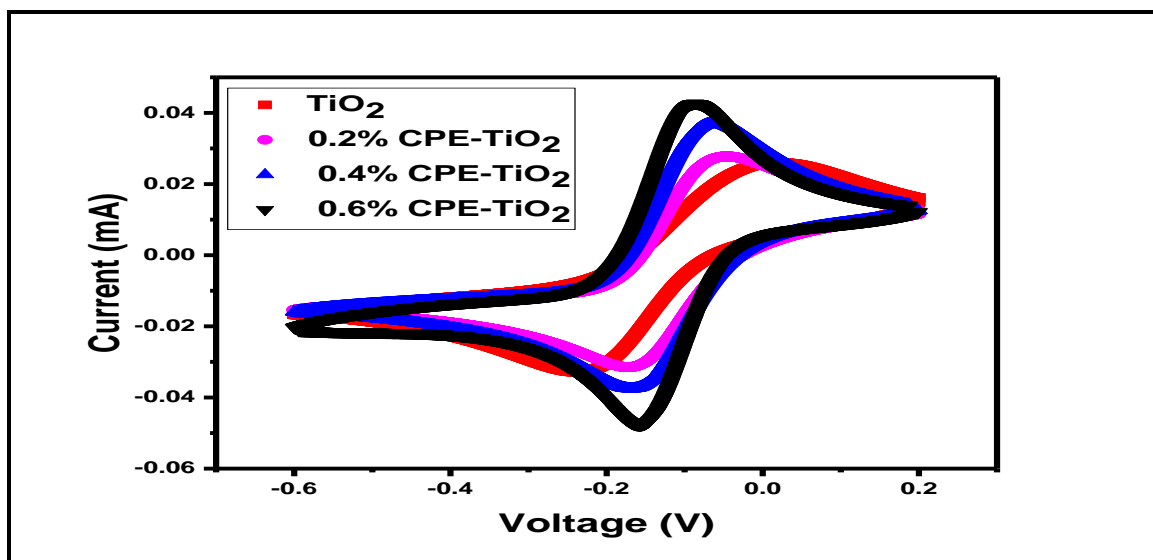


**Figure A 1:** CV curve for (A)  $\text{TiO}_2$  and CPE- $\text{TiO}_2$  at varying polyene percentage modification

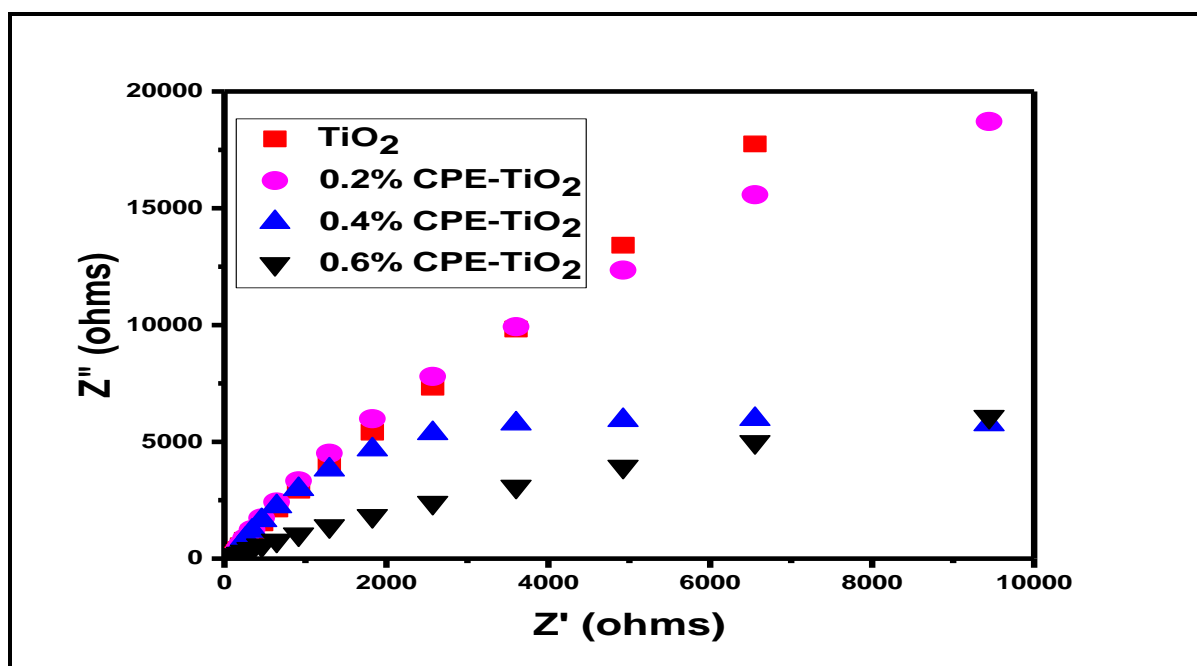


**Figure A 2:** The EIS Nyquist plots of  $\text{TiO}_2$  and CPE- $\text{TiO}_2$  at varying polyene percentage modification and

**APPENDIX B:** Optical behaviour of bare  $\text{TiO}_2$  and the modified  $\text{TiO}_2$  at varying polyene percentages

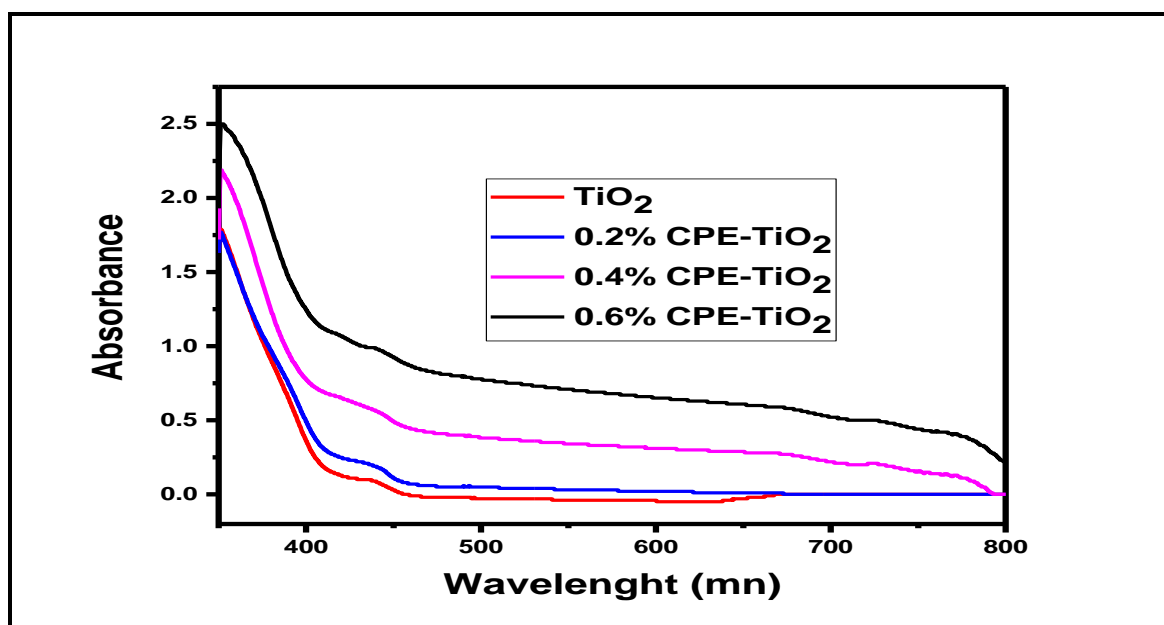


**Figure B 1:** The EIS Nyquist plots of  $\text{TiO}_2$  and CPE- $\text{TiO}_2$  at varying polyene percentage modification

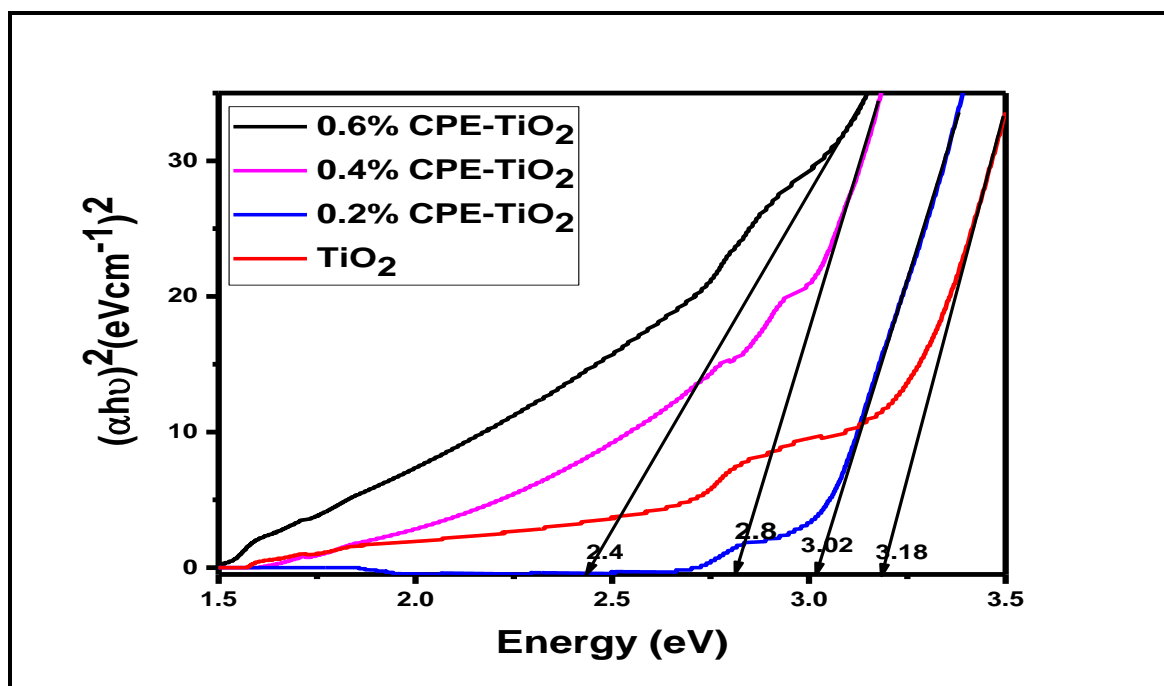


**Figure B 2:** The EIS Nyquist plots of  $\text{TiO}_2$  and CPE- $\text{TiO}_2$  at varying polyene percentage modification

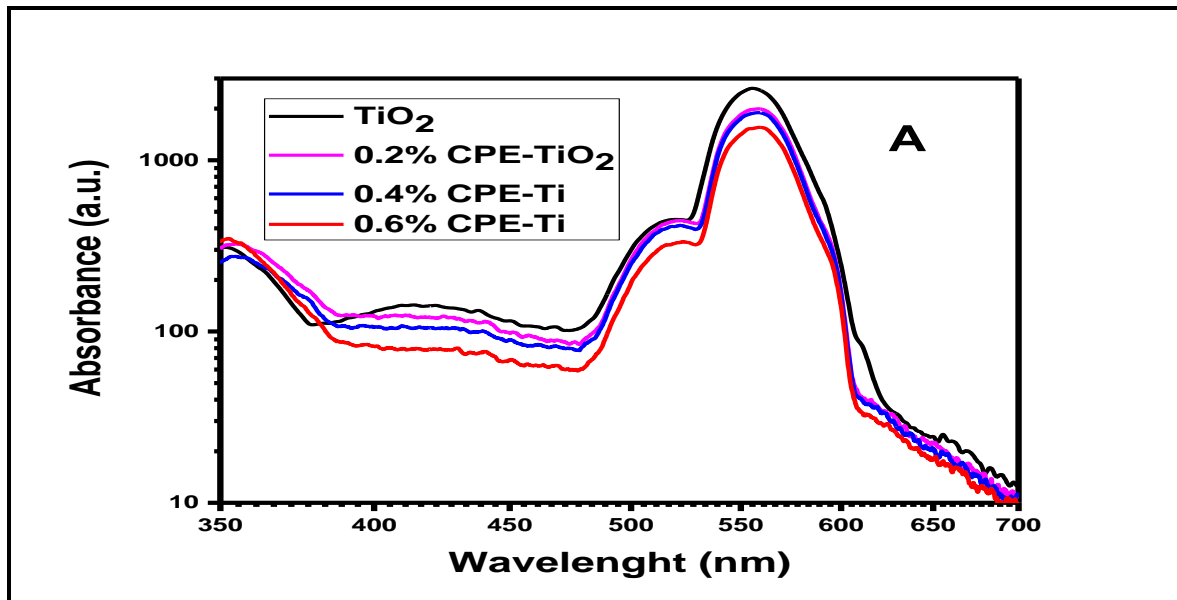


**Figure B 3:** The photoluminescence (PL) spectra of (A)  $\text{TiO}_2$  and CPE- $\text{TiO}_2$  at varying polyene percentage modification

## APPENDIX C: HPLC photocatalytic degradation monitoring.

**Table C 1:** Detected Intermediate products and their retention time during photocatalytic degradation.

Molecule	Retention time $t_R$ (Min)
Paracetamol	9.8
Hydroquinone	5.6
benzoquinone	6.9
p-nitrophenol	10.9
1,2,4-trihydroxybenzene	29.2
Acetaminophen	5.6
Oxamic acid	2.2
Succinic acid	2.7